Responsive Lanthanide Complexes for Metal Ion Sensing

Aileen Congreve

Department of Chemistry
University of Durham

A thesis submitted in part-fulfilment for the degree of Doctor of Philosophy

February 2004

Abstract

Responsive Lanthanide Complexes for Metal Ions Sensing

Aileen Congreve

The speciation and distribution of zinc (II) within cells is not well established and the range of zinc (II) probes available are of limited use.

The quest was to develop responsive lanthanide complexes to bind selectively and respond (by change in hydration state) to biologically relevant concentrations of zinc at physiological pH for possible application in MRI and luminescence.

A pyridyl sulfonamide ligand with an α-$CH_2NHSO_2CF_3$ substituent was found to have the desired properties for strong zinc (II) coordination. The presence of a methyl group at 6', inhibited the formation of related square planar copper (II) complexes.

Pyridyl amide appended europium and gadolinium (III) complexes, based on cyclen were developed with C_2 and C_3 spacers separating the macrocyclic ring and the amide. The mono-aqua C_2 complex exhibited fast water exchange, due to the steric hindrance of the seven-membered chelate between the amide carbonyl and the lanthanide centre. The increase in steric hindrance caused by the eight-ring chelate in the C_3 analogue rendered it q = 0.

A trifluoromethanesulfonamide moiety at the 6' position of the pyridine group resulted in a mono-aqua complex for the C_2 and C_3 appended systems. This system showed no change in hydration state on addition of Zn^{2+}. The addition of α-N-carboxyalkyl groups to give a GdaDO3A system resulted in the formation of q = 2 complexes which showed no zinc (II) responsive properties. However, the C_2-linked species exhibited a high binding affinity to HSA which resulted in a dramatic increase in the relaxivity.

Eu and Gd complexes of an octadentate N_5O_3 pyridyl sulfonamide containing ligand were developed as pH and pZn responsive probes. The pyridyl nitrogen bound irreversibly to the lanthanide centre, resisting protonation even in the presence of zinc and copper ions, for which the pyridyl sulfonamide group has an establiblished high affinity.

Declaration

The work described herein was carried out in the Department of Chemistry, University of Durham between October 2000 and February 2004. All the work is my own unless otherwise stated and no part of it has been submitted for a degree at this or any other university.

Statement of Copyright

Acknowledgements

Sincere thanks the following people:

First and foremost, Professor David Parker for giving me the opportunity to undertake this research under his supervision and for all his help, advice, encouragement and patience as well as cunning plans on post-it notes.

The analytical people in the department, without whom this work would not have been possible and so much gossip would have gone unknown! Dr Alan Kenwright, Catherine Heffernan and Ian McKeag for NMR (and therapy); Dr Mike Jones and Lara Turner for Mass Spectrometry, Jarka Dorstal for CHN analysis, Dr Tony Royston for NMRD, Dr Ritu Kataky for electrochemistry and speciation.

Mark Knell for determining the pK_a values, speciation of the pyridyl sulfonamide ligands and pH dependant cyclic voltammetry.

Dr Horst Puschmann for solving and refining the crystal structures, fitting NMRD profiles, sorting out numerous computer issues and above all his friendship.

Professor Mauro Botta and Dr Eliana Gianolio for fitting NMRD and ^{17}O profiles.

Dr Andy Beeby and Dr Gareth Williams for invaluable discussions and references, and help with luminescence and lifetime measurements.

The members of the CG27 & CG133; in particular Dr Kanthi Senanayke, my chemistry mummy, who did the initial pyridyl-sulfonamide work; Dr Rachel Dickins for all her help, especially with the wiggly lines of Eu NMRs; Nicola Thompson for dealing splendidly with the HSA and providing an excellent extra pair of hands when required; also Dr Lowe, JIB, SW, Gaaaaaaab, SDK, PA, AB ☺, JC, YB, DM, MO'H, SB, LF and LW whose help, expertise, patience, friendship and ability to eat cake has been invaluable.

My friends, especially Kate Adamson, Clare Crossland, Andrew Wilkinson, Matthew Hampson, Nadine Koch and Christina Schumacher for their companionship, and ongoing support. Also, the members of the Graduate Society Boat Club 2000-2003 for providing a distraction from chemistry.

Everyone in the chemistry department who has assisted me in some way, from repairing and Aileen-proofing my glassware to ordering stuff, making interesting tea and coffee and generally making it such a nice friendly place to work.

EPSRC for funding.

Last, but by no means least, thanks to my parents and family for their encouragement and support.

'You can go and collect some fir-cones for me', said Kanga, giving them a basket. So they went to the Six Pine Trees, and threw fir-cones at each other until they had forgotten what they came for...

The House at Pooh Corner
A.A. Milne

Table of Contents

Abbreviations

aDO3A	1,4,7,10-tetraazacyclododecane-1,4,7-tri(adipic acid)
BOC	*tert*-butoxycarbonyl
CHEF	chelation enhanced fluorescence
CN	coordination number
CNS	central nervous system
COSY	correlation spectroscopy
CSD	Cambridge Structural Database
CV	cyclic voltammetry
cyclen, $12N_4$	1,4,7,10-tetraazacyclododecane
DCM	dichloromethane
DMF	dimethylformamide
DO3A	1,4,7,10-tetraazacyclododecane-1,4,7-triacetate
DOTA	1,4,7,10-tetraazacyclododecane-1,4,7,10-tetraacetic acid
DPA	bis(2-pyridylmethyl)amine, di-2-picolylamine
DTPA	diethylenetriaminepentaacetic acid
EDC	1-(3-dimethylaminopropyl)-3-ethylcarbodiimide
EDTA	ethylenediamine-*N,N,N'N'*-tetraacetate
Et	ethyl
EtOAc	ethyl acetate
EtOH	ethanol
EI	electron ionisation
FAB	fast atom bombardment
FTIR	fourier transform infra red
HOBt	hydroxybenzotriazole
HSA	human serum albumin
Hz	hertz
ICT	internal charge transfer
IR	infra red
ISC	intersystem crossing

LFSE	Ligand Field Stabilisation Energy
LMCT	ligand to metal charge transfer
Ln	lanthanide
m.p.	melting point
MeCN	acetonitrile
MeOH	methanol
MLCT	metal to ligand charge transfer
MOPS	3-(N-morpholino) propanesulfonic acid
MRI	Magnetic Resonance Imaging
MS	mass spectrometry
NHS	*N*-Hydroxysuccinimide
NMR	Nuclear Magnetic Resonance
NMRD	Nuclear Magnetic Relaxation Dispersion
PET	photoelectron transfer
q	number of primary coordination sphere water molecules
R_{1p}	relaxation rate caused by paramagnetic species
r_{1p}	relaxivity caused by paramagnetic species
R_f	retention function
SU	Standard Uncertainty
T_1	longitudinal relaxation time
TBAP	tetrabutylammonium perchlorate
^{t}Bu	*tert*-butyl
TETA	1,4,8,11-tetraazacyclotetradecane-1,4,8,11-tetraacetate
TFA	trifluoroacetic acid
THF	tetrahydrofuran
TLC	Thin Layer Chromatography
tosyl	*p*-toluenesulfonyl
TPEN	N,N,N′,N′-tetra(2-picolyl)ethylenediamine
TSQ	6-methoxy-8-p-toluene-sulfonamido-quinoline
UV	ultra violet
WE	working electrode
τ_R	rotational correlation time/ reorientational correlation time

Chapter 1

Introduction

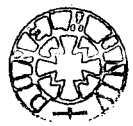

1 Introduction

Metal ions play essential roles, both structural and catalytic, in the regulation of many cellular functions, including metabolism, signal transduction, gene expression and proliferation.[1] Small, selective and sensitive sensor molecules that can penetrate through cell membranes without harming the cell are necessary tools that can allow the role of metal ions in such mechanisms to be evaluated.[2]

1.1 Biological Importance of Zinc

Zinc is the second most abundant transition metal within the human body: an average 70 kg person contains approximately 2.3 g of zinc.[3] For more than a century, zinc has been known to be an essential trace element in eukaryotes[4] and in 1934[5] zinc was shown to be essential for the normal growth of mammals. However, due to the spectroscopically silent nature of zinc (II), it is difficult to monitor. Consequently, details of the chemical speciation and compartmentalisation of zinc (II) within cells are not currently well established.[6]

The total zinc (II) ion concentration in serum is of the order of 10 to 20 micromolar and this rises towards the millimolar levels in mammalian cells.[3] There are thought to be two pools of intracellular zinc. The first contains zinc that is tightly complexed to proteins and thus is invisible to cytological stains. The second pool, which can be visualised histochemically, contains approximately 10% of the total cellular zinc (II).[7] This zinc is free and ionised and found in vesicles, that are rich in glutamate and aspartate.[7]

A study by Outten and O'Halloran[8] has revealed that although the concentration of zinc (II) within the cell is in the millimolar range, the availability of free zinc (II) within the cytoplasm is very stringently controlled. Their study showed that only a femtomolar concentration of zinc (II) may be required for the triggering of zinc-responsive transcription factors. This hypothesis is inconsistent with the possibility of a cytosolic pool of free zinc (II) ions, suggesting that any zinc within cells must be very tightly bound, either in vesicles or to proteins. Cells must have a very tight control over cytosolic metal ion concentrations.

Zinc (II) has numerous cellular functions and is important in the various processes associated with cell activation and growth[7,9,10]: these include gene expression, apoptosis, neurotransmission, signal transduction, enzyme regulation and catalysis.

In gene expression,[1,3,11] zinc (II) is involved in the transcription and replication of genetic material. Zinc fingers are special zinc containing proteins, which recognise DNA base sequences and serve in the selective activation and regulatory control of genetic transcription. Zinc (II) is also present in transcription factors and core proteins of DNA.

Zinc forms an essential part of more than 300 enzymes.[7,12] Each of the six classes of enzyme[13] are known to employ zinc in either a catalytic or structural role. At the active site of many hydrolytic enzymes, zinc lowers the pK_a of coordinated oxygen ligands: the potential for undesired electron transfer is avoided as zinc (II), being d^{10}, has no readily accessible redox state.

Elevated levels of zinc (II) are localised in areas of the brain, especially the hippocampus.[11] Here, there is a requirement for high activity of many peptide triggers and hormones such that their release and removal must be rapid. It is thus concluded that a huge range of hormones have a connection with zinc biological action.

High levels of free ionic zinc are exhibited throughout the mammalian central nervous system (CNS).[14] Hippocampal synaptic nerve vesicles typically contain a 200 - 300 μM concentration of zinc (II).[10,15] Stimulated release of this metal ion from zincergic neurons in the hippocampus is thought to be important in neurotransmission.[13]

Zinc deficiency[3,16] in humans may cause a variety of symptoms such as loss of appetite, reduced sense of taste and an enhanced disposition for inflammations and an impairment of the immune system. However, free zinc (II) at physiologically reasonable concentrations can cause the precipitation of human Aβ amyloid protein, the major constituent of plaques in Alzheimer's disease and thus may play

a role in its pathophysiology.[15] Zinc has also been implicated in stroke and in aetiology of excitotoxic cell death in seizures, a condition in which vesicular zinc is vigorously released.[17]

Total intracellular zinc (II) content can be readily measured by standard analytical techniques, but the detection and measurement of available zinc (II) within cells is more challenging.[7] The role of intravesicular zinc remains enigmatic[15] and the importance of zinc-specific probes is particularly apparent in understanding zinc chemistry in the brain.[13] As more roles for non-enzymatic zinc become apparent, so has the need for cell permeant chemical probes of zinc biology.

1.2 Zinc Solution Chemistry

Under physiological conditions zinc occurs in its dicationic state.[3] It is diamagnetic and colourless due to its closed d shell (d^{10}) configuration.[4,18]

This d^{10} electron configuration has four biologically important consequences:[4]

- Zn^{2+} has no ligand field stabilisation energy (LFSE) when coordinated by ligands in any geometry. For ligands with partially filled d shells, this electronic energy term can favour certain arrangements of ligands over others.
- In hard-soft acid-base theory, zinc is regarded as a borderline acid, so zinc can interact with a variety of ligand types including sulfur, nitrogen, oxygen and water.
- Divalent zinc is not redox active; neither the potential oxidised form Zn^{3+}, nor the potential reduced form is accessible under physiological conditions.
- Zn^{2+} is relatively labile in kinetic terms. It undergoes ligand exchange reactions relatively rapidly.

Zinc (II) has a highly concentrated charge as it has a small ionic radius; 0.65Å in a six-coordinate geometry[11] and 0.60 Å in a four-coordinate geometry.[19] A combination of this highly localised charge and high electron affinity make zinc a

very effective attacking group. This is used in enzymes in the activation of small molecules, which cannot be handled by organic groups in a multipoint attachment.

Zinc (II) is a good electron acceptor or Lewis acid. It polarises groups to which it binds and either increases the attacking power of a bound base or increases the probability of attack on the bound group by acting as an acid.[20]

1.3 Complexation Chemistry of Zinc (II)

In order to design chemical probes for the detection of zinc (II), it is important to understand its chemical properties. The probe molecule must be able to selectively and reversibly coordinate the metal ion of interest.

1.3.1 Donor Atoms

When trying to complex a specific metal, the selection of the correct donor atom can lead to an increase in the complex stability.

Metals can be sorted into two groups according to their preference for various ligands; this is the concept of Hard and Soft Acids and Bases.[20] Metals are Lewis acids and ligands are Lewis bases. Hard metals are ones that retain their valence electrons very strongly: they are of a small size and high charge and are not readily polarised. Soft metals, conversely, are relatively large and easily polarisable. They do not retain their valence electrons firmly. Ligands containing highly electronegative donor atoms (O, N, F) that are hard to polarise are classified as hard bases. These include ammonia, amines, water, phosphate and sulfate. Soft bases are large and easily polarisable (e.g. I^-, $\underline{C}O$, R_3P). Stable complexes are formed as a result of interactions between hard acids and hard bases or soft acids and soft bases. Hard-soft interactions are weak.

Zinc (II) is classified as a borderline acceptor and therefore should tolerate both hard and soft bases.

1.3.2 Complex Stability

The Irving-Williams series[21] shows the binding preference for a given ligand across the divalent first row transition metal ions. There is an increase in stability across the series reaching a maximum at copper.

$$Mn(II) < Fe(II) < Co(II) < Ni(II) < Cu(II) > Zn(II)$$

This order can be related to the decrease in ionic radii across the series leading to stronger metal to ligand bonds.

1.3.3 Geometrical Preferences

To change the order of ligand binding preference, the ligand must be able to bind the desired metal more strongly than its neighbours. Synthesising a ligand that only binds in the preferred geometry for the desired metal can lead to greater selectivity. The preferred binding geometries for divalent cobalt, nickel, copper and zinc are shown in Table 1.1.

Table 1.1 Preferred binding geometry of some transition metals.[22]

Metal	Preferred Geometry
Cobalt (II)	Octahedral
Nickel (II)	Octahedral / Square Planar
Copper (II)	Jahn-Teller distorted / Square Planar
Zinc (II)	Tetrahedral

The partially filled d orbitals of cobalt (II), copper (II) and nickel (II) favour these geometries because the LFSE is maximised. As zinc (II) is d^{10}, LFSE does not affect the geometry of the complex formed. In the absence of any other preferred geometry, a tetrahedral arrangement of ligands is favoured as this minimises repulsion between donor groups.[18]

1.3.4 Chelation Effects

The coordination of two or more donor atoms from a single ligand to a central metal ion leads to an unusual increase in the stability. This is derived in part from the favourable entropic factor accompanying the release of non-chelating ligands.[5]

1.3.5 Zinc Specificity.

Koike and coworkers[23] have shown that zinc (II) has a strong affinity for aromatic sulfonamides. Zinc (II) forms a strong bond to a deprotonated sulfonamide nitrogen at physiological pH. However, copper (II), which is also an essential element, typically binds more tightly to nitrogen containing ligands than Zn (II).[21]

As copper (II) is a d^9 transition metal, it prefers to occupy a square planar or tetragonally distorted octahedral coordination geometry, whereas zinc prefers to have a tetrahedral environment. By making a ligand with sulfonamide nitrogen donors that have steric restrictions to prevent binding in an octahedral or square planar geometry, specificity for zinc may be obtained.[24]

1.4 Zinc Sensors

Chemosensors are typically molecules of abiotic origin that are able to bind selectively and reversibly to the molecule of interest.[2,25] Chemosensors usually consist of three different components: a receptor which selectively binds; an active unit whose properties change upon complexation and a spacer that can change the geometry of a system and change the electronic interaction between the receptor and active unit, Figure 1.1. Chemosensors allow the analyte to be monitored in real time and real space.

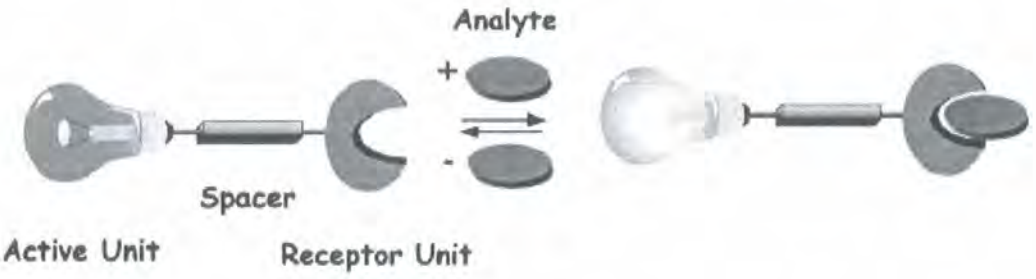

Figure 1.1 Schematic representation of a luminscent chemosensor.[2]

Fluorescence based chemosensors are currently the most common and present many advantages as fluorescence measurements are low cost, easy to perform, versatile and very sensitive (single molecule detection is possible).[2]

The zinc sensors currently available can be divided into four main groups: fluorophore appended cyclic amines, fluorophore appended acyclic amines, quinolines and proteins/peptides.

As the majority of zinc (II) sensors are currently fluorescent molecules, they will be discussed now with the limited number of lanthanide systems, both luminescent and MRI active, being addressed later.

1.4.1 Fluorophore Appended Azamacrocycles.

Macrocyclic polyamines with appended fluorophores have been synthesised by several groups as potential cellular zinc probes. This group of sensor molecules all work on the same principle. A fluorophore is directly linked to a macrocyclic polyamine, which strongly complexes with transition metal ions such as zinc (II). In the absence of zinc (II), fluorescence is quenched by a photoinduced electron transfer (PET). This is an intramolecular quenching mechanism caused by the lone pair of electrons of an amine nitrogen.[26,27] However, when zinc (II) is complexed by the nitrogen atoms of the macrocycle, the lone pair of electrons on nitrogen become coordinated to the metal. This prevents PET occurring, so fluorophore fluorescence is not quenched. As a result of this, an increase in the fluorescence emission is observed with increasing zinc (II) concentration (Figure 1.2). These probes have the disadvantage that the amine nitrogen can become protonated at low pH. This protonation can also cause inhibition of PET, resulting in an increase in fluorescence.

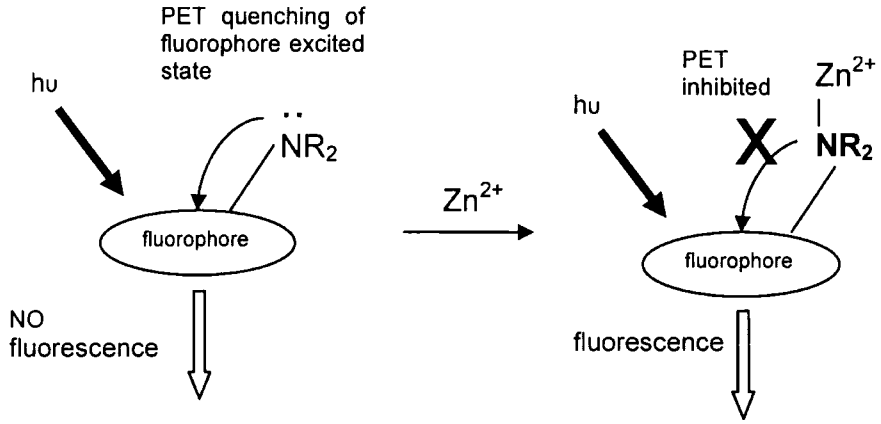

Figure 1.2 Schematic representation of zinc (II) binding inhibiting fluorescence by inhibiting PET.

Aromatic sulfonamides have a high affinity for zinc (II). The strong bond that forms between zinc (II) and deprotonated sulfonamides at physiological pH[28] has formed the basis of a series of ligands (**1 - 4**) which has been sequentially developed by Kimura and co-workers.[13,28,29,30]

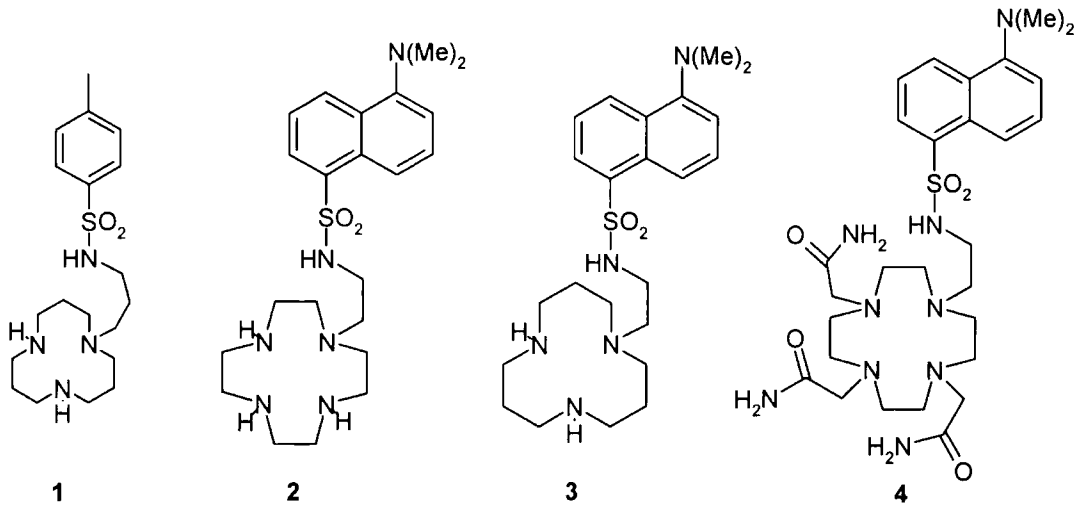

Tosylamidopropyl[12]aneN$_3$ **1** was initially shown to form a stable 1 : 1 tetrahedral complex with zinc (II) at physiological pH.[28] [12]aneN$_4$ (cyclen), which forms a much more stable complex with zinc (II), replaced the [12]aneN$_3$ to bind the zinc (II) while a dansylamide with an ethyl link was adopted as a new fluorophore **2**.[13] Chelation enhanced fluorescence (CHEF) resulted with the binding of zinc (II), with the fluorescence emission increasing linearly with zinc (II) concentration until a 1 : 1 ligand : zinc (II) ratio was reached ($K_a = 7 \times 10^9\ M^{-1}$, pH 7.0).[13] In order to make the ligand responsive to zinc (II) at intracellular concentrations, the cyclen was replaced with [12]aneN$_3$ **3** in a homologous system.[29] This resulted in a zinc (II) fluorophore that is responsive to zinc (II) in a micromolar concentration. It was also found that by functionalising cyclen with three carbamoylmethyl groups along with a dansylamide pendant arm **4**,[30] a system was obtained that bound zinc (II) but did not fluoresce in its presence. In this latter case the sulfonamide nitrogen is not coordinating.

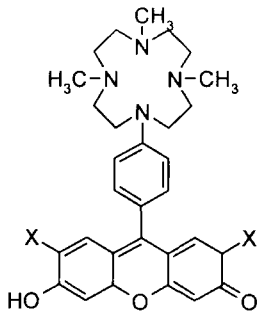

5 X = H, ACF-1
6 X = Cl, ACF-2

Fluorescein-appended cyclic amines **5** and **6** that use cyclen to bind zinc (II) have been developed by Nagano *et al.*[31] A 1 : 1 complex forms slowly (> 100 minutes) in the presence of zinc (II). This complexation hinders PET, resulting in a 14-fold fluorescence enhancement at micromolar zinc (II) concentrations at physiological pH (detection limit: 0.5 μM, pH 7.5). However, the slow complexation rate makes these ligands unsuitable for use in a biological system.

Fluorescein is a good fluorophore for use in biological systems as it is excited using visible light. Short wavelength ultra violet light, which is often required by simpler fluorophores, is potentially damaging to cells.

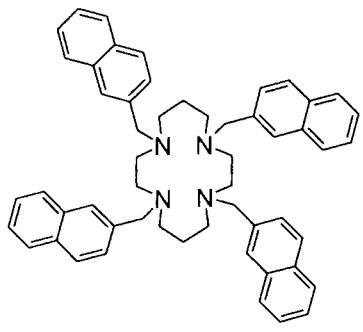

7

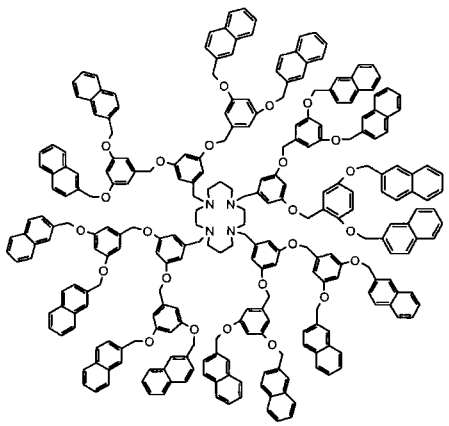

8

Naphthyl dendrimers attached to a 1,4,8,11-tetraazacyclotetradecane (cyclam) core, **7** and **8**, have been shown by Sauden and co-workers[32] to form luminescent complexes with zinc (II). In the absence of Zn (II), exciplexes form between the cyclam nitrogen and the naphthyl groups. Zinc(II) complexation engages the nitrogen lone pairs, preventing exciplex formation and resulting in intense

naphthyl fluorescence. The fluorescence has been shown to increase linearly with zinc (II) concentration until a 1 Zn (II) : 7 or 1 Zn (II) : 2 8 complex, i.e. $[Zn(8)_2]^{2+}$ has formed. The complexes that form are very stable ($K_a > 10^7 M^{-1}$ for 7 and $K_a > 10^{13} M^{-2}$ for 8). These molecules would be of limited use as biological probes because they are not water soluble.

1.4.2 Fluorophore Appended Acyclic Amines

Fluorophore appended acyclic amines are being investigated by many groups for possible application as sensors for biological zinc (II). In general, these probes work on the same principle as the flurophore appended cyclic amines, whereby the complexation of free zinc (II) involves binding of the lone pair of electrons on the amine nitrogen, preventing PET. This results in an increase in fluorescence intensity. In the absence of metal ions (or protons), the fluorescence of the active unit is quenched by the occurrence of a PET process between the lone pair on the nitrogen and the appended chromophore.[2]

Lippard and coworkers[10,14,33,34] have recently developed the Zinpyr family of high affinity, selective fluorescent sensors for zinc. (The name Zinpyr comes from both the utilisation of pyridine ligands and the ability to "peer" at zinc concentrations within the cell.) These probes all have sub-nM dissociation constants. They consist of a fluoroscein core, which can be excited at visible wavelengths, coupled to a zinc (II) chelator; DPA (bis(2-pyridylmethyl)amine) in the case of **9** (Zinpyr-1) and **10** (Zinpyr-2) and BPAMP [2-{bis(2-pyridylmethyl)aminomethyl}-N-methylaniline) in **11** (Zinpyr-4).

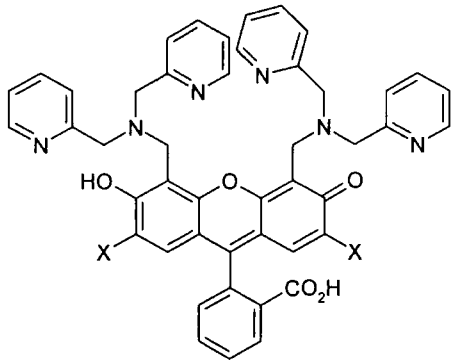

9 X = H, Zinpyr-1
10 X = Cl, Zinpyr-2

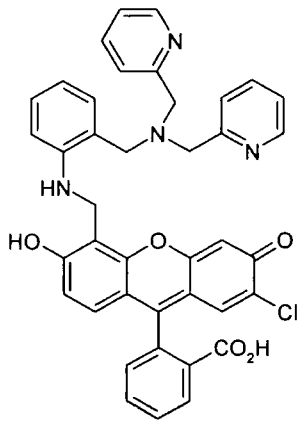

11, Zinpyr-4

The chelation of zinc (II) prevents the PET from the benzylic amine lone pair from quenching the fluorescein emission in each of these Zinpyr probes. However, the fluorescence enhancement on zinc coordination of **9** and **10** is greater at higher pH, due to protonation of the tertiary amines at physiological pH (apparent pK_a 8.3 (**9**), 9.4 (**10**)). This problem was addressed with the modified zinc binding moiety of **11**, which has a lower pK_a and so is less sensitive to protonation under physiological conditions. Although **11** is more sensitive to zinc (II) than the previous zinpyr sensors, it has the disadvantage that, unlike the others, it is not membrane permeant.[35] Zinpyr-1 has been applied to cells and was found to preferentially stain the Golgi apparatus and acidic cellular compartments.[10] However, this staining may be due to the acidic conditions within these compartments protonating the benzylic amine, preventing PET, rather than elevated concentrations of zinc (II) in these areas.

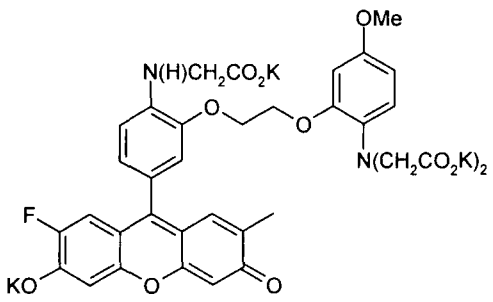

12 Fluo-Zin3

Fluoroscein appended acyclic amines have also been synthesised by Nagano *et al.*[36,37] and Gee and Kennedy.[38] **12** is tetra-anionic and therefore cell impermeant, although it has been used to show zinc (II) secretion from pancreatic cells.[38] It is sensitive to zinc (II) at nanomolar concentrations (K_d 15 nm) and fluorescence emission is not affected by pH over the physiological range (pH 6 - 9).

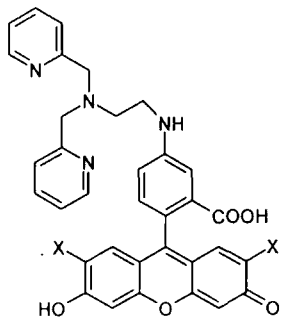

13 X = H, ZnAF-1
15 X = F, ZnAF-1F

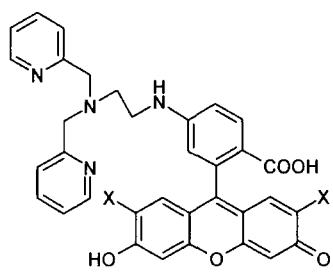

14 X = H, ZnAF-2
16 X = F, ZnAF-2F

The probes synthesised by Nangano and coworkers[36,37] use N,N,N',N'-tetra(2-picolyl)ethylenediamine (TPEN) to coordinate to zinc (II). The initial probes **13** and **14**, although showing an increase in fluorescence intensity in the presence of zinc (II), have the disadvantage of having a fluorescence intensity that is dependent on pH (pK_a 6.2). This was rectified with the development of **15** and **16** wherein the electron-withdrawing fluorine substituents on the fluorescein reduced the phenolic pK_a, resulting in a system with stable fluorescence under physiological conditions. This system has the added advantage of being able to distinguish between zinc (II) and cadmium (II). The increase in ionic radius of cadmium, compared with zinc, results in the cadmium ion being coordinated by the carboxylate rather than the benzylic nitrogen. PET can still occur so fluorescence is quenched when Cd (II) is bound. These probes are not cell permeant, but their diacetyl derivatives are more lipophilic and able to pass though cell membranes. Inside the cell they are cleaved by esterase enzymes and so are retained within the cell.

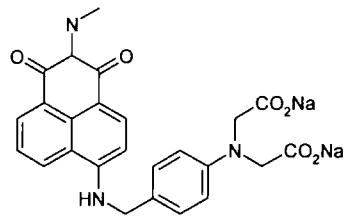

17

The water soluble naphthalimide derivative **17** is a zinc (II) chemosensor developed by Gunnlaugsson *et al.*[39] This molecule shows an increase in fluorescence intensity with increasing zinc (II) concentration at pH 7.4, due to the 1 : 1 binding of zinc (II) to the carboxylates of the iminodiacetate and the benzylic nitrogen. This results in a reduction of the ability of the nitrogen lone pair to quench the naphthalimide fluorescence via PET.

A ratiometric probe was also developed by Nagano *et al.*,[40] which employs an internal charge transfer (ICT) mechanism. A fluorophore containing an electron-donating group (e.g. amino) conjugated to an electron-withdrawing group undergoes ICT from the donor to the acceptor upon excitation by light. If the electron rich terminal interacts with a cation, a partial positive charge is

photogenerated adjacent to the cation, and that affects the absorption or excitation spectral wavelength of the fluorophore with an ICT excited state. Therefore, a cation-induced blue-shift is expected in the absorption or excitation spectra. Fluorescence emission spectra are less affected due to cation ejection during the lifetime of the excited state.

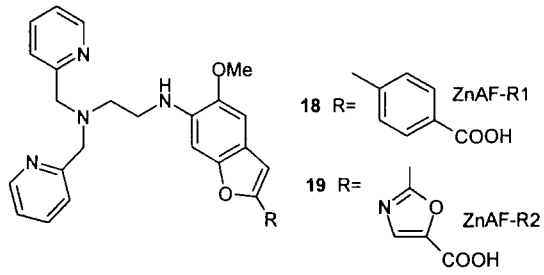

The probes **18** and **19** were generated using benzofuran derivatives as the fluorophore and TPEN derivatives as the chelators of zinc (II). Although the probe is not cell permeable, the ethyl ester derivative is. The study[40] has shown that the ethyl ester passes into cells, where it is transformed into **19** by the action of esterases in the cytoplasm. These probes have been shown to selectively bind zinc (II) in a nanomolar range (K_d 0.79 mM **18**, and K_d 2.8 nM **19**). The nature of this probe makes it possible to detect zinc (II) ratiometrically, thereby eliminating most, if not all of the possible variability due to differences in instrument efficiency and content of effective dye.

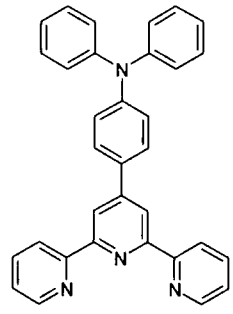

20

Another system which employs an ICT mechanism resulting in a large red-shift in emission, was recently developed by Goodall and Williams.[41] Terpyridine **20** is highly fluorescent and its emission is affected very distinctively and ratiometrically upon coordination to zinc (II) ions. The ligand binds zinc (II) in a 2L : 1Zn complex

(K_d 4.3 nM^{-2}). Water insolubility does not allow the use of this system in physiological studies.

1.4.3 Quinoline Based Zinc (II) Molecular Probes

The most widely used fluorescent probes for biological zinc (II) used at the present time are based on based on 8-*p*-toluenesulfonamidoquinoline systems.[6,7,9,42,43,44,45] There are three main compounds **21** TSQ, **22** zinquin and **23** 2-Me-TSQ, although many derivatives have been made.[46,47]

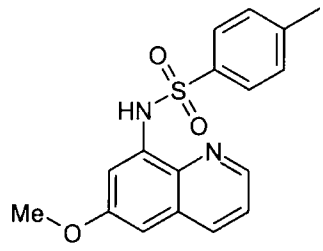

21
TSQ

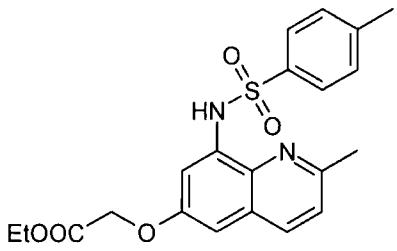

22
Zinquin

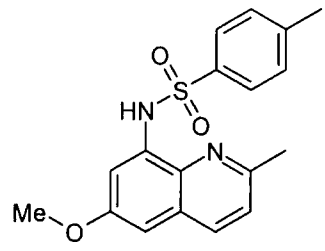

23
2-Me-TSQ

These 8-*p*-toluenesulfonamidoquinoline systems are cell permeable and have been utilised for the detection of zinc (II) in neurochemical and histochemical staining procedures.[12,15,42] They can detect zinc (II) at 100 pM to 10 nM concentrations. In all cell lines tested, these probes show zinc (II) pools localised in vesicle-like regions.

The ester functionality was introduced to TSQ to form Zinquin in a desire to improve cellular retention.[48] It was thought that cleavage of the ester by esterases in the cytoplasm to produce anionic zinquin acid would prevent the molecule from passing out through cell membranes. However, as the derivatives formed were membrane bound and uncharged,[49] it was concluded that the cleavable ester function was not necessary for cellular zinc staining.

In a study by O'Halloran,[49] 2-Me-TSQ, **23**, and a series of TSQ analogues were synthesised and their properties characterised. Crystallographic studies[49] showed that 2-Me-TSQ, **23**, forms a neutral [Zn(2-Me-TSQ)$_2$] complex with the coordination of the two nitrogen atoms from each ligand giving a highly distorted tetrahedral centre. The methyl group at the 2-position of the quinoline provides geometric

restrictions and along with the sulfonamide oxygens hinders the formation of both square planar and octahedral complexes, thus providing a steric selection for tetrahedral coordination that is not available in TSQ.

Addition of zinc results in a greater than 100-fold increase of the fluorescence intensity for each of these quinoline sulfonamides. This is independent of pH. The fluorescence of the uncoordinated ligand is quenched by the presence of the sulfonamide proton and the effects of the hydrogen bonding of the solvent molecules to the quinoline nitrogen. Only the coordination of the diamagnetic zinc (II) to the quinoline nitrogen can suppress this quenching.

However, despite the ability of these quinoline probes to image intracellular zinc (II),[50] mixed complexes can form with partially coordinated zinc (II) in cells, generating uncertainty in the measurement of free zinc (II). Usefulness is also limited by their poor water solubility and requirement for potentially damaging UV radiation. A longer wavelength of light is required to prevent damage to living tissues. These quinoline probes have a limited range of dissociation constants (sub-nanomolar), whereas the effective study of the numerous functions of Zn (II) requires many sensors with a wide array of binding affinities.

1.4.4 Protein and Peptide Sensors

In general, proteins do not show suitable fluorescence properties to be useful luminescent sensors. This problem has been overcome by covalently appending auxiliary fluorophores into the peptide sequence. The binding of zinc (II) causes a conformational change within the peptide, resulting in a change in the fluorophore environment, which in turn causes fluorescence to occur. The zinc binding affinity of protein and peptide probes can be optimised for selectivity and affinity, as well as water solubility, by variation of the overall amino acid sequence and the chelating residues.

Imperiali and coworkers[51,52] have used polypeptide architectures to make fluorescent chemosensors which are sensitive to zinc (II) in water at pH 7. Polypeptides have been prepared that include amino acid building blocks bearing

bipyridyl zinc (II) coordination sites, a cyanoanthracene chromophore, and an L-3,4-dimethoxy-DOPA donor unit which is able to quench the fluorophore fluorescence. This sensor works by undergoing a reversible metal induced conformation change in the presence of micromolar concentrations of zinc. This results in PET luminescence quenching. This has the disadvantage that fluorescence is quenched in the presence of zinc (II).

Zinc finger domains have been modified for use as sensitive and selective zinc receptors.[52,53] A dansylated β-aminoaniline amino acid derivative replaced a residue in the peptide sequence so the metal binding could be monitored. Metal binding caused the peptide to fold, resulting in the dansyl fluorophore becoming shielded from the solvent, leading to an increase in the fluorescence intensity. A linear and reversible response was observed with increasing zinc (II) levels between 0.1 and 1.0 μM.

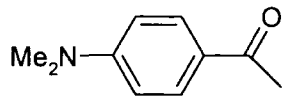

24
DMP

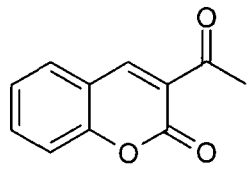

25
CMN

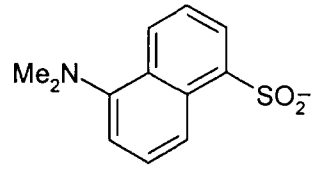

26
DNS

Fluorophores **24**, **25** and **26** have been incorporated into peptides based on zinc finger domains by Walkup and Imperiali.[52] Fluorescent peptidyl sensor for zinc (II) with high oxidative stability and high selectivity and binding affinity (K_d 7 pM - 65 nM) were obtained.

In order to be able to incorporate the fluorosensor onto a water-solvated resin to build a regenerable device, it was necessary to make the sensor smaller. Walkup and Imperiali[43,51] incorporated 8-hydroxyquinoline into a peptide seven residues in length to form Fmoc-2Oxn-OH **27** and Fmoc-5Oxn-OH **28**.

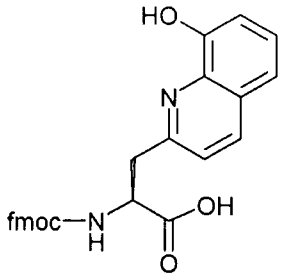

27

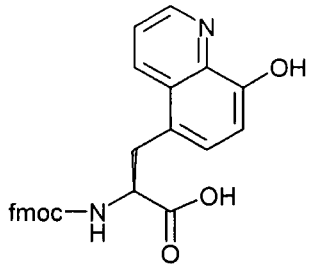

28

The sequence of peptides was designed to promote folding and cysteine was incorporated to favour zinc (II) selectivity. Under normal handling conditions, Fmoc-5Oxn-OH was found to undergo oxidation. Fmoc-2Oxn-OH formed 1 : 1 complexes with Zn (II) leading to a 170 fold increase in fluorescence with a sensitivity that was sub micromolar (< 250 nm). This has been further developed to contain a sulfonamido moiety.[54]

A ratiometric fluorescent probe for Zn (II) was reported by Godwin and Berg.[55] It has a receptor based on a zinc finger consensus peptide which binds zinc tightly (K_d = 5.7 pM, pH 7) and selectively, resulting in a change in flexibility and structure. The peptide was modified to covalently link two fluorescent moieties with fluorescein **29** as the donor and lissamine **30** as the acceptor.

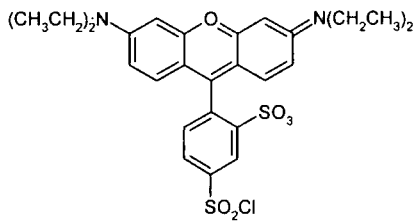

29

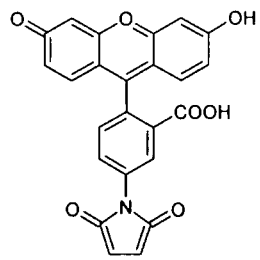

30

In the unfolded conformation, the fluorophores are relatively far apart and do not interact much. In the presence of zinc (II) ions, a 1 : 1 complex forms and folding is induced. This brings the fluorophores close together and intramolecular energy transfer occurs. The fluorescence spectrum that occurs has two maxima corresponding to the fluorescein (521 nm) and lissamine (592 nm) emission. The relative intensity of the peaks changes with increasing zinc (II) concentration, resulting in a ratiometric chemosensor. As the emission occurs in the visible region,

it is not covered by other cellular components, so it is a good candidate for *in vivo* studies.

A green fluorescent biosensor protein which binds zinc (II) (K_d = 50 μM) enhancing fluorescence intensity two-fold has been developed by Barondeau *et al.*[56] The green mutant protein binds zinc to a tridentate chromophore resembling half a porphyrin. Unfortunately it also binds Cu (II) (K_d = 24 μM) but this quenches fluorescence. Copper (II) binds with a different coordination geometry resulting in a change in the absorption spectrum: the maximum moves from 379 to 444 nm when bound.

The major disadvantage of using proteins and peptides as biological sensors is that peptides usually do not pass through cell membranes and are subject to degradation by peptidases. As a result, they must be introduced into the cell by microinjection. Introduction of the sensor molecules to cells by transinfection allows it to be targeted to specific tissues, organelles or cellular locations.

1.4.5 Zinc Sensor Problems

Many indicators for zinc (II) ions have been described in the recent literature.[57] However, very few of these have proved useful in addressing the problem of determining the biological function of zinc (II). This is for three main reasons.

1. Biological systems contain an abundance of magnesium (II) and calcium (II) ions which can potentially interfere with the probe molecules. Most other potentially interfering metal ions e.g. Cu (II), Ni (II), Co (II) are open shell and paramagnetic so quench fluorescence, and Cd (II) and Hg (II) are typically present at very low concentrations in biological systems.

2. Sensitivity: concentrations of free or weakly bound zinc (II) apparently range from the low millimolar within zinc secretory vesicles to femtomolar levels with in the cytoplasm of normal healthy resting cells. The probe must be able to bind to zinc (II) selectively and reversibly, therefore a selection of probes with different association constants would be useful to investigate the role of zinc (II) in different environments.

3. Quantification: it is difficult to relate fluorescence intensity to analyte concentrations. This can be overcome by the development of ratiometric indicators, where the ratio of intensities at two different excitation or emission wavelengths is related to the analyte concentration.

There is still much scope for improvement in probes for the detecting biological zinc (II) species. Responsive lanthanide systems are a current area of interest.

1.5 Emissive Lanthanide Complexes

The world of chemical sensors is currently dominated by small fluorescent organic molecules but highly emissive lanthanide complexes are becoming more common and offer many advantages, including a more extensive excited state chemistry. In general, complexes have all the excited state levels associated with organic molecules along with the dd and ff transitions of metals. Analyte binding can cause a direct effect on the luminescence i.e. quenching or triggering. Alternatively, an alteration in the emission or excitation wavelength maxima may result.[26]

1.5.1 Lanthanides

Lanthanides have very different characteristics to transition metals because the 4f orbitals are well shielded from external fields by $5s^2$ and $5p^6$ shells. As a result the f orbitals interact weakly with ligand orbitals.[18] This results in ligand field splittings being small (typically 100 cm^{-1}). The forbidden nature of f-f transitions (Laporte or parity forbidden) means that absorption coefficients are very low and typically < 1 $dm^3mol^{-1}cm^{-1}$. The wavelengths of *ff* transition bands are nearly independent of coordination environment resulting in fixed emission wavelengths: the emission bands are very sharp and narrow even in solution. Vibrations of the ligands and accompanying changes in M-L distances have very little effect on the energy levels of the excited states.[70]

1.5.2 Lanthanide Luminescence

Many lanthanide (III) ions luminesce in solution including Sm(III), Eu(III), Gd(III), Tb(III) and Dy(III). Absorption of light promotes the lanthanide (III) ion to an

excited state and luminescence occurs when the ion loses its energy and returns to the ground state.[58]

Currently most research involves Eu (III) and Tb (III) as they have relatively large energy gaps and low rates of radiationless decay. Their excited energy levels are not too high in energy and so are relatively easy to populate, and they emit strongly in the visible region of the spectrum.[26]

1.5.3 Advantages of Lanthanides Complexes

Lanthanide complexes have many advantages over conventional small fluorescent organic molecules as chemical sensors. These include: [26,58,70]

- **Very large Stokes shifts**. The wavelength of emission is much greater than the excitation wavelength, typically 250 - 350 nm (compared to 28 nm for fluorescein). This allows the elimination of background fluorescence from cellular components, such as amino acids, because the lanthanide luminescence occurs where fluorescence from biological samples is minimal. These large Stokes shifts also mean that concentration dependent self-absorption problems do not arise.

- **Long lived luminescence.** The spin forbidden nature of lanthanide transitions leads to long luminescent lifetimes, typically 0.1 - 10 ms in the case of europium and terbium (compared to 1 -100 ns for organics). This allows the use of time resolved detection systems to discriminate against background fluorescence. A pulse excitation light source can be used to irradiate a sample and the long lived luminescence is monitored after suitable delay

- **Emission spectra consist of narrow lines characteristic of the lanthanide ions.** Luminescence can be monitored by observing specific Ln^{3+} emission lines. These lines shift no more than ± 2 nm with changing conditions.

1.5.4 Direct and Sensitised Excitation Pathways

There are various problems to be overcome with lanthanide (III) luminescence, including difficulties in populating the excited states. Absorption bands of lanthanide (III) ions are very weak because the transitions of interest involve the same f^n configuration and electronic dipole. Transitions between such states are parity (Laporte) forbidden, leading to very low extinction coefficients, typically 0.1 $mol^{-1}dm^3cm^{-1}$.[70] The excited states can be achieved either by direct or sensitised excitation.

1.5.4.1 Direct Excitation

Lanthanide (III) ions have low molar absorption coefficients. As a result the excited states are not readily populated by direct absorption of light unless a very intense source is used.[26] One solution is to use laser light to match the energy gap, another is sensitised emission.

1.5.4.2 Use of Sensitising Chromophores

Sensitised excitation has the advantage that lower intensities of light can be used. For energy transfer to occur efficiently, the distance between the chromophore and lanthanide ion must be small. This can be achieved by incorporating the chromophore into the same ligand as the lanthanide ion. The chromophore absorbs light energy and transfers it to the lanthanide excited state.[26,70] This is illustrated by the antenna effect, Figure 1.3.

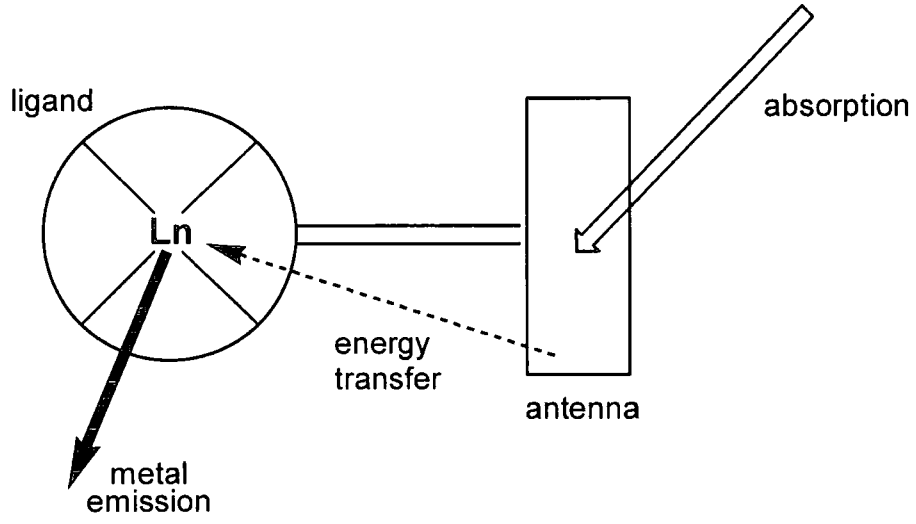

Figure 1.3 The Antenna Effect[26]

For energy transfer to occur efficiently, the energy of the excited state of the chromophore should exceed that of the emissive state of the lanthanide, as illustrated in the Jablonski Diagram, Figure 1.4. Efficient energy transfer requires that resonance of the emission band of the excited species (**S1**) should overlap the absorption spectrum of the metal. However, if the energy gap is too small (<1700 cm^{-1}), back energy transfer can occur, resulting in a decrease in lifetime and emission intensity. The donor excited state must be long-lived enough for energy transfer to compete effectively with other deactivation pathways. Singlet states are usually too short-lived for energy transfer to occur so triplet states dominate as the donor. If the energy gap between donor and acceptor is too small, it can lead to thermally activated back energy transfer from the metal to the chromophore, which competes with emission, leading to reduced lifetimes and quantum yields.

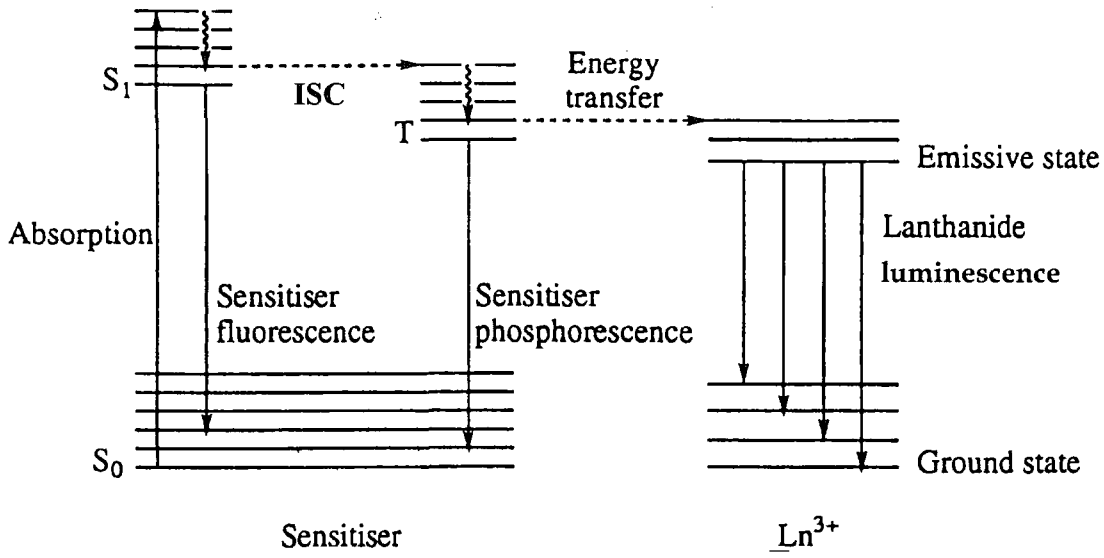

Figure 1.4 Jablonski Diagram for Sensitised Emission.[59]

1.5.4.3 Lanthanide Emission

Once the lanthanide (III) has been excited there are three excited states that may be perturbed leading to emission (Figure 1.5). These are the singlet excited state of the sensitising chromophore, the intermediate triplet excited state of the chromophore and the excited state of the lanthanide itself.[58]

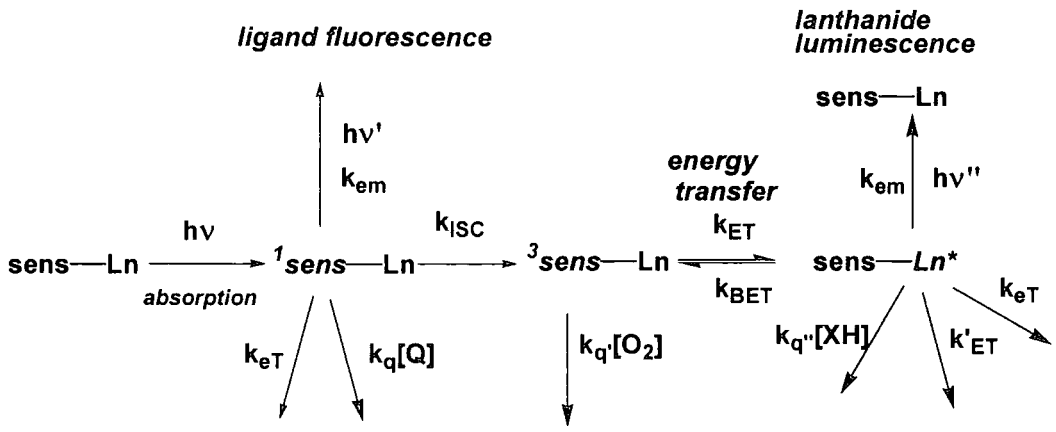

Figure 1.5 Excited states that may be perturbed prior to lanthanide emission.[58]

1.5.5 Quenching Effects of Water on Lanthanide Luminscence

Lanthanide (III) emissive states can be deactivated, or quenched, by vibrational energy transfer to the high energy O-H stretching vibrations of coordinated or closely diffusing water molecules. This process is strongly dependent on the distance between the lanthanide and the OH oscillator. Water coordinated directly to the lanthanide centre has a much larger quenching effect. This reduces both the lifetime and the emission intensity and quantum yields. Lanthanide complexes must therefore be made to exclude water molecules.[60]

The stretching vibration energy of O-D is much less than that of O-H. This results in the lifetimes and luminescence intensity recorded in D_2O being much greater than that in H_2O,[61] except where q = 0.

1.5.6 Structure and Stability of Lanthanide Complexes

Lanthanide (III) aqua ions are very toxic *in vivo*. As potential applications are concerned with biological samples and low concentrations, it is important that the lanthanide ion is chelated within a stable complex which does not dissociate at low concentrations in water over an appropriate pH range.[58]

1.5.7 Lanthanide Complexing Agents

Lanthanide ions are most commonly 8 or 9 coordinate and form stable complexes with ligands with donor atoms which satisfy the demands of hard polarising ions.[62]

Lanthanide (III) ions favour polydentate ligands with nitrogen and/or oxygen coordination. Suitable ligands include polyaminocarboxylate ligands based on DOTA (1,4,7,10-tetraazacyclododecane-1,4,7,10-tetraacetic acid) and DTPA (diethylenetriaminepentaacetic acid). These satisfy all Ln (III) ligand requirements and have been derivatised with a variety of sensitising groups in close proximity of the lanthanide ion. They form well defined 1 : 1 complexes with high formation constants and are kinetically inert to proton and cation mediated dissociation pathways. They are also water soluble and exclude all but one water molecule from the metal centre.[26,70]

1.6 Responsive Lanthanide Complexes

Sensitised emission offers particular scope for controlled modulation of lanthanide luminescence. The excited state properties of the antenna chromophore can be designed to be perturbed in response to interaction with a specific analyte. This in turn can result in changes in the emission intensities and lifetimes. Alternatively, water bound to the lanthanide centre can be reversibly displaced leading to an increase in the intensity and lifetime of the emission.[26,58]

1.6.1 PET Dependent Luminescence

The first excited singlet state of aromatic fluorophores may be quenched by PET from oxidisable groups such as amines (Figure 1.2). Inhibition of this process by amine protonation or metal ion binding may lead to large increases in fluorescence intensity. If a fluorophore is being used to sensitise a lanthanide then the effect can be mirrored by a corresponding change in Ln (III) emission intensity.[26]

1.6.2 Water Displacement from Lanthanide Centre

Excited Ln (III) ions are subject to quenching by vibrational energy transfer (e.g. by H_2O). If a species can reversibly bind directly to the Ln^{3+} centre, either intermolecularly or intramolecularly, displacing these water molecules, then the emission intensity and lifetime can increase markedly. Also, the spectral form will change, allowing ratiometric analysis.[63,64,65]

Responsive lanthanide probes containing europium (III) or terbium (III) are useful in luminescence imaging. If the luminescent lanthanide ion is replaced with gadolinium (III), it is possible to generate a probe useful in magnetic resonance imaging.

1.7 Magnetic Resonance Imaging

Magnetic resonance imaging (MRI) is a powerful medical diagnostic technique.[66,67,68,69] It is effectively a sophisticated NMR experiment which visualises water molecules within the human body. It allows a highly detailed, three dimensional image of the body to be generated in a non-invasive manner.

MRI can be used to build up an image because the water protons within the body are in different chemical environments and concentrations. The image obtained can be made to have better resolution by use of a contrast agent. Contrast agents are currently used in over 30% of MRI investigations,[68] with this percentage predicted to increase further with the development of more effective and target specific contrast agents.

The intensity of the MRI signal obtained is dependent upon the longitudinal (T_1) and the transverse (T_2) water proton relaxation times. Increasing the relaxation rates of these water protons usually results in an increase in the intensity of the signals obtained.

Contrast agents use a paramagnetic centre to increase the relaxation rate of water protons. When water is located close to a highly paramagnetic species such as Gd^{3+} or Mn^{2+}, a substantial increase in the rate of relaxation of the water proton is observed. This is caused by a dipolar interaction between the electronic magnetic moment of the paramagnetic ion and the smaller magnetic moments of the proximate water molecules.[70] Gadolinium (III) is one of the best paramagnetic ions for MRI as it has seven unpaired f-electrons, a large magnetic moment (S=7/2) and a relatively slow electronic relaxation rate.

The efficacy of a contrast agent is described by its relaxivity (r_1). Relaxivity is the enhancement of the total paramagnetic relaxation rate of the free water protons (R_{1p}) per unit concentration of the paramagnetic species (units are $mM^{-1}s^{-1}$), equation (1.1)

$$r_1 = \frac{R_{1p}}{[Gd]} \tag{1.1}$$

The overall relaxivity of water protons R^{obs} is described by equation (1.2), where R_{1d} is the diamagnetic contribution to the rate of water relaxation, i.e. in the absence of any paramagnetic solute, and R_{1p} is the paramagnetic contribution to the measured relaxation rate.

$$R^{obs} = R_{1d} + R_{1p} \tag{1.2}$$

The magnetic field generated around the paramagnetic centre decreases rapidly with increasing distance from the metal centre, so interactions that bring water protons into the proximity of the paramagnetic centre are important in the transfer of the paramagnetic effect to the bulk water. For Gd (III) complexes this interaction includes contributions from the water molecules bound in the first coordination sphere of the metal ion (inner sphere) R_{1p}^{IS}, in the second coordination sphere (second sphere) R_{1p}^{SS} and also from those which diffuse in proximity to the paramagnetic complex (outer-sphere) R_{1p}^{OS}, (Figure 1.6).

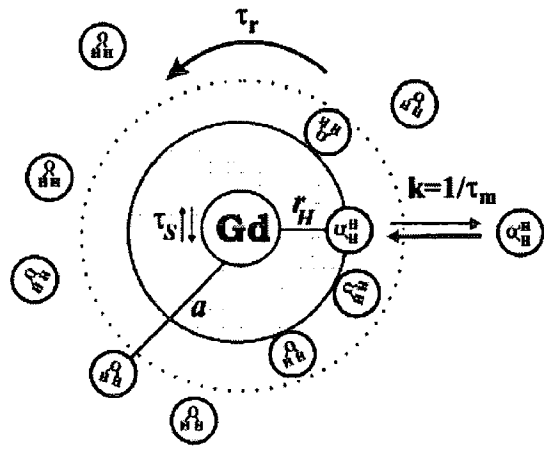

Figure 1.6 Schematic representation of the three idealised hydration layers around a Gd^{3+} complex and the most relevant parameters of paramagnetic relaxation.[71]

The paramagnetic contribution is made up from these three terms, equation (1.3).

$$R_{1p} = R_{1p}^{IS} + R_{1p}^{OS} + R_{1p}^{SS} \tag{1.3}$$

1.7.1 Inner Sphere Relaxation

The inner-sphere contribution, R_{1p}^{IS}, originates from dipolar interactions between the paramagnetic ion and the proton nuclei of directly bound water molecules. The paramagnetic effect is then transferred to the bulk through chemical exchange of the coordinated water with the bulk.

$$R_{1p}^{IS} = \frac{Cq}{55.6} \cdot \frac{1}{T_{1M} + \tau_M} \tag{1.4}$$

The inner sphere contribution is largest and provides the area of greatest control for change in relaxivity, equation (1.4), where C = molar concentration of the paramagnetic compound, q = number of bound water molecules, T_{1M} = longitudinal relaxation time of the bound water protons and τ_m = mean residence lifetime in the coordination site. Changing these parameters can lead to more efficient contrast agents.[68]

The parameters determining T_{1M}, the longitudinal relaxation time are expressed in Solomon, Bloembergen and Morgan theory,[72,73,74] through equations (1.5) and (1.6)

$$T_{1M} = \frac{2}{15} \cdot \frac{\gamma_H^{\,2} g^2 \beta^2 S(S+1)}{r6} \times \left[\frac{7\tau_c}{1+\omega_S^{\,2}\tau_C^{\,2}} + \frac{3\tau_C}{1+\omega_H^{\,2}\tau_C^{\,2}} \right] \tag{1.5}$$

$$\frac{1}{\tau_C} = \frac{1}{\tau_R} + \frac{1}{\tau_S} + \frac{1}{\tau_M} \tag{1.6}$$

γ_H is the gyromagnetic ratio of proton nuclei; g is the electronic Landé factor; β is the Bohr magneton; S is the electronic spin quantum number; r, the distance of the inner sphere water proton from the paramagnetic metal ion; τ_C, the effective rotational correlation time; τ_R, the molecular reorientational correlation time; τ_S, the electronic relation time and ω_S and ω_H are the Larmor frequencies for the electron and proton respectively.

When proton exchange is very slow, $\tau_M \geq T_{1M}$, the rate of water exchange will be the determining factor for relaxivity. However, if the exchange rate is fast enough that $T_{1M} \geq \tau_M$, then the observed relaxivity will be determined by the relaxation rate of the coordinated protons, which in turn is dependent on the rate of proton exchange, rotation rate and electronic relaxation. In each of these limiting cases, the number of bound water molecules (q) and the Gd-H distance (r) are variables whose influence can be easily seen. Influences of parameters such as rotational correlation time and electronic relaxation are less predictable due to their dependence on magnetic field.

1.7.2 Second Sphere and Outer Sphere Relaxation

A significant proportion of the relaxation rate is a consequence of second and outer sphere relaxation. Water molecules that are not bound directly in the first coordination sphere may remain in the proximity of the paramagnetic ion for a relatively long time due to hydrogen bond bridges with the ligand. These water molecules give rise to the second sphere contribution and can play a significant role in the overall paramagnetic contribution to the water proton relaxation rate. Due to the difficulty in separating outer and second sphere effects, the second sphere contribution is rarely considered individually and is reported as part of the overall outer sphere contribution.

The outer sphere relaxivity stems from modulation of dipolar proton interactions brought about by loosely diffusing water molecules from the bulk solvent and the paramagnetic centre. It is governed by a set of equations developed by Freed[75] and depends on the electronic relaxation time of the metal ion, the distance of closest approach of the solvent and solute (a) and the sum of solvent and solute diffusion coefficients (D). C^{os} is a constant ($5.8 \times 10^{-13}\ s^{-2}M^{-1}$) and the dependence on the electronic relaxation times is expressed in the non-Lorentzian spectral density functions $J(\omega_i)$, equation (1.7).

$$R_{ip}^{OS} = C^{os}\left(\frac{1}{aD}\right)[7J(\omega_S) + 3J(\omega_H)] \qquad (1.7)$$

1.8 Contrast Agents for MRI

Gadolinium (III) is rather toxic (LD_{50} ~ 0.1 mmol kg^{-1} in rats),[19] so must be administered in a form that is highly stable *in vivo* especially as the administered dose is high (typically 0.1 mmol kg^{-1}). Clinically approved contrasts agents are thermodynamically and kinetically stable, highly water soluble complexes of gadolinium (III) and based on polyaminocarboxylate systems, Figure 1.7.

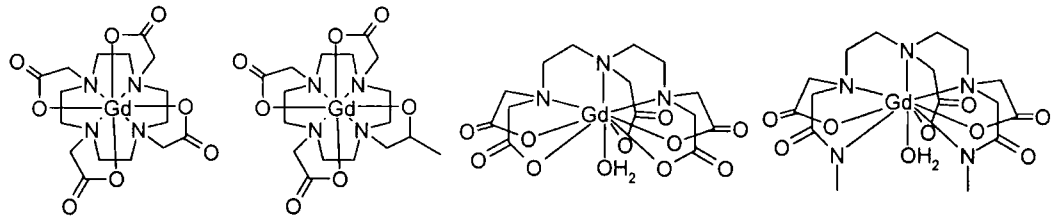

Figure 1.7 Gadolinium complexes which are currently in clinical use for MRI.

$Gd(DOTA)^-$ (DOTAREM) **31**, and $Gd(DTPA)^{2-}$ (MAGNEVIST) **33**, were the first complexes put into clinical use, Gd(DTPA-BMA) (OMNISCAN) **34** and GdHPDO3A (PROHANCE) **32** were introduced later; as they are neutral complexes they have a reduced osmotic potential and are used for applications that require a higher dose of contrast agent. These are all examples of perfusion agents which distribute non-specifically through plasma and interstitial spaces and are excreted rapidly.

Research is ongoing to develop the next generation of contrast agents which require a reduced administered dose. This can be achieved through 'smart' and high relaxivity contrast agents.

1.8.1 'Smart' Contrast Agents

'Smart' or responsive contrast agents have a relaxivity which is modulated by a change in the physiological environment such as pH,[63,76,77,78,79,80,81] metal ion concentration,[82,83,84] partial pressure of oxygen[85,86,87] or enzyme activity.[88,89,90] Changes in the environment result in a change in one or more of the parameters outlined in equation (1.5).

1.8.2 High Relaxivity Contrast Agents

The relaxivity of a contrast agent can be enhanced maximally by optimising each of the inner, second and outer sphere contributions.

Inner sphere relaxation is directly proportional to the number of bound water molecules (q), therefore increasing the number of bound water molecules will increase the relaxivity. However, the gadolinium (III) ion is toxic and must be chelated in a thermodynamically and kinetically stable complex. Most attempts to make contrast agents where q = 2 have failed. This is usually because the inner sphere water molecules are displaced by anions[64,91] or protein carboxylate side chains present within serum.[72]

Another problem found with heptadentate ligands was that the derived complex was not sufficiently stable with respect to cation-mediated or acid dissociation to be safe for *in vivo* use. Furthermore τ_M, the water exchange lifetime tended to be too long, limiting the overall relaxivity.[92]

One example of a q = 2 complex, **35**, GdaDO3A, was recently synthesised by Messeri *et al.*[93] The anionic side chains inhibit the interaction with proteins and anions. A high relaxivity (12.3 $mM^{-1}s^{-1}$, (20 MHz, 298 K)), is reported in the presence of serum.

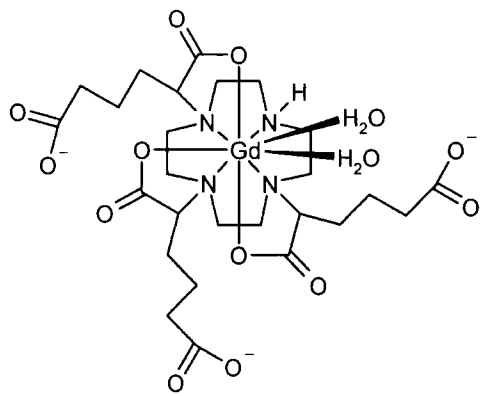

35
GdaDO3A

The longitudinal relaxation time of bound water molecules T_{1M} is dominated by the molecular reorientation (rotational correlation) time, τ_R, at 20 - 60 MHz (0.5 - 1.5 T),

the magnetic field strength used in MRI scanners. The more slowly the Gd (III) complex tumbles, the longer the reorientational correlation time, τ_R, the higher the relaxivity. Various approaches have been used to lengthen τ_R. Attaching the Gd (III) complex to a slowly tumbling macromolecule such as a polysaccharide,[94] protein[95] or dendrimer[96] has been used to reduce the tumbling rate of the Gd (III) complex. Complexes with hydrophobic groups form host-guest complexes with human serum albumin (HSA): this large protein tumbles slowly in solution with the small Gd (III) chelate compartmentalised within, also tumbling slowly. Significant increases in values of τ_R have been seen for **36**, MS-325,[97] τ_R 10.1 ns, r_1 42.0 $mM^{-1}s^{-1}$ when fully bound to HSA, compared to τ_R 115 ps, r_1 6.6 $mM^{-1}s^{-1}$ when free at 20 MHz, 310 K.

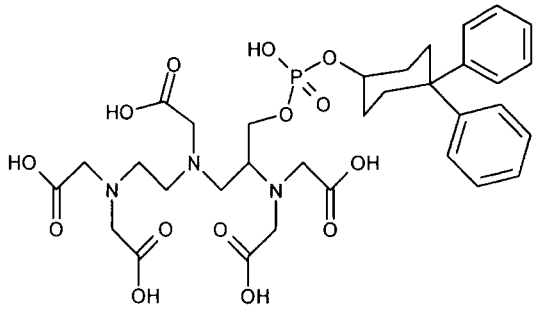

36
MS-325

1.9 Responsive Lanthanide Metal (II) Signalling Systems

Reany *et al.*[98,99] synthesised pentadentate europium (III) and terbium (III) complexes **37** and **38** to signal changes in zinc (II) concentration.

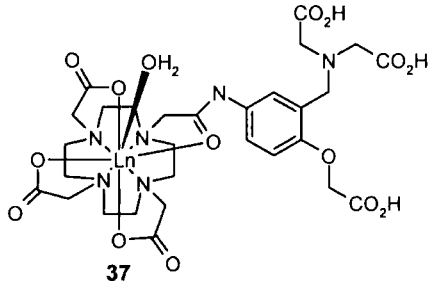

37

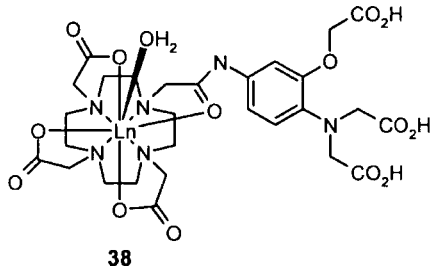

38

These complexes show both a change in the form of the ligand emission and absorption spectra and also an increase in the intensity of delayed lanthanide emission with zinc (II) binding. The coordination of zinc to the pentadentate

sensitising group inhibits PET from the benzylic nitrogen to the aryl group. This is mirrored in enhancement of the lanthanide emission intensities. Zinc (II) sensitivity and selectivity is observed with **38**, but its short excitation wavelength renders it unsuitable for cellular analyses. Ideally the system would exhibit a change in the emission spectrum of lifetime of the lanthanide reporter group. This would have to involve either a change in the rate of quenching of the lanthanide excited state or a change in the lanthanide coordination environment.

Nagano and coworkers have made a MRI contrast agent[84] and a luminescent lanthanide probe[100] **39** which responds to changes in zinc (II) concentration.

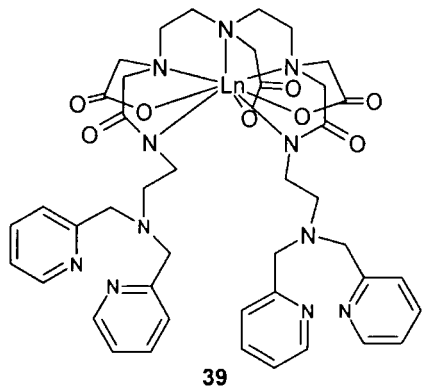

39

The probe is a Ln(III) DTPA complex with an TPEN moiety to coordinate with zinc (II).[84] This gadolinium complex shows a reduction in relaxivity upon coordination with zinc (II), the maximum decrease in relaxivity corresponds to the presence of one equivalent of zinc (II) (r_{1p} 6.06 $mM^{-1}s^{-1}$, 25°C, 300 MHz, pH 8). The presence of more than one equivalent results in an increase in the relaxivity until it returns to its original value (r_{1p} 3.98 $mM^{-1}s^{-1}$, 25°C, 300 MHz, pH 8) in the presence of two zinc equivalents. This complex does not complex to zinc (II) in a desirable range for biological systems and even if it did, then it would be difficult to apply it in a 1 : 1 ratio to observe the maximum decrease in relaxivity. This relaxivity change can be ascribed to the binding of Zn (II) causing a change in the second sphere hydration state[62] rather than the change in conformation and gadolinium hydration state, as suggested by Nagano.[84]

The europium and terbium (III) analogues of this complex[100] show an linear increase in emission intensity with increasing zinc (II) concentrations up to a 1 : 1 molar ratio of the lanthanide complex to Zn (II) (apparent K_d 2.6 nM), the intensity remained at a plateau upon the addition of more zinc (II) ions. This has been ascribed to a conformational change resulting in better energy transfer between the pyridyl moieties and the lanthanide centre. However, this is not in agreement with the decrease, followed by increase in relaxivity observed in the gadolinium analogue.

Meade *et al.*[82,83] have developed a calcium responsive lanthanide complex. DOPTA-Gd, **40**. This displays a relaxivity increase of 77% from 3.26 $mM^{-1}s^{-1}$ to 5.76 $mM^{-1}s^{-1}$ (25°C, 500 MHz) following addition of micromolar concentrations of calcium (II), K_d 0.96 μM. The change in relaxivity was seen to be most striking between the levels of 0.1 and 10 μM.[83] As cellular calcium (II) is present in micromolar concentrations,[1] this sensor will only be responsive when internalised inside a cell. A much higher K_d value is required.

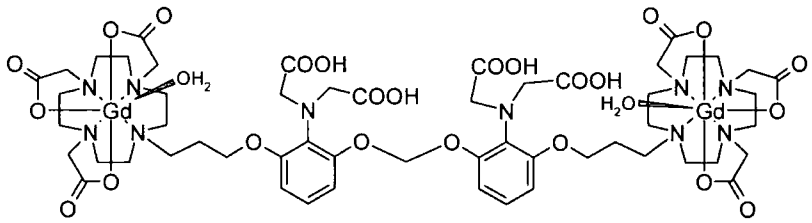

40
DOPTA-Gd

The terbium analogue shows[82] that an increase in calcium concentration leads to an increase in the hydration state of the lanthanide centre. In the absence of calcium, one water molecule may be present at a distance of about 3.3 - 3.4 Å. This could indicate the presence of one water proton hydrogen bonded to a carboxylate of the macrocycle. Alternatively, two second sphere water molecules could be coordinated at a distance of about 3.8 Å from the metal ion, or a larger number of water molecules at larger distance.[83]

After Ca^{2+} is bound to DOPTA-Gd **40**, the molecule undergoes a substantial conformational change that opens up the hydrophilic face of tetraazacyclododecane

macrocycle. This change dramatically increases the accessibility of chelated Gd (III) ion to bulk solvent.[82]

pH responsive lanthanide complexes **41**, **42** and **43** (Figure 1.8) have been synthesised by Lowe *et al.* [63,77]

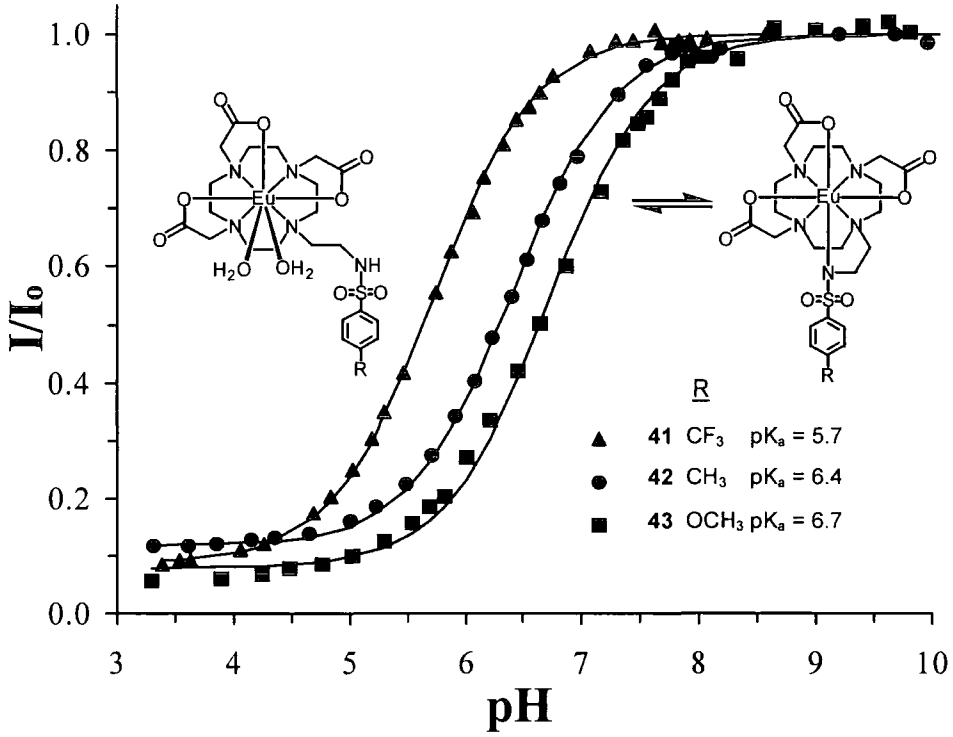

Figure 1.8 pH Responsive lanthanide probe.[63]

These sulfonamide appended DO3A complexes[63] exhibit a reversible change in hydration state over a defined pH range. The pH range was varied by using different substituents at the para position of the benzyl sulfonamide. At low pH, the sulfonamide is protonated and water binds to the lanthanide centre resulting in a luminescence inactive species. Increasing pH causes the deprotonation of the sulfonamide nitrogen which then binds to the lanthanide centre preventing water from binding. This results in a decrease in observed relaxivity and an increase in luminescence. The converse effect was seen with the gadolinium analogue; at low pH, water can bind to the gadolinium centre so a high relaxivity is observed. An increase in pH causes deprotonation of the sulfonamide, and the anionic nitrogen

binds to the gadolinium preventing water from binding, q = 0. This results in a significant decrease in observed relaxivity.

1.10 Scope of Work

Following the work of Lowe,[63,77] the aim of this study was to synthesise and characterise ligands that selectively complex to zinc (II) at physiological pH, for possible application in luminescence sensors and as contrast agents in MRI.

The initial task was to develop a simple pyridyl sulfonamide ligand which would selectively complex zinc (II) in a biological concentration and pH range. This ligand could then be appended to a macrocyclic lanthanide system which would exhibit a change in hydration state, and thereby lead to a switching on and off of luminescence and relaxivity, with changing zinc (II) concentration.

In order to make this system work for clinical MRI applications, it would be necessary to have an appropriate association constant, such that the Zn[LnL] complex would form even though the complex (after introduction to the body by injection) would be present at very low concentrations.

As zinc (II) is of a higher concentration in the hippocampus of the brain and central nervous system, a long-term aim would be to seek a zinc specific contrast agent that may be of use in brain imaging, providing it can cross the blood brain barrier.

Chapter 2

Simple Pyridyl-sulfonamide Ligands

2 Simple Pyridyl-sulfonamide Ligands

2.1 Introduction

Initial work was directed towards the synthesis and characterisation of some simple pyridyl-sulfonamide ligands $\mathbf{L^1}$, $\mathbf{L^2}$, $\mathbf{L^3}$, and $\mathbf{L^4}$, to examine their binding to zinc (II) and to compare the structure and solution behaviour of the zinc complexes formed with those of neighbouring transition metals, namely Co (II), Ni (II) and Cu (II).

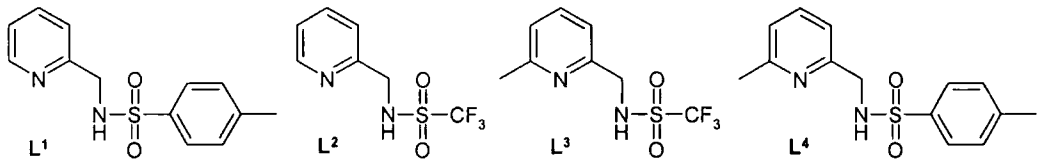

A model ligand system was sought from this series, capable of forming a well-defined neutral complex with zinc (II) under ambient pH conditions, when the zinc (II) concentration is within the range 100 - 0.1 nm. The most appropriate ligand was then to be incorporated into a related system suitable for MRI and luminescent applications.

2.1.1 Electronic Control

The electron donating ability of the sulfonyl nitrogen atom was varied by altering the sulfonamide substituent from tolyl to trifluoromethyl. A neutral secondary sulfonamide is a weak acid that may be deprotonated in basic media to generate an anionic conjugate base. The protonation constant characterising this equilibrium (pK_a) is primarily determined by the nature of the sulfur substitutuent. For example, arylsulfonamides typically have pK_a values around 12,[101] while $CF_3SO_2NH_2$ has a pK_a of 7.[102] Thus the donor ability of the sulfonamide N may be controlled by variation of the sulfur substituent.

2.1.2 Steric Control

An α-methyl substitutent was introduced to sterically inhibit the formation of square planar ML_2 complexes. The simple ligand $\mathbf{L^1}$ may act as a mono-anionic bidentate donor through chelation of each nitrogen. In $\mathbf{ML_2}$ complexes, limiting square planar or tetrahedral geometries may be adopted at the metal centre whose

relative stability can be varied by introduction of a substituent at the 6-position of the pyridyl ring e.g. L^3. The more bulky this substituent, the more a tetrahedral geometry is expected to be favoured. Such an analysis is well established in coordination chemistry. For example, whilst 2,2-bipyridine forms well-defined square planar complexes with Cu(II), introduction of an α-methyl substituent in each ring destabilises this coordination mode and favours formation of a tetrahedral complex - as revealed in the stabilisation of the Cu(I) complex with the ligand neocuproin.[103] An α-methyl substituent was introduced into the fluorescent zinc probe 'TSQ'[49] to inhibit the formation of square planar and octahedral complexes and thus disfavour the binding of the ligand to Cu (II).

2.2 Synthesis

2.2.1 Ligand synthesis

The sulfonamide ligands L^1 and L^2 were prepared by the reaction of 2-(amino-methyl)pyridine with toluenesulfonyl chloride or trifluoromethanesulfonyl chloride, in dry pyridine (Scheme **2.1**).

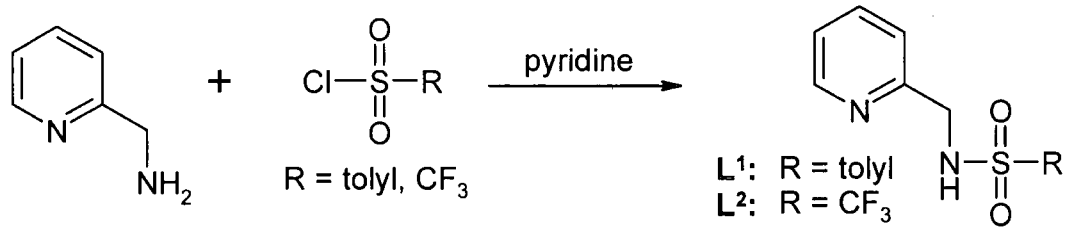

Scheme 2.1 Synthesis of ligands L^1 and L^2

The related 6-Me derivatives L^3 and L^4 were prepared from 6-methyl-2-pyridinecarboxaldehyde. Reaction with hydroxylamine hydrochloride following the method of Fuentes and Paudler,[104] yielded the imine **44.** Hydrogenation of the imine using a palladium on carbon catalyst gave the amine **45**. Initially, an attempt was made to synthesise the amine **45** using a zinc/acetic acid reduction.[105] This route was abandoned as it gave rise to a mixture of the desired amine **45** and an hydroxylamine. Ligands L^3 and L^4 were then prepared by sulfonylation of the

amine **45** with toluenesulfonyl chloride and trifluoromethanesulfonyl chloride in 53% and 30% yields respectively (Scheme 2.2).

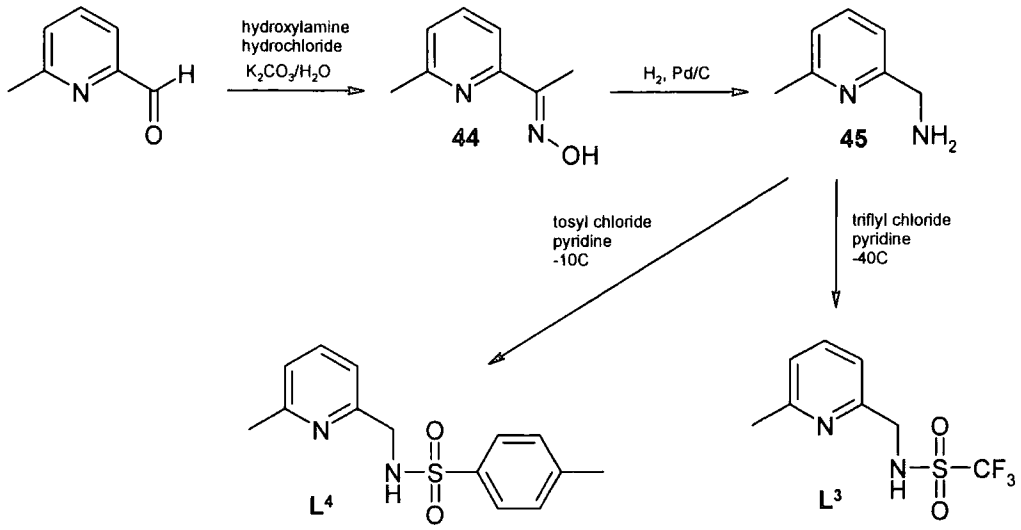

Scheme 2.2 Synthesis of ligands L^3 and L^4

2.2.2 Metal Complex Synthesis

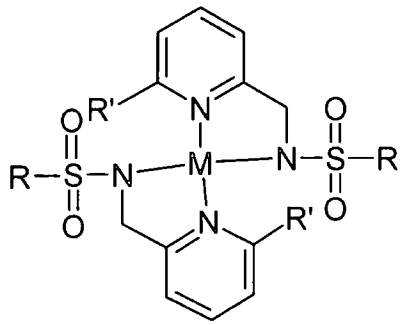

L^1 R = *p*-MePh, R' = H
L^2 R = CF_3, R' = H
L^3 R = CF_3, R' = Me
L^4 R = p-MePh, R' = Me
M = Co^{2+}, Ni^{2+}, Cu^{2+} or Zn^{2+}

The ML_2 complexes were formed by mixing two molar equivalents of ligand with one of the metal acetate salt in boiling methanol. In the case of $[Ni(L^1)_2]$ and $[Co(L^1)_2]$, it was found to be necessary to form the potassium salt of the ligand prior to complex formation. On cooling, crystals of the neutral complex were deposited, usually over the course of several days. It was then possible to recrystallise each of the complexes from hot methanol or ethanol.

Attempts were made to prepare the corresponding iron (II) and manganese (II) complexes of L^1 using this procedure but this was not successful; only manganese (IV) oxide and iron (III) hydroxide were obtained.

2.3 X-ray Analysis

Single crystal X-ray diffraction experiments were carried out by Dr Horst Puschmann, using SMART CCD area detectors and graphite-monochromated MoK_α radiation. The structures were solved by direct methods and refined against F^2 of all data, using SHELXTL programs.[106]

Each of the sixteen neutral complexes had its structure determined by X-ray crystallography at 100 - 120 K. Table 2.1 shows views of each of the crystal structures and Table 2.2 details the unit cell and crystallographic information.

Ligand	Co	Ni	Cu	Zn
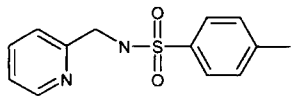 L^1	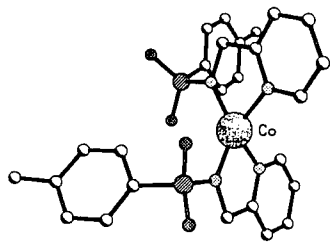	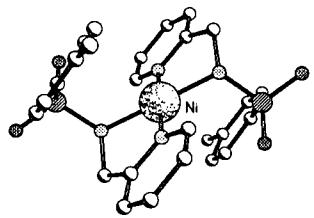	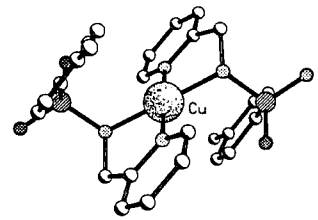	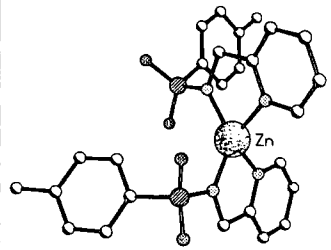
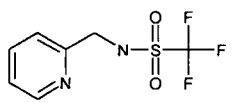 L^2	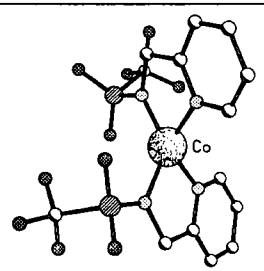	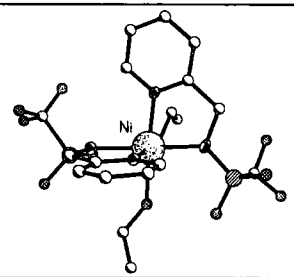	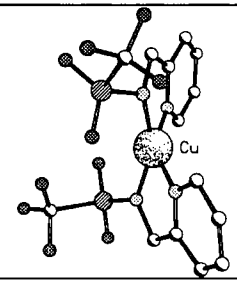	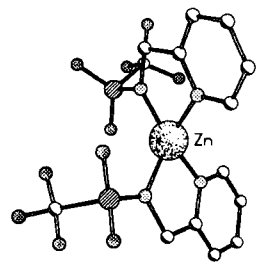
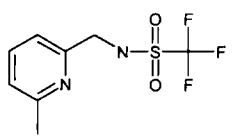 L^3	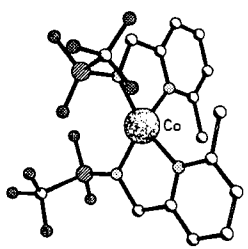	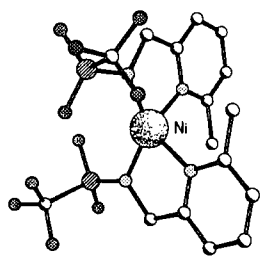	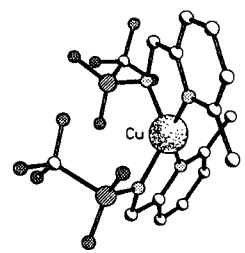	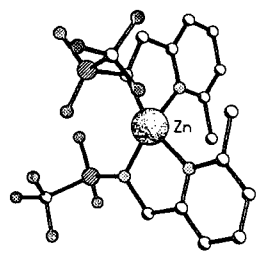
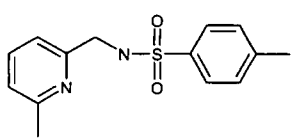 L^4	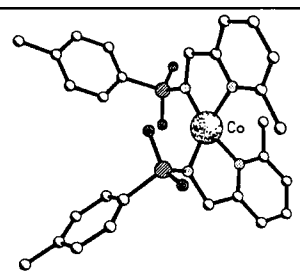	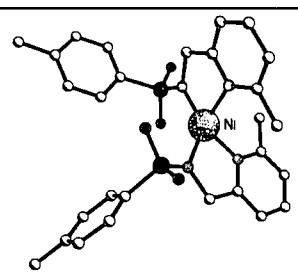	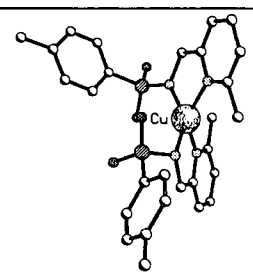	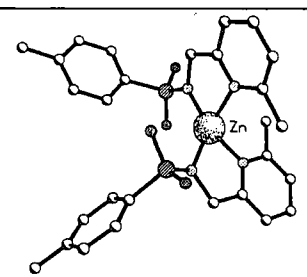

Table 2.1 View of the crystal structures of the Co(II), Ni (II), Cu (II) and Zn(II) complexes of L^1 - L^4

Complex	a/Å	b/Å	c/Å	α/°	β/°	γ/°	Volume /Å^3	System	S.Gr	Z	μ/mm^{-1}	T/K	R_{int}/%	Rw/%	R/%
L1	26.831(4)	5.958(1)	16.576(2)	90	99.967(3)	90	2610.1(6)	Monoclinic	C2/c	8	0.249	110	3.05	9.20	3.84
Zn(L1)2	30.505(2)	8.010(1)	27.309(1)	90	123.815(3)	90	5543.8(9)	Monoclinic	C2/c	8	1.081	100	8.30	10.94	4.83
Zn(L2)2	8.296(1)	9.721(1)	13.035(1)	93.193(4)	95.817(4)	107.145(4)	995.27(17)	Triclinic	P$\bar{1}$	2	1.529	100	2.06	6.64	2.72
Zn(L3)2	7.973(1)	9.432(1)	14.746(1)	81.984(1)	81.130(1)	81.744(10)	1076.38(5)	Triclinic	P$\bar{1}$	2	1.419	105	2.56	8.35	2.99
Zn(L4)2	28.129(1)	12.033(1)	16.726(1)	90	91.701(1)	90	5658.54(17)	Monoclinic	I2/a	8	1.057	120	2.48	6.65	2.69
Cu(L1)2	7.293(1)	17.089(1)	9.912(7)	90	99.176(4)	90	1219.56(15)	Monoclinic	$P2_1/c$	2	1.11	100	4.14	8.99	3.31
Cu(L2)2§§	9.04(5)	10.29(5)	20.70(5)	90	91.71(5)	90	1923(10)	Monoclinic	Pc	4	1.442	100	5.60	36.05	14.10
Cu(L3)2	10.450(1)	14.023(1)	15.197(1)	90	106.221(1)	90	2138.19(10)	Monoclinic	$P2_1/c$	4	1.301	105	5.26	8.17	3.45
Cu(L4)2	26.673(1)	14.539(1)	14.980(1)	90	102.051(1)	90	5680.9(3)	Monoclinic	C2/c	8	0.96	110	15.03	18.56	7.32
Ni(L1)2	7.335(1)	17.058(1)	9.822(1)	90	99.139(1)	90	1213.25(8)	Monoclinic	$P2_1/c$	2	1.015	120	5.46	20.24	6.99
Ni(L2)2	10.458(1)	16.052(2)	29.546(4)	90	90	90	4960.1(11)	Orthorhombic	Pbca	8	1.038	100	4.21	15.38	5.89
Ni(L3)2	7.936(1)	9.450(1)	14.716(1)	80.519(0)	80.609(1)	81.548(1)	1065.77(6)	Triclinic	P$\bar{1}$	2	1.191	100	2.42	9.33	3.36
Ni(L4)2	32.016(1)	11.932(4)	16.782(8)	90	118.86(2)	90	5615(4)	Monoclinic	C2/c	8	0.881	120	4.23	11.8	4.35
Co(L1)2	29.967(6)	7.977(1)	26.183(5)	90	121.349(5)	90	5345.2(17)	Monoclinic	C2/c	8	0.838	100	5.23	9.00	3.73
Co(L2)2	8.270(1)	9.801(1)	13.050(1)	93.015(1)	95.599(1)	108.418(1)	994.84(6)	Triclinic	P$\bar{1}$	2	1.158	110	3.19	9.47	3.69

§ Remaining solvent electron density was refined to 0.13 molecules of water.

§§These crystals were badly twinned, despite appearing perfectly well formed. Satisfactory anisotropic refinement was not possible.

Table 2.2 Unit Cell and Crystallographic Data for Zn, Cu, Ni and Co Complexes of L^1 - L^4

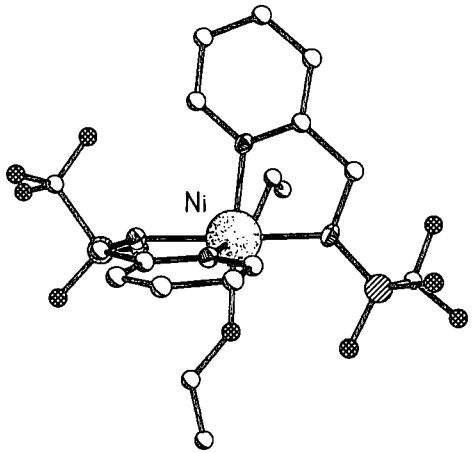	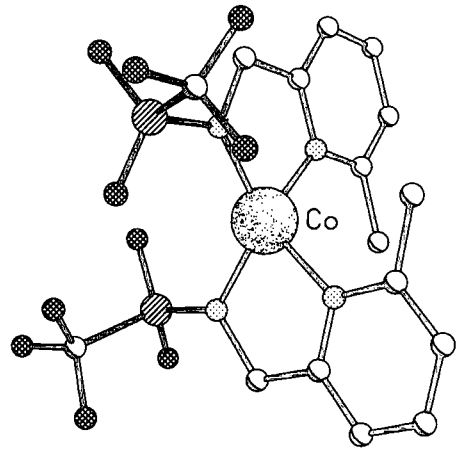
Octahedral: 6-coordinate $[Ni(L^2)_2.2EtOH]$	Distorted Tetrahedral $[Co(L^3)_2]$
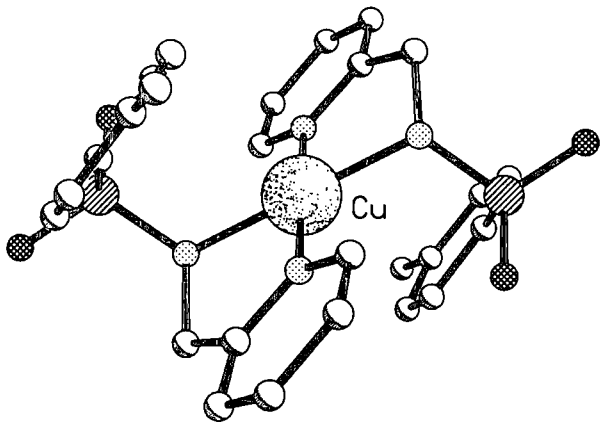	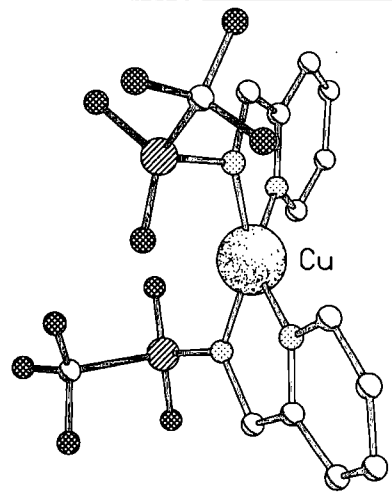
Square planar $[Cu(L^1)_2]$, also $[Ni(L^1)_2]$	Distorted Tetrahedral $[Cu(L^2)_2]$

Table 2.3 Highlighting the three different structures of the complexes. Each complex, with the exceptions of $[Cu(L^1)_2]$ (square planar), $[Ni(L^1)_2]$ (square planar) and $[Ni(L^2)_2.2EtOH]$ (octahedral), adopted a distorted tetrahedral conformation.

2.3.1 Coordination Geometry

Each of the complexes was found to form 2 ligand : 1 metal systems with the ligands coordinating in a bidentate manner. With three exceptions, they were four-coordinate and adopted a distorted tetrahedral geometry (Table 2.3).

The coordination geometry at the zinc and cobalt centres was invariably distorted tetrahedral. This arrangement minimises the steric congestion around the metal and offers a slightly favourable ligand field stabilisation effect in the case of cobalt. A similar distorted tetrahedral arrangement was found in the case of copper with ligands L^2, L^3 and L^4. However, the less sterically demanding ligand L^1 allowed the formation of a square planar complex. Nickel was found to form the same distorted tetrahedral arrangement with the α-methyl substituted ligands, L^3 and L^4. $[Ni(L^1)_2]$ adopted a square planar arrangement, while $[Ni(L^2)_2]$ adopted an octahedral arrangement with two ethanol molecules *cis*-coordinated and the sulfonamide nitrogens *trans*-related.

During the course of this study, a related square planar complex was reported by Gutierrez *et al.*[107,108]

2.3.2 Bond Angle Analysis

Two extreme geometries exist for four-coordinate complexes; square planar and tetrahedral. In an ideal tetrahedral complex, the angles between adjacent donor atoms and the central atom are 109°. Square planar complexes have 90° angles between adjacent coordinated atoms. Only $[Ni(L^1)_2]$ and $[Cu(L^1)_2]$ can be described as square planar and with the exception of the octahedral complex, $[Ni(L^2)_2]$, each of the other complexes adopted a distorted tetrahedral geometry (Table 2.4).

The degree of distortion of these complexes is primarily related to the 5-ring chelate bite angle, which averaged 82°. This is imposed by the bidentate ligand structure. The intra-ligand N-M-N′ bond angles in the series average 83° and 82° for the set of zinc and cobalt complexes respectively. This relatively constant bite angle is also maintained (83 ± 3°) in the square planar and octahedral nickel complexes.

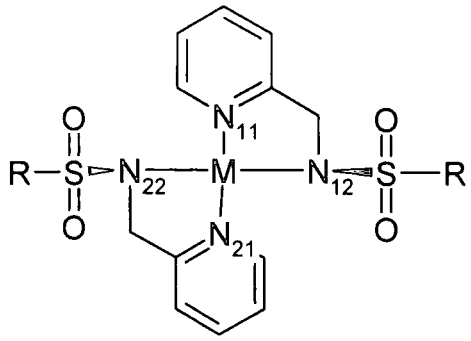

L^1 R = Ts, R' = H

L^2 R = CF_3, R' = H

L^3 R = CF_3, R' =Me

L^4 R = Ts, R' = Me

Table 2.4 Bond angles, in degrees between the central metal ion and the coordinating nitrogen atoms.

Complex	N_{11}-M-N_{12}	N_{11}-M-N_{21}	N_{11}-M-N_{22}	N_{12}-M-N_{21}	N_{12}-M-N_{22}	N_{21}-M-N_{22}
$[Zn(L^1)_2]$	82.96(11)	122.40(10)	121.54(11)	117.73(11)	134.92(11)	82.59(10)
$[Zn(L^2)_2]$	83.12(6)	124.98(6)	124.75(6)	114.93(7)	131.99(7)	82.44(6)
$[Zn(L^3)_2]$	82.81(6)	113.20(6)	125.79(7)	123.81(7)	131.73(7)	83.32(6)
$[Zn(L^4)_2]$	82.8(2)	113.3(2)	129.8(3)	117.47(8)	134.01(8)	82.01(7)
$[Cu(L^1)_2]$	83.23(6)	180.00(8)	96.77(6)	96.77(6)	180.00(7)	83.23(6)
$[Cu(L^2)_2]^{\S}$	82.3	147.3	105.6	105.6	154.7	81.0
$[Cu(L^3)_2]$	84.07(8)	150.57(9)	112.72(8)	103.40(8)	131.34(9)	83.92(8)
$[Cu(L^4)_2]$a	83.0(2)	140.66(19)	109.3(2)	107.2(2)	145.0(2)	84.2(2)
$[Cu(L^4)_2]$b	82.2(2)	128.82(19)	115.0(2)	110.6(2)	145.4(2)	82.7(2)
$[Ni(L^1)_2]$	94.4(2)	180.00(17)	85.6(2)	85.6(2)	180.0(3)	94.4(2)
$[Ni(L^2)_2]$	79.48(12)	91.01(12)	94.27(13)	97.31(13)	173.27(13)	80.18(13)
$[Ni(L^3)_2]$	82.13(7)	108.20(7)	124.26(8)	124.25(7)	137.32(8)	82.23(7)
$[Ni(L^4)_2]$	81.82(8)	110.69(8)	116.45(8)	133.00(8)	134.63(8)	81.64(7)
$[Co(L^1)_2]$	81.85(9)	122.08(9)	119.28(10)	119.19(10)	137.24(10)	82.59(9)
$[Co(L^2)_2]$	82.25(8)	125.16(8)	122.17(8)	116.01(9)	135.44(8)	81.83(8)
$[Co(L^3)_2]$	82.88(8)	115.13(8)	124.51(8)	127.66(9)	129.35(9)	82.12(8)
$[Co(L^4)_2]$	81.97(8)	114.45(8)	119.17(8)	128.57(8)	134.20(8)	81.94(7)

[§]Twinned Crystal. Structure of poor quality. SU's are estimated at ± 5 in the last digit.

2.3.3 CSD Bond Angle Analysis.

There are two limiting geometries for four-coordinate complexes; square planar and tetrahedral. To quantify the deviation from these extremes in the complexes being examined here, a search of the CSD[109] was undertaken, examining all of the four-coordinate first row transition metal complexes with nitrogen or oxygen donors. In the April 2001 version, 284 of these were zinc complexes. The bond

angles around the central metal ion, which determine the overall geometry of the complex, were obtained from the database. The sum of these angles is 656° in a tetrahedral complex and 720° in a square planar system. However, the sum itself is not a sufficient measure of geometry; in the case of a perfect tetrahedron all the angles must be identical, whilst for a perfect square planar arrangement, two of the angles must be 180° and the others must be 90°. A measure of distortion is obtained from the average deviation of all six angles; in the case of a perfect tetrahedron, this should be 0° and for a square planar complex, it should be 40°, [(2x60)+(4x30)]/6. A plot of the average angular deviation (y axis) versus the sum of the six angles is given for all the CN = 4 first row transition metal complexes where the donor atoms are nitrogen or oxygen only (Figure 2.1). In this plot, the square planar complexes, $[Cu(L^1)]$ and $[Ni(L^1)]$, appear in the top right hand corner. $[Cu(L^2)_2]$ has an angular deviation of ~25° whereas the rest of the structures examined (with the exception of octahedral nickel which has been excluded as CN = 6) form a cluster around 18 - 20°. The degree of distortion examined here can be primarily related to the 5-ring chelate with constant bite angle of approx. 82°. This method may be extended to related polyhedron such as octahedron and trigonal bipyramids.

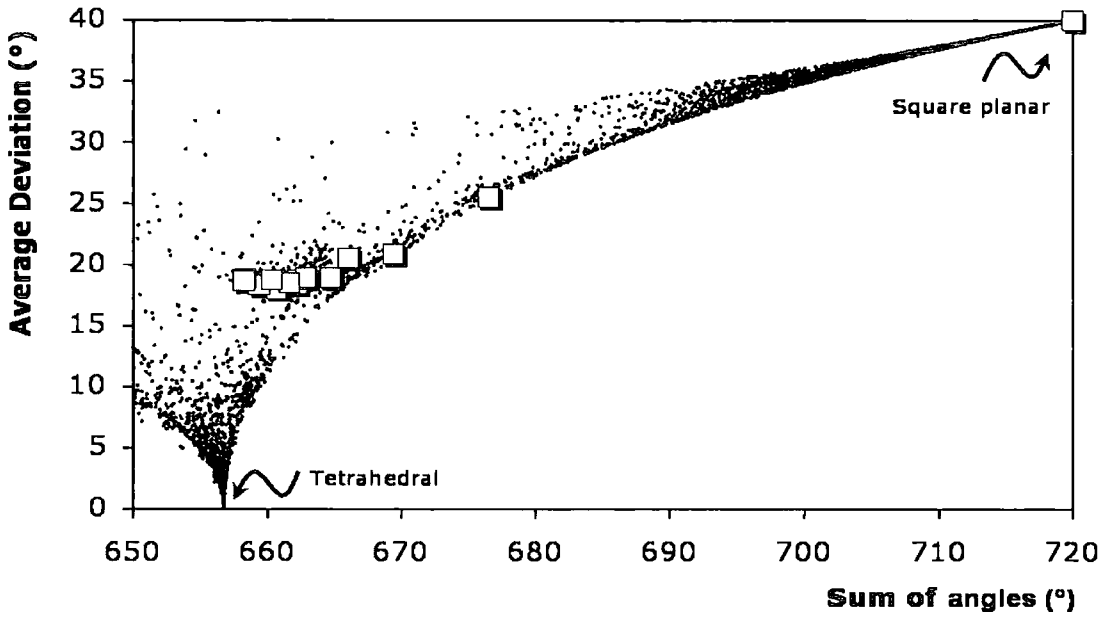

Figure 2.1 Plot of the sum of the six bond angles versus the average deviation of these angles for all four-coordinate first row transition metal complexes involving N and O donors (CSD 2001). The squares represent the complexes of L^1 - L^4.

An alternative method of 1-D analysis exists for the unique case of tetrahedral distortion. Analysis involves the examination of the dihedral angle between the two ML_2 planes with limits of 0 and 90° for ideal square planar and tetrahedral geometry respectively. The advantage of this system is that it gives the absolute configuration for chiral systems. Such an analysis has been carried out on the four-coordinate systems described here. For each of the tetrahedrally distorted cobalt (II), nickel (II) and zinc (II) systems examined, the deviation from the tetrahedral limit was not more than 10°. Distortion was more evident with the copper systems. For $[Cu(L^2)_2]$ the dihedral angle was 45° whereas for $[Cu(L^3)_2]$ and $[Cu(L^4)_2]$, the angles were 29° and 33° respectively. The 2-D plot in Figure 2.1 provides additional information. For example, tetragonal distortion of a square planar complex gives an angle sum of 720° and an angular distortion of > 40°; no cases were found of this for first row transition metals with N or O donors.

2.3.4 Bond Length Analysis

Table 2.5 Bond Lengths, in Å, from the metal ion to the coordinating pyridyl (N_1) and sulfonamide (N_2) nitrogens and average distances.

Complex	M-N_{11}	M-N_{12}	M-N_{21}	M-N_{22}	av M-N_1	av M-N_2	Av M-N
$[Zn(L^1)_2]$	2.049(3)	1.942(3)	2.049(3)	1.956(3)	2.049	1.949	1.999
$[Zn(L^2)_2]$	2.023(2)	1.972(2)	2.043(2)	1.967(2)	2.033	1.969	2.001
$[Zn(L^3)_2]$	2.048(2)	1.965(2)	2.057(2)	1.966(2)	2.052	1.965	2.009
$[Zn(L^4)_2]$	2.050(7)	1.954(2)	2.089(2)	1.929(2)	2.069	1.941	2.004
$[Cu(L^1)_2]$	1.996(1)	1.998(1)	1.996(1)	1.998(2)	1.996	1.998	1.997
$[Cu(L^2)_2]$	1.949	1.939	1.998	1.916	1.974	1.928	1.951
$[Cu(L^3)_2]$	1.979(2)	1.973(2)	1.962(2)	1.969(2)	1.971	1.971	1.971
$[Cu(L^4)_2]$a	2.067(5)	1.920(5)	2.019(5)	1.944(5)	2.043	1.932	1.988
$[Cu(L^4)_2]$b	2.067(5)	1.914(5)	2.058(5)	1.918(5)	2.063	1.916	1.989
$[Ni(L^1)_2]$	1.924(5)	1.960(5)	1.924(5)	1.960(5)	1.924	1.960	1.942
$[Ni(L^2)_2]$	2.090(3)	2.123(3)	2.060(3)	2.099(3)	2.075	2.111	2.093
$[Ni(L^3)_2]$	2.021(2)	1.941(2)	2.028(2)	1.946(2)	2.025	1.944	1.9845
$[Ni(L^4)_2]$	2.040(2)	1.905(2)	2.014(2)	1.929(2)	2.027	1.917	1.972
$[Co(L^1)_2]$	2.031(2)	1.960(2)	2.037(2)	1.937(2)	2.034	1.949	1.9915
$[Co(L^2)_2]$	2.028(2)	1.962(2)	2.031(2)	1.968(2)	2.030	1.965	1.9975
$[Co(L^3)_2]$	2.040(2)	1.972(2)	2.035(2)	1.965(2)	2.038	1.969	2.0035
$[Co(L^4)_2]$	2.061(2)	1.934(2)	2.052(2)	1.960(2)	2.056	1.947	2.001

a) In CN=4, mean ionic radii for Zn, Cu, Ni and Co(II) ions are 0.60, 0.57, 0.55 and 0.58Å.[19]
b) $[Cu(L^4)_2]$ This complex has two independent molecules per unit cell.

Within the series of zinc and cobalt complexes, average bond lengths (Table 2.5) from the metal centre to the sulfonamide nitrogen were marginally longer with the more electron-poor trifluoromethyl substituted ligands $\mathbf{L^2}$ and $\mathbf{L^3}$. Also, the 6-methyl substituted ligands form complexes with slightly longer M-N_{py} bond lengths. Bond lengths to pyridyl and sulfonamide nitrogens were in line with literature values for four and five-coordinate zinc complexes.[110,111,112,113] For example, in the 2,2-bipyridyl zinc complex of cyclohexane-1,2-diylbis(methane-sulfonamide) the sulfonamide N-Zn bond length was 1.94 Å with a bpy-N-Zn length of 2.05Å.[110] With the copper (II) complexes, average bond lengths were slightly longer for the square planar example.

The X-ray structure of $\mathbf{[Cu(L^1)_2]}$ has recently been reported at 273 K:[107, 108] structural details echo those reported herein.

Overall, there is a remarkable constancy in the M-N bond lengths. This can again be related to the fixed chelate bite angle associated with each ligand, and the similarity of the ionic radii of four-coordinate Co^{2+}, Ni^{2+}, Cu^{2+} and Zn^{2+} ions.

2.4 Mercury Complexes

Mercury (II) complexes of $\mathbf{L^1}$ and $\mathbf{L^2}$ were synthesised in an analogous manner, and the crystal structures of complexes $\mathbf{[Hg(L^1)_2]}$ and $\mathbf{[Hg(L^2)_2]}$ were obtained (Figure 2.2). The crystallographic information is summarised in Table 2.6.

Figure 2.2 Structure of mercury (II) complexes of ligands L^1 and L^2.

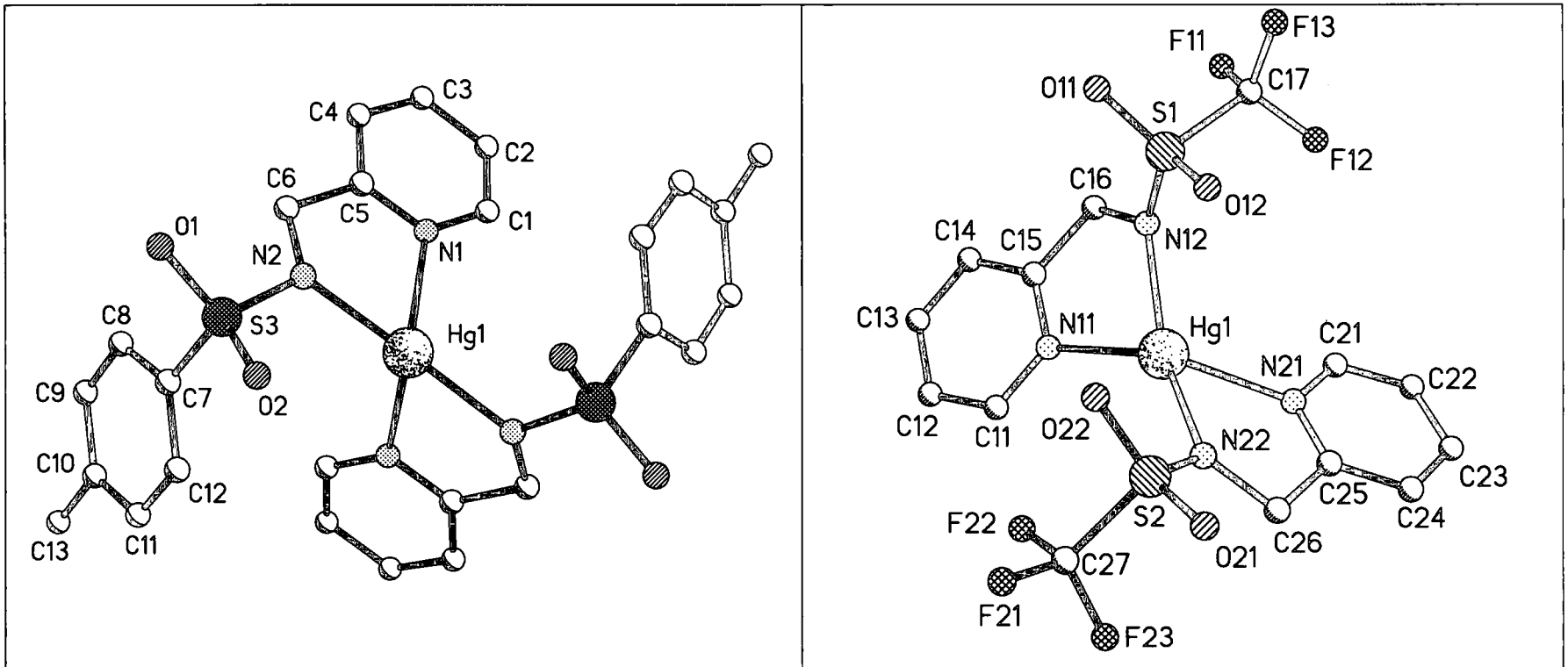

$[Hg(L^1)_2]$ $[Hg(L^2)_2]$

Table 2.6 Unit Cell and Crystallographic Data for Complexes $[Hg(L^1)_2]$ and $[Hg(L^2)_2]$.

Complex	a/Å	b/Å	c/Å	α/°	β/°	γ/°	Volume /Å^3	System	S.Gr	Z	μ/mm^{-1}	T/K	R_{int}/%	Rw/%	R/ %
$Hg(L^1)_2$	9.227(1)	9.227(1)	31.966(1)	90	90	90	2721.2(1)	Tetragonal	P-4	4	5.848	120	3.80	3.25	1.43
$Hg(L^2)_2$	10.908(1)	10.008(1)	18.044(1)	90	96.522(1)	90	1957.0(1)	Monoclinic	P2(1)/n	4	8.165	120	2.88	4.25	1.77

2.4.1 Bond Lengths and Angles of $[Hg(L^1)_2]$ and $[Hg(L^2)_2]$

The mercury (II) complexes of L^1 and L^2 crystallised with a distorted tetrahedral geometry. The angles and bond lengths between the central mercury (II) ion and the coordinating nitrogens are summarised in Table 2.7 and Table 2.8.

Table 2.7 Bond angles (°) between the mercury ion and the coordinating nitrogens.

Complex	N_{11}-M-N_{12}	N_{11}-M-N_{21}	N_{11}-M-N_{22}	N_{12}-M-N_{21}	N_{12}-M-N_{22}	N_{21}-M-N_{22}
$[Hg(L^1)_2]$	73.78(7)	101.48(9)	114.57(7)	114.57(7)	167.62(11)	73.78(7)
$[Hg(L^2)_2]$	74.12(7)	122.92(7)	129.20(8))	110.31(8)	150.89(8)	73.82(7)

Table 2.8 Bond lengths (Å) between the mercury ion and coordinating nitrogens.

Complex	M-N_{11}	M-N_{12}	M-N_{21}	M-N_{22}	av M-N_1	av M-N_2
$[Hg(L^1)_2]$	2.460(1)	2.073(1)	2.460(1)	2.073(1)	2.460	2.073
$[Hg(L^2)_2]$	2.350(2)	2.165(2)	2.376(2)	2.135(2)	2.363	2.150

In the complexes of the first row transition metals, the angle between the central metal ion and the coordinating nitrogens of the same ligand (e.g. N_{11}-M-N_{12}), were constrained by the bite angle of the five-membered chelate ring to approximately 82°. In both of the mercury complexes, this bite angle is drastically reduced to 74°.

Although four-coordinate mercury has a greater ionic radius (1.10 Å),[19] the metal to nitrogen bond lengths do not increase proportionally. In the first row transition metal complexes, the average metal to pyridyl (M-N_1) bond length was 2.0 Å and the average metal to sulfonamide nitrogen (M-N_2) bond length was 1.95 Å. In the mercury complexes, it can be seen that M-N_2 bond increases by approximately 8% in length whereas the M-N_1 bond increases by approximately 18% in length. This indicates that the sulfonamide nitrogen anion is a much stronger donor to the mercury ion than the pyridyl nitrogen. This difference in the donor ability and thus the bond lengths from the two coordinating nitrogens results in a distortion of the bite angle of the chelate ring.

2.5 Absorption Spectra.

Absorption spectra were recorded for each of the soluble coloured complexes in acetonitrile solution at 1 mM concentration. Absorption maxima and extinction coefficients are summarised in Table 2.9.

Table 2.9 Absorption Spectral Data (MeCN, 295 K) for cobalt, copper and nickel (II) complexes (λmax ; ε/$M^{-1}cm^{-1}$ in parenthesis)

	Co(II)	Ni (II)	Cu (II)
L^1	513 (300), 579 (290)	Insoluble	639 (70)
L^2	500 (45)	367 (50), 597 (3)	672 (230)
L^3	533(400), 564 (380)	544 (190), 733 (50)	410 (405), 764 (70)
L^4	532 (580), 564 (540)	544 (70), 760 (30)	448 (2020), 784 (215)

2.5.1 Absorption Spectra of Cobalt (II) Complexes

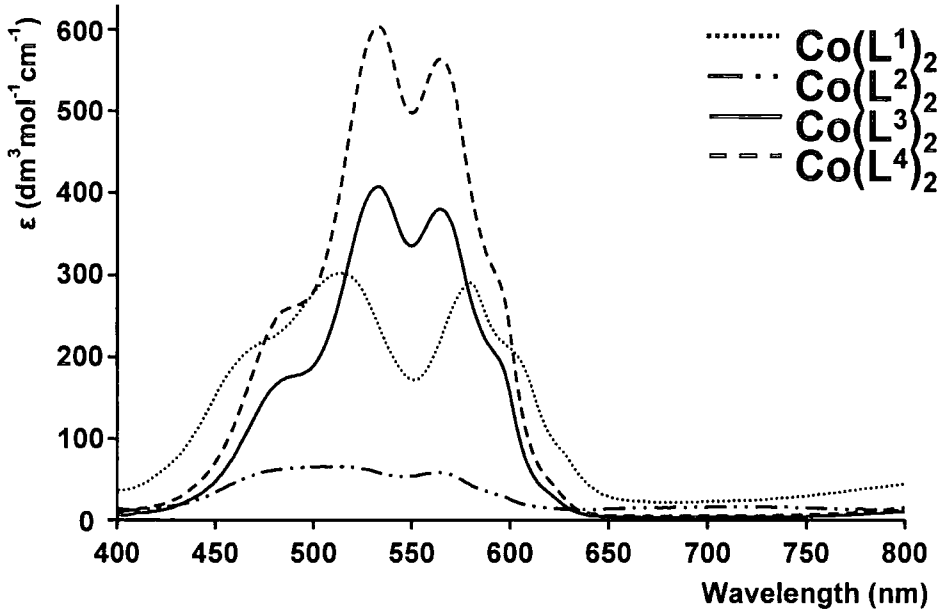

Figure 2.3 Absorption spectra of neutral cobalt (II) complexes of L^1 - L^4. (1 mM complex), (2 mM for L^2), MeCN)

For the series of Co (II) complexes (Figure 2.3), the absorption spectra were similar, with the exception of $[Co(L^2)_2]$ which was much more pale coloured in solution. Molar absorption coefficients, ε, increased in the sequence $[Co(L^2)_2] << [Co(L^1)_2] < [Co(L^3)_2] < [Co(L^4)_2]$. It is generally appreciated that the visible transitions in tetrahedral cobalt (II) complexes are an order of magnitude more intense than for equivalent octahedral systems.[114] Absorption spectra tend to be dominated by the

$^4A_2 \rightarrow {}^4T_1(P)$ transition for tetrahedral systems and the $^4T_{1g}(F) \rightarrow {}^4T_{1g}(P)$ transition for octahedral examples. Fine structure is imposed by a number of transitions to doublet excited states, which gain intensity by spin orbit coupling. Thus for $[Co(L^2)_2]$, the complex must be octahedral in solution, binding two additional solvent molecules, as revealed in the X-ray analysis of $[Ni(L^2)_2(EtOH)_2]$. The reflectance spectra for each cobalt complex, obtained from crystalline samples, were more or less identical in form and intensity, in support of this idea.

2.5.2 Absorption Spectra of Copper (II) Complexes

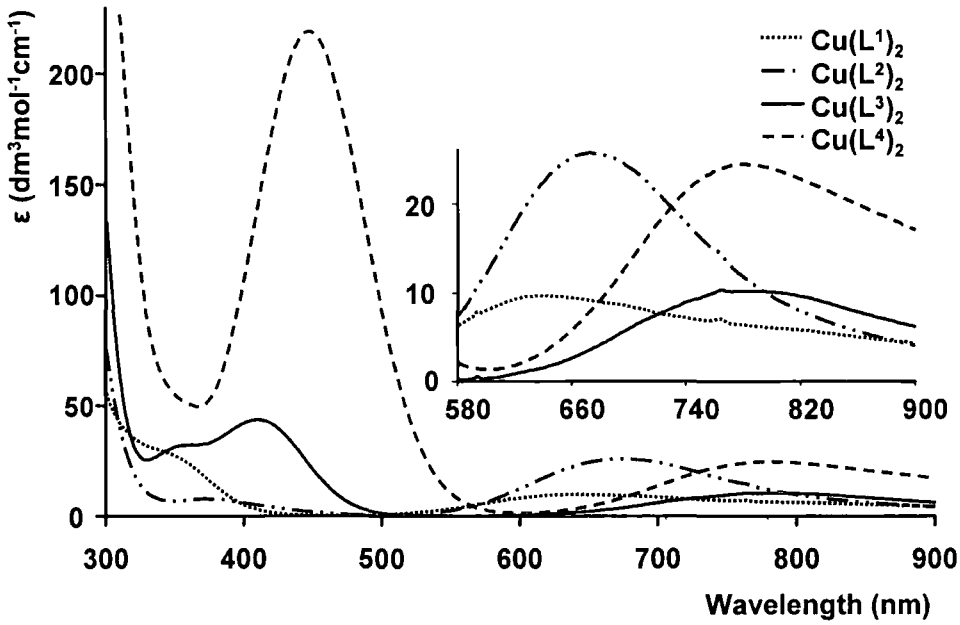

Figure 2.4 Absorption spectra of neutral copper (II) complexes of L^1 - L^4, the inset highlights the position of the $^2E_{2g} \rightarrow {}^2T_{2g}$ transition.

Complexes of copper (II) with N_4 donors typically give rise to two main transitions, associated with a d-d transition in the range 500 - 700 nm and with an LMCT band to shorter wavelength.

The tetrahedrally distorted copper complexes, $[Cu(L^3)_2]$ and $[Cu(L^4)_2]$, were lime-green and orange-brown in solution, reflecting the intensity of the relatively intense LMCT bands at 410 and 448 nm respectively (Figure 2.4). The position of the d-d transition was shifted in the sequence $[Cu(L^1)_2] > [Cu(L^2)_2] > [Cu(L^3)_2] > [Cu(L^4)_2]$ associated with the increase in LFSE for square planar complexes, with the more polarisable NTs ligand in L^1 affording the greatest crystal field splitting.

2.5.3 Absorption Spectra of Nickel (II) Complexes

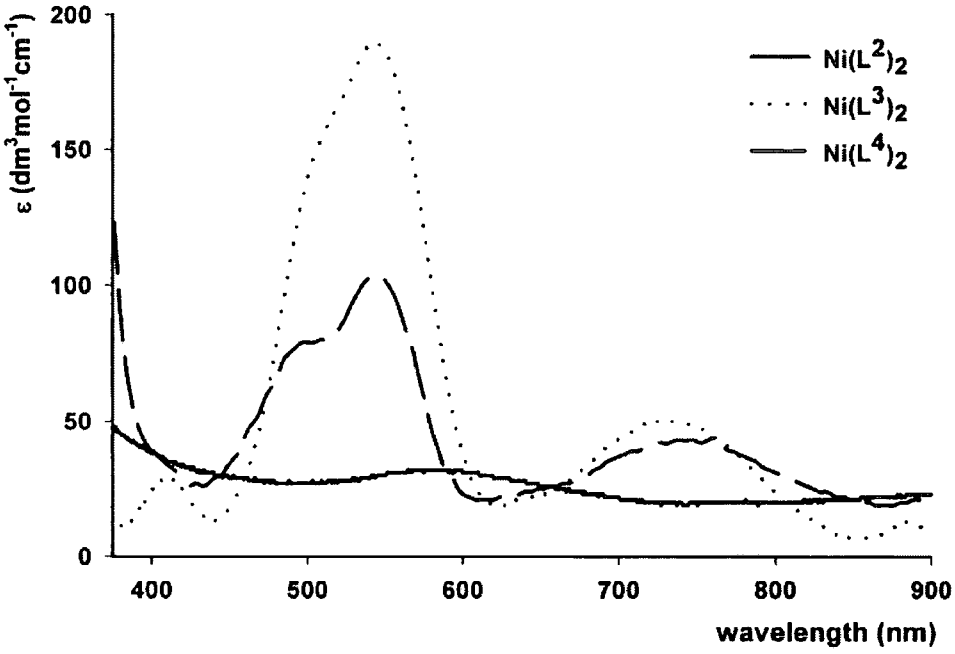

Figure 2.5 Absorption spectra of neutral nickel (II) complexes of L^2 - L^4.

The complexes $[Ni(L^3)_2]$ and $[Ni(L^4)_2]$ have a much more intense absorption than $[Ni(L^2)_2]$. The crystallographic information shows that $[Ni(L^3)_2]$ and $[Ni(L^4)_2]$ adopt a distorted tetrahedral configuration, whereas $[Ni(L^2)_2]$ adopts an octahedral arrangement. Whilst a relatively intense absorption typically arises from the $^3T_1(F) \rightarrow {}^3T_1(P)$ transition in tetrahedral d^8 complexes, the transition from $^3A_{2g} \rightarrow {}^3T_{1g}$ in octahedral d^8 complexes results in a much weaker absorption.[18] Such features are evident in the spectra obtained here (Figure 2.5). It was not possible to measure the absorption spectrum for complex $[Ni(L^1)_2]$ as it was insoluble in acetonitrile.

2.6 Cyclic Voltammetry

Cyclic voltammetry is a controlled potential sweep technique, which applies a triangular waveform of potential to the working electrode (WE) of an electrochemical cell. A cyclic voltammogram is produced: this is a plot of the current through the electrode as the potential is increased linearly (Figure 2.6).[115]

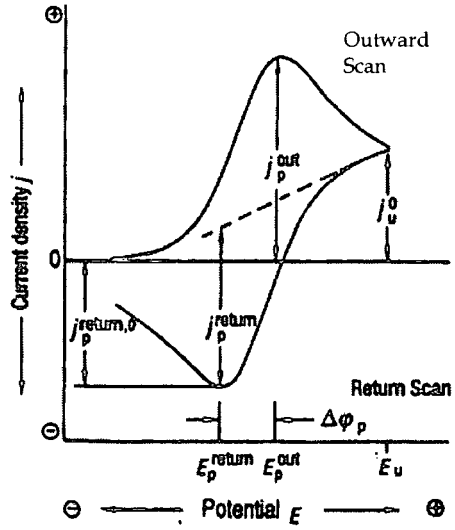

Figure 2.6 Cyclic voltammogram for a reversible redox system in unstirred solution for a single triangular potential excursion: for fast electron transfer, the peaks are separated by 57mV at 298 K[115]

The applied waveform is controlled by a potentiostat. It sweeps at a constant scan rate, from a negative start potential up to a positive limit, and then returns to the initial potential. The driving of the electrode to more positive potentials, with respect to the reference electrode, causes an oxidation current to flow from the solution to the electrode. Similarly, driving the electrode to negative potentials causes a reducing current to flow from the electrode to the solution. At a critical point, the analyte will oxidise or reduce and cause the peak current (i_p) to flow resulting in a peak in the voltammogram. These critical potentials are referred to as standard potentials and are unique to the analyte.[115]

A background electrolyte of tetrabutylammonium perchlorate, TBAP, was used in these experiments. This reduces the resistance of the cell and carries most of the current between the electrodes. This allows the effects of migration on the electroactive species of interest to be ignored.

2.6.1 Cyclic Voltammetry Studies of Copper Complexes

The Cu^{II}/Cu^{I} redox couple was examined by cyclic voltammetry (MeCN, 0.1M Bu_4NClO_4, 295K) for each of the four complexes Figure 2.7 and Table 2.10.

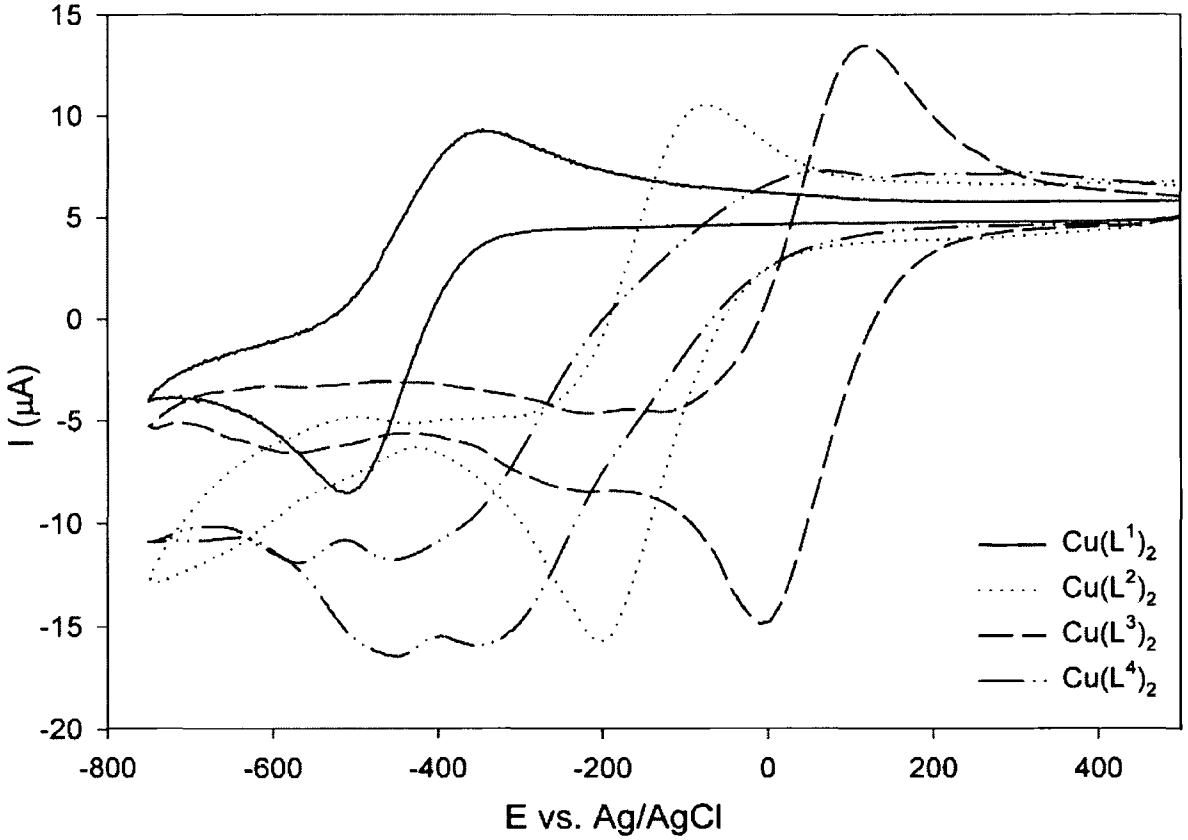

Figure 2.7 Cyclic voltammogram of copper (II) complexes of L^1 - L^4 (295 K, 0.1 M Bu_4NClO_4, 100 scans per minute)

Table 2.10 Cyclic voltammetry data for copper (II) complexes of ligands L^1 - L^4.

Complex	Scan rate (scans per minute)	Peak current oxidation (μA)	Peak voltage oxidation (mV)	Peak current reduction (μA)	Peak voltage reduction (mV)	ΔV (mV)	ΔV /2 (mV)
$Cu(L^1)_2$	50	-13.24	-532	11.27	-322	210	105
	100	-8.50	-514	9.30	-346	168	84
	150	-17.26	-532	8.546	-346	186	93
	200	-20.90	-546	15.24	-300	246	123
$Cu(L^2)_2$	50	-10.12	-196	12.482	-72	124	62
	100	-15.68	-202	10.549	-72	130	65
	150	-20.13	-206	16.27	-68	138	69
	200	-24.13	-224	23.43	-60	164	82
$Cu(L^3)_2$	50	- 9.82	-0.0007	9.379	120	120	60
	100	-14.86	-8.001	13.466	118	126	63
	150	-19	-12.0	17.37	128	140	70
	200	-22.5	-18.0	18.7	128	141.7	70.8
$Cu(L^4)_2$	50	-13.75	-338				
	100	-15.95	-352	7.308	68	420	210
	150	-20.57	-354	9.227	116	470	235
	200	-23.77	-354	9.767	120	474	237

The $E_{½}$ values (Table 2.11) for $[Cu(L^1)_2]$ reflect the larger stabilisation energy of the Cu(II) state as provided in a square planar configuration in the tosylamide complex. The complexes with the α-methyl substituents, $[Cu(L^2)_2]$ and $[Cu(L^3)_2]$, are much more readily reduced. This is consistent with the destabilisation of the Cu(II) state in a distorted tetrahedral conformation.[115,116] In each of the cases of L^1, L^2 and L^3 a quasi-reversible behaviour was exhibited ($i_p \approx i_{ai}$ $i_a \propto \nu^{½}$). The tetrahedrally distorted complex $[Cu(L^4)_2]$ exhibited more complex redox behaviour with an apparent redox couple at *ca.* -240mV.

Table 2.11 $E_{1/2}$ values (*vs* Ag/AgCl) for copper complexes of ligands L^1 - L^4.

Complex	$E_{½}$ *vs* Ag/AgCl (mV)
$Cu(L^1)_2$	-430
$Cu(L^2)_2$	-137
$Cu(L^3)_2$	+55
$Cu(L^4)_2$	-240

2.7 pH Dependent Cyclic Voltammetry

For the Cu(II)/L^1 system, it was possible to vary the pH over the range 4 - 10 in order to control the relative proportion of $[CuL^1]$ and $[Cu(L^1)_2]$ species. Thus, for a ligand concentration of 10 mM at pH 5, the predominant species is $[CuL^1]$, whereas at pH > 7, $[Cu(L^2)_2]$ is the major species. With this in mind, cyclic voltammetry was used to examine the Cu(II)/Cu(I) redox couple as a function of pH. These measurements were undertaken by Mark Knell in Durham.

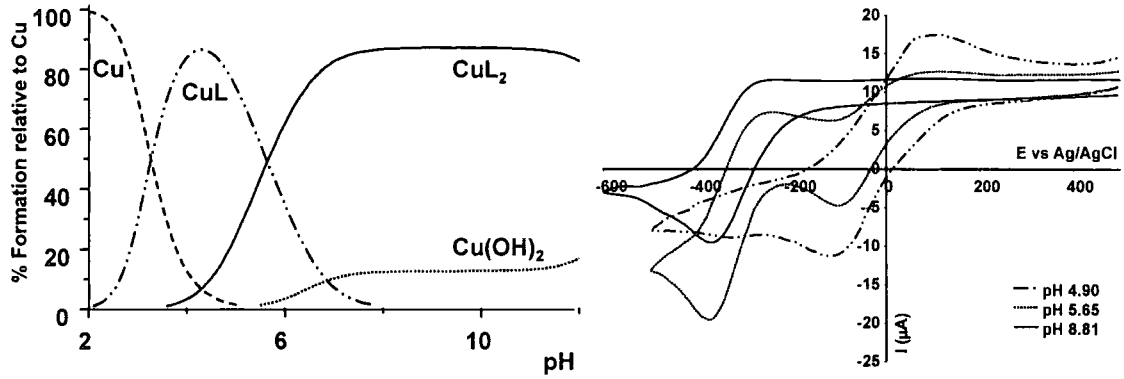

Figure 2.8 Left: Species distribution plot for Cu^{2+}/L^1 (10 mM L^1, 5 mM Cu^{2+}, 298K, 80% MeOH, 20% H_2O, 0.1 M NMe_4NO_3). Right: cyclic voltammograms recorded under the same conditions at pH 4.9, 5.65 and 8.81 (υ = 100 mVs^{-1}).

Figure 2.8 shows that at pH 4.9 (10 mM L^1; 5 mM $Cu(CF_3SO_3)_2$; 298 K; 0.1 M NMe_4NO_3, 80% MeOH/ H_2O), the reversible wave observed at *ca* -10 mV may be ascribed to $[CuL^1]$, whereas at pH 8.8, the redox couple shifts to -315 mV and is associated with the square planar complex $[Cu(L^1)_2]$.

At the intermediate pH of 5.65, both species are present in nearly equal amounts, and the observation of separate redox waves for each species is consistent with the rate of electron transfer being faster than any associative ligand exchange process involving $[CuL^1]$ and $[Cu(L^1)_2]$. Given that different redox active ML species may be observed simultaneously, for example using different pulse voltammetry, and that their relative concentrations is pH dependent, such work suggests that by immobilizing ligands related to L^1 at an electrode surface, the selection detection and assay of a mixture of metal ions may be expedited using sensitive stripping voltammetric techniques.

2.8 Ligand and Complex Speciation in Solution

2.8.1 Ligand Protonation Constants

Equilibrium constants associated with stepwise protonation of the anionic ligands L^1, L^2 and L^3 were measured by Mark Knell in Durham using standard pH-metric methods in 80% MeOH/H_2O in a background of 0.1 M NMe_4NO_3. Data were corrected[117] to allow for the variation of water dissociation constant at this solvent composition and analysed using the programme HYPERQUAD.[118,119,120]

Table 2.12 Ligand Protonation Constants.

Ligand	pKa_1	pKa_2	β_2
L^1	3.31(3)	12.23(6)	15.54
L^2	2.69(3)	7.51(3)	10.20
L^3	3.23(3)	7.61(3)	10.84
L^4	2.92	12.55	10.88

The successive ligand protonation constants are summarised (Table 2.12) and are defined as $K_1 = [LH]/[L^-][H^+]$ and $K_2 = [LH_2^+]/[LH][H^+]$.

The log K_1 values measured for L^2 and L^3 were 7.51 and 7.61 respectively, similar to the literature values for simple trifluoromethylsulfonamides.[121] The *p*-toluene-sulfonyl analogue, L^1, possesses a much more basic sulfonamide N, log K_1 = 12.23, in line with published data for related arylsulfonamides.[122]

The pyridyl nitrogen is much less basic in each case, with a pK_a in the range 2.7 to 3.3. The introduction of the 6-methyl substituent slightly enhances proton affinity. Thus, around ambient pH conditions, the ligands L^2 and L^3 exist as almost 50% of the monoanionic species.

2.9 Metal complex formation constants

Metal complex formation constants were measured by Mark Knell for Cu(II) and Zn(II) complexes of ligands L^1, L^2 and L^3, taking into account metal ion hydrolysis.[118,119,120] Separate titrations at 1 : 1 and 1 : 2 metal : ligand ratios were undertaken in order to measure both the ML and ML_2 formation constant.

Table 2.13 Selected Metal Complex Formation Constants (298 K, I = 0.1 M NMe_4NO_3, 80% MeOH - 20% H_2O)

	log K_{ZnL}	log K_{ZnL_2}	log K_{CuL}	log K_{CuL_2}	log K_{CoL}	log K_{CoL_2}
L^1	7.66(6)	6.91(7)	11.40(5)	9.16(7)		
L^2	5.25(5)	5.12(7)	6.74(5)	6.42(8)	5.11(6)	5.19(5)
L^3	precipitate formed	precipitate formed	6.26(4)	6.09(8)		

From the data summarised in Table 2.13 it can be seen that ligand L^2 formed slightly more stable complexes with copper than zinc in accord with the Irving-Williams series,[21] although a direct comparison of the tetrahedrally distorted Cu-L^3 /ZnL^3 systems is not possible here, owing to the insolubility of the zinc complex under the standard conditions used. The difference in the stability of the copper and zinc complexes is much greater with L^1, as the copper complex in that case is square planar and the zinc complex is tetrahedral.

The relative magnitude for the stepwise formation constants (log K_{ML} *vs* log K_{ML_2}) for zinc, copper and cobalt was very similar, although there was no evidence for positive cooperativity in the formation of the ML_2 species.

The harder trifluoromethanesulfonamide N favours binding to Cu (II) less than the more basic and softer tosylsulfonamide N in L^1. Systems favouring tetrahedral coordination should also enhance the relative stability of zinc (II) compared to copper (II), as the LFSE contribution is significantly diminished for Cu (II) when deviations from planarity or square pyramidal geometry occur.

2.9.1 Complex Speciation Plots

Species distribution diagrams as a function of pH and M/L concentrations were obtained from the data in Table 2.12 and Table 2.13 in which the percentage of the insoluble metal hydroxide is calculated by extrapolation. Considering the Zn^{2+}/L^1 and L^2 systems, the pH-dependent distribution of complex species has been calculated at fixed ligand concentrations of 10 mM, 1 mM and 0.1 mM with varying $[Zn^{2+}]$ values.

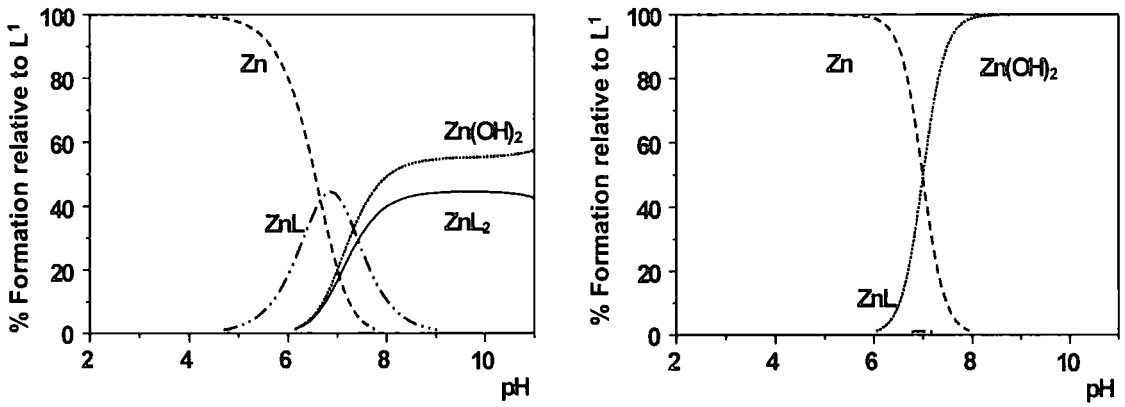

Figure 2.9 Species distribution plots for Zn^{2+}/L^1: left, 10 mM ligand 1 mM Zn^{2+}; right, 0.1 mM L^1, 10 μM Zn^{2+}.

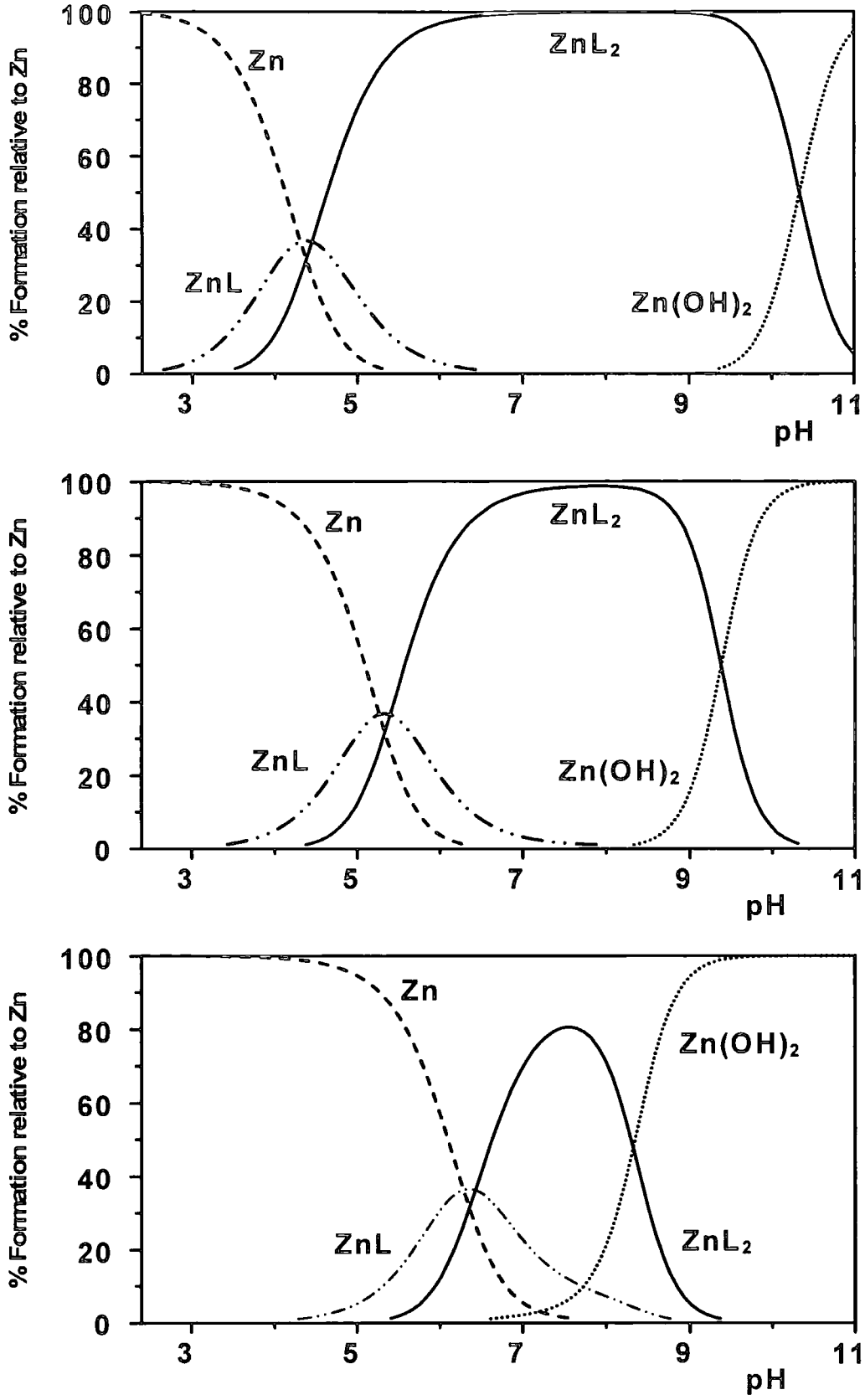

Figure 2.10 Species distribution plots for Zn^{2+}/L^2 : Upper, 10 mM ligand, 1 mM Zn^{2+}; centre, 1 mM L^2, 0.1 μM Zn^{2+}; lower, 0.1 mM L^2, 0.1 μM Zn^{2+}. (80% MeOH, 20% H_2O; 298 K; 0.1 M Me_4NNO_3).

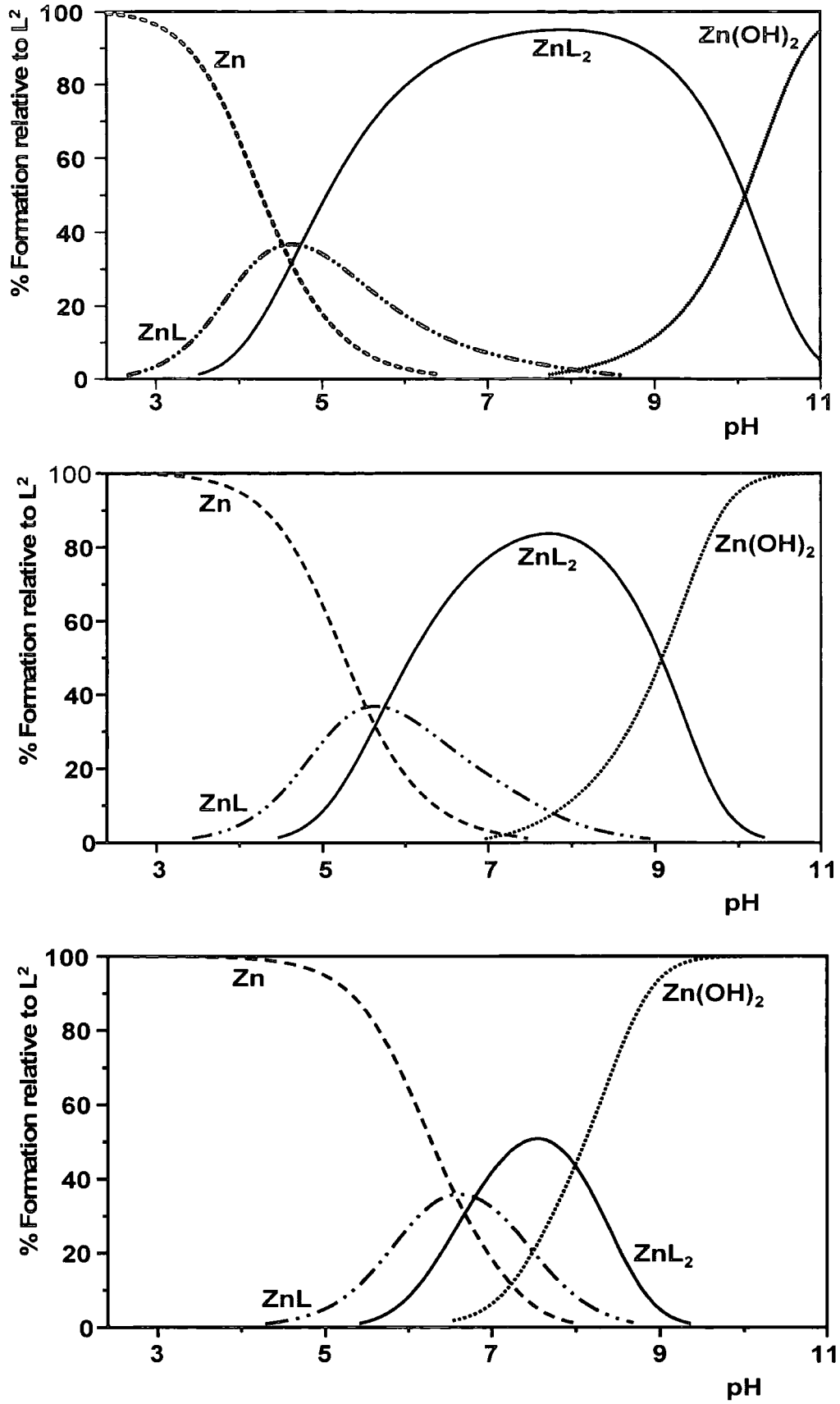

Figure 2.11 Species distribution plots for Zn^{2+}/L^2 with ligand to metal ratio of 2 : 1 *upper*, 2 mM ligand, 1 mM Zn^{2+}; *centre*, 0.2 mM L^2, 0.1 mM Zn^{2+}; *lower*, 0.2 μM L^2, 0.1 μM Zn^{2+} (80% MeOH, 20% H_2O; 298 K; 0.1 M Me_4NNO_3).

With the L^2 system (Figure 2.10) a particular feature is that the $[Zn(L^2)_2]$ species predominates at ambient pH and even with $[L^2]_{tot}$ = 0.1 mM and $[Zn^{2+}]$ = 0.1 μM, more than 80% of all Zn bound species is in the form of the neutral 2 : 1 complex $[Zn(L^2)_2]$. However, for the tosylamide ligand L^1 (log K_1 = 12.2), even when $[L^1]_{tot}$ = 10 mM and $[Zn^{2+}]_{tot}$ = 1 mM, the major species at pH 7.4 is the metal hydroxide, with significant $[ZnL^1]$ formed (Figure 2.9). At lower ligand concentrations, only a very small amount of the $[ZnL^1]$ species is present. In summary, it can be seen that L^2 and L^3 offer scope as the basis for practicable Zn(II) probes in neutral aqueous media, possessing sufficient affinity for the Zn^{2+} ion at ambient pH to form a major 2 : 1 species, even with low total ligand concentrations.

2.10 Conclusion

Ligands L^2 and L^3 are suitable basic ligand systems that form neutral ML_2 complexes at ambient pH when the free zinc (II) concentration is in the micro to nanomolar range. Based on these ligands, appropriately conjugated variants were then considered for potential use as pZn sensitive MRI or luminescence probes, and are discussed in the following chapters.

Chapter 3

Simple Macrocyclic Ligands

3 Simple Macrocyclic Ligands

3.1 Introduction

Once the most appropriate zinc (II) binding ligands had been identified as the pyridyl trifluoromethanesulfonamides, L^2 and L^3, a suitable linkage group to attach it to a macrocyclic system had to be established.

Macrocyclic ligands based on triacetate (e.g. DO3A: N,N',N''-tris(carboxymethyl)-1,4,7,10-tetraazacyclododecane) and triacetate-monoamide derivatives of cyclen (1,4,7,10-tetraazacyclododecane) have been shown to form well-defined and kinetically robust complexes with lanthanide (III) ions in solution.[62] Therefore, DO3A-type complexes with appended pyridyl amide groups were designed and synthesised, with both ethyl and propyl chains linking the amide group to one nitrogen of the 12-N_4 ring.

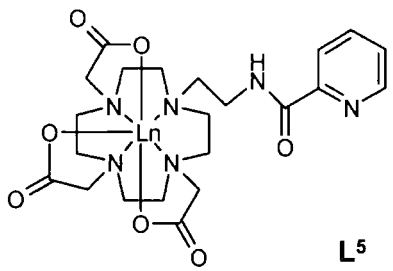

L^5

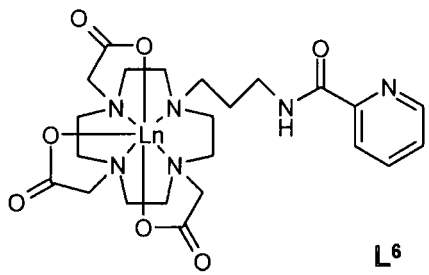

L^6

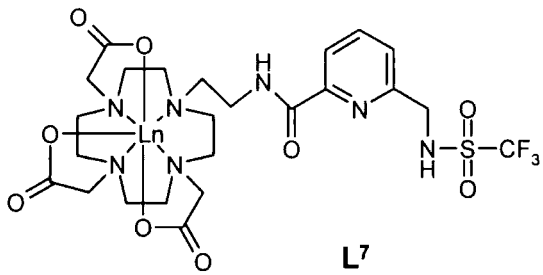

L^7

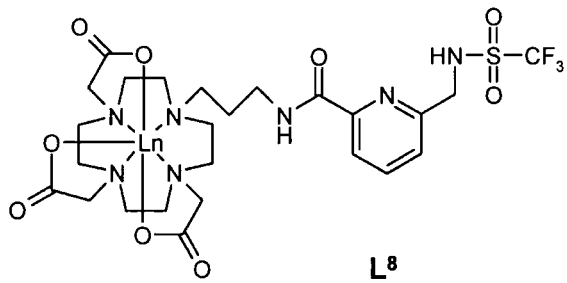

L^8

The europium (III) and gadolinium (III) complexes of ligands L^5 and L^6 were synthesised and characterised as model complexes for the trifluoromethane-sulfonamide systems L^7 and L^8, which are potentially pZn MRI probes or precursors of luminescent probes.

The amide carbonyl group was anticipated to ligate intramolecularly to the central lanthanide ion. Enlarging from a seven membered chelate ring (L^5) to an eight membered chelate ring (L^6) was expected to disfavour amide carbonyl binding. If

this intramolecular ligation was rendered reversible, it would then be possible to create a responsive system, sensitive to the presence of added metal ions, provided that the binding of the carbonyl group to the lanthanide centre also prevented water from binding to the lanthanide ion. The result was hypothesised to be a switching between q = 0 and q = 1 or 2 system, following the addition of metal ions (Scheme 3.1).

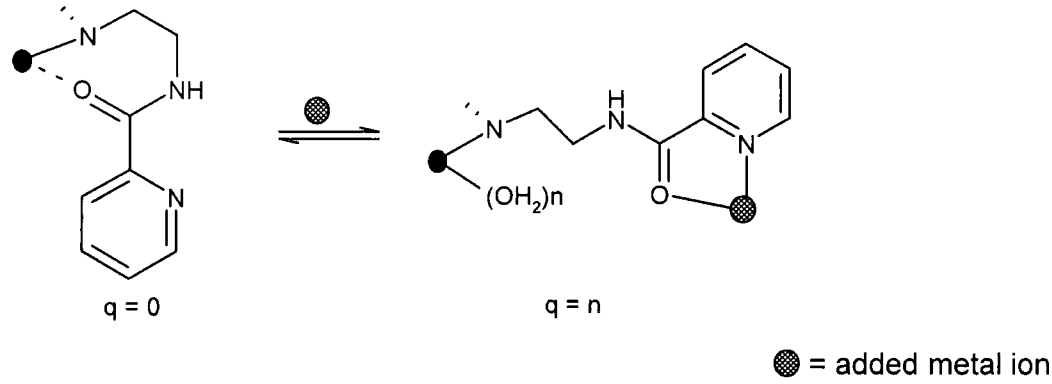

Scheme 3.1

3.2 Synthesis

The synthesis of ligand L^5 (Scheme 3.2), commenced with the EDC coupling of 2-pyridine carboxylic acid with ethanolamine to give the corresponding amide **46**. The terminal alcohol was then brominated using carbon tetrabromide and triphenylphosphine to give **47** which was then used to alkylate 1,4,7-tris(*tert*-butoxycarbonylmethyl)-1,4,7,10-tetra-azacyclododecane, **48**, in the presence of base in hot acetonitrile. The resulting tetrasubstituted cyclen, **49**, was deprotected with trifluoroacetic acid to afford the desired ligand L^5 as the TFA salt. Lanthanide complexes were prepared in aqueous solution following reaction of the ligand with hydrated $LnCl_3$ at pH 5.5 (90°C, 18 hours).

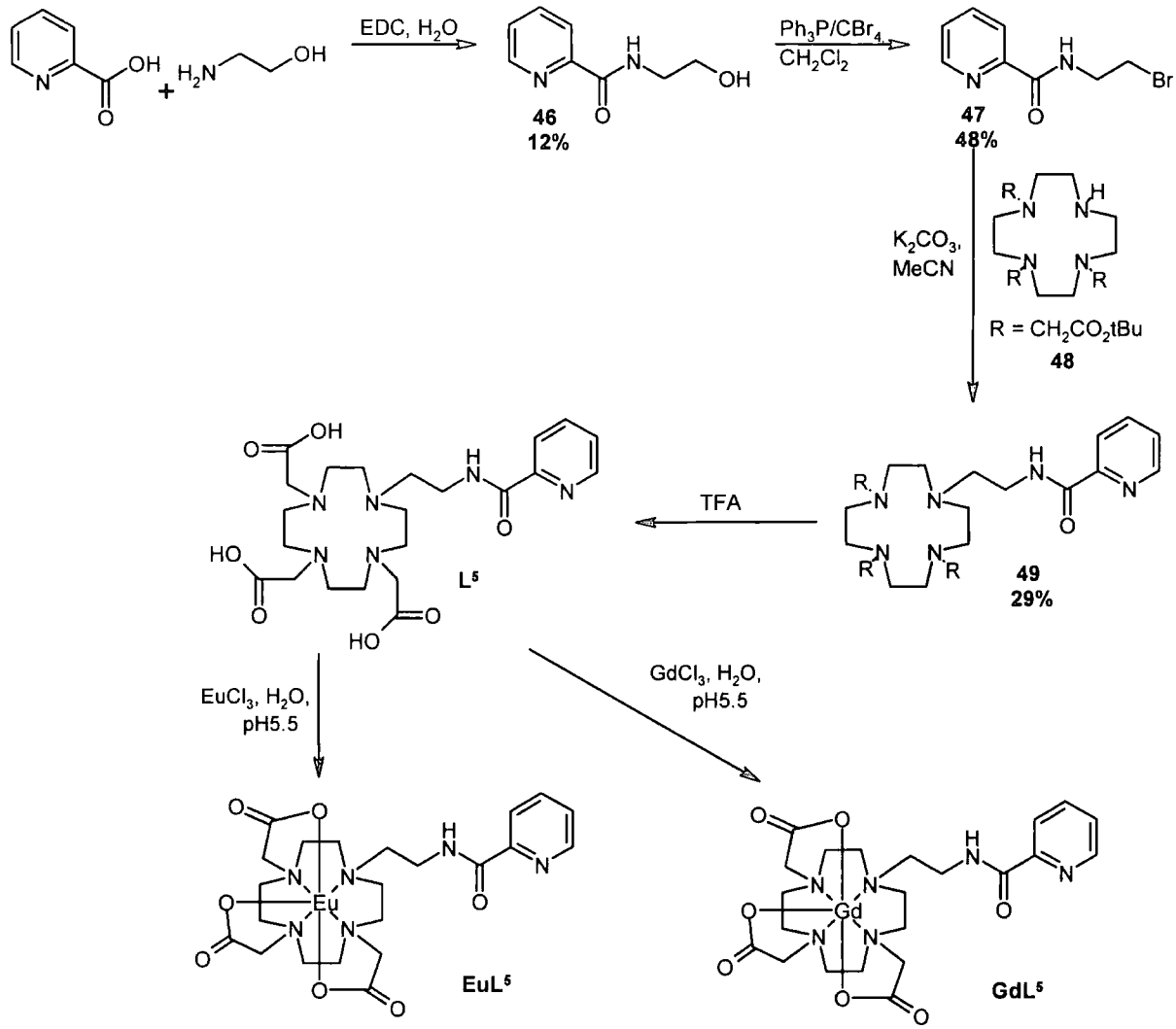

Scheme 3.2 Synthesis of Lanthanide (III) Complexes of L^5.

Ligand L^6 was prepared in a similar fashion: EDC coupling of 2-pyridine carboxylic acid with n-propanolamine yielded the amide **50**. Carbon tetrabromide and triphenylphosphine were used to brominate the alcohol, and the resulting bromoalkane **51** was reacted with 1,4,7-tris(*tert*-butoxycarbonylmethyl)-1,4,7,10-tetraazacyclododecane **48** in the presence of base. The t-butyl protecting groups were then removed from the tetra-substituted cyclen **52** with TFA, and the desired ligand L^6 was complexed with the lanthanide ion (Scheme 3.3).

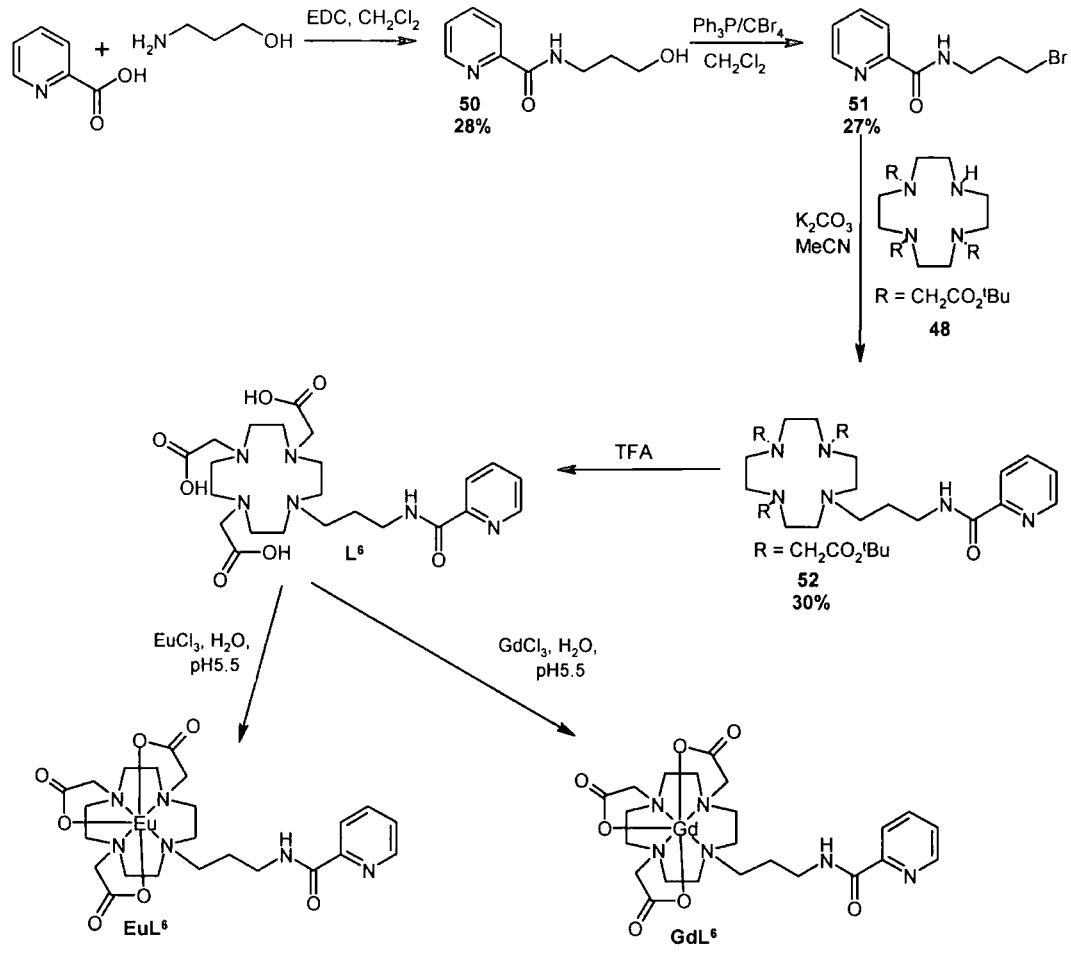

Scheme 3.3 Synthesis of Lanthanide (III) Complexes of L^6.

These four complexes were then studied using various physicochemical techniques to establish the speciation and constitution of the complexes in solution and determine whether the ethyl or propyl linkage gives rise to more appropriate properties in the desired lanthanide complex.

3.3 Emission excited state lifetimes of Eu (III) complexes: evaluation of hydration state, q.

The number of water molecules (q) coordinated to the europium ion was assessed by measuring the rate constants for the depopulation of the Eu $^5D_0$ excited states in H_2O (k_{H_2O}) and D_2O (k_{D_2O}) and applying equation (3.1), where x is the number of exchangeable amide NH groups bound to the europium (III) ion.[61,123]

$$q_{Eu} = \Delta\left(k_{H_2O} - k_{D_2O} - (0.25) - (0.075x)\right) \qquad (3.1)$$

Table 3.1 Rate decay constants and number of bound waters at pH 7 of complexes [EuL^5] and [EuL^6]. The values of q obtained assumes that the amide nitrogen is not bound to the europium centre.

Complex	k_{H_2O} (ms^{-1})	k_{D_2O} (ms^{-1})	q_{Eu}
[EuL^5]	1.65	0.47	1.11
[EuL^6]	0.87	0.58	0.04

The hydration state of the europium (III) centre changes with ligand. The q values obtained (Table 3.1), show that there is one water molecule bound to the europium (III) centre in **[EuL^5]** whereas **[EuL^6]** has no bound water. The parent systems **[EuDOTA]$^-$** and **[EuDO3A]** are known to form q = 1 and q = 2 complexes respectively.[92] As the hydration state for **[EuL^6]** is q = 0, the pyridyl amide group must be binding to the europium (III) centre giving rise to considerable steric demand at the Eu (III) centre, thereby preventing water from binding. It is also worth noting that in the 14-N_4-tetraacetate complex, **[EuTETA]$^-$**, no water is bound to the Eu (III) ion.[124] This has been ascribed to the increased steric demand imposed by the introduction of the two six-ring chelates of the macrocyclic ring (Table 3.2).

Table 3.2 [EuTETA]$^-$, [EuDOTA]$^-$ and [EuDO3A] are q = 0, q = 1 and q = 2.

[EuTETA]$^-$	[EuDOTA]$^-$	[EuDO3A]
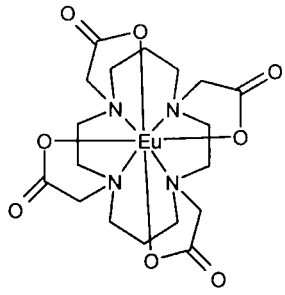	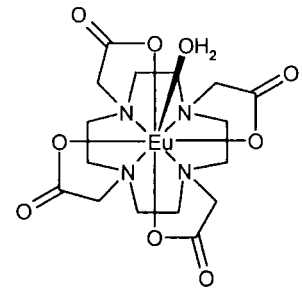	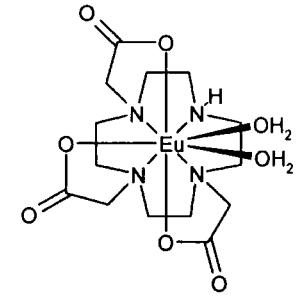
q = 0	q = 1	q =2

Caravan *et al.*[92] found that alcoholic oxygen, pyridyl nitrogen and amide oxygen donor atoms (X) gave rise to the greatest contribution to the increase in stability to lanthanide (III) chelation of the neutral donors that they investigated (Scheme 3.4). Table 3.3 details the relative affinities of different donor atoms for Ln(III) ions; here, Δlog K refers to the free energy difference in binding after taking into account the difference in ligand basicity.

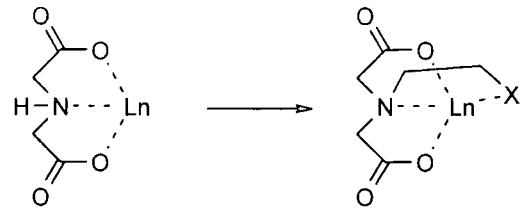

Scheme 3.4

Table 3.3 Relative affinity of different donor atoms for Ln(III) ions.[92]

	Δ log K
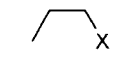	
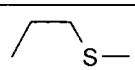	0.0
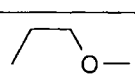	1.6
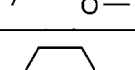	2.9
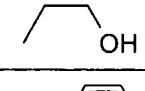	3.3
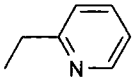	3.38

Although pyridyl nitrogen and amide oxygen have been shown to have a relatively high affinity for lanthanide (III) ions, this is in a 5-membered ring chelate system. The ligands L^5 and L^6 cannot form 5-membered chelate rings between either the pyridyl nitrogen or the amide oxygen. In the case of **[EuL^5]**, a seven-membered chelate ring could exist between the amide oxygen or an eight membered ring with the pyridyl nitrogen; and in the case of L^6, an eight-membered chelate ring would have to form between the amide oxygen or a nine membered ring with the pyridyl nitrogen. Nevertheless, the lifetime studies are consistent with the intramolecular coordination, in each case. The nature of this coordination was therefore studied further.

3.3.1 Variation of Lifetime with pH.

The lifetimes of the europium (III) complexes L^5 and L^6 were measured in water at pH 4 and 7. If the pyridyl nitrogen were reversibly bound to the lanthanide centre, protonation at low pH would result in the pyridyl group no longer being ligated to the europium and an increase in the hydration state would be expected to result.

Table 3.4 Rate decay constants (k_{H_2O}, ms^{-1}) of [EuL^5] and [EuL^6] at pH 4 and 7

pH	k_{H_2O} (ms^{-1})	
	[EuL^5]	[EuL^6]
4	1.73	0.92
7	1.65	0.87

From the lifetime values given in Table 3.4, it can be seen that there is no significant variation of lifetime with pH. Thus it can be concluded that the number of water molecules bound to the europium (III) centre (q) does not vary with pH over the range studied, and the pendant group does not bind to the europium (III) centre in a pH dependent manner.

3.3.2 Effect of Zinc (II) Concentration on Lifetime

Pyridyl and amide groups can each coordinate to zinc (II) either independently or as a chelate. If zinc (II) coordination occurred in **[EuL^6]**, a 5-membered chelate ring system would form, similar to that observed in the zinc (II) complexes of L^1 - L^4. Zinc (II) acetate was added to solutions of the europium complexes **[EuL^5]** and **[EuL^6]**. Formation of a zinc complex, **Zn[EuL]$_2$**, was postulated as in Scheme 3.5. The bound zinc (II) might then inhibit the pyridyl amide from binding to the europium (III) centre and instead allow water to bind to the europium. The increase in the number of bound water molecules, in turn, would result in an decrease in the measured Eu (III) excited state lifetime.

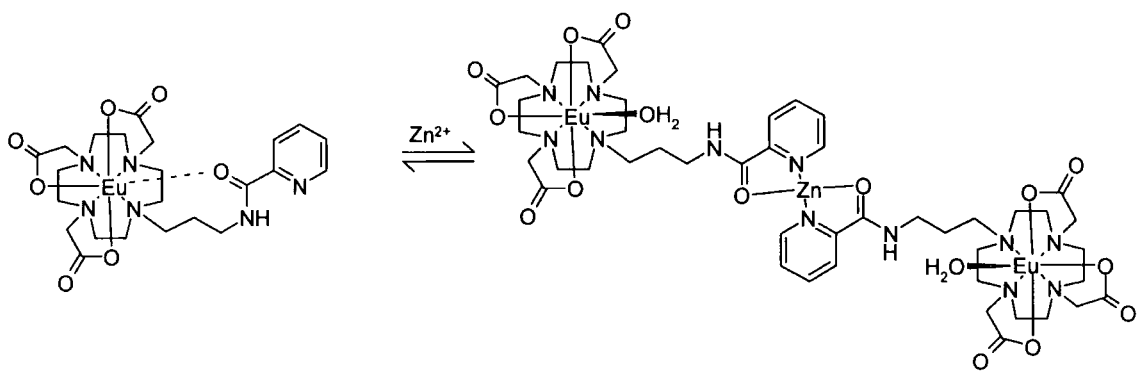

Scheme 3.5 Proposed mechanism for the binding of Zn (II) to [EuL^6], resulting in the coordination of water to the europium centre and so causing a decrease in excited state lifetime.

The lifetimes of the europium complexes **[EuL^5]** and **[EuL^6]** were measured at pH 4 and 7 in the presence of 10 equivalents of zinc (II) acetate.

Table 3.5 Rate decay constant of [EuL^5] and [EuL^6] in the presence of 10 equivalents of Zn (II) at pH 4 and 7.

pH	k_{H_2O} (ms^{-1})	
	[EuL^5]	**[EuL^6]**
4	1.76	0.96
7	1.64	0.91

The k_{H_2O} values obtained at different pH values (Table 3.5) in the presence of zinc (II) show that the lifetime does not vary with changing zinc (II) concentration. The **[EuL^5]** complex remains a mono-aqua species and **[EuL^6]** remains q = 0. This suggests that in the case of **[EuL^6]**, the pyridyl amide group must be strongly coordinated to the europium centre in an irreversible manner, preventing coordination of water to the europium centre.

3.4 Luminescence studies of [EuL^5] and [EuL^6].

Examination of the form and relative band intensity in europium (III) emission spectra following direct (λ_{exc} 397 nm) or sensitised (λ_{exc} 268 nm) excitation can be used to provide further information about the coordination environment at the lanthanide centre.[125,126]

Comparison of the emission spectra of **[EuL^5]** and **[EuL^6]** (Figure 3.1) reveals an increase in the relative intensity of emission of the ΔJ = 2 transition, centred at 616 nm, for **[EuL^6]** in comparison with **[EuL^5]**. The ΔJ = 2 band provides information about the nature of the axial donor binding to the europium. In general, the more polarisable the axial donor, the greater the ratio of the intensity of the $\Delta J = 2/\Delta J = 1$ bands. This increase in intensity is consistent with the different hydration states in the two complexes. An enhanced relative intensity of emission would be expected for **[EuL^6]** as there are no water molecules bound to the europium (III) centre. In contrast **[EuL^5]** has one bound water molecule, which would not only quench the overall Eu (III) emission, resulting in a decrease in the

total emission intensity, but also has been characterised by a low $\Delta J = 2/\Delta J = 1$ intensity ratio for several related mono-aqua complexes.[125]

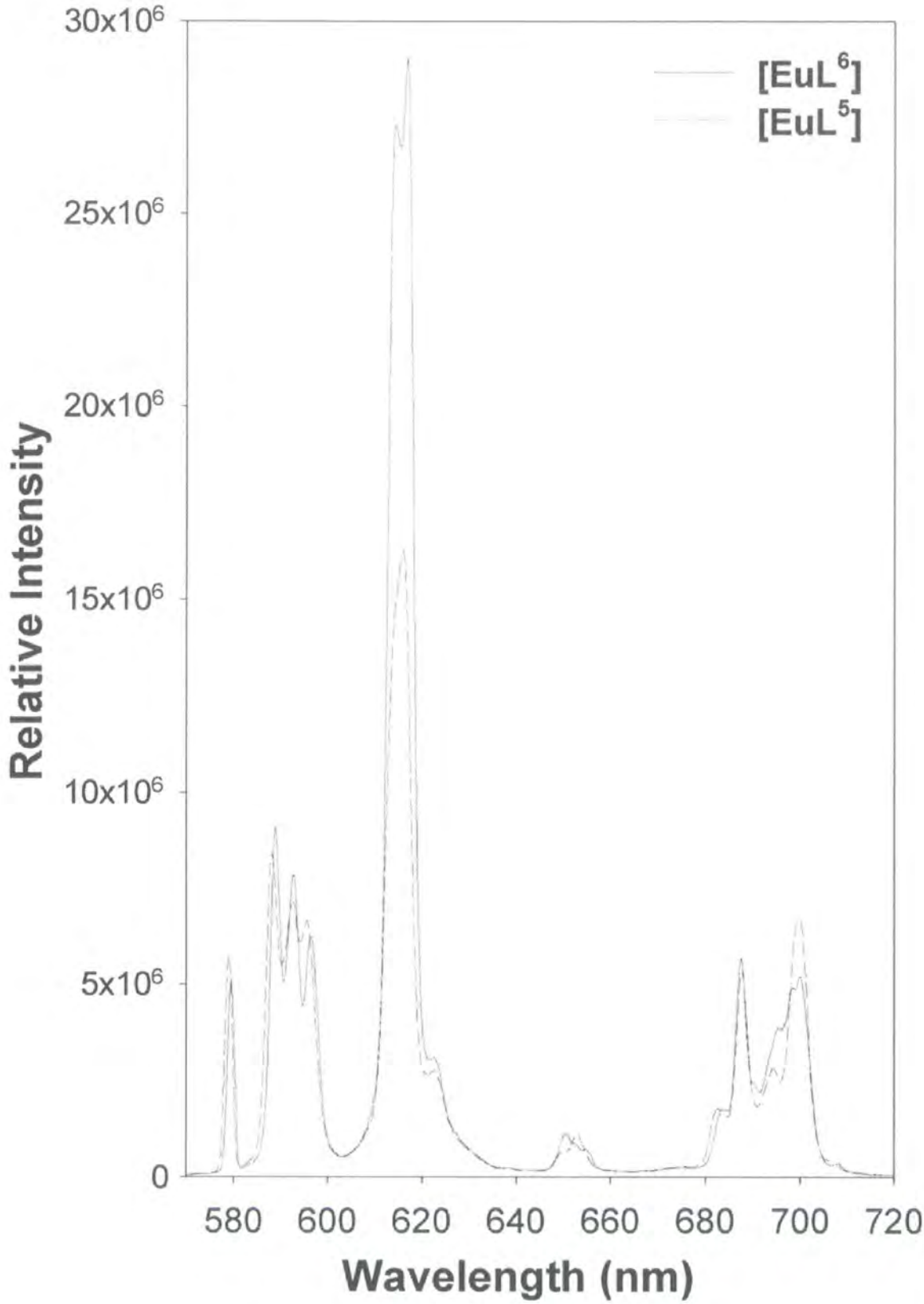

Figure 3.1 Emission spectra of [EuL^5] and [EuL^6], λ_{exc} = 268nm.

3.4.1 Effect of pH on luminescence

Measurements of lifetimes at various pH values had shown that there was no change in the hydration state of **[EuL^6]**. This was confirmed by changing the pH and recording the emission spectrum. No change in the spectral form was observed between pH 4 and 9 with direct or sensitised excitation, confirming that the europium (III) coordination environment was not changed.

3.4.2 Effect of Zinc (II) on luminescence

Emission spectra were also used to confirm that there was no change in the hydration state of **[EuL^6]** with increasing added zinc (II) concentration. Zinc (II) acetate solution was added in small aliquots containing one equivalent, until 10 equivalents had been added. No change was observed in the spectral form with direct or sensitised excitation at either pH 4 or pH 7. It can therefore be concluded that **[EuL^6]** remains q = 0, i.e. unhydrated, in the presence of an excess of Zn (II) ions.

3.4.3 Dilution Effects

For **[EuL^6]** to be a q = 0 complex, part of the pyridyl amide subsituent must be binding to the europium (III) centre. As seven (C=O) or eight (pyridyl N) membered chelate rings are not usually formed, intermolecular binding was considered to be a possibility.

Recording the emission spectra with sensitised emission at increasingly dilute concentrations might result in a change in the spectral form when the concentration fell below the binding affinity of the pyridyl amide of one complex to the europium (III) centre of another.

Dilution of a solution of **[EuL^6]** from 250 μM to 7.3 μM resulted in a decrease in the overall intensity of the observed emission spectrum, but no change to the spectral form was observed. This suggests that the antennae group is bound to the europium (III) centre intramolecularly. If the antennae group was bound intermolecularly, a change in the spectral form might have been expected.

Electrospray mass spectrometry suggests that it is possible that a high affinity dimer has formed. However, this is seems unlikely as the dissociation constant would be $K_d < 10^{-6}$ M; anions have been to have a much lower affinity than this for lanthanide centres, ca. 10^{-4} M.[64]

3.4.4 Sensitised [EuDO3A] emission with a pyridyl chromphore

Compound **50**, which contains the chromophore in **[EuL^5]** and **[EuL^6]**, was added to a solution of **[EuDO3A]** and the sensitised emission spectrum was recorded. If **50** is a good donor for europium (Scheme 3.6) then it was hypothesised that it might coordinate in solution and sensitised emission would occur when the excitation wavelength matched the absorption spectral profile of the chromophore.

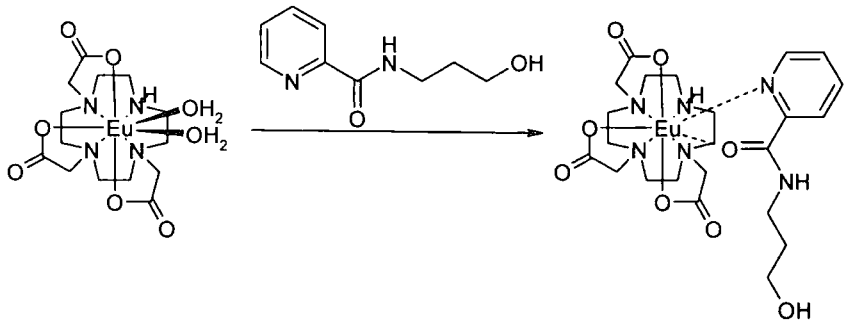

Scheme 3.6 Proposed method of coordination of pyridyl chromophore 50 to [EuDO3A] allowing sensitised emission (λ_{exc} = 268 nm) to occur.

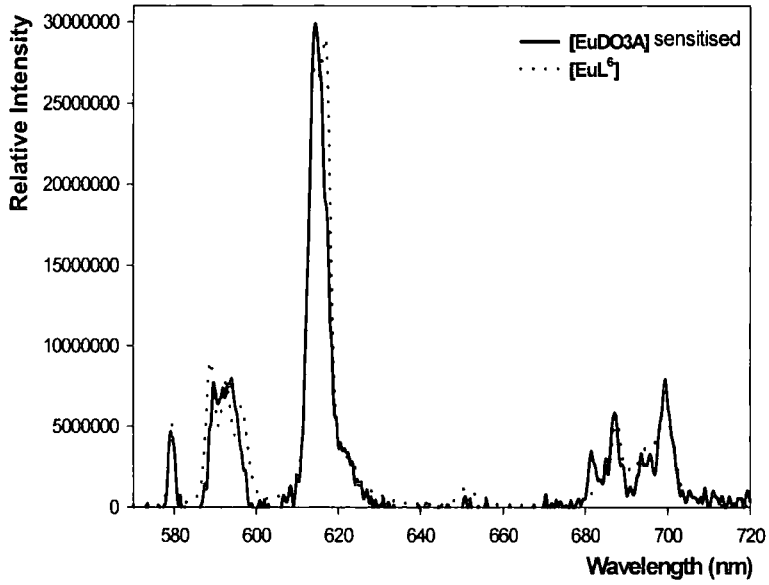

Figure 3.2 Emission spectrum of [EuDO3A] sensitised with one equivalent of pyridyl amide (50) scaled to compare with [EuL^6]. λ_{exc} = 268nm, 315 nm filter.

The spectrum obtained for the sensitised emission of **[EuDO3A]** and one equivalent of **50**, when put on the same scale as the emission spectra of **[EuL^6]** (Figure 3.2), shows that there is a striking similarity in the spectral form of **[EuL^6]** and **[EuDO3A]** sensitised with **50**. However, the spectrum for **[EuDO3A]** is of poorer resolution. The ΔJ = 2 band, which is most sensitive to axial coordination, is of a similar form and relative intensity suggesting that the pyridyl amide group coordinates to the europium centre in the same way, irrespective of whether it binds intermolecularly or intramolecularly.

3.5 Relaxivity Behaviour of the Gadolinium Complexes

The relaxivity (r_{1p}) of the gadolinium (III) complexes describes the bulk water proton relaxation rate per mmol of complex. The magnitude of the measured relaxivity gives an indication of the number of water molecules bound to the gadolinium (III) centre. Information on water exchange rates is usually deduced in separate studies measuring the ^{17}O transverse relaxation rate as a function of temperature.

The relaxation rate (R_{1p}) was determined from the measured T_1 values via equations 3.2 and 3.3. Proton T_1 values were measured using either a Bruker Minispec mq60 NMR analyser, which operates at 37.0°C and 60 MHz, or using a homemade 65 MHz NMR machine, which operates at ambient temperature (22°C).

$$\frac{1}{T_1^{obs}} = R_1^{obs} = R_{1p} + R_{1d} \tag{3.2}$$

$$R_{1p} = \frac{1}{T_1^{obs}} - \frac{1}{T_1^{diamag}} \tag{3.3}$$

The diamagnetic contribution to water relaxation was determined from a dilution series of a gadolinium standard and the values used were 0.26 s^{-1} (60 MHz, 37°C) and 0.38 s^{-1} (65 MHz, 22°C).

The concentration of the relaxivity samples were determined by digesting them in 2.5 M nitric acid. The relaxivity of gadolinium (III) in 2.5 M nitric acid was determined to be 8.74 $mmol^{-1}s^{-1}$ with a diamagnetic correction factor of 0.24 s^{-1} at

60 MHz, 37°C, compared to 11.66 $mM^{-1}s^{-1}$ with a diamagnetic correction factor of 0.40 s^{-1}, at 65 MHz, 22°C).

The relaxivity was determined by equation 3.4.

$$r_{1p} = \frac{R_{1p}}{[Gd]} \tag{3.4}$$

3.5.1 Relaxivity of [GdL^5] and [GdL^6]

The relaxivities of **[GdL^5]** and **[GdL^6]** were determined at both 60 MHz and 65 MHz (Table 3.6).

Table 3.6 Relaxivities of gadolinium (III) complexes at pH 7.

Complex	Relaxivity ($mM^{-1}s^{-1}$)	
	60 MHz, 37°C	65 MHz, 22°C
[GdL^5]	2.89	3.50
[GdL^6]	2.18	2.45

The relaxivity values obtained for **[GdL^5]** are higher than those obtained for **[GdL^6]**, which is consistent with the higher hydration state of **[GdL^5]**. The values obtained at the measured field and temperatures lie within the expected range for low molecular weight gadolinium systems with q = 1 and q = 0 hydration states for **[GdL^5]** and **[GdL^6]** respectively.[92]

The relaxivity values obtained at 37°C are consistently lower than those obtained at 22°C because under conditions of fast water exchange, relaxivity is inversely proportional to temperature, as it depends primarily on the rotational correlation time, τ_R, of the whole complex.

3.5.2 Variation of Relaxivity with pH

The relaxivity of gadolinium (III) complexes **[GdL^5]** and **[GdL^6]** was measured at pH 4, 7 and 9 at 37°C and 60 MHz using the Bruker Minispec mq60.

Table 3.7 Variation of relaxivity (60 MHz, 37°C) of complexes [GdL^5] and [GdL^6] with pH.

pH	Relaxivity ($s^{-1}mmol^{-1}l$)	
	[GdL^5]	[GdL^6]
4	3.14	3.16
7	2.89	2.30
9	2.83	2.25

The relaxivity of both **[GdL^5]** and **[GdL^6]** increased slightly at low pH (Table 3.7). This could be caused by the onset of protonation of the pyridine, resulting in an increased second sphere of hydration around the gadolinium centre and hence an increase in the observed relaxivity.

3.5.3 Zinc (II) Dependence of Relaxivity

The relaxivity of both **[GdL^5]** and **[GdL^6]** was measured in 0.1 M MOPS buffer at pH 7.4, in the presence of increasing zinc (II) concentration, using the Bruker Minispec mq60 (Table 3.8).

Table 3.8 Relaxivity (60 MHz, 37°C) of complexes [GdL^5] and [GdL^6] in the presence of 1 and 10 equivalents of Zn(II) acetate at pH 7.4.

Relaxivity ($mM^{-1}s^{-1}$)			
[GdL^5]		[GdL^6]	
1 equiv Zn	10 equiv Zn	1 equiv Zn	10 equiv Zn
2.89	2.96	2.24	2.38

The **[GdL^5]** complex shows no change in the relaxivity with increasing Zn (II) concentration. As the complex is a q = 1 species, the observed relaxivity is dominated by the inner sphere effect.

A small but significant increase can be seen in the relaxivity of **[GdL^6]** with increasing zinc (II) concentration. Titration of small aliquots of zinc acetate solution (1.88 µl, 5 mM), containing one equivalent of zinc (II), into a solution of **[GdL^6]** (200 µl, 0.47 mM) in 0.1 M MOPS buffer at pH 7.4 (Figure 3.3), shows that the relaxivity (60 MHz, 37°C) increases most significantly with the addition of between

one and five zinc (II) equivalents and then reaches a saturation value. Such behaviour may be associated with weak binding between **[GdL^6]** and Zn (II). By assuming a 1 : 1 binding model, an estimated apparent binding constant of 0.53 mM^{-1} was calculated by iterative least squares fitting.

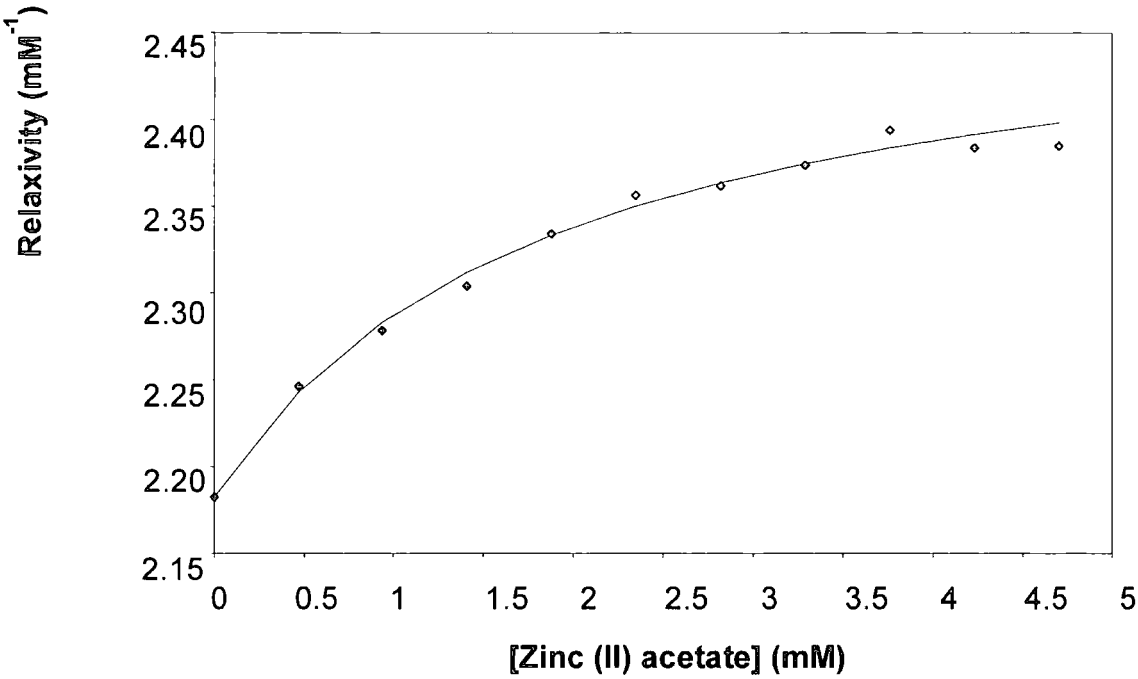

Figure 3.3 Increase in relalaxivity of [GdL^6] (0.47mM) with increasing zinc (II) concentration. (60 MHz, 37°C).

The 65 MHz NMR machine at 22 °C was also used to determine the relaxivity of **[GdL^6]** at 0.5 mM and 11.5 mM concentration in the presence of 10 equivalents of zinc (II). At each concentration investigated, the relaxivity of **[GdL^6]** increased from 2.4 $mM^{-1}s^{-1}$ (65 MHz, 22 °C) to 4.3 mM^1s^{-1} in the presence of 10 equivalents of zinc (II) acetate. As a control, 10 equivalents of sodium acetate were added to another sample of **[GdL^6]**. The relaxivity was relatively unchanged at 2.5 $mM^{-1}s^{-1}$ (65 MHz, 22 °C). The **[GdL^6]** complex shows a 75% increase in relaxivity at this temperature in the presence of zinc (II). As the addition of sodium acetate caused no change in the relaxivity, it can be concluded that there is no anion binding effect. The increase in relaxivity can be ascribed to outer sphere binding of zinc (II) to the complex, which markedly changes the local hydration of the complex, resulting in an increase in the relaxivity. From studies with the europium analogue, it was

earlier shown that the q value does not change in the presence of added Zn (II) ions. The increase in the relaxivity is therefore most likely to be an outer sphere effect.

The relaxivity increase in the presence of zinc (II) is greater than that shown by the only published zinc (II) sensitive contrast agent, **39**, which has a maximum decrease in relaxivity of 33% in the presence of one equivalent of Zn (II).[84] This relaxivity change has also been ascribed to the binding of Zn (II), presumable caused by a change in the second sphere hydration state.[62]

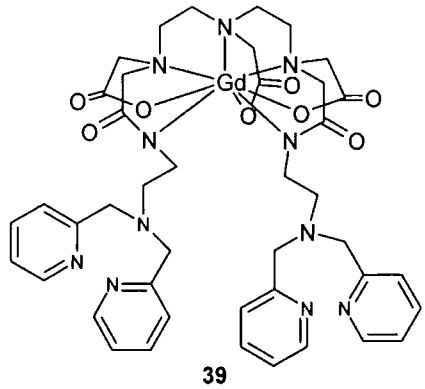

39

Large changes in relaxivity have been reported for other cases of q = 0 complexes, as a consequence of 'outer sphere' binding. Examples of this include the tetrabenzylphosphinate **53**[127] in which the steric bulk of the phosphinate groups above the complex prevents the coordination of water molecules to the gadolinium centre, rendering it a purely outer sphere complex. The relaxivity has no inner sphere component and the NMRD profile represents the archetypal case of a complex exhibiting only 'outer sphere' relaxivity.

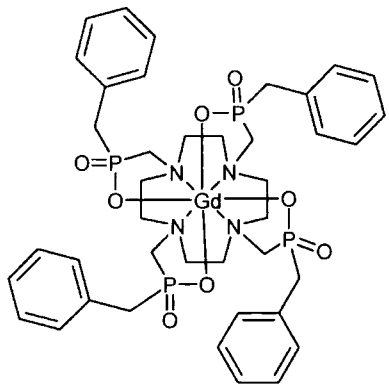

53

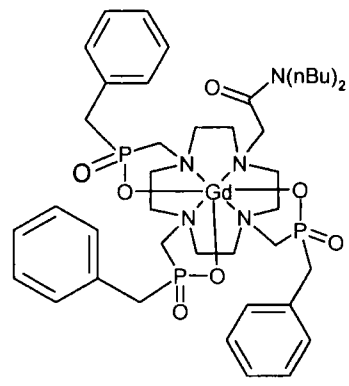

54

Substitution of one of the phosphinate groups with a less bulky carboxamide e.g. **54** favours the access of water to the paramagnetic centre.[128,129] The NMRD profile obtained has a shape typical of a q = 1 complex but the magnitude is significantly lower. A small hump in the NMRD profile at 100 MHz characterises a dependence of the relaxivity on the rotational dynamics (τ_R) of the complex. The increase in the relaxivity on passing from the pure outer sphere system **53** to **54** can be assigned to the presence of a tightly bound water molecule in the second coordination sphere with a long coordination lifetime.[128] The water molecule was proposed to be hydrogen bonded to the carboxamide oxygen atom, resulting in a metal proton distance that is sufficiently short to markedly affect the relaxivity.

A divalent calcium-sensitive MRI contrast agent DOPTA-Gd **40** developed by Meade and co-workers,[83] has a relaxivity increase of 77% from 3.26 $mM^{-1}s^{-1}$ to 5.76 $mM^{-1}s^{-1}$ (25°C, 500 MHz) following addition of micromolar concentrations of calcium (II).

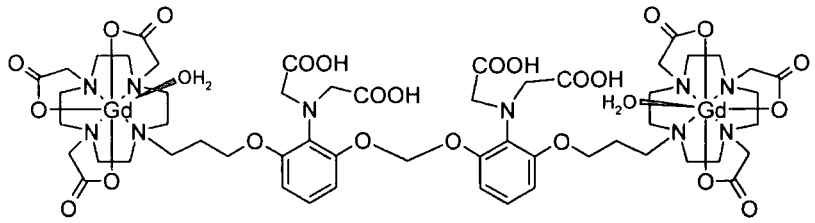

40
DOPTA-Gd

It has been proposed that the metal ion chelation perturbs the second sphere rather than the inner sphere water molecules, causing the increase in relaxivity,[62] although Meade *et al.* were unaware of this in their original publications[83] where they postulated changes in the coordination environment at the gadolinium centre, without any experimental proof.

3.6 NMRD Profiles of Complexes [GdL^5] and [GdL^6].

Nuclear Magnetic Resonance Dispersion (NMRD) profiles which record the magnetic field dependence of relaxivity were recorded in Durham at 25°C (Figure 3.4) and at 37°C using a Stelar field-cycling relaxometer. The NMRD profiles were fitted (Table 3.9) by Professor Mauro Botta and Dr Eliana Gianolio at the Universitá

di Torino based on the following theoretical arguments, and using ^{17}O data to determine τ_M (Section 3.7).

The relaxation rate of inner sphere water, R_{1p}^{His}, arises from the exchange of the metal-bound waters and is given by:

$$R_{1p}^{His} = \frac{Cq}{55.6} \frac{1}{T_{1M}^{H} + \tau_M^H} \tag{3.5}$$

where C is the concentration of the Gd (III) complex in mM; q is the number of metal bound water molecules and τ_M^H is their residence lifetime.

T_{1M}^H is the longitudinal relaxation time of the inner-sphere water protons and is given by:

$$\frac{1}{T_{1M}^H} = \frac{2}{15} \frac{\gamma_H^2 g_e^2 \mu_B^2 S(S+1)}{r_H^6} \left[\frac{3\tau_{c1}}{1+\omega_H^2 \tau_{c1}^2} + \frac{7\tau_{c2}}{1+\omega_S^2 \tau_{c2}^2} \right] \tag{3.6}$$

where S is the electron spin quantum number (7/2 for Gd(III)); γ_H the proton nuclear magnetogyric ratio; μ_B the Bohr magneton; g_e the Landè factor for the free electron; r_H the distance between the metal ion and the inner-sphere water protons; ω_H and ω_S the proton and electron Larmor frequencies ($\omega_S = 658\ \omega_H$) respectively and τ_{ci} ($i = 1,2$) the correlation times related to the modulation of the electron-proton dipolar coupling. The modulation may occur by the reorientation of the paramagnetic species, τ_R, by the water exchange with a rate $k_{ex} = 1/\tau_M$ and by the electron relaxation , T_{iE}:

$$\tau_{ci}^{-1} = \tau_R^{-1} + \tau_M^{-1} + T_{iE}^{-1} \tag{3.7}$$

For Gd(III) complexes T_{1E} and T_{2E} are related to the modulation of the zero field splitting (ZFS) of the electronic spin states due to the dynamic distortions of the ligand field interaction and, according to the Bloembergen-Morgan theory,[74] their magnetic field dependence is given by the following equations:

$$\left(\frac{1}{T_{1e}}\right)^{ZFS} = \frac{1}{25} \Delta^2 \tau_v \{4S(S+1) - 3\} \left(\frac{1}{1+\omega_s^2 \tau_v^2} + \frac{4}{1+4\omega_s^2 \tau_v^2} \right) \tag{3.8}$$

$$T_{2r}^{-1} = \frac{1}{50}\Delta^2\tau_v\left[4S(S+1)-3\right]\left(3+\frac{5}{1+\omega_S^2\tau_v^2}+\frac{2}{1+4\omega_S^2\tau_v^2}\right) \qquad (3.9)$$

where Δ^2 is the the square of the average (transient) ZFS tensor and τ_V the correlation time related to its modulation. The outer sphere term, R_{1p}^{Hos}, describes the contribution arising from the water molecules diffusing near the paramagnetic chelate and, according to the Freed model,[75] may be related to the minimum distance between the metal and the diffusing water molecules, a, the relative solute-solvent diffusion coefficient, D, and the electronic relaxation times, T_{iE}:

$$R_{1p}^{Hos} = C^{os}\left(\frac{1}{aD}\right)\left[7J(\omega_S)+3J(\omega_H)\right] \qquad (3.10)$$

where C^{os} is a constant (5.8×10^{-13} $s^{-2}M^{-1}$) and the dependence on the electronic relaxation times is expressed in the non-Lorentzian spectral density functions $J(\omega_i)$.

Figure 3.4 Experimental NMRD profiles for [GdL^5] (solid squares) and [GdL^6] (open squares) in aqueous solution (pH 6) The values were all obtained at 25°C with the exception of the 65 MHz values which were obtained at 22°C. The solid lines through the data are best-fitting curves obtained using the above theory, using parameters given in Table 3.9.

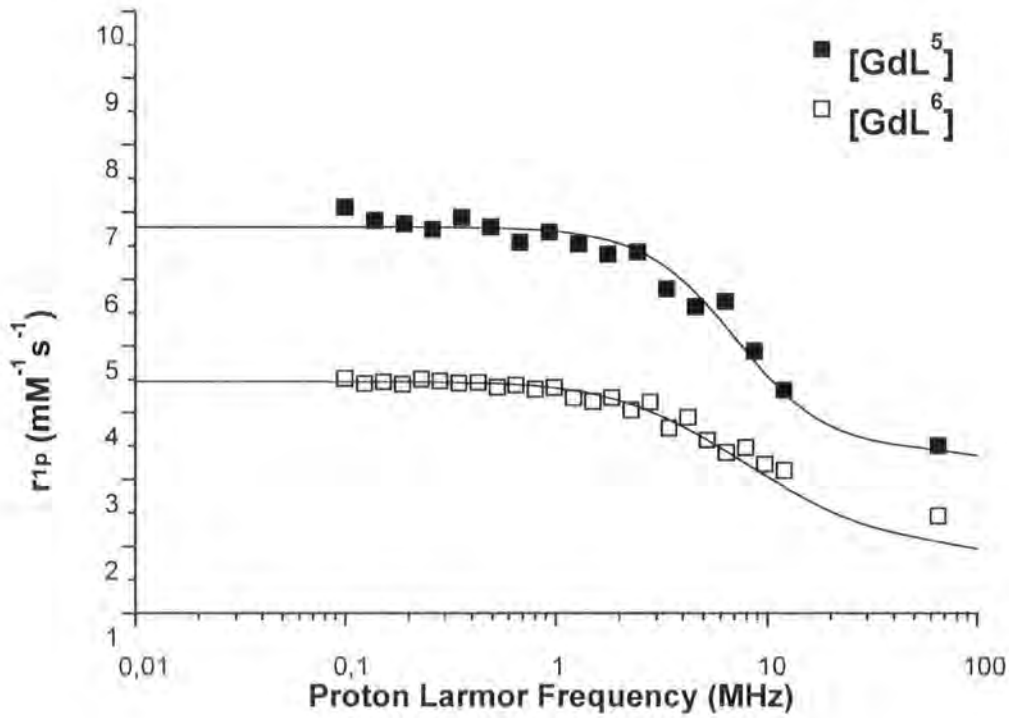

Table 3.9 **Best fitting parameters obtained from the analysis of the NMRD profiles for the gadolinium (III) complexes [GdL^5] and [GdL^6] at 25°C and pH 6.**

Complex	q	Δ^2 ($s^{-2}x10^{19}$)	τ_v (ps)	τ_R (ns)	r (Å)	a (Å)	D($cm^2s^{-1}x10^{-5}$)
[GdL^5]	1	5.6	16	54	3.13	4	2.24
[GdL^6]	0	4	12.9	54	-	3.7	2.24

[GdL^5] has an NMRD profile (Figure 3.4) typical of a small Gd^{3+} complex possessing a single coordinated water molecule. Fitting of the data (Table 3.9) shows that the gadolinium (III) to water proton distance is quite long, 3.13 Å. The gadolinium (III) to outer water distance is 4 Å, which is consistent with the inner and outer sphere water molecules being hydrogen bonded together.

Fitting of the data for **[GdL^6]** shows the complex to be q = 0, whilst the profile obtained for **[GdL^5]** has a shape characteristic of a low molecular weight Gd (III), q = 1 complex. However, the magnitude of relaxivity across the entire magnetic field range, is lower than typically expected for a q = 1 complex. The relaxation behaviour of **[GdL^6]** is however inconsistent with purely outer-sphere properties. The Gd-H distance of coordinated water molecules has been estimated as 3.7 Å, which is shorter than the distance that would be expected in a purely outer sphere complex.[69,92] It can probably be accounted for by hydrogen bonding of the water molecules in the second hydration sphere to the pyridyl amide group. This would result in the water being bound at an equilibrium distance from the metal that is longer than in inner sphere complexes, but the residence lifetime, τ_M, is significantly longer than the time necessary for the solute and solvent to diffuse apart. Such behaviour is reminiscent of the monoamide triphosphinate gadolinium complexes described in section 3.5.3.

3.7 Variable Temperature ^{17}O NMR Studies

The temperature dependence of the solvent water ^{17}O transverse relaxation rate can provide information about the hydration number and the water exchange rate.[60,128,129] The residence lifetime of a water molecule directly coordinated to a paramagnetic metal ion (τ_M^O) may be evaluated by measuring the temperature

dependence of the paramagnetic contribution (R_{2p}^{O}) to the observed ^{17}O water solvent transverse relaxation rate:

$$R_{2p}^{O} = R_{2obs}^{O} - R_{2d}^{O} \tag{3.11}$$

where, by analogy with the relaxivity, R_{2d}^{O} is the diamagnetic term. R_{2p}^{O} is related to τ_M^O through the values of $\Delta\omega_M^O$ (the ^{17}O chemical shift difference between coordinated and bulk water resonances) and R_{2M}^{O} (the transverse relaxation rate of the coordinated water oxygen):

$$R_{2p}^{O} = \frac{qC}{55.6}\tau_M^{O\,-1}\frac{R_{2M}^{O\,2} + \tau_M^{O\,-1}R_{2M}^{O} + \Delta\omega_M^{O\,2}}{\left(R_{2M}^{O} + \tau_M^{O\,-1}\right)^2 + \Delta\omega_M^{O\,2}} \tag{3.12}$$

The temperature dependence of $\Delta\omega_M^O$ is given by the following equation:

$$\Delta\omega_M^O = \frac{g_e\mu_B S(S+1)B_0}{3k_BT}\frac{A}{\hbar} \tag{3.13}$$

where B_0 is the magnetic field strength and $A/\hbar$ is the Gd-^{17}O scalar coupling constant which, for polyaminocarboxylate Gd(III) complexes, may be reasonably fixed to -3.8 x 10^6 rad s^{-1}.

For relatively small-sized Gd(III) chelate R_{2M}^{O} is dominated by the electron-nucleus scalar interaction:

$$R_{2M}^{O} = \frac{1}{3}\left(\frac{A}{\hbar}\right)^2 S(S+1)\left(\tau_{E1} + \frac{\tau_{E2}}{1+\omega_s^2\tau_{E2}^2}\right) \tag{3.14}$$

$$\tau_{Ei}^{-1} = T_{iE}^{-1} + (\tau_M^O)^{-1} \tag{3.15}$$

Finally, the temperature dependence of R_{2p}^{O} is expressed in terms of the Eyring relationship for τ_M^O and τ_V:

$$(\tau_j)_T^{-1} = \frac{\left(\tau_j^{-1}\right)^{298}T}{298}\exp\left[\frac{\Delta H_j}{R}\left(\frac{1}{298} - \frac{1}{T}\right)\right] \tag{3.16}$$

where j refers to the two different dynamic processes involved (j = v, M) and ΔH_j is the corresponding activation enthalpy.

3.7.1 ^{17}O Measurements of [GdL^5] and [GdL^6]

The ^{17}O linewidths were measured in Durham at 500 MHz and pH 6 over the temperature range 275 - 365 K for 21 mM and 32 mM solutions of complexes [GdL^5] and [GdL^6] respectively. The ^{17}O data were fitted (Figure 3.5 and Table 3.10) by Professor Mauro Botta and Dr Eliana Gianolio at the Universitá di Torino according to equations 3.11 - 3.16.

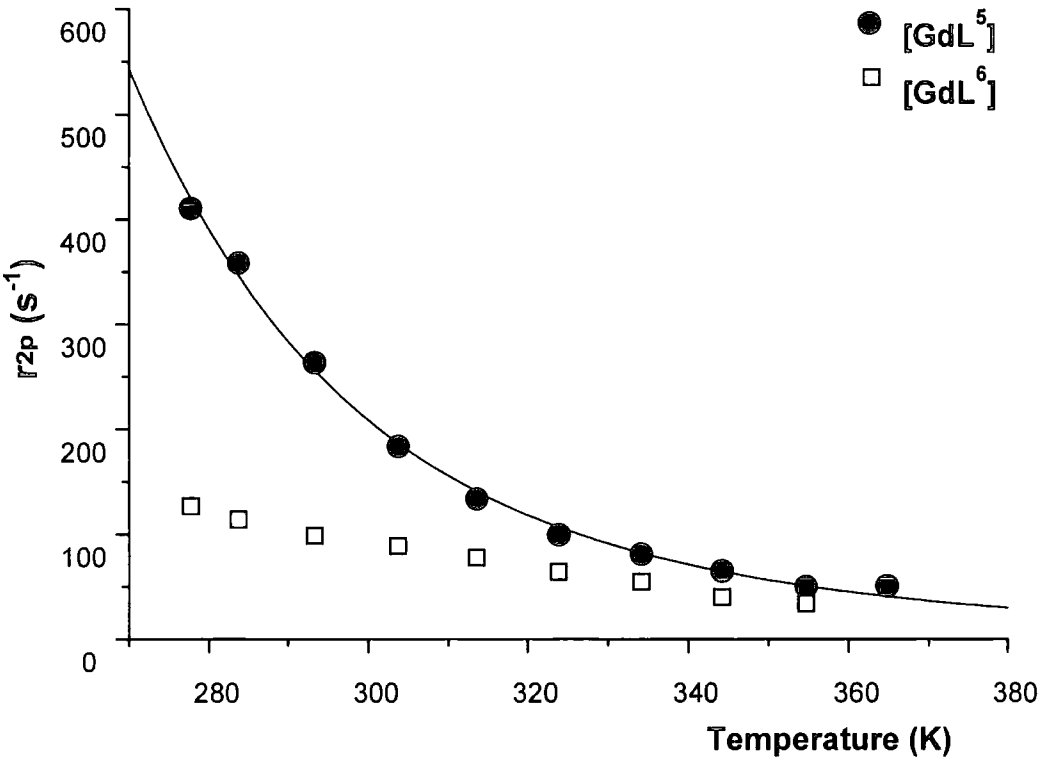

Figure 3.5 Temperature dependence of ^{17}O transverse relaxation rate at 500 MHz and pH 6 of [GdL^5] (21 mM) and [GdL^6] (32 mM). The line for [GdL^5] shows the fit to the experimental data.

Table 3.10 ^{17}O NMR best-fitting parameters obtained from the analysis of the temperature dependence of R_{2p} for 21 mM aqueous solution of [GdL^5]

Complex	q	Δ^2 ($s^{-2}x10^{19}$)	τ_v (ps)	τ_M (ns)	τ_R (ps)	r (Å)	ΔH_v ($kJmol^{-1}$)	ΔH_M ($kJmol^{-1}$)
[GdL^5]	1	5	14	8.6	55	2.50	2	21

[GdL^6] has no water molecules directly coordinated to the gadolinium (III) centre so the ^{17}O profile obtained for this complex is almost flat, i.e. no bound water is

present. The form of the ^{17}O profile (Figure 3.5) of **[GdL^5]** is consistent with fast water exchange. The calculated value of the mean residence lifetime, τ_M (25°C) for **[GdL^5]** is 8.6 ns which is very fast, indeed it is two orders of magnitude faster than occurs for $[Gd(DOTA)H_2O]^-$ (τ_M 244 ns, 25°C) and $[Gd(DTPA)H_2O]^{2-}$ (τ_M 303 ns, 25°C).[130] This suggests that the sterical demands of the pyridyl amide moiety result in a steric destabilisation of the Ln-water binding interaction which in turn causes fast water exchange to occur.

Systems with increased steric demands at the water binding sites have been shown by Merbach and coworkers[131,132,133] to exhibit increased water exchange rates. By the replacement of one five-membered NCCN ring of DOTA or a pendant arm of DTPA, by a more sterically demanding six-membered analogue they have synthesised systems that exhibit an exchange rate which is an order of magnitude faster than the parent system.

The fitted data also is consistent with the presence of a relatively long Gd-$\underline{O}H_2$ bond (2.50 Å). This is in agreement with the long Gd-H bond lengths derived from the fitting to the NMRD data.

3.8 Infra Red Spectroscopy

Infra red (IR) spectra of lyophilised samples of **[LnL^5]** and **[LnL^6]** were recorded in a KBr matrix and compared. The infra red spectra of the complexes of ligands L^5 and L^6 shows them to be virtually identical in the region 1750 - 1500 cm^{-1}, with a (coordinated) amide stretch at 1636 cm^{-1} (cf. 1660 cm^{-1} for the unbound amide carbonyl stretch). This would suggest that the amide carbonyl coordinates to the lanthanide centre in the same manner in each case. The pyridine ring vibrations have been tentatively assigned at 1591 and 1560 cm^{-1}. This is consistent with the absence of pyridine nitrogen ligation.[134]

3.9 Conclusions

Pyridyl amide groups in the studied complexes of L^5 and L^6 bind very well to both europium and gadolinium centres. In the case of **[LnL^6]**, the pyridyl amide binds irreversibly to the lanthanide centre, forming a kinetically stable q = 0 complex

which resists protonation and binds the central lanthanide ion more strongly than Zn (II). Inspection of molecular models confirms that the mode of binding is through the carbonyl oxygen, is relatively unstrained and accords with IR and emission luminescence studies.

Reducing the alkyl chain length linking the pyridyl amide to the macrocyclic ring nitrogen from propyl to ethyl, reduces the steric demand at the lanthanide centre, giving rise to a q = 1 complex. Molecular models confirm that because of the rigidity of the amide group it is not possible for the pyridyl nitrogen to bind to the lanthanide ion, but it is possible for the amide carbonyl oxygen to bind. The steric demands of this seven-membered chelate ring results in a steric compression of the water ligand binding site, causing the Ln-water bond to be long and the water exchange rate to be fast.

The relaxivity of **[GdL^6]** (65 MHz, 22°C) shows a 75% increase in the presence of excess added zinc (II). This increase is not an anion effect, a pH effect nor a result of a change in the gadolinium (III) inner sphere hydration state. The increase can be tentatively ascribed to the binding of zinc (II) to the complex resulting in an increase in the extent of complex hydration and thus an increase in the measured relaxivity.

Although neither of the complexes **[LnL^5]** or **[LnL^6]** showed a change in lanthanide coordination environment with changing pH or Zn (II) concentration, the presence of carboxyalkyl subsituents on the cyclen nitrogens instead of a DO3A type system along with a trifluoromethanesulfonamide group in the six position of the pyridine may prevent the pyridyl amide from binding so strongly to the lanthanide ion.

Both the ethyl and propyl linkage groups were therefore used to link the pyridyl sulfonamide to the central macrocycle for use in potentially pZn sensitive MRI probes and the results of these studies are discussed in the following chapter.

Chapter 4

pZn Responsive Lanthanide System

4 pZn Responsive Lanthanide System

4.1 Introduction

Having established the parent macrocyclic system with either ethyl or propyl amide groups linking the pyridyl moiety to the macrocyclic core, the parent zinc (II) binding trifluoromethanesulfonamide ligand, L^3, was incorporated into pyridyl sulfonamide appended macrocyclic system with the aim of providing a greater affinity for zinc (II), Figure 4.1.

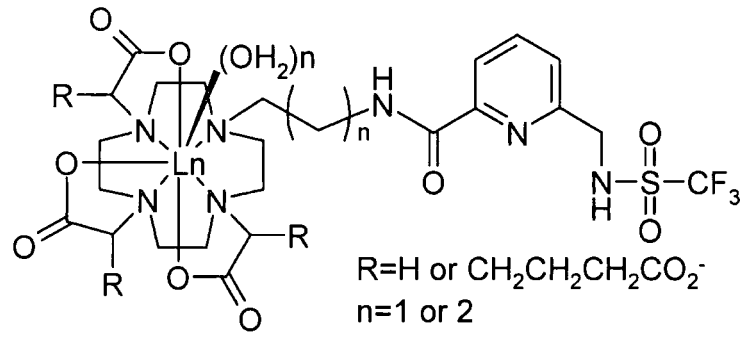

Figure 4.1 Pyridine trifluoromethanesulfonamide appended lanthanide complex.

This pyridyl trifluoromethanesulfonamide appended macrocyclic complex was intended to have pZn (II) responsive properties for potential MRI and luminescence applications. The amide carbonyl group had been shown in the parent systems **[LnL^5]** and **[LnL^6]** (Chapter 3) to ligate intramolecularly the lanthanide centre forming q = 1 and q = 0 systems respectively. Although these parent systems exhibited no reversible pZn dependent binding properties, it was hypothesised that the addition of the trifluoromethanesulfonamide group to the system would significantly increase the affinity of the pendant group for zinc (II).

The proposed mechanism through which **[LnL^8]** responds to increased concentrations of zinc (II) is illustrated in Scheme 4.1. The amide carbonyl was hypothesised to bind to the lanthanide (III) centre in a reversible manner in response to changes in zinc (II) concentration.

In the absence of Zn (II), the lanthanide (III) ion is eight coordinate and binding of water is inhibited by the presence of the carbonyl group.

Addition of zinc (II) to the system could result in the formation of a $[Zn(L^3)_2]$ type complex between the pendant arm and the free zinc (II) ions; the resulting complex will have 2 Gd^{3+} : 1 Zn^{2+}. The amide carbonyl was anticipated to participate in octahedral zinc (II) binding leaving a co-ordination site free on the lanthanide (III) ion for water to bind. The result was hypothesised to be a switching between a q = 0 and a q = 1 or 2 system, following the addition of zinc (II) ions.

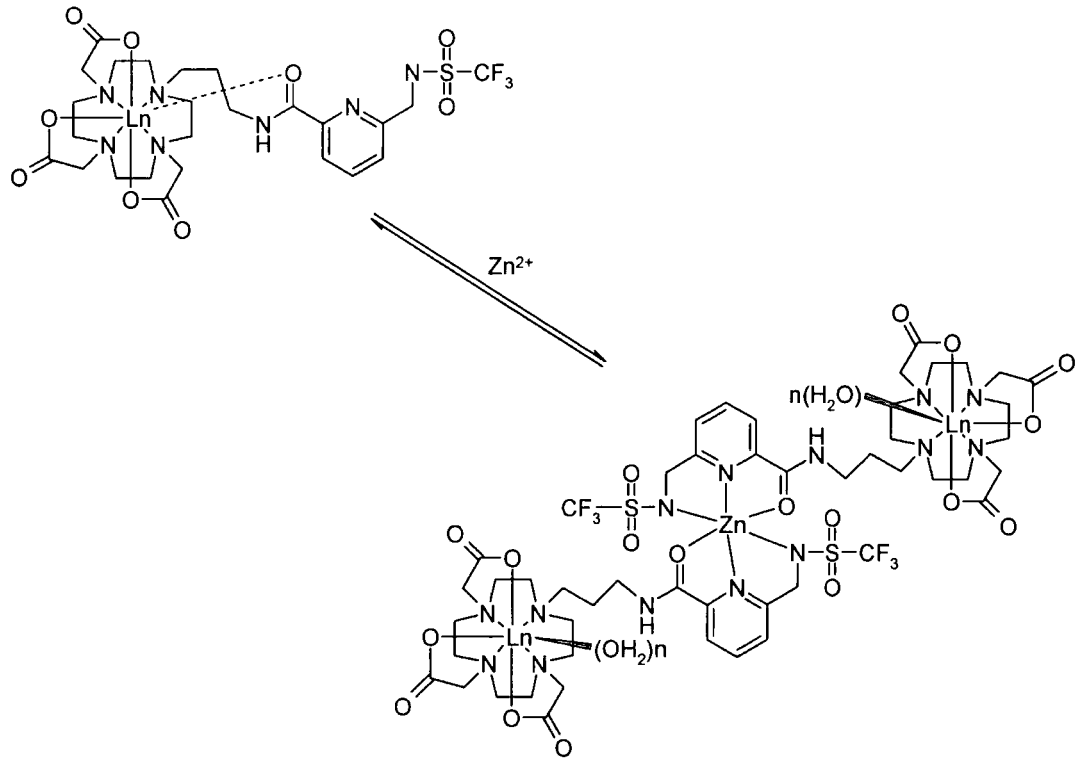

Scheme 4.1 Proposed mechanism through which [LnL^8] binds zinc (II) ions. The amide carbonyl participates in the octahedral ligation of Zn (II) resulting in an increase in the hydration state of the lanthanide centre.

The initial target complexes prepared to prove the concept were the Eu (III) and Gd (III) complexes of DO3A-derived ligands, L^7 and L^8. It was appreciated that when the complex was not intermolecularly ligated, then the binding of endogenous anions[64,77] or proteins might displace the bound waters and suppress the relaxivity of the Gd (III) complexes.[135] Therefore, the related ligands L^9 and L^{10} were also prepared (Figure 4.2). The presence of the carboxyalkyl subsituents had earlier been demonstrated to inhibit intermolecular anion binding at a coordinatively unsaturated lanthanide centre.[64]

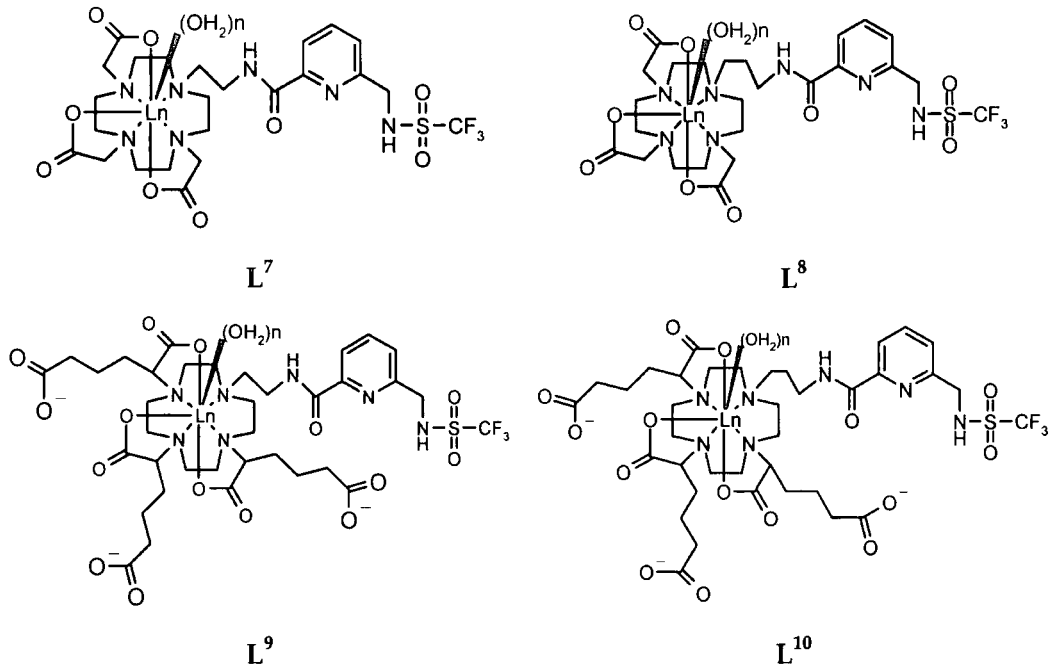

L^7 L^8

L^9 L^{10}

Figure 4.2 Target complexes [LnL^7], [LnL^8], [LnL^9] and [LnL^{10}].

4.2 Synthesis

The synthesis of ligands L^7, L^8, L^9 and L^{10} was more complicated than initially anticipated; many different routes were investigated before one was found which led to the production of the desired products.

The synthetic pathway started with the synthesis of pyridine-2,6-dicarboxylic acid diethyl ester **55**, which was prepared by esterification of commercially available 2,6-pyridinedicarboxylic acid with ethanol. Following the method of Bretonièrre,[136] the ester was reduced using sodium borohydride to give the monoalcohol **56**. A one-pot reaction was used to convert the alcohol **56** into azide **57**.[136] The alcohol was first mesylated using methanesulfonyl chloride in the presence of triethylamine in toluene. When the reaction was shown to be complete by TLC, it was heated under reflux in a two phase system with sodium azide in water using tetrabutyl ammonium bromide as a phase transfer reagent. The reaction proceeded with an overall yield of 63%. Azide **57** was then hydrogenated using a palladium on carbon catalyst, under 30 psi hydrogen gas using Parr's hydrogenator apparatus to produce amine **58.** The amine was acidified using trifluoroacetic acid, prior to concentration, to prevent polymerisation from occurring.

The trifluoromethanesulfonamide **59** was then prepared by the reaction of **58** with trifluoromethanesulfonyl chloride in dry pyridine. The ester functionality of **59** was then converted into an amide by stirring, at room temperature, with the desired amine; in this case ethanolamine or 3-aminopropan-1-ol. However, this resulted in the cleavage of the sulfonamide, resulting in the production of amines **60** and **61** respectively (Scheme 4.2).

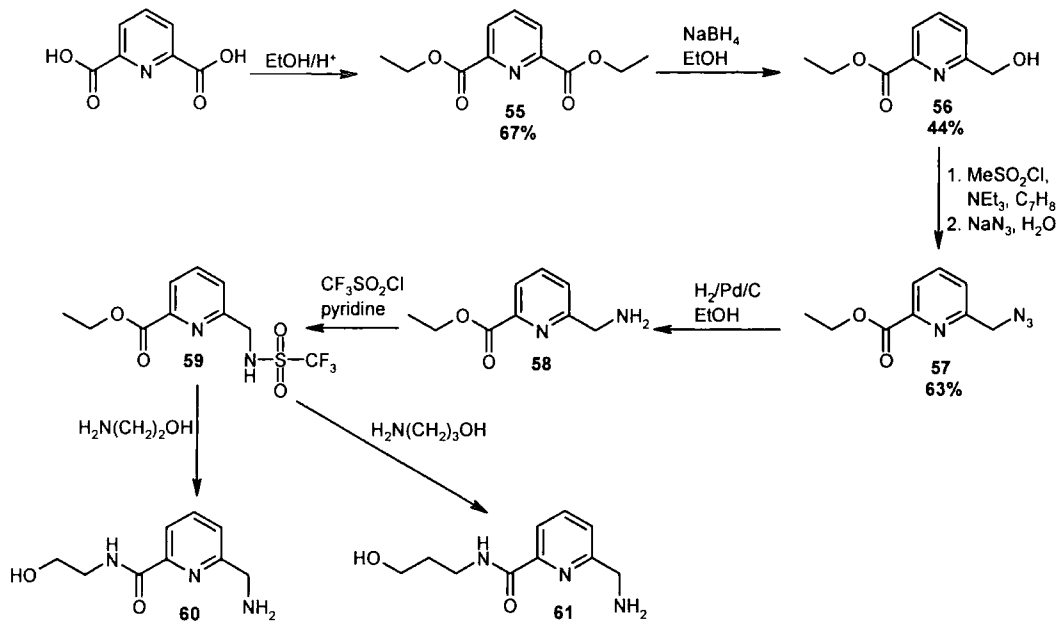

Scheme 4.2 Synthesis of 60 and 61.

As the hydrolysis of the sulfonamide was not desirable at this stage, it was decided to BOC protect amine **58**, then form the amide, deprotect the amine and then form the sulfonamide.

The BOC protected amine **62** was formed by stirring **58** with di-*tert* butyl dicarbonate in methanol. It was later discovered that the BOC protected amine could be formed in a one-pot reaction from the azide **57**. Following the method of Saito and coworkers,[137] the azide and di-*tert* butyl dicarbonate were dissolved in ethyl acetate and the solution was shaken under a hydrogen atmosphere (40 psi) in a Parr's hydrogenator. The BOC protected amine **62** was formed cleanly in 91% yield (Scheme 4.3).

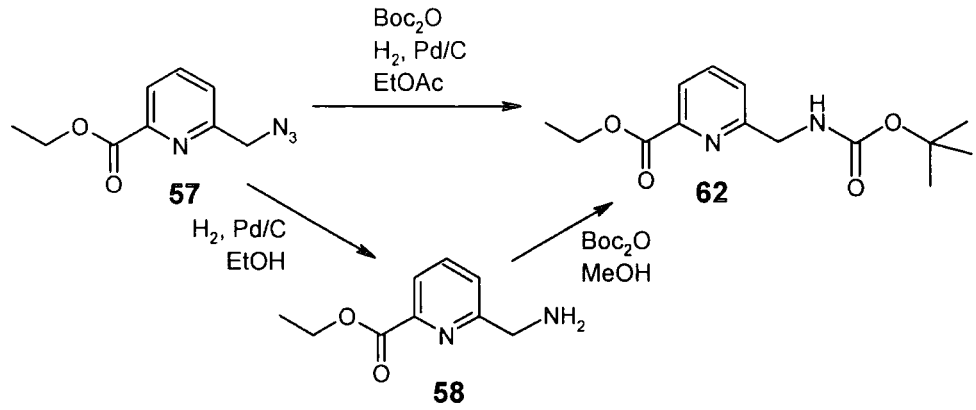

Scheme 4.3 Alternative route for the production of BOC protected amine 62.

The ester functionality of **62** was converted into an amide by stirring with ethanolamine or 3-aminopropan-1-ol at room temperature to give **63** and **64** respectively. The BOC protecting group was then removed with TFA to give **65** (**66**). The sulfonamides **61** and (**67**) were then formed under anhydrous conditions with trifluoromethanesulfonyl chloride in the presence of Hunig's base (Scheme 4.4).

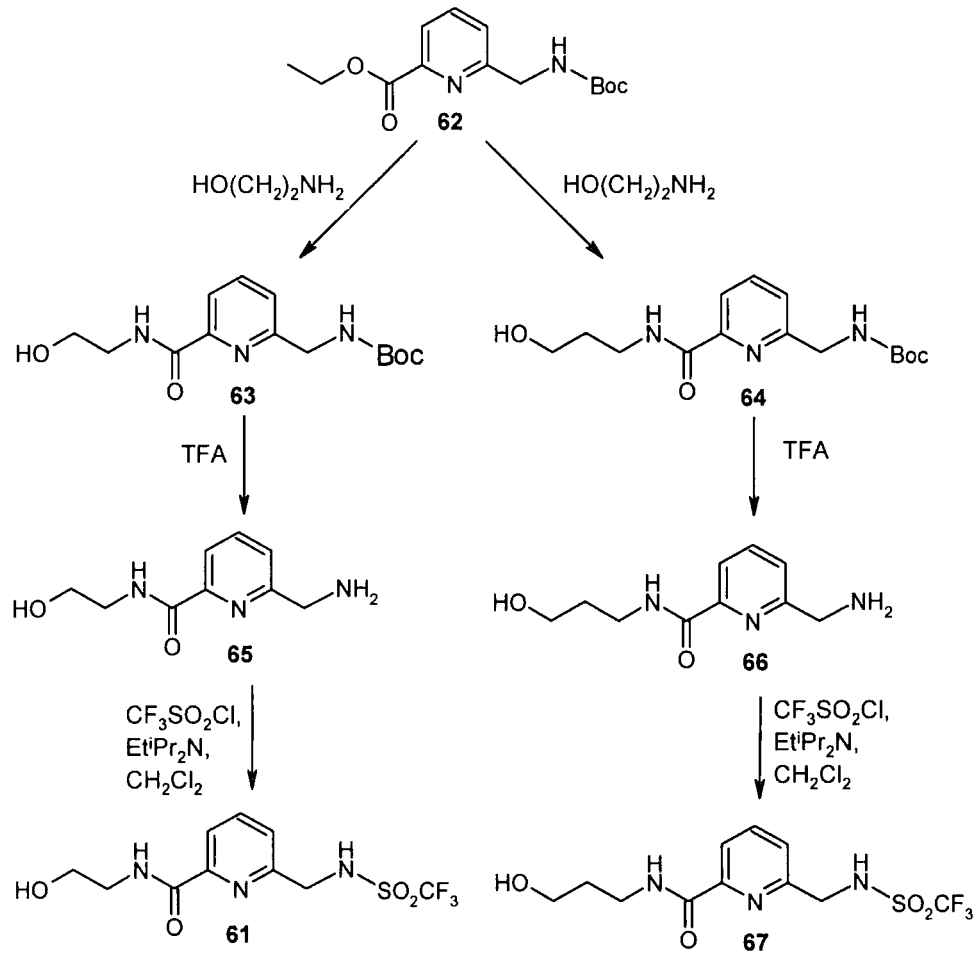

Scheme 4.4 Formation of sulfonamides

Difficulties arose in attaching a leaving group to the hydroxy sulfonamides **67** and **61** so that they could be joined on to the cyclen core. Carbon tetrabromide and triphenyl phosphine were used in an attempt to brominate the alcohol. However, under a variety of conditions, no reaction occurred. Attempts were then made to sulfonylate the alcohol using trifluormethanesulfonyl chloride and trifluoromethanesulfonyl anhydride under different conditions, but the desired product was never isolated.

As it was surprisingly tricky to attach a leaving group to **61** (**67**), it was decided to attach the BOC protected pyridyl amide to the cyclen core and then deprotect it and try to form the trifluoromethane sulfonamide derivative at a later stage.

The hydroxy amides **63** and **64** were therefore converted into the corresponding bromides, **68** and **69** respectively following the reaction of the alcohol with triphenyl phosphine and carbon tetrabromide in dichloromethane. Attempts were made to substitute these bromides on to trisubstituted cyclen **48** in dry acetonitrile in the presence of base. Unfortunately, this did not result in the production of tetrasubstituted cyclen as desired. The bromide molecules instead underwent an intramolecular reaction, resulting in the production of aziridine **70** and azetidine **71**. A similar result was obtained on reacting the bromides with tri-adipate substituted cyclen **72** (Scheme 4.5).

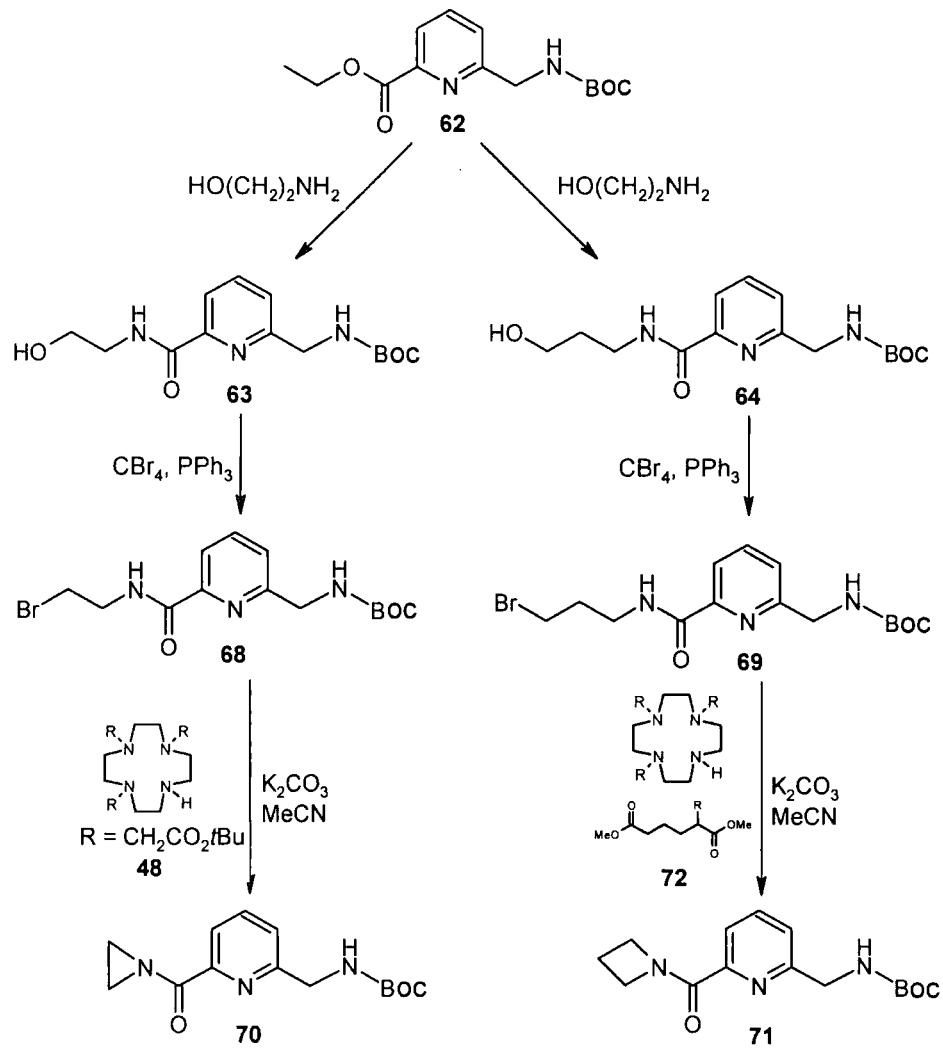

Scheme 4.5 Attempt to alkylated tri-substituted cyclen ring with BOC protected bromo amides.

With this disappointing result, a new approach was attempted. Ester **59** was hydrolysed in lithium hydroxide solution, yielding acid **73**. Attempts were made to undertake an EDC coupling of **73** and **74**, an ethylamine appended DO3A compound which had been prepared independently by Luca Frullano in the laboratory (Scheme 4.6).

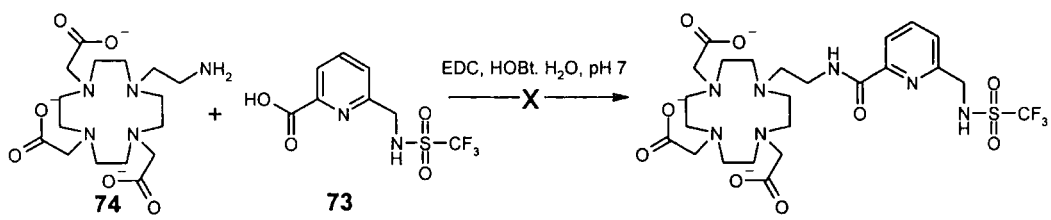

Scheme 4.6 Attempted EDC coupling of 73 and 74.

Unfortunately Scheme 4.6 was not successful so the coupling was attempted again, this time using the methyl ester of **74**. The DO3A compound was converted into the methyl ester by refluxing in dry methanol in the presence of a catalytic amount of acid to give **75**. The coupling reaction was then undertaken as outlined in Scheme 4.7. This reaction also did not lead to the isolation of the desired product.

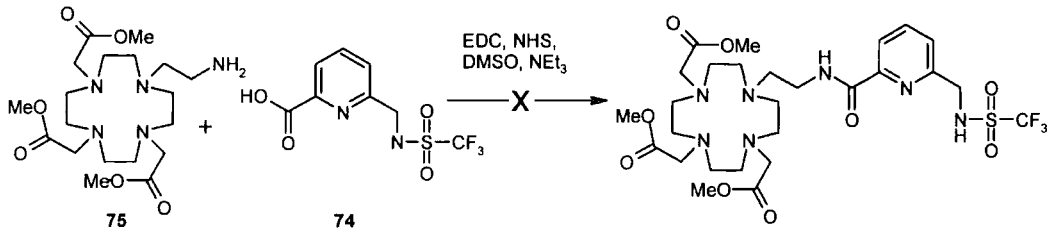

Scheme 4.7 Attempted EDC coupling of 73 and 75.

The next plan of attack involved the monoalkylation of cyclen with the bromo BOC protected amine **68 (69)**, followed by the addition of the three other N-substituents, either carboxymethyl or α-dimethyl adipate **76**, on to the cyclen core.

It was found possible to monoalkylate cyclen quantitatively with both **68** and **69** in dry chloroform in the presence of excess cyclen to give **77** and **78** respectively (Scheme 4.8). To prevent over alkylation, the reaction was carried out in a dilute solution, with the excess of cyclen which also acted as a base. The reaction proceeded more rapidly with **69** possibly because it has a C_3 spacer separating the electron withdrawing C-N bond.

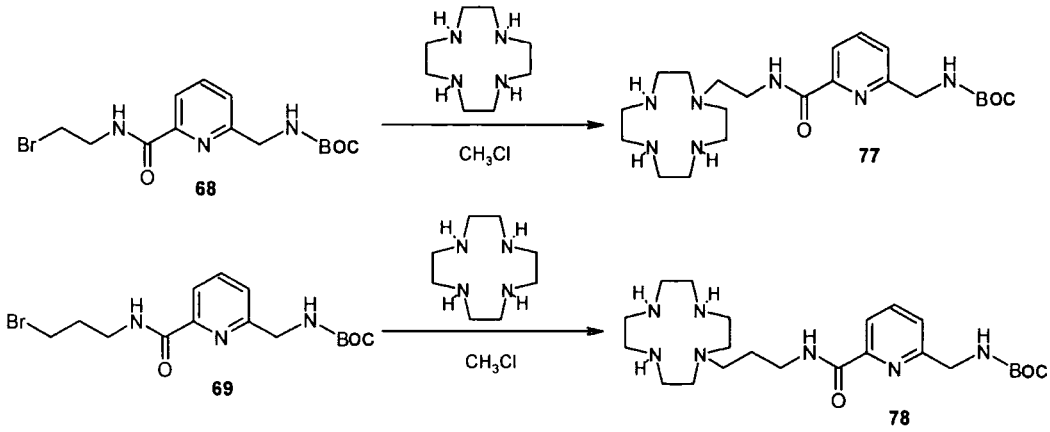

Scheme 4.8 Alkylation of cyclen in dry chloroform.

Following the production of the monoalkylated cyclen, the product was split into two batches. One batch was to undergo substitution with *t*-butylbromoacetate to then go on and form the DO3A type system for L^7 and L^8. The other batch was to be substituted with dimethyl α-bromoadipate, to form the basis for the carboxyalkyl ligands L^9 and L^{10}.

The DO3A system was synthesised first in order to establish a synthetic route for the more synthetically challenging carboxyalkyl ligands. For this reason the synthesis of the DO3A system will be discussed first.

Alkylation of the three remaining cyclen amines of the monosubstituted system was achieved by stirring **77** (or **78**) with *t*-butylbromoacetate at 60°C in dry acetonitrile under argon in the presence of base to yield **79** (or **80**). The BOC protection group was then removed using trifluoroacetic acid; this also resulted in the removal of the *t*-butyl protecting group on the acetate arms resulting in **81** and L^{11} respectively (Scheme 4.9).

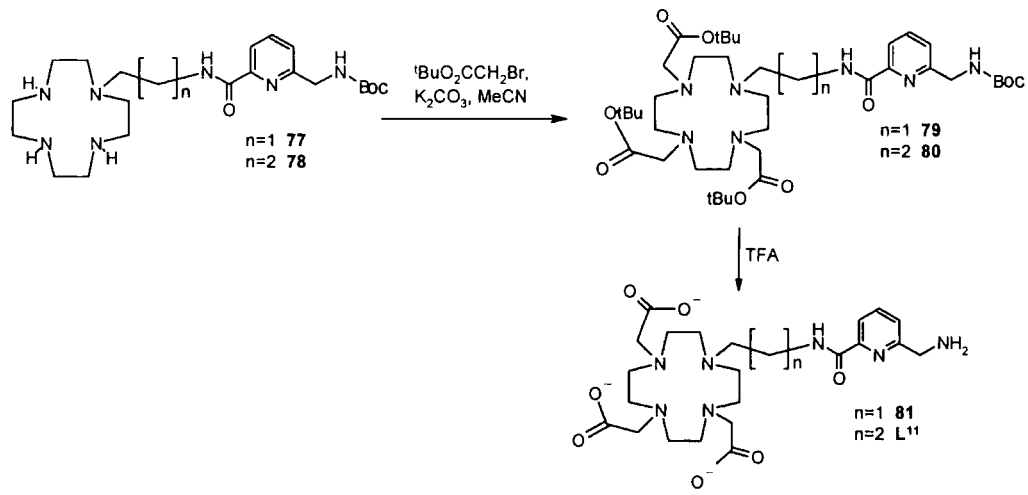

Scheme 4.9 Alkylation and deprotection of 77.

The resulting ligand L^{11} was then complexed with europium (III) under standard conditions and attempts were made to sulfonylate the complex **[EuL^{11}]** in a two-phase system. The europium complex was dissolved in water and layered on top of trifluoromethanesulfonyl chloride and Hünig's base dissolved in dichloro-methane. The reaction mixture was stirred gently and the reaction was anticipated

to occur at the interphase of the two solvents. No reaction occurred (Scheme 4.10). It was concluded that nothing happened because trifluoromethanesulfonyl chloride reacts too rapidly with water with the production of hydrochloric acid and trifluoromethanesulfonic acid. The reaction was then repeated with trifluoromethanesulfonic anhydride, as this reacts more gently with water. Similarly, the desired product was not isolated, only unreacted starting material. From this is it was concluded that sulfonylation using trifluoromethanesulfonyl chloride must be undertaken in a dry non-polar organic solvent.

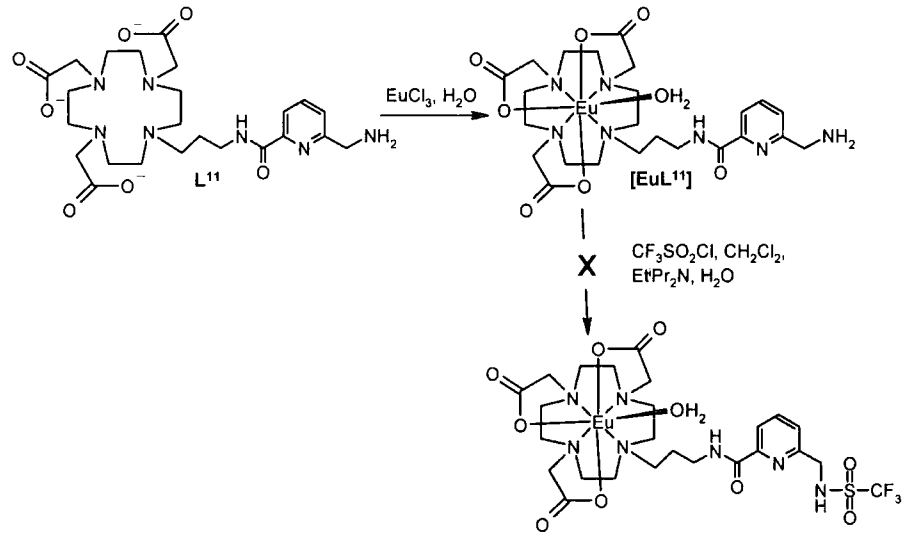

Scheme 4.10 Complexation of L^{11} and subsequent attempt to sulfonylate complex.

As complex **[EuL^{11}]** was not soluble in non-polar organic solvent, it was necessary to find a different route to the target complex. Following the removal of the *t*-butyl protecting groups from the acetate arms of the DO3A system with TFA, **L^{11}** was also insoluble in dichloromethane. The ligand was rendered soluble in dichloromethane by converting the acetate arms to the methyl ester. This was achieved by heating the acid **81** (**L^{11}**) in dry methanol under reflux, in the presence of dry HCl, generated *in situ* from acetyl chloride. In hindsight, it would have been more efficient to transesterify the *t*-butyl ester into a methyl ester, by heating under reflux in methanol, and then removing the BOC protecting group with TFA.

The triester **82** (**83**) was soluble in dichloromethane and able to react with trifluoromethanesulfonyl chloride under anhydrous conditions. Amine **82** (**83**) was

sulfonylated with trifluoromethanesulfonyl chloride in the presence of Hunig's base in dichloromethane resulting in the production of the desired sulfonamide **84** (**85**). The methyl esters were subsequently hydrolysed in 0.5 M lithium hydroxide solution to give ligand L^7 (L^8) which was complexed by heating at 90°C with the lanthanide chloride salt in aqueous solution at pH 5.5 (Scheme 4.11).

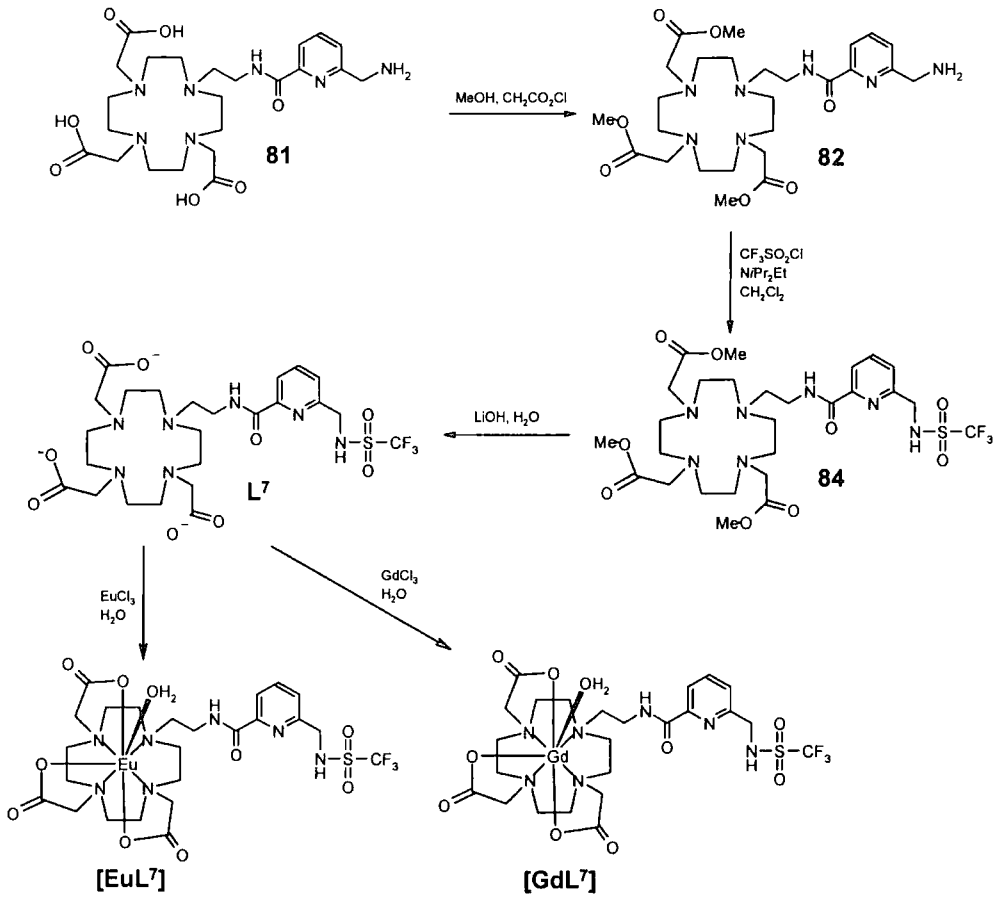

Scheme 4.11 Final steps leading to the production of [EuL^7] and [GdL^7]

Having finally established a route to the target complexes, the carboxyalkyl substituted analogue was prepared by a similar route. The monosubstituted cyclen **77** (or **78**) was alkylated with dimethyl α-bromoadipate **76** in the presence of base to form **86** (and **87**). This reaction took approximately one week to reach completion whereas the equivalent *t*-butylbromoacetate reaction reached completion overnight. This difference in rate was probably caused by the dimethyl adipate groups being bulkier and their addition being more sterically hindered. The BOC protecting group was then removed from the tetrasubsituted cyclen **86** (**87**) using trifluoro-acetic acid, to give **88** (**89**). As this was done under anhydrous conditions, the

methyl ester protecting groups were not affected. Trifluoromethanesulfonyl chloride was then used to form the sulfonamide **90** (**91**). Lithium hydroxide solution was used to remove the methyl ester protecting groups and the resulting ligand L^9 (L^{10}) was complexed with the lanthanide (III) chloride salt in aqueous solution at pH 5.5 (Scheme 4.12).

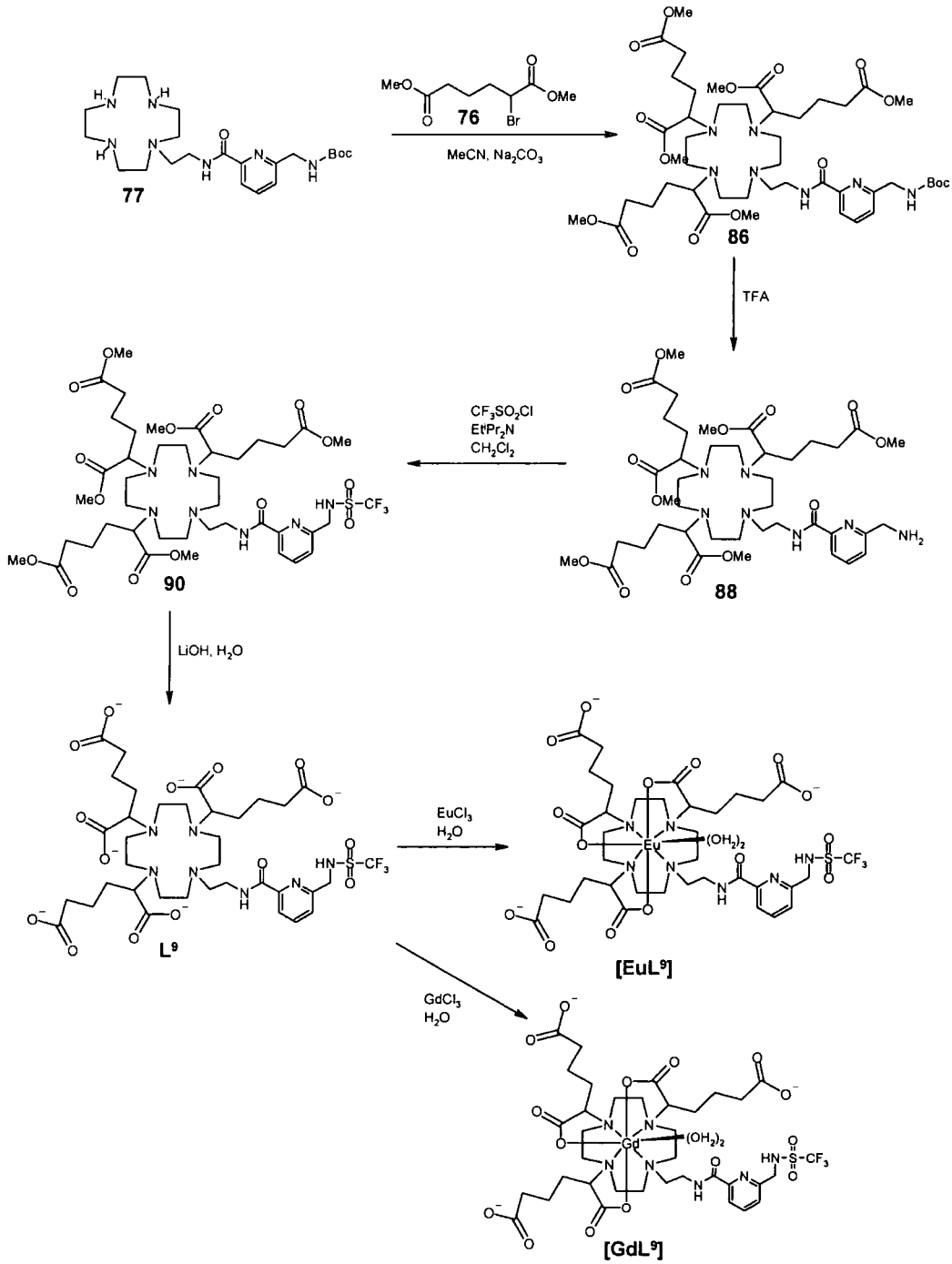

Scheme 4.12 Final steps in the synthesis of the carboxyalkyl subsitituted complexes.

The synthesis of the desired complexes was therefore finally achieved in thirteen steps, as outlined in Scheme 4.13 and Scheme 4.14.

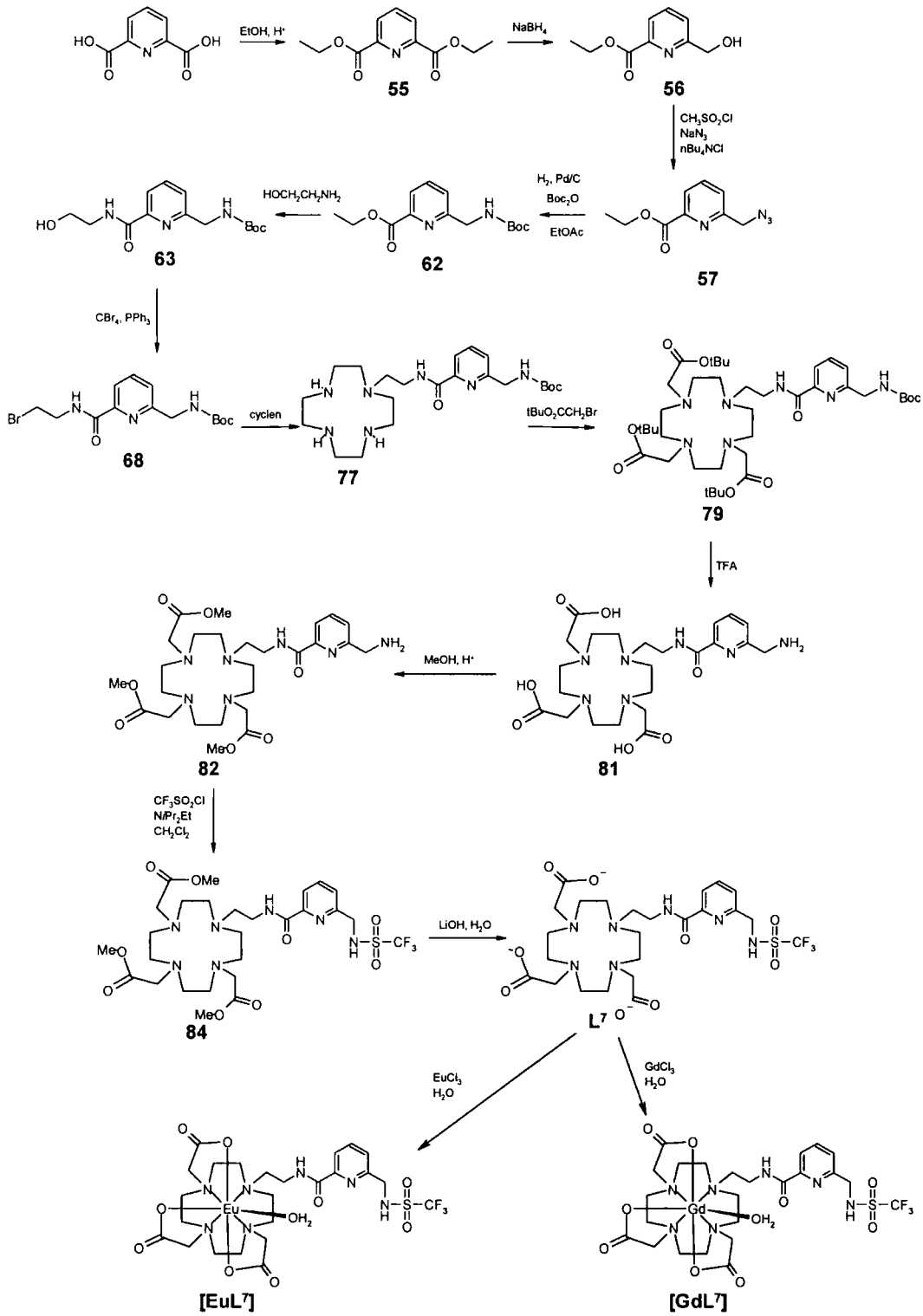

Scheme 4.13 Overall successful synthesis of europium (III) and gadolinium (III) complexes of L^7. L^8 was synthesised in an analogous manner using 3-amino-propan-1-ol instead of ethanolamine.

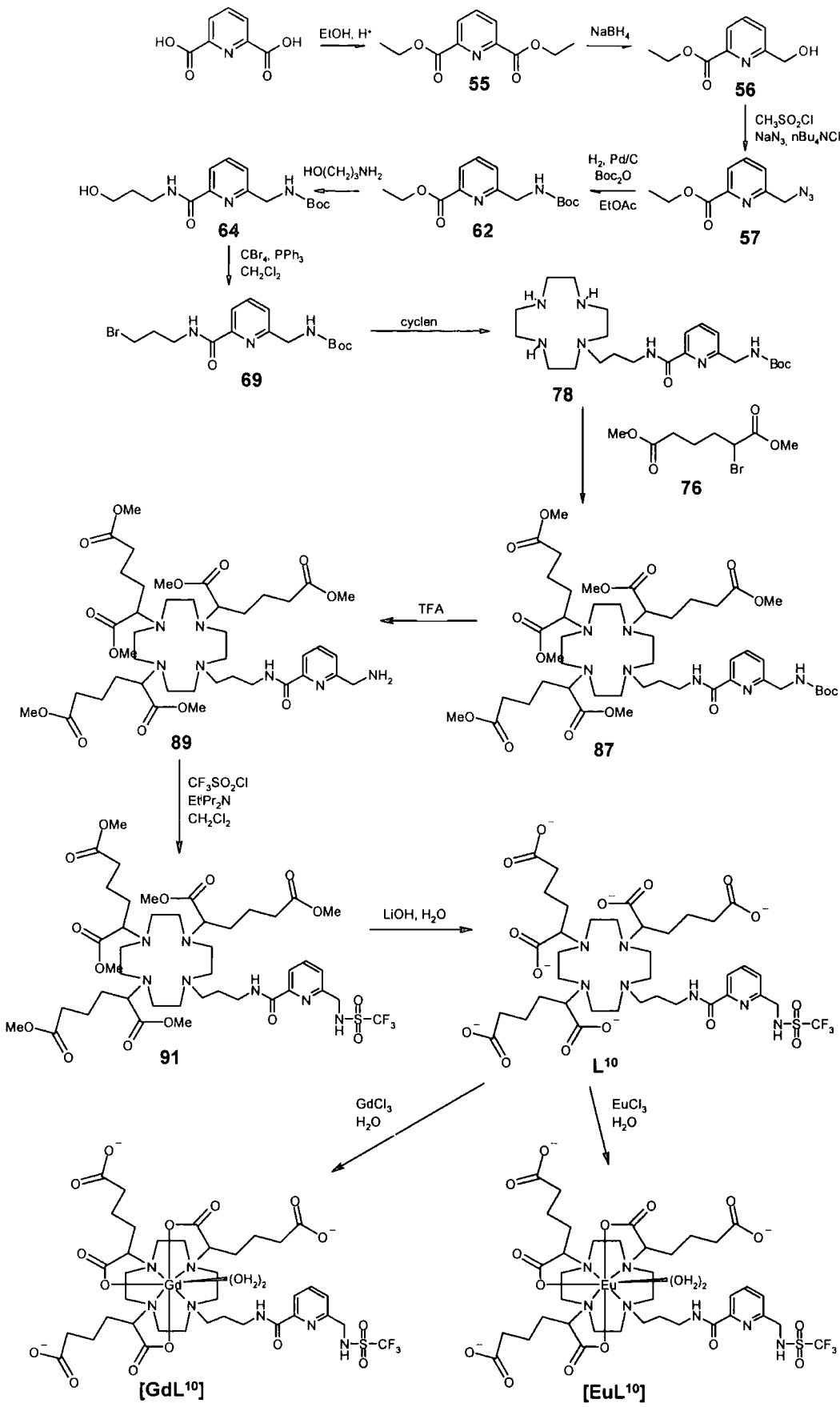

Scheme 4.14 Overall successful synthesis of europium (III) and gadolinium (III) complexes of L^{10}. L^{9} was synthesised in an analogous manner using ethanolamine instead of 3-aminopropan-1-ol.

4.3 Luminescence Studies of Europium Complexes

4.3.1 Emission Excited State Lifetimes of Eu (III) Complexes: Evaluation of q

The number of water molecules (q) coordinated to the europium (III) ion was assessed by measuring the rate constants for the depopulation of the Eu $^5D_0$ excited states in H_2O (k_{H_2O}) and D_2O (k_{D_2O}) as described in Section 3.3.

Table 4.1 Radiative rate constants *k* and derived hydration states (q) for decay of europium luminescence at pH 7.

	[EuL^5]	[EuL^6]	[EuL^7]	[EuL^8]	[EuL^9]	[EuL^{10}]	[EuL^{11}]
k_{H_2O} (ms^{-1})	1.65	0.87	1.57	1.69	2.05	1.84	1.91
k_{D_2O} (ms^{-1})	0.47	0.58	0.503	0.49	0.26	0.22	0.62
q_{Eu}	1.11	0.04	0.98	1.14	1.85	1.65	1.24

Assessment of the radiative rate decay constants obtained for the europium complexes (Table 3.1) shows that DO3A type complexes **[EuL^7]**, **[EuL^8]** and **[EuL^{11}]** possess only one coordinated water molecule, whereas each of the carboxyalkyl substituted complexes, **[EuL^9]** and **[EuL^{10}]**, possess two water molecules bound to the europium (III) centre. This suggests that the presence of the carboxyalkyl substituents prevents the coordination of the pyridyl amide moiety to the europium centre, thus allowing the coordination of a second water molecule.

Comparison of the q values obtained for the three C_3 appended DO3A complexes **[EuL^6], [EuL^8] and [EuL^{11}]** (Table 4.2) reveals that while **[EuL^8] and [EuL^{11}]** have one water molecule coordinated to the europium centre, whereas **[EuL^6]** has no coordinating water molecules. From this observation, it can be concluded that the presence of the trifluoromethanesulfonamide, or of just a free methylamine group on the 6′ position of the pyridyl group, provides sufficient steric bulk to prevent the amide carbonyl from coordinating to the europium (III) centre. This also sterically inhibits water from binding.

Table 4.2 Comparison of q values of C_3 appended ligands

[EuL^6]	[EuL^8]	[EuL^{11}]
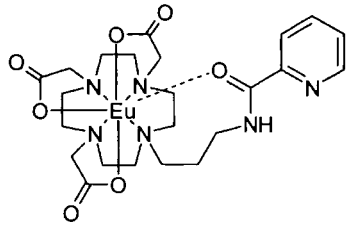	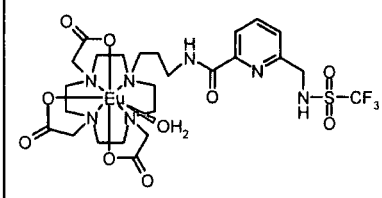	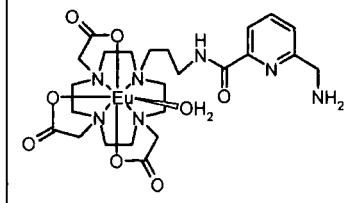
q = 0	q = 1	q =1

4.3.2 Effect of Zinc (II) Concentration on Excited State Lifetime

It was anticipated that as ligand L^3 has been shown to have a high affinity for zinc (II), the pyridyl sulfonamide moieties of the europium complexes would become coordinated to any free zinc present in an octahedral fashion involving amide carbonyl ligation. This would leave a coordination site free on the europium ion, allowing the binding of another water molecule, resulting in a switching from a q = 1 to q = 2 complex (Scheme 4.15).

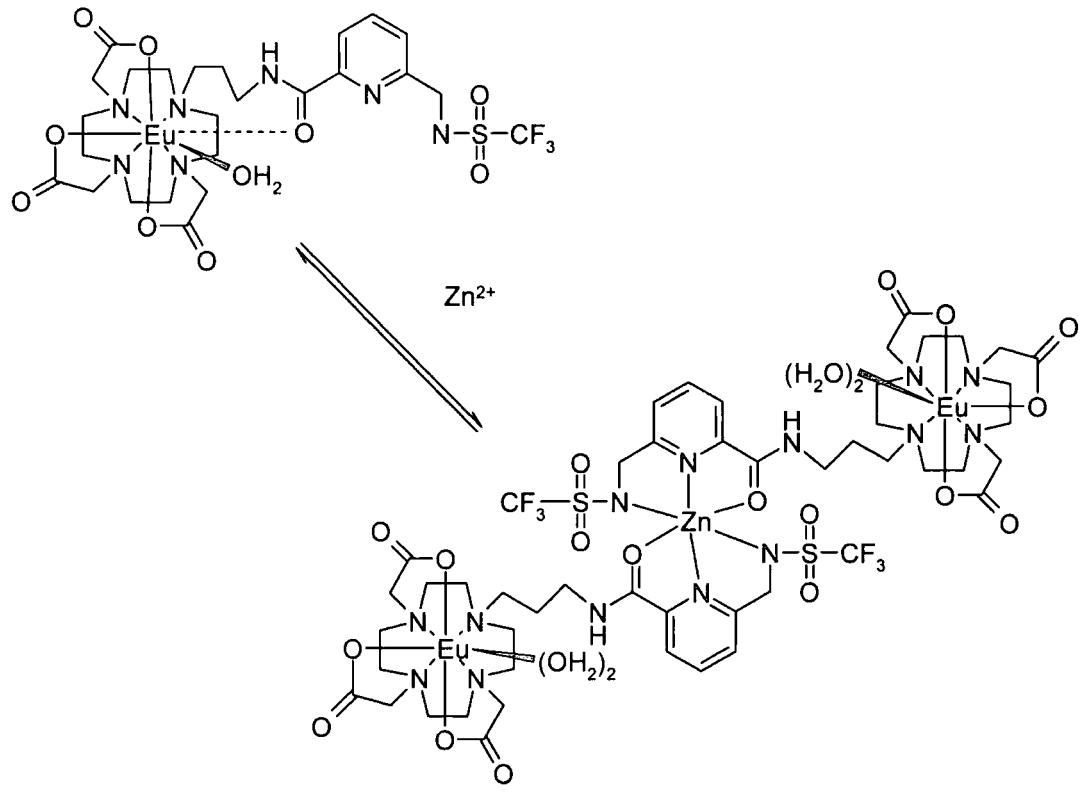

Scheme 4.15 Proposed mechanism through which [EuL^8] may bind zinc (II) ions. The amide carbonyl participates in the octahedral ligation of Zn (II) resulting in an increase in the hydration state of the europium centre.

The europium complexes [EuL^7], [EuL^8], [EuL^9] [EuL^{10}], and [EuL^{11}] were dissolved in 0.1 M MOPS buffer (pH 7.4). The excited state lifetimes (k_{H_2O}) were measured in the presence of 0, 0.5 and 1 equivalents of zinc. A pH of 7.4 was chosen because the speciation plots (section 2.9) showed that at this pH, zinc was bound as an ML_2 complex.

Table 4.3 Excited state lifetimes of Eu (III) complexes in the presence of Zn (II).

No. of zinc (II) equivalents added	Lifetime τ (ms)				
	[EuL^7]	[EuL^8]	[EuL^9]	[EuL^{10}]	[EuL^{11}]
0	0.70	0.59	0.16	0.29	0.52
0.5	0.72	0.64	0.16	0.29	0.44
1	0.79	0.65	0.16	0.30	0.45

The excited state lifetimes (Table 3.5) reveal that none of the trifluoromethane-sulfonamide complexes show any significant change in lifetime in the presence of added zinc (II) ions. This proves that there is no change in the hydration state of the europium (III) centre with increasing free zinc (II) concentration.

4.3.3 Emission Spectra of [EuL^7], [EuL^8], [EuL^9], [EuL^{10}] and [EuL^{11}]

The emission spectra of the europium complexes were recorded both in water (pH 5.5) and in 0.1 M MOPS buffer (pH 7.4). The spectra recorded were identical, suggesting that the MOPS buffer had no effect on the coordination environment of the europium (III).

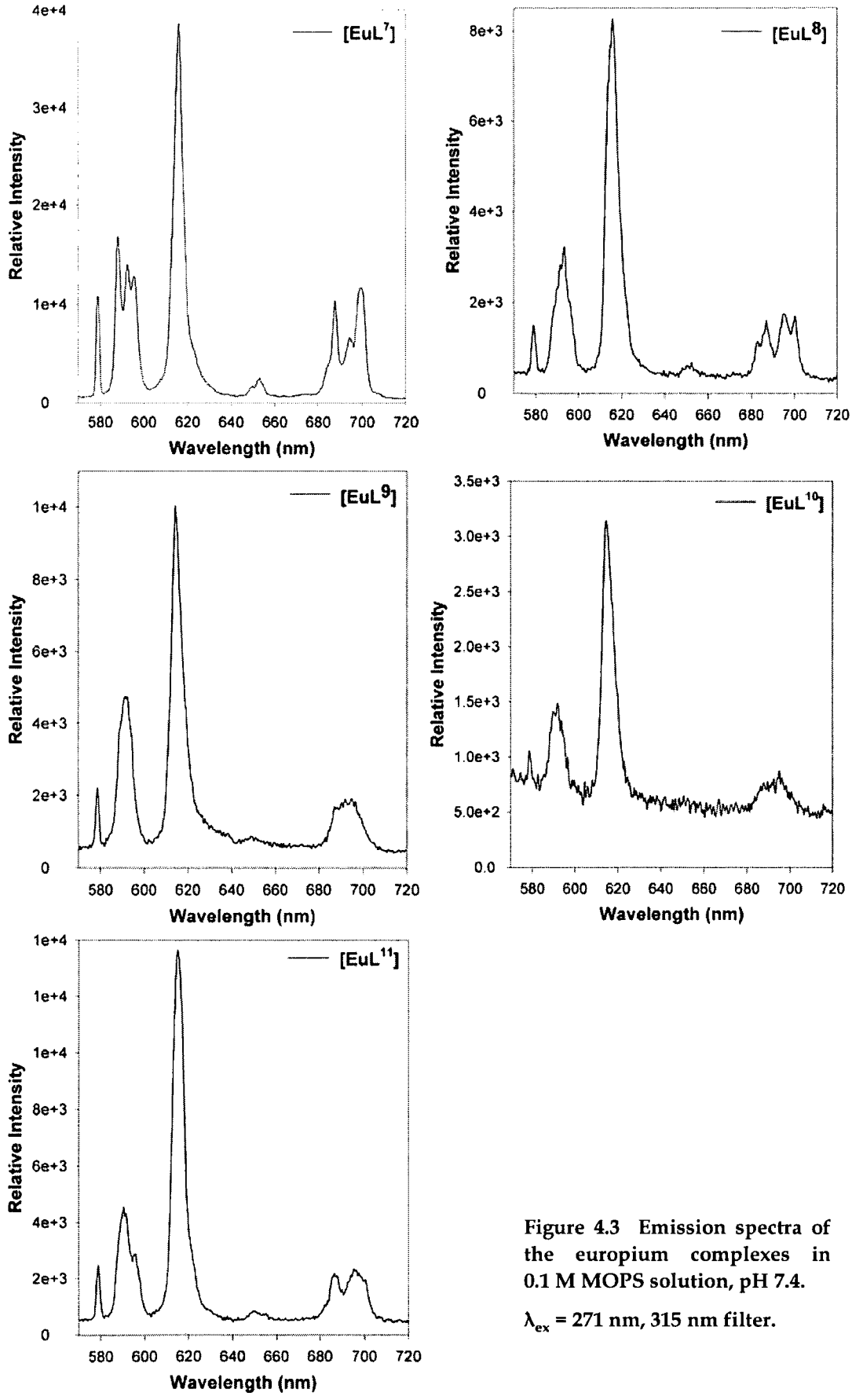

Figure 4.3 Emission spectra of the europium complexes in 0.1 M MOPS solution, pH 7.4.

λ_{ex} = 271 nm, 315 nm filter.

Comparison of the emission spectra of the europium complexes [EuL^7], [EuL^8], [EuL^9], [EuL^{10}] and [EuL^{11}], (Figure 4.3) shows that the coordination environment at the europium centre is significantly different for each of these complexes. The poor signal to noise ratio and resolution of the [EuL^9] and [EuL^{10}] spectra is a result of the complexes being dihydrated; coordinated water molecules quench europium emission markedly.[26]

The emission spectrum of [EuL^7] has a very similar form to that of the pyridyl amide complex [EuL^5] . This suggests that the amide carbonyl group coordinates to the europium centre in a similar manner in each complex.

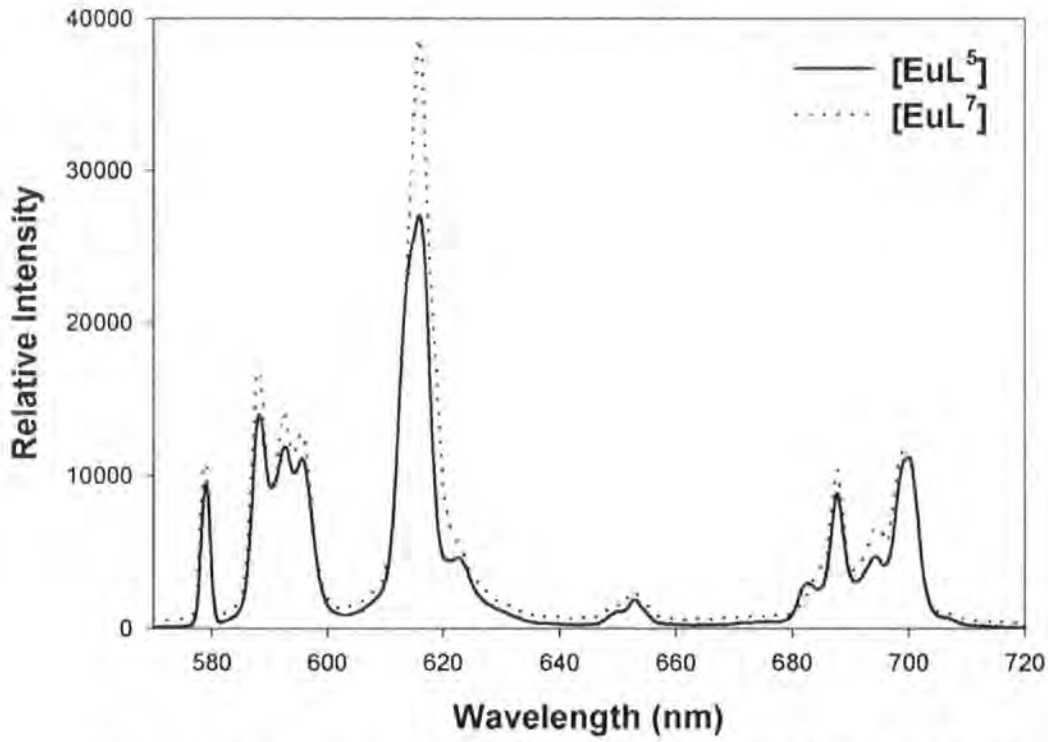

Figure 4.4 Sensitised europium emission spectra of [EuL^7] and [EuL^5]. These spectra have a very similar form suggesting a similar europium coordination environment.

The sensitised europium emission spectra of the three C_3 appended DO3A type complexes [EuL^6], [EuL^8] and [EuL^{11}], differ in their spectral form. This is in agreement with the measured differences in hydration state, as revealed by examination of their excited state lifetimes (Section 4.3.1). The complex [EuL^6], has no group attached to the 6′ position of the pyridine ring. This allows the amide carbonyl to coordinate to the europium centre in such a way as to prevent water

from coordinating as well. The trifluoromethanesulfonamide and aminomethyl group on the pyridyl 6′ position in complexes **[EuL^{8}]** and **[EuL^{11}]** respectively, increase the apparent steric demand of the aryl moiety. This prevents the coordination of the amide carbonyl to the europium centre and in addition inhibits the direct coordination of a second water molecule to the lanthanide centre. Seven-coordinate monohydrated systems have also been synthesised by Bretonnière *et al.*[65] In these systems the presence of a sterically demanding acridone moiety prevents the lanthanide centre being dihydrated.

4.3.4 Effect of Zinc (II) on Emission Spectra of Europium (III) Complexes

The sensitised emission spectra of the europium complexes **[EuL^{7}]**, **[EuL^{8}]**, **[EuL^{9}]**, **[EuL^{10}]** and **[EuL^{11}]** were recorded in 0.1M MOPS buffer (pH 7.4) in the presence of 0, 0.5 and 1 equivalents of zinc (II).

The trifluoromethanesulfonamide complexes showed no change in either spectral form or intensity with the increase in zinc concentration. This is in agreement with the absence in variation in excited state lifetimes, consistent with no change in the hydration state of these complexes with added zinc (II) ions. It also shows that there is no change in the coordination environment at the europium centre. Such behaviour suggests that in the case of the q = 1, DO3A complexes, possessing a coordinated amide carbonyl group, the affinity of the amide carbonyl for the proximate lanthanide (III) centre is greater than its affinity for zinc (II). These results show that the pyridyl trifluoromethanesulfonamide moieties do not bind as hypothesised to free zinc (II) in an octahedral fashion. However, it does not rule out the possibility that free zinc (II) is bound in a four-coordinate complex, leaving the europium coordination environment unaffected.

As complexes **[EuL^{9}]** and **[EuL^{10}]** have two bound water molecules, it is unlikely that the coordination of zinc (II) to the trifluoromethanesulfonamide moiety would result in any change in the coordination environment of the europium (III) centre.

4.3.5 Effect of Zinc (II) on Excitation Spectra of Europium Complexes

Information about the europium coordination environment can also be ascertained from the excitation spectrum.[126] The excitation spectra of **[EuL^7]**, **[EuL^8]**, **[EuL^9]** **[EuL^{10}]**, and **[EuL^{11}]** were recorded as a function of zinc (II) whilst observing the 616 nm emission band.

The form of the excitation spectrum of all of the Eu (III) complexes remained unchanged with increasing zinc (II) concentration. This proves that there is no change in the coordination environment of europium, i.e. no reversible ligation, with changing zinc (II) concentration.

4.3.6 Effect of Zinc (II) Concentration on Pyridyl Emission and Absorption Spectra

The pyridyl emission spectra and absorption spectra of the europium complexes **[EuL^7]**, **[EuL^8]**, **[EuL^9]** **[EuL^{10}]**, and **[EuL^{11}]** were recorded in the presence of 0, 0.5 and 1 equivalents of zinc (II) (λ_{ex} = 271 nm). No change in the absorption or the spectral form or intensity of the pyridyl emission was observed. This strongly suggests that the pyridyl coordination environment of all of these complexes remains unchanged in the presence of excess zinc (II).

4.4 Relaxivity Behaviour of Gadolinium Complexes

The behaviour of the gadolinium (III) complexes **[GdL^7]**, **[GdL^8]**, **[GdL^9]** and **[GdL^{10}]** was assessed by ^{1}H NMR relaxivity studies. The relaxivity values were determined from the measured T_1 values and were calculated as described in Section 3.5.

4.4.1 Relaxivity of [GdL^7], [GdL^8], [GdL^9] and [GdL^{10}]

The relaxivities of **[GdL^7]**, **[GdL^8]**, **[GdL^9]** and **[GdL^{10}]** were determined at both 60 MHz, 22°C and at 65 MHz and 37°C (Table 4.4).

Table 4.4 Relaxivities of Gadolinium Complexes, pH 6.

Relaxivity ($mM^{-1}s^{-1}$)	Complex			
	[GdL^7]	[GdL^8]	[GdL^9]	[GdL^{10}]
65 MHz, 22°C	6.74	6.56	13.40	19.9
60 MHz, 37°C	4.34	4.35	8.71	13.6

The relaxivity values obtained for complexes **[GdL^7]** and **[GdL^8]** lie within the expected range for low molecular weight gadolinium complexes with one water molecule coordinated to the Gd (III) centre.[92]

[GdL^9] and **[GdL^{10}]** have high relaxivity values, even for q = 2 complexes. The relaxivities are significantly higher than the value shown by the parent GdaDO3A system,[93] which exhibits a relaxivity of 12.3 $mM^{-1}s^{-1}$ (20 MHz, 298 K).

High relaxivity values result from the concomitant effect of two inner sphere water molecules and the increase in molecular size. A linear relationship has been observed between the relaxivity and the molecular weight of diaqua gadolinium complexes.[138] consistent with the expected effect of an increasing τ_R, under conditions of fast water exchange.

The relaxivity values obtained for each of the gadolinium complexes studied, i.e. **[GdL^7]**, **[GdL^8]**, **[GdL^9]** and **[GdL^{10}]** are in agreement with the hydration states observed for the related europium complexes.

4.4.2 Effect of Zinc (II) on Relaxivity

Although the presence of an excess of zinc (II) ions showed no effect in the related europium complexes, it is possible that the trifluoromethanesulfonamide moiety binds to zinc but without any change in the lanthanide coordination environment. In the europium complexes, only a change in the coordination environment or hydration state would result in a change in the sensitised europium emission of excited state lifetime.

Addition of zinc (II) to the gadolinium system may result in the formation of a 2 : 1 complex with 2 Gd^{3+} : 1 Zn^{2+}. The increased size of this molecule will cause it to

tumble more slowly in solution; slower tumbling in solution results in an increase in τ_R[138] and consequently the relaxivity will increase (Scheme 4.16). In the case of the q = 1 DO3A complexes, **[GdL^7]** and **[GdL^8]**, it would be possible that the free zinc was bound in a four coordinate manner between the sulfonamide and pyridyl nitrogen atoms, while the amide carbonyl remains bound to the lanthanide centre. This would cause no change in the lanthanide coordination environment.

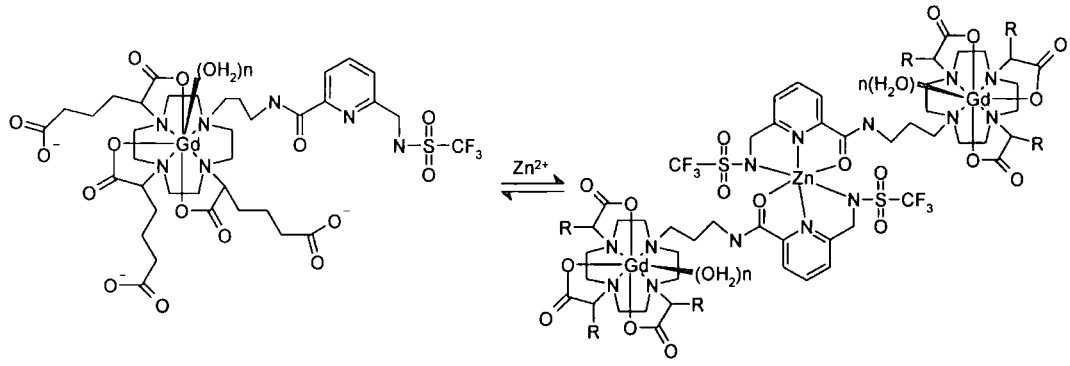

Scheme 4.16 The coordination of the trifluoromethane sulfonamide pyridyl moiety of [GdL^{10}] to zinc may result in the formation of a 2 : 1 complex, resulting in an increase in molecular size and consequently an increse in relaxivity.

The gadolinium (III) complexes **[GdL^7]**, **[GdL^8]** and **[GdL^{10}]** were dissolved in 0.1 M MOPS buffer (pH 7.4). Due to problems with solubility, possibly due to oligomerisation at high pH, **[GdL^9]** was dissolved in water at pH 5.5. Small aliquots containing 0.5 equivalents of zinc (II) acetate were added to the solutions of the complexes. The T_1 values were determined at 60 MHz, 37°C.

Table 4.5 Effect of zinc (II) on the relaxivity of gadolinium complexes [GdL^7], [GdL^8], [GdL^9] and [GdL^{10}].

No. of zinc (II) equivalents added	Relaxivity ($mM^{-1}s^{-1}$)			
	[GdL^7] (60 MHz, 37°C)	[GdL^8] (65 MHz, 22°C)	[GdL^9] (65 MHz, 22°C)	[GdL^{10}] (60 MHz, 37°C)
0	4.34	6.56	8.70	13.63
0.5	4.35	6.50	8.71	12.89
1	4.45	6.76	8.72	12.45

It can be seen from Table 4.5 that the presence of free zinc (II) results in no significant increase in the measured relaxivity for each of the gadolinium complexes. From this information it can be concluded that the pyridyl trifluoro-methanesulfonamide moiety does not have a sufficiently high affinity for zinc (II) under the conditions of the present study.

The slight decrease in relaxivity observed for **[GdL^{10}]** at increased zinc concentrations may be a result of the acetate anion perturbing the second sphere of hydration.

4.5 Protein Binding Studies

Human serum albumin (HSA) is the most abundant protein in blood plasma and is the major transport protein for zinc (II).[139] Blood plasma has a zinc concentration of ca. 19 μM, most of which is bound to HSA with an affinity constant of $\log K_d = -7.53$.[140]

The interaction of gadolinium chelates with proteins has been widely investigated in recent years.[69] Research has focussed on gadolinium chelates which will bind to HSA either through a covalent or non-covalent interaction resulting in a ternary macromolecular paramagnetic complexes. HSA tumbles slowly in solution with the small Gd (III) chelate compartmentalised within, also tumbling slowly.

At the magnetic field strength used in MRI scans (20 - 60 MHz), the longitudinal relaxation time of bound water molecules T_{1M} is dominated by the rotational correlation time (τ_R). If the gadolinium complex tumbles more slowly, τ_R increases and this leads to an increase in the relaxivity. The length of τ_R for a small Gd complex is usually in the picosecond range (typically 50 - 200 ps) whereas τ_R for albumin is in the nanosecond range (ca. 50 ns).[68]

Many gadolinium chelates have been synthesised which contain a hydrophobic moiety which binds to HSA,[69] this is then attached to the gadolinium chelate through a rigid linker so that the motion of the protein is coupled to that of the gadolinium, leading to an increase in τ_R of Gd (Figure 4.5).

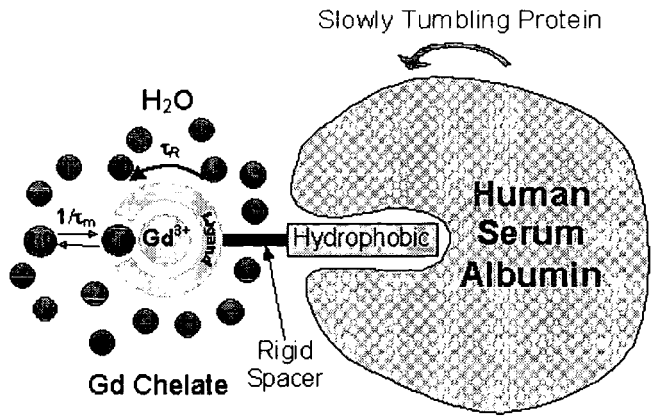

Figure 4.5 Schematic representation of a Gd (III) chelate binding to HSA leading to an increase in τ_R.[69]

As well as providing increased relaxivity values through the increase in τ_R, contrast agents which bind HSA target the blood pool allowing selective enhancement of veins and arteries. They also have an increased half-life *in vivo* allowing higher resolution images to be obtained.[141]

The high affinity of the pyridine trifluoromethanesulfonamide moiety for zinc (II) coupled with the hydrophobic nature of this group suggested that this might make a good HSA binding system. With this in mind, HSA was added to solutions of the gadolinium (III) complexes and relaxivity was measured as a function of added HSA.

4.5.1 Binding Affinity of Gd Complexes to Human Serum Albumin

The binding interaction of gadolinium complexes **[GdL^7]**, **[GdL^8]**, **[GdL^9]** and **[GdL^{10}]** to human serum albumin (HSA) were assessed by measuring the water proton relaxation times of solutions containing the paramagnetic complex in the presence of increasing concentrations of the protein. These titrations were carried out in collaboration with Nicola Thompson using the Bruker Minispec mq60 (60 MHz, 37°C).

In addition to yielding an estimate of the binding strength K_A (by assuming one binding site on the protein) by iterative least squares fitting, these measurements also provide a direct assessment of the relaxivity of the putative macromolecular adduct.

The relaxivity values obtained in these protein binding studies have been quoted in terms of molality ($mMolal^{-1}s^{-1}$). Defining relaxivity in terms of $mM^{-1}s^{-1}$ in protein solution, such as human serum albumin, can be misleading as high concentrations of protein are usually dissolved. As a result, more than 20% of the volume is occupied by protein and hence less than 80% by water. [92,142]

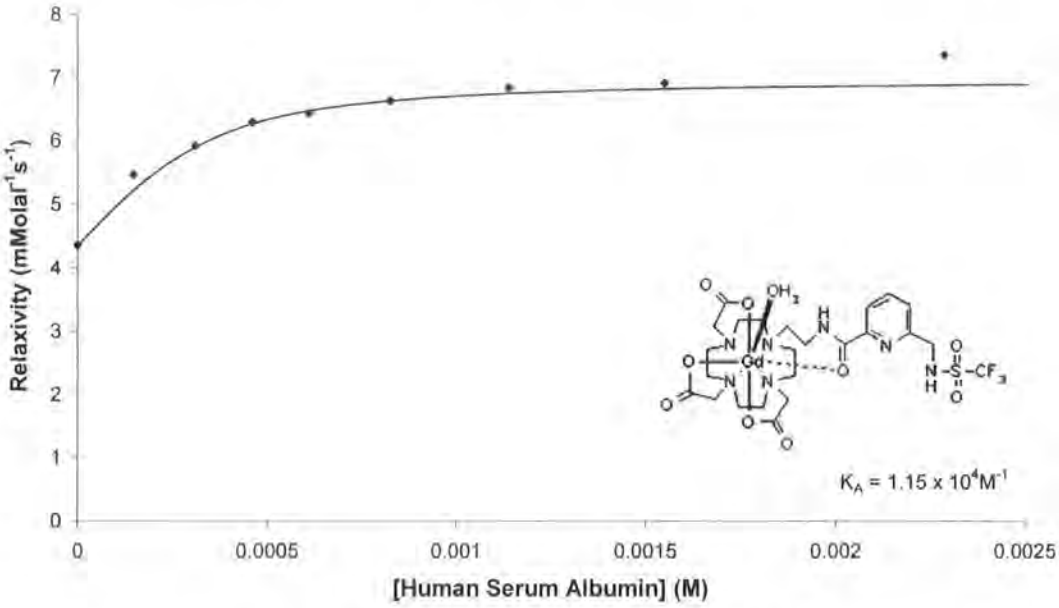

Figure 4.6 Increase in relaxivity of [GdL^7] (0.32 mM) with increasing HSA concentration (60 MHz, 37°C).

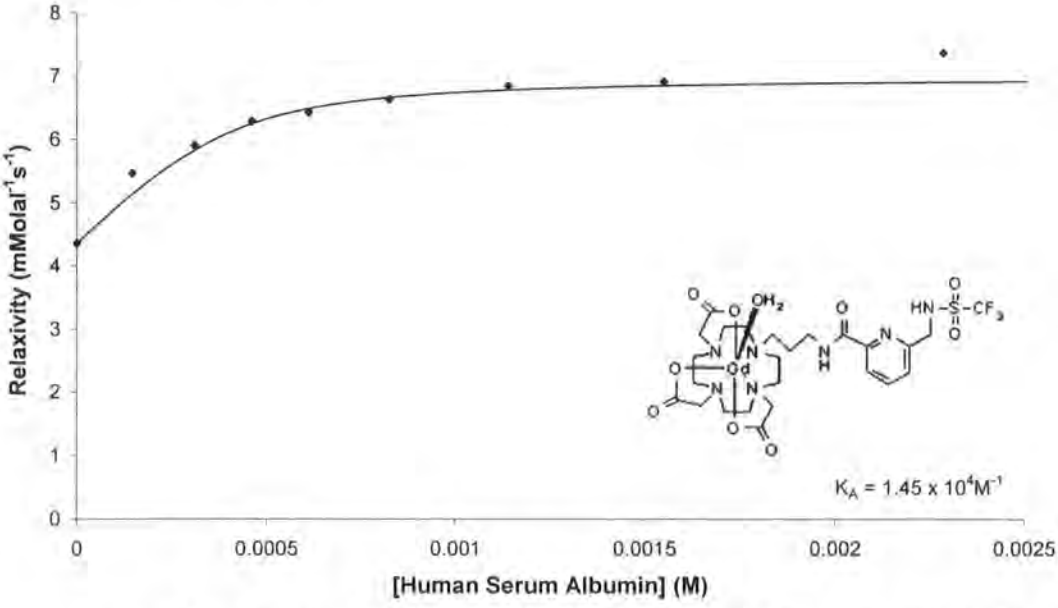

Figure 4.7 Increase in relaxivity of [GdL^8] (0.40 mM) with increasing HSA concentration (60 MHz, 37°C).

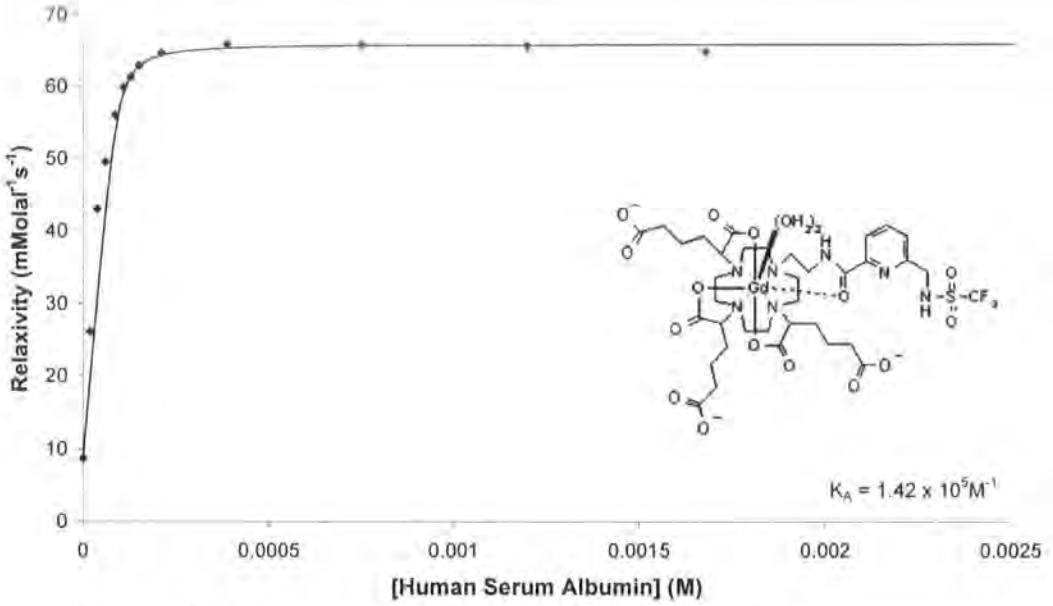

Figure 4.8 Increase in relaxivity of [GdL^9] (0.05 mM) with increasing HSA concentration (60 MHz, 37°C).

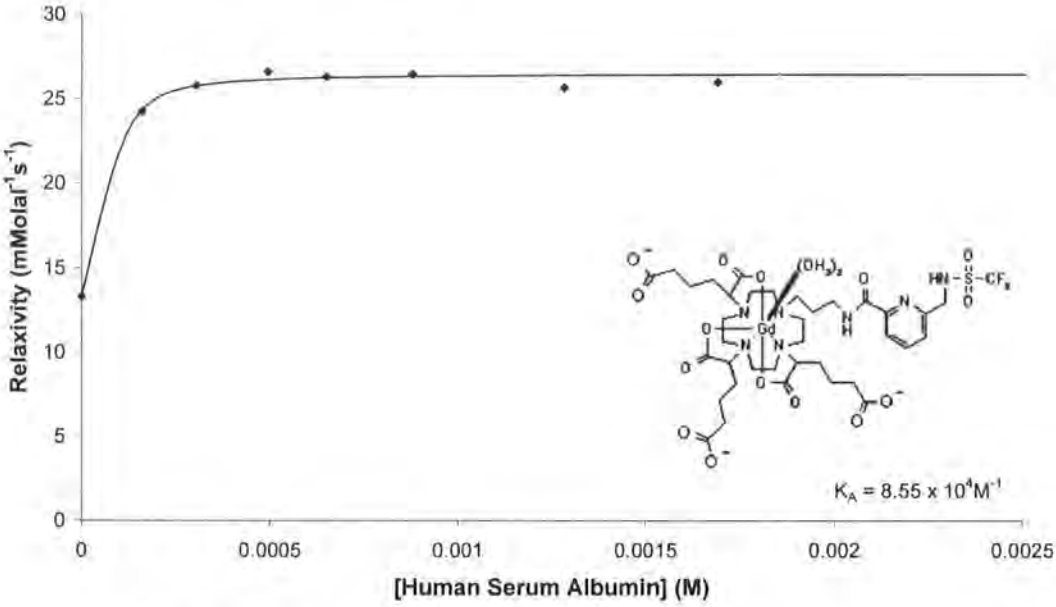

Figure 4.9 Increase in relaxivity of [GdL^{10}] (0.12 mM) with increasing HSA concentration (60 MHz, 37°C).

The binding curves for the gadolinium complexes to HSA, Figure 4.6 - Figure 4.9 and the association constants (Table 4.6) reveal that the complexes with carboxy-alkyl substituents, **[GdL^9]** and **[GdL^{10}]**, show a much higher binding affinity and greater increase in relaxivity with the addition of HSA compared to the charge neutral DO3A analogues.

The q = 1 DO3A complexes show approximately 60% increase in relaxivity on binding to HSA. Whereas the relaxivity of the q = 2 **[GdL^{10}]** system doubles and **[GdL^{9}]** shows approximately a 700% increase in relaxivity.

Table 4.6 Binding constants (K_A) for the gadolinium complexes to HSA.

Complex	K_A (M^{-1})
[GdL^{7}]	1.15×10^4
[GdL^{8}]	1.45×10^4
[GdL^{9}]	2.71×10^5
[GdL^{10}]	8.55×10^4

The concentration of HSA in the blood is 0.6 mM.[139] From the experimental binding affinities, it can bee seen that complexes **[GdL^{9}]** and **[GdL^{10}]** have reached the maximum saturated relaxivity value at this concentration.

The tri-negative charge on the **[GdL^{9}]** and **[GdL^{10}]** complexes may have caused an increase in the electrostatic interaction between the gadolinium chelate and the HSA resulting in the carboxyalkyl substituted complexes having a higher affinity for HSA compared to the neutral complexes.

The greater relaxivity enhancement shown by **[GdL^{9}]** compared to **[GdL^{10}]**, is probably caused by the C_2 linker being more rigid than the C_3 analogue. Free rotation about the alkyl chain could result in the slow tumbling rate of HSA not being transferred efficiently to the gadolinium chelate in **[GdL^{10}]**.[69]

It is likely that hydrogen bonding between the pyridyl nitrogen and the amide proton will result in the **[GdL^{9}]** and **[GdL^{10}]** adopting different conformations in solution, Figure 4.10. This hydrogen bonding between a pyridyl nitrogen and amide proton has been observed in a 2,6-diamide substituted pyridine system synthesised by Hunter and Purvis.[143] The different conformations of the two analogues may be associated with the different binding affinities to HSA.

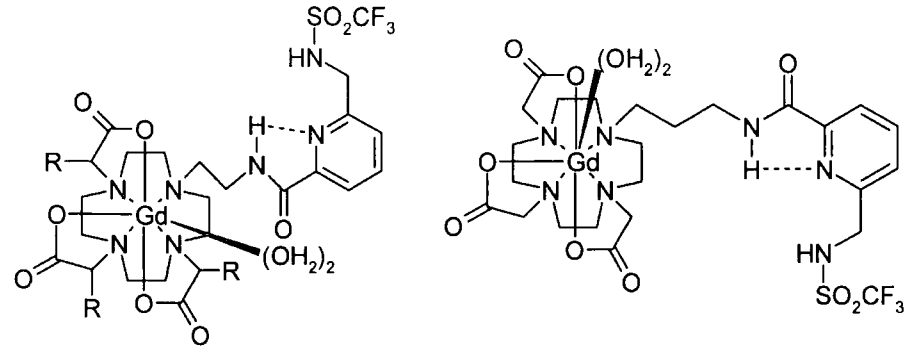

Figure 4.10 Proposed conformation of [GdL^9] and [GdL^{10}]

The affinity constant of **[GdL^9]** for HSA is in line with the affinity constant shown by **L^2** for zinc (II). This suggests that a complex may form between **[GdL^9]** and a zinc (II) ion present within the HSA protein.

In previous examples of diaqua gadolinium complexes, the expected relaxation enhancement on binding to a macromolecule such as HSA has not been observed. This is generally because the inner sphere water molecules are displaced by a donor atom either from the protein (e.g. a carboxylate group) or through the coordination of a bidentate anion (e.g. carbonate or phosphate).[138]

4.5.2 NMRD Profiles of Gadolinium Complexes bound to HSA

NMRD profiles are highly diagnostic of the formation of adducts between gadolinium complexes and slowly tumbling substrates such as proteins, as they show a characteristic relaxivity peak centered at about 20 - 30 MHz. [130]

NMRD profiles of the gadolinium complexes were recorded in Durham and will be fitted according to the theoretical arguments presented in Section 3.6. The profiles were recorded at 25°C in the presence and absence of a saturated level of HSA, Figure 4.11 - Figure 4.14.

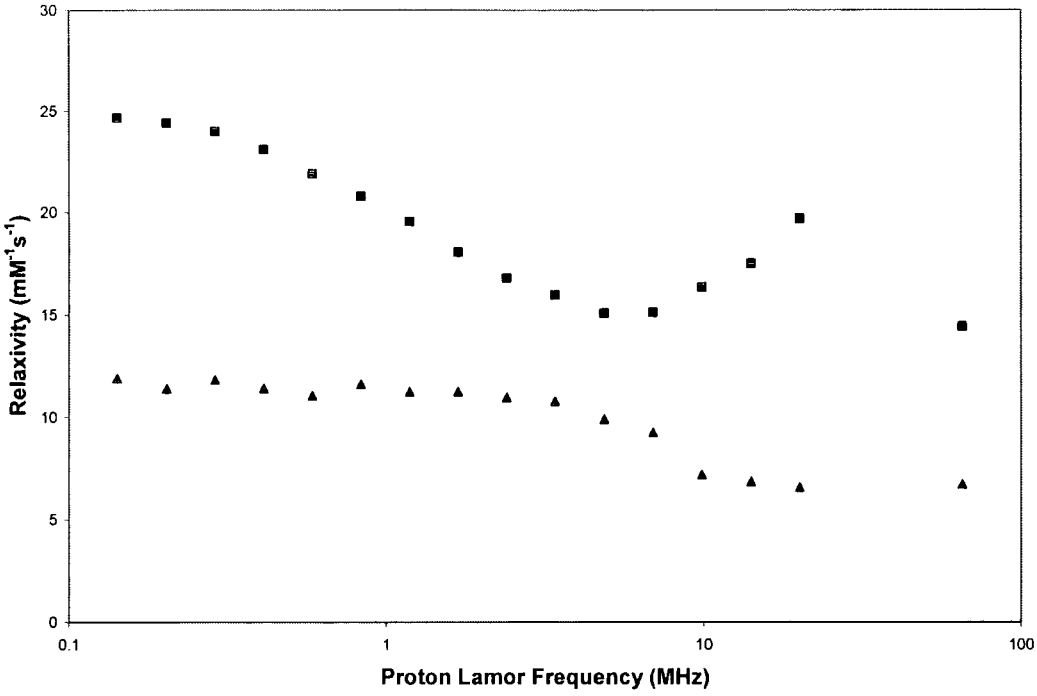

Figure 4.11 NMRD profile of [GdL^{7}] in the presence ■ and absence▲ of HSA, 25°C.

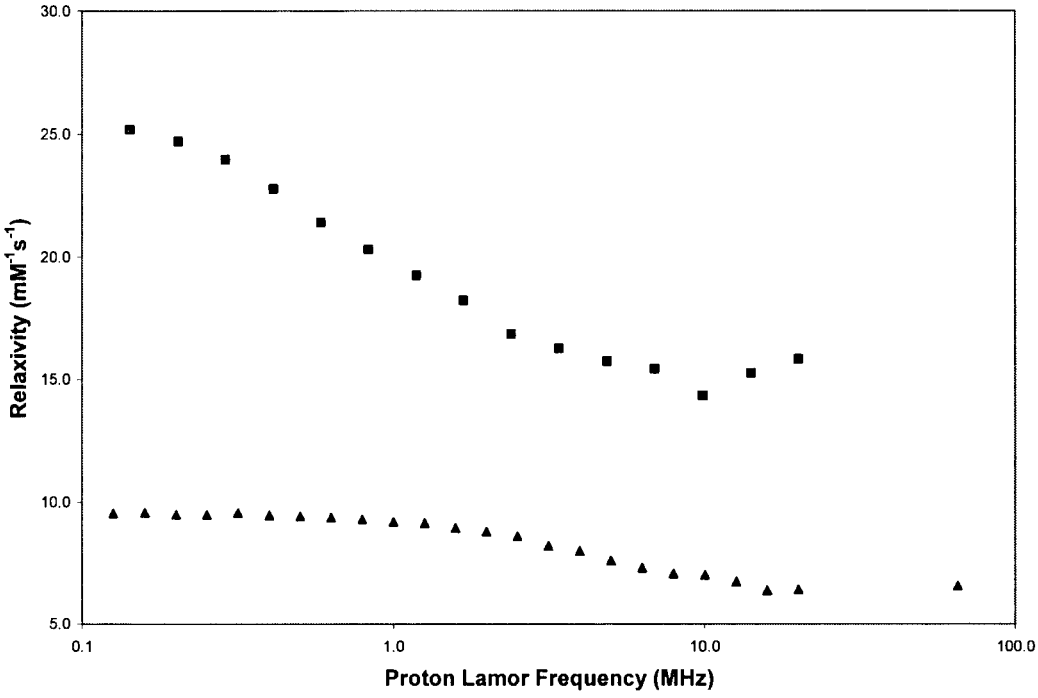

Figure 4.12 NMRD profile of [GdL^{8}] in the presence ■ and absence▲ of HSA, 25°C.

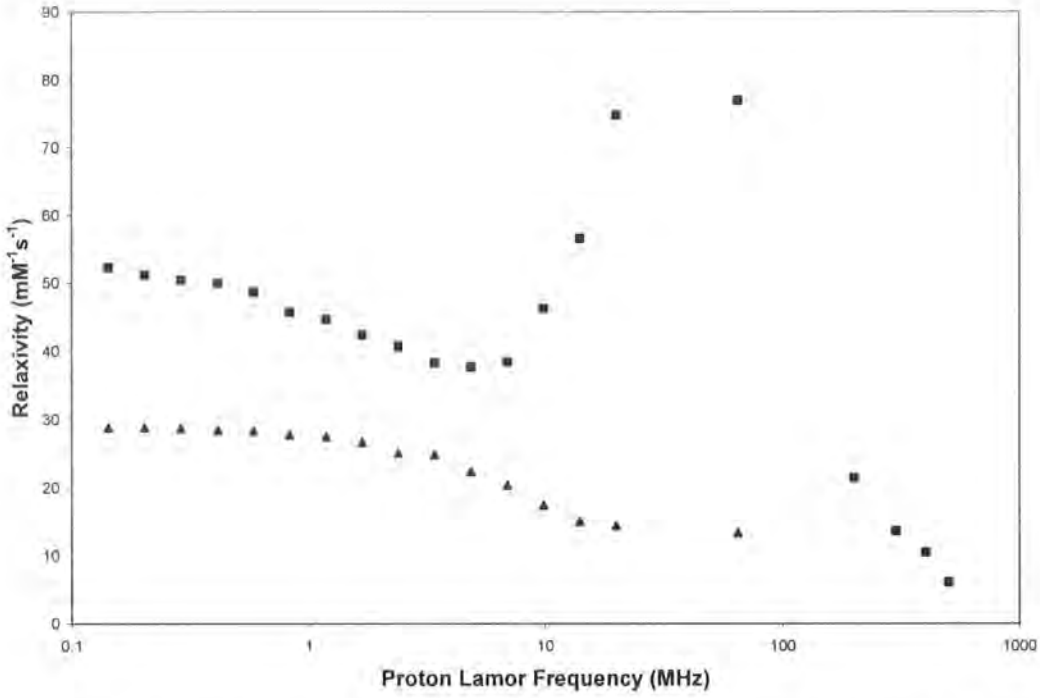

Figure 4.13 NMRD profile of [GdL^9] in the presence ■ and absence ▲ of HSA, 25°C.

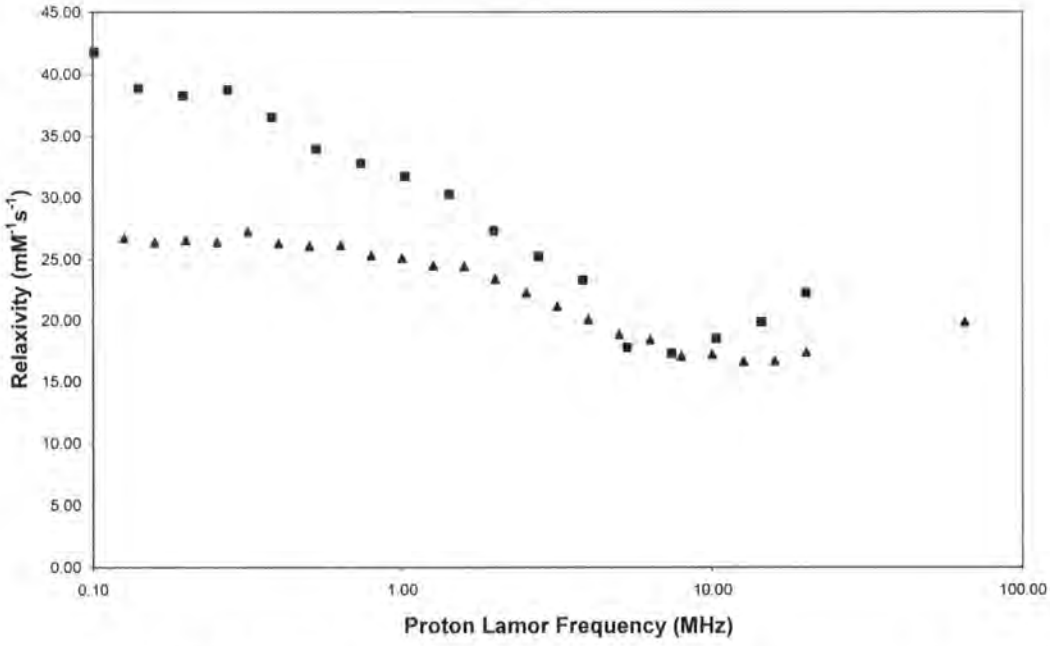

Figure 4.14 NMRD profile of [GdL^{10}] in the presence ■ and absence ▲ of HSA, 25°C.

From the NMRD profiles of the DO3A complexes **[GdL^7]** and **[GdL^8]** (Figure 4.11 and Figure 4.12) it can be seen that the addition of HSA causes a doubling of the

observed relaxivity. The appearance of a relaxivity peak at the high field end of the spectrum is characteristic of an increased τ_R. The effect on τ_R is more pronounced in **[GdL^7]** than in **[GdL^8]**. This is probably because the C_2 spacer is less conformationally mobile than the C_3 spacer. Thus, the C_3 spacer allows free rotation between the HSA-pyridylsulfonamide moiety and the gadolinium chelate, the C_2 spacer is more rigid so the protein and gadolinium chelate tumble coherently and the increased τ_R of the HSA is effectively transferred to the gadolinium ion.

This effect is also apparent in the behaviour of carboxyalkyl analogues **[GdL^9]** and **[GdL^{10}]**, Figure 4.13 and Figure 4.14. The relaxivity increase in the high field region caused by the increased τ_R is much greater in the C_2 example, again suggesting that the C_3 linkage group allows more rotational freedom.

The relaxivity enhancement exhibited by **[GdL^9]** is quite remarkable. Previous examples of q = 2 gadolinium chelates have always displayed a much lower relaxivity value than expected. This is usually caused by the displacement of the bound water molecules by protein side chains (e.g. aspartate or glutamate carboxylate groups) or anions, or free rotation occuring in the spacer group so that the long τ_R of the HSA is not effectively transferred to the gadolinium centre.[138] Complex **[GdL^9]** is unique in that it maintains its q = 2 hydration stae in the presence of HSA and apparently tumbles coherently with the protein. This results in an unprecedented relaxivity value and has a relaxivity value[92] close to the calculated maximum value for such a system.[69]

As these results were so unexpected, the complex was sent to Turin for independent verification. The relaxivity value at 40 MHz was also measured as this appeared, from the NMRD profiles, to be the frequency at which the maximum relaxivity value would occur.

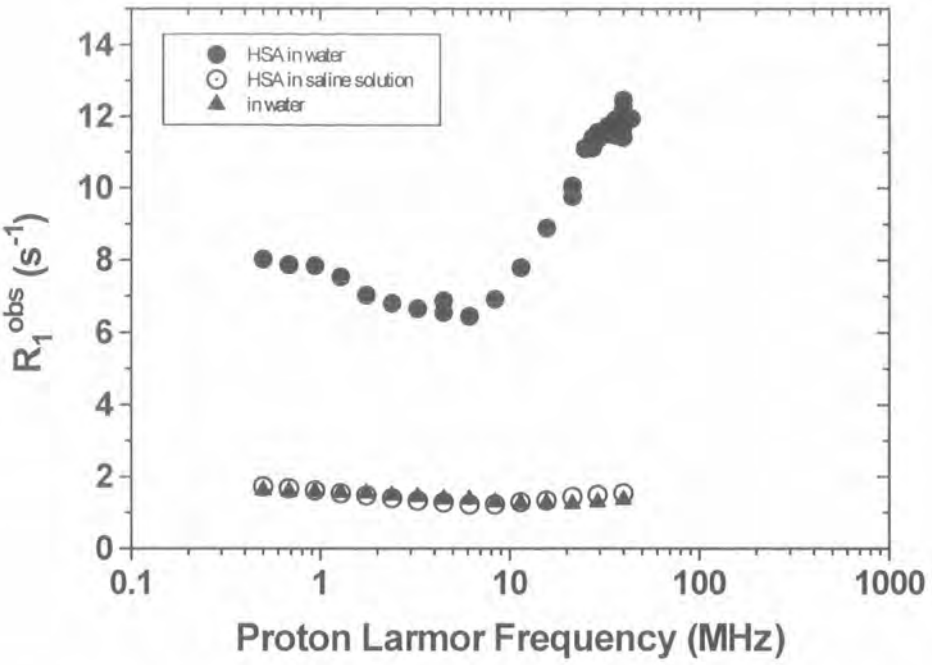

Figure 4.15 NMRD Profile of [GdL^9] in the presence of HSA, measured in Turin.

Figure 4.15 shows the relaxation rate of **[GdL^9]** in the presence of HSA. This data is in agreement with that obtained in Durham and suggests that the maximum relaxivity is obtained at ca. 40 MHz. This value appears to be approximately 20% higher than the relaxivity at 20 MHz suggesting a maximum relaxivity value of ~ 90 $mM^{-1}s^{-1}$ (40 MHz, 25°C)

4.5.3 Effect of Human Serum on Relaxivity

Complex **[GdL^9]** exhibits high relaxivity in the presence of HSA, suggesting that it binds very well to the protein and this reduces its rate of tumbling in solution. Also, the complex retains its dihydrated state in the presence of HSA.

Most q = 2 contrast agents which have been synthesised so far exhibit a binding of the protein carboxylate side chains to the lanthanide centre resulting in the water molecules being displaced with a subsequent reduction in the observed relaxivity.

Although the relaxivity was maintained in GdaDO3A, the relaxivity did not increase so markedly in the presence of either HSA or human serum.[93,142]

The relaxivity of **[GdL^9]** was determined in the presence of human serum (60 MHz, 37°C).

Table 4.7 Relaxivity (60 MHz, 37°C) of [GdL^9] in the presence of human serum.

	Relaxivity ($mM^{-1}s^{-1}$) (60 MHz, 37°C)
[GdL^9]	8.7
[GdL^9] in 0.6mM HSA	67.5
[GdL^9] in human serum	14.1

The relaxivity of **[GdL^9]** is shown to be much smaller in serum than in serum albumin, Table 4.7. This suggests that anions from the serum bind to the gadolinium centre displacing the water molecules leading to a significant reduction in relaxivity. Although **[GdL^9]** has a high affinity for HSA in serum, leading to an increase in relaxivity through an increase in τ_R, the loss of the dihydrated state of the gadolinium leads to a feeble relaxivity enhancement.

The relaxivity of **[GdL^9]** in human serum was monitored as a function of pH over the range 9 to 4. N-Alkylation of the macrocyclic ring is known to lead to a higher affinity for anion binding at lanthanide centres.[64] It was hypothesised that a reduction of pH might prevent anions such as bicarbonate or phosphate from binding. However, no significant change in relaxivity was observed with decreasing pH, suggesting that lactate, as well as phosphate and bicarbonate is a likely competeing ion.

4.5.4 Effect of Anions on Relaxivity

As the binding of anions to the gadolinium centre was hypothesised as the cause for the reduction in relaxivity observed in serum, the relaxivity of **[GdL^{10}]** was recorded as a function of the concentration of biological anion background.

Aliquots of a simulated anion background solution containing carbonate (30 mM), phosphate (0.9 mM), citrate (0.13 mM) and lactate (2.3 mM) were added to a solution of **[GdL^{10}]** and the transverse relaxation time (60 MHz, 37°C) was recorded.

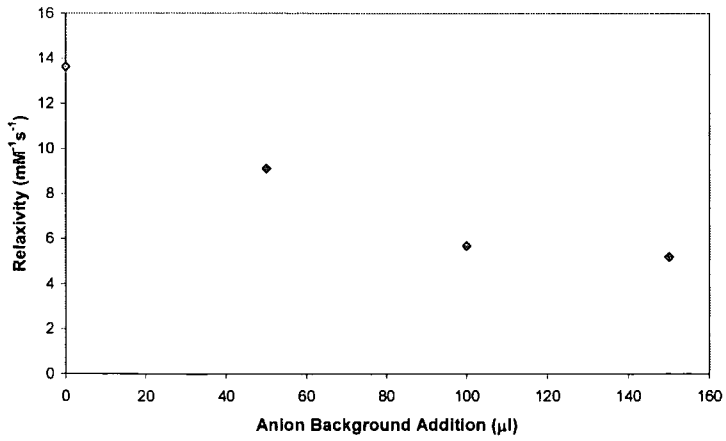

Figure 4.16 Relaxivity of [GdL^{10}] as a function of biological anion concentration.

From Figure 4.16 it can be seen that the relaxivity decreases significantly as the biological anion concentration increases. This suggests that it is the binding of extra-cellular anions which cause the decrease in relaxivity in serum. The relaxivity of **[GdL^{10}]** in anion background was monitored as a function of pH. The relaxivity remained constant between pH 3 and pH 9. This is in agreement with the observations made in serum.

4.5.5 Effect of Anions and pH on Luminescence of [EuL^9]

Further to the observation that relaxivity of **[GdL^{10}]** did not vary with pH in an extra-cellular anion background; the sensitised emission spectrum of **[EuL^9]** was recorded in an extra-cellular anion background as a function of pH.

Europium luminescence is effectively quenched by the OH oscillators in bound water molecules.[61] The displacement of these water molecules by coordinating anions can be detected by an increase in the emission intensity, Scheme 4.17.

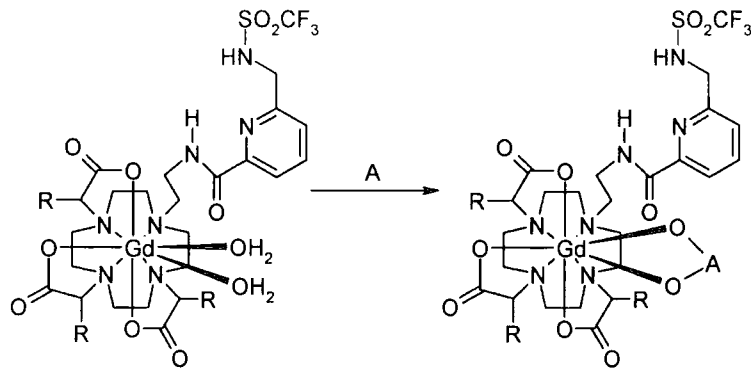

Scheme 4.17 Formation of ternary complex-anion (A) adduct, resulting in the displacement of bound water.

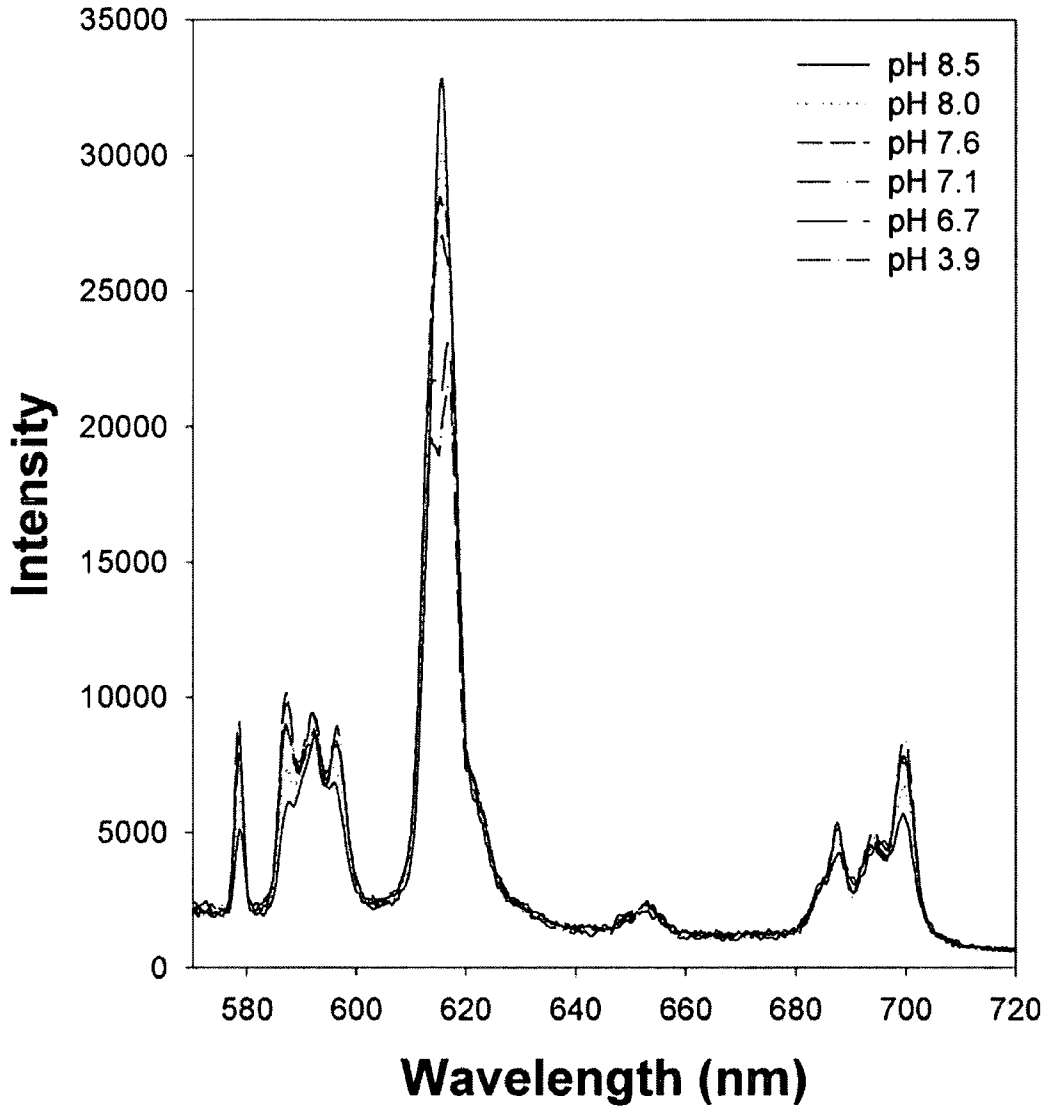

Figure 4.17 Effect of pH on sensitised emission (λ_{ex} 271 nm) of [EuL^9] in an extracellular anion background.

The sensitised europium emission spectrum (Figure 4.17) of **[EuL^9]** in an extracellular anion background shows that as the pH decreases there is a change in the

spectral form but the intensity of emission remains constant. This suggests that anions are bound to the europium centre over the whole pH range investigated, unlike in the parent GdaDO3A system where the anions only bound at pH>7.5.[142] At high pH (>7.5), the hypersensitive $\Delta J = 2$ band is very sharp and intense and the $\Delta J = 1$ band is broad. A decrease in pH results in a change in the spectral form at ~pH 7.5. The intensity of the $\Delta J = 2$ band decreases and resolves into two distinct bands and the intensity of both the $\Delta J = 4$, $\Delta J = 1$ and $\Delta J = 0$ bands increase, with the $\Delta J = 1$ transition displaying three bands. This suggests that the anion coordinated to the europium centre varies with pH.

In order to unequivocally prove which anion is bound to the europium centre, the sensitised emission spectrum of **[EuL^9]** was recorded in solutions containing only one anion.

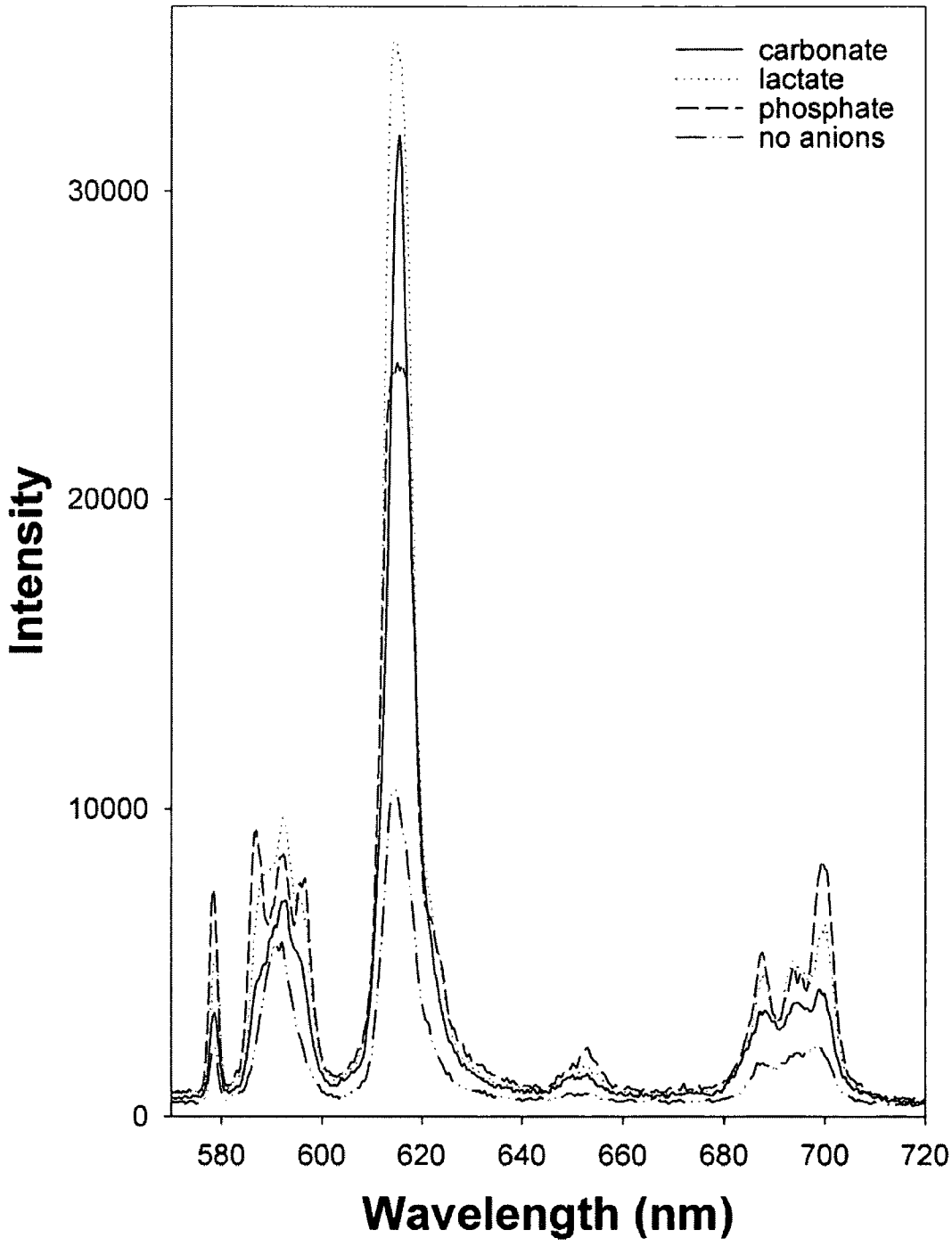

Figure 4.18 Effect of lactate, phosphate and carbonate on the sensitised emission of [EuL^9].

The sensitised emission spectra of **[EuL^9]** in the presence of lactate, phosphate and carbonate show significant differences in spectral form, (Figure 4.18). The displacement of the water molecules bound to the europium centre by the anions results in a large increase in emission intensity.

Comparison of Figure 4.17 with Figure 4.18 reveals that at high pH (>pH 7.5), carbonate is bound to **[EuL^9]** and as the pH decreases the carbonate is displaced by phosphate.

4.6 Conclusions

Pyridine trifluoromethanesulfonamide appended lanthanide complexes **[LnL^7]**, **[LnL^8]**, **[LnL^9]** and **[LnL^{10}]** did not show any behaviour, either emissive or relaxometric, which was responsive to zinc (II) ions in the range investigated. A zinc (II) binding group with a higher affinity at physiological pH must be sought.

Protein binding studies revealed that **[GdL^9]** has a very high affinity (K_A = 1.4×10^5 M^{-1}) for HSA. The binding of **[GdL^9]** to HSA results in the formation of a ternary adduct with a very high relaxivity: unbound r_{1p} = 8.7 $mM^{-1}s^{-1}$ (60 MHz, 37°C) compared to r_{1p} = 67.5 $mM^{-1}s^{-1}$ (60 MHz, 37°C) when bound to 0.6 mM HSA. This increase in relaxivity shows that **[GdL^9]** remains q =2 even when bound to protein and the increase in τ_R of the protein increases the observed relaxivity. However, this relaxivity is not maintained in the presence of serum. The presence of anions in the serum displaces the inner sphere water molecules from the gadolinium, resulting in a significant reduction in relaxivity. Sensitised emission spectra of the europium analogue have revealed that at pH > 7.5, carbonate anions bind to the gadolinium whereas at pH < 7.5 phosphate anions displace the water from the lanthanide centre.

Chapter 5

pH and pZn Responsive Lanthanide System

5 pH and pZn Responsive Lanthanide System

5.1 Introduction

The pyridyl trifluoromethanesulfonamide ligand L^2 was incorporated into a DO3A-type macrocyclic complex **[LnL^{12}]**, which was destined to have pH and pZn (II) responsive properties for potential MRI and luminescence applications. The complex has an anionic sulfonamide donor which was hypothesised to bind to the lanthanide (III) centre in a reversible manner in response to changing pH and zinc (II) concentration.

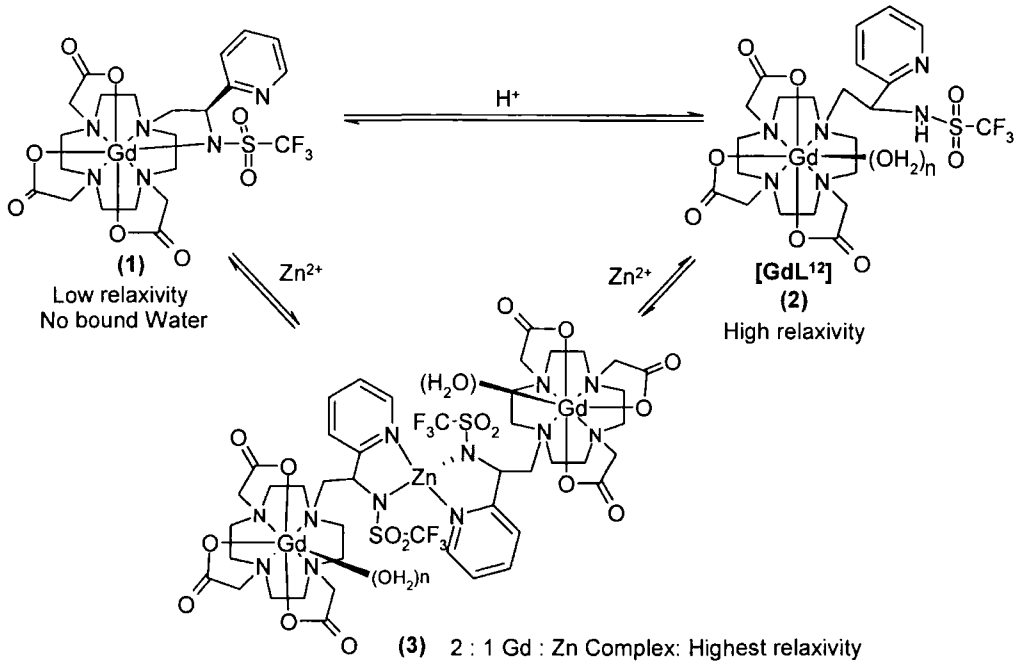

Scheme 5.1 Proposed mechanism for the responsive behaviour of [GdL^{12}] with variation of pH and pZn (II).

The proposed mechanism through which **[GdL^{12}]** enhances the water relaxation rate in response to increased concentrations of zinc (II) and pH is illustrated in Figure 5.1.

At high pH and in the absence of Zn (II), complex **(1)**, the gadolinium (III) ion is eight coordinate, and binding of water is inhibited by the presence of the coordinated trifluoromethanesulfonamide group, leading to a complex with low relaxivity.

In the presence of acid, the sulfonamide nitrogen will be protonated and the binding of the sulfonamide nitrogen to gadolinium is suppressed; complex **(2)** may then form. This leaves a co-ordination site free on the Gd (III) for water to bind, leading to an increase in the relaxivity of the complex. The pH dependence of this process has been defined in recent work by Lowe *et al.*[63,77]: the pH at which complex protonation occurs may be controlled by variation of the sulfonamide group or by changing the substituent α to the ring nitrogen. Complexes with pK_{aH} values in the range 5.7 to 7.2 have been characterised in Lowe's work.

Addition of zinc (II) ions to the system will disturb this equilibrium, resulting in the stepwise formation of **(3)**, which is a 2 : 1 complex with 2 Gd^{3+}: 1 Zn^{2+}. The increased size of this molecule will cause it to tumble more slowly in solution; slower tumbling in solution results in an increase in τ_R and consequently the relaxivity will increase.

The europium analogue **[EuL^{12}]** was also synthesised. It is proposed that at high pH, no water will be coordinated to the europium centre, so the intensity of emission will be high. As pH increases, the sulfonamide nitrogen will protonate and water will be able to bind to the europium centre, leading to a quenching of the emission. Similarly, at high concentrations of zinc (II) ions, the sulfonamide nitrogen will bind to zinc, allowing water to bind to the europium, again resulting in a decrease in the intensity of emission.

5.2 Synthesis

Many different routes were investigated in an attempt to synthesise ligand **L^{12}**. Initially, work was directed towards the synthesis of enantiomerically pure 2-pyridylglycine, Scheme 5.2.

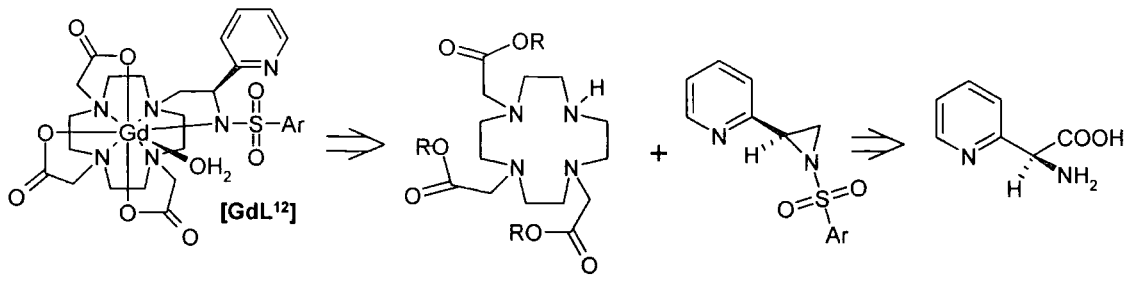

Scheme 5.2 The first target in the overall sequence requires the synthesis of enantiometrically pure 2-pyridylglycine

Early attempts that were made to synthesis 2-pyridylglycine are shown in Scheme 5.3. The initial intention was to prepare the N-acetyl derivative and use hog renal acylase[144] to resolve it. 2-Pyridinecarboxaldehyde was converted into the oxazole **92** using the Bucherer-Burgs reaction.[145] Subsequent hydrolysis with 2M sodium hydroxide solution[145,146] yielded a mixture of 2-pyridylgycine **93** and pyridine-2-ylmethyl-urea **94** in variable ratios and yields. Strong cation exchange resin was used to remove the salt from the products. However, the liberation of protons in exchange for Na^+ resulted in the decarboxylation of the amino acid and the production of unwanted 2-aminomethylpyridine **95**.

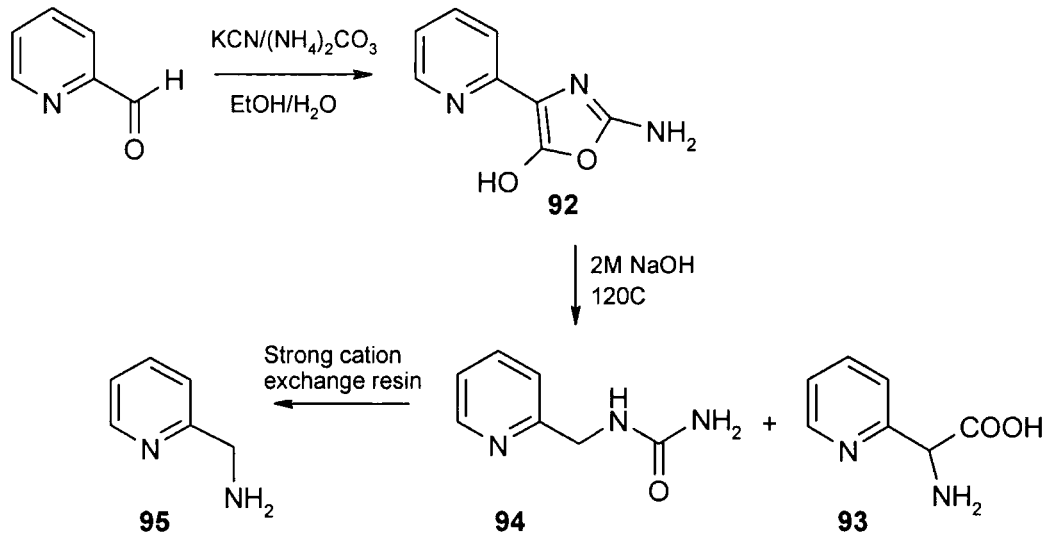

Scheme 5.3 Initial attempt to synthesise 2-pyridyl glycine 93.

An alternative route, Scheme 5.4, was therefore devised for the synthesis of N-acyl 2-pyridylglycine **96**. The oxime **97** was formed by reacting sodium nitrite with ethyl(2-pyridyl)acetate as described by Van Zyl *et al.*[147] Following the method of Kolar and co-workers,[148] **97** was reduced using zinc dust and acetic anhydride to

form the racemic amide **98**. Hydrolysis of the ethyl ester was achieved with 0.02 M sodium hydroxide solution to yield N-acyl 2-pyridylglycine **96**.

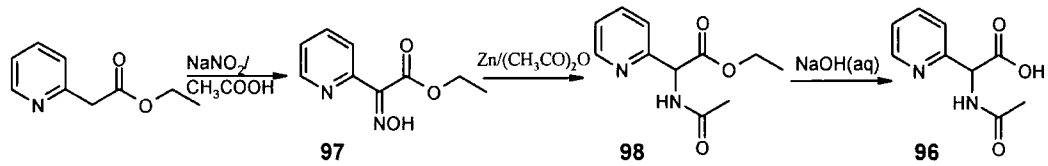

Scheme 5.4 Synthesis of N-acyl 2-pyridylglycine.

Hog renal acylase was then used in an attempt to make enantiomerically pure 2-pyridyl glycine from **96**. Unfortunately both enantiomers were obtained, with no significant resolution.

α-Chymotrypsin was then used in an attempt to hydrolyse ester **98** to enantimerically pure N-acyl protected 2-pyridyl glycine. This also resulted in the isolation of unresolved material.

As the ligand was more challenging than expected to synthesise, it was decided to concentrate on the chemistry of the racemic mixture. The target could be then synthesised subsequently in an enantiomerically pure form.

Initial efforts to reduce ester **98** to the alcohol used borane.THF at low temperatures. This proved to be too powerful a reducing agent, reducing both the ester and the amide functional groups. Lithium borohydride proved to be more gentle, and reduced only the ester functionality to the alcohol to give **99** in 41% yield. The amide protecting group was then removed by hydrolysis in 6M hydrochloric acid to give **100** quantitatively. Trifluoromethanesulfonyl chloride in the presence of Hünig's base was then used to prepare the sulfonamide **101**.

Problems arose in attaching a leaving group to **101** so that it could be linked to the protected DO3A core. Triphenyl phosphine and carbon tetrabromide were used in an attempt to brominate the alcohol. However, under a variety of conditions no reaction occurred. Attempts were made to sulfonylate the alcohol **101** with trifluormethanesulfonyl chloride, trifluoromethanesulfonic anhydride, and

trifluoromethanesulfonyl imidazole under different conditions, but the desired product was never isolated.

As it did not seem possible to attach a leaving group to **101**, it was decided to go back to the protected amine stage (**99**), and endeavour to join the pyridyl amide on to the DO3A core and then sulfonylate it. It was found possible to brominate **99** using triphenyl phophine and carbon tetrabromide. The bromide **102** was then used to alkylate protected DO3A **48**, but this led directly to the formation of the aziridine **103**. Attempts were made to alkylate the protected DO3A using the aziridine, which was produced by stirring the bromide in potassium hydroxide solution. The aziridine proved to be very stable and resisted ring opening even when heated to 160°C (Scheme 5.5).

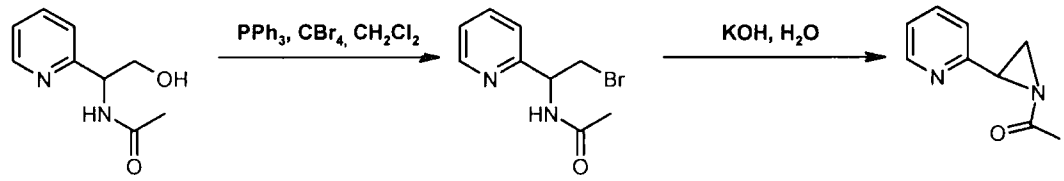

Scheme 5.5 Formation of stable aziridine 103.

As joining the pyridyl moiety with the protected amine group onto DO3A was difficult, further attempts were pursued using the sulfonamide **101**. This time it was decided not to isolate the product with the leaving group as this was probably causing intermolecular reactions to occur. Instead, attempts were made to react it on *in situ*.

Methanesulfonyl chloride was then used to mesylate the alcohol of **101**. The disappearance of the alcohol was monitored by TLC and a single spot, presumed to be **104**, was formed. This was then reacted *in situ* with the addition of 1,4,7-tris(tert-butoxycarbonylmethyl)-1,4,7,10-tetraazacyclododecane **48**, in hot acetonitrile, in the presence of potassium carbonate. The resulting tetrasubstituted cyclen **105** was deprotected with trifluoroacetic acid to afford the desired ligand L^{12} as the TFA salt. Lanthanide (III) complexes, **[EuL^{12}]** and **[GdL^{12}]** were prepared in aqueous solution

following reaction of the ligand with hydrated $LnCl_3$ at pH 5.5 (90°C, 18 hours), Scheme 5.6.

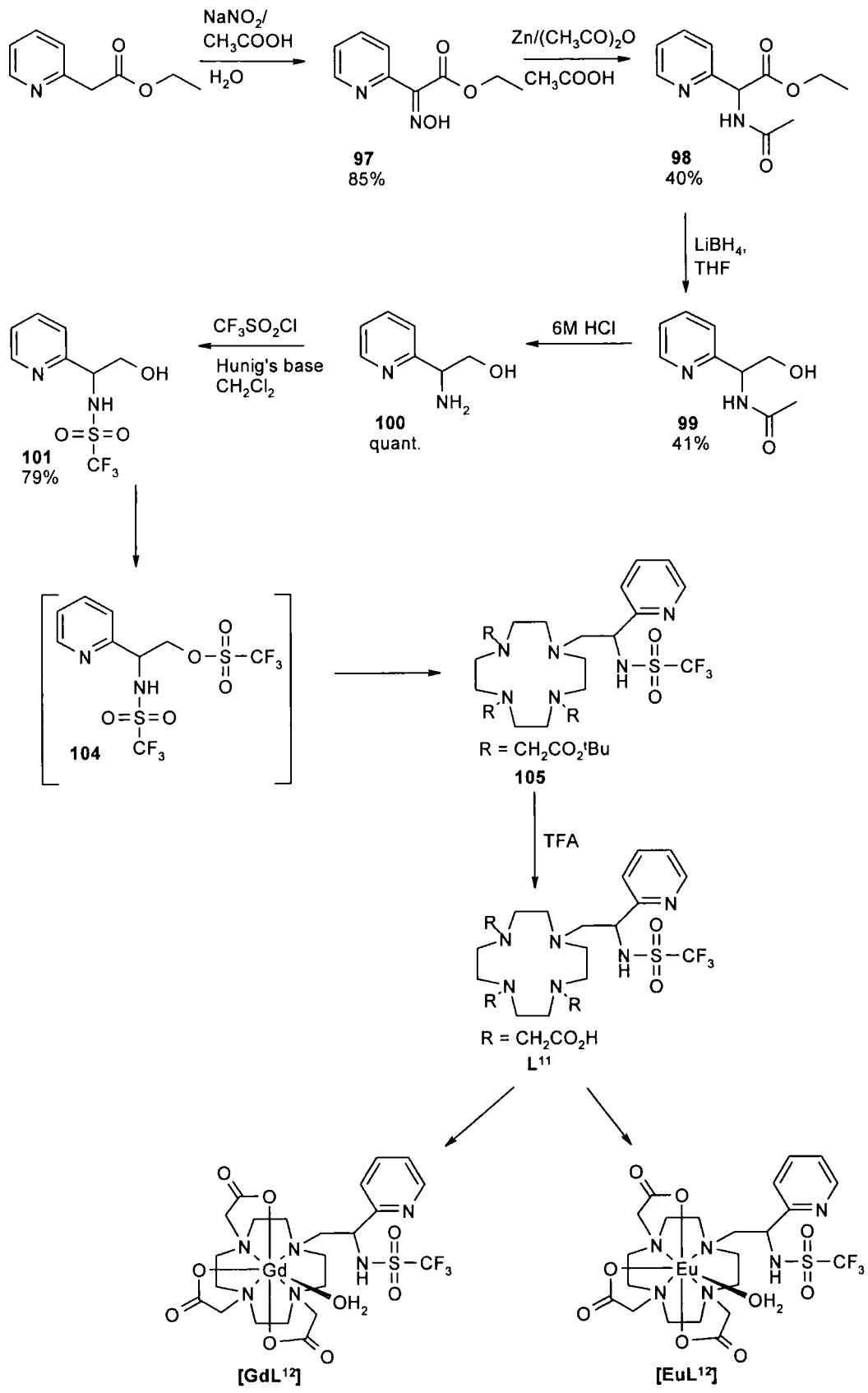

Scheme 5.6 Successful overall synthesis of lanthanide (III) complexes of ligand L^{12}.

5.3 Luminescence Studies of [EuL^{12}]

5.3.1 Effect of pH on Emission Spectrum of [EuL^{12}]

Information about the nature of the lanthanide (III) coordination environment as a function of pH was provided by examination of the europium emission spectrum following sensitised excitation (262 nm). It was anticipated that as the pH decreased, the sulfonamide nitrogen would become protonated, resulting in the sulfonamide nitrogen ceasing to bind to the lanthanide centre (Scheme 5.7). This would then allow water to bind to the lanthanide centre, resulting in a change in spectral form and a decrease in the intensity of emission. Also, the increased distance between the pyridyl chromophore and europium (III) centre would result in less efficient energy transfer between the sensitising group and the lanthanide ion.

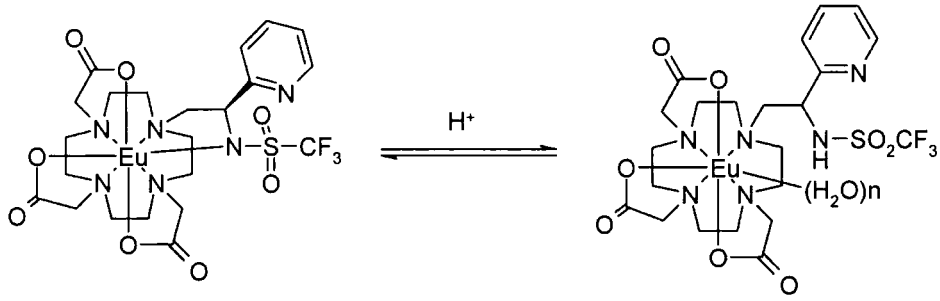

Scheme 5.7 Hypothesised effect of pH on the constitution of [EuL^{12}].

The pH of a solution of **[EuL^{12}]** was adjusted to pH 10 using sodium hydroxide solution. Small aliquots of 0.1 M HCl were added and the luminescence spectra were recorded at each point following excitation at 262 nm.

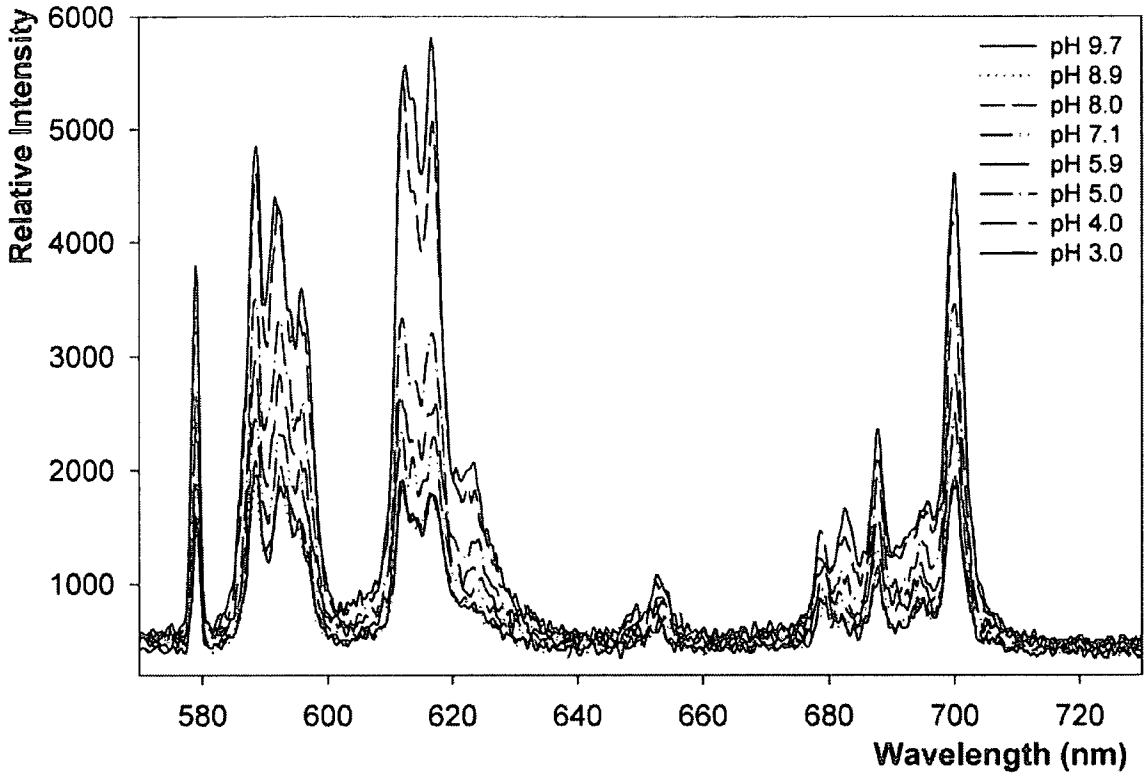

Figure 5.1 Effect of pH on the Sensitised Emission (λ_{exc} 262 nm) of [EuL^{12}] (315 nm filter).

The emission spectrum (Figure 5.1) shows no change in spectral form between pH 3 and pH 10. As the pH decreases, the intensity of emission can be seen to increase slightly although the ratio of the $\Delta J = 2 : \Delta J = 1$ bands remains constant. This suggests that there is no change in the europium coordination environment over the pH range investigated. It can therefore be concluded that there is no reversible ligation of the europium centre with changing pH.

If the pyridyl nitrogen were irreversibly bound to the europium (III) centre, then the protonation of the unbound sulfonamide nitrogen with decreasing pH may result in the slight increase in intensity of the spectrum, as it would be less hydrated than in an anionic form.

5.3.2 Variation of Excitation Spectra of [EuL^{12}] with pH

Information about the europium coordination environment can also be ascertained from the excitation spectrum. The excitation spectrum was also recorded as a function of pH whilst observing the 616 nm emission band.

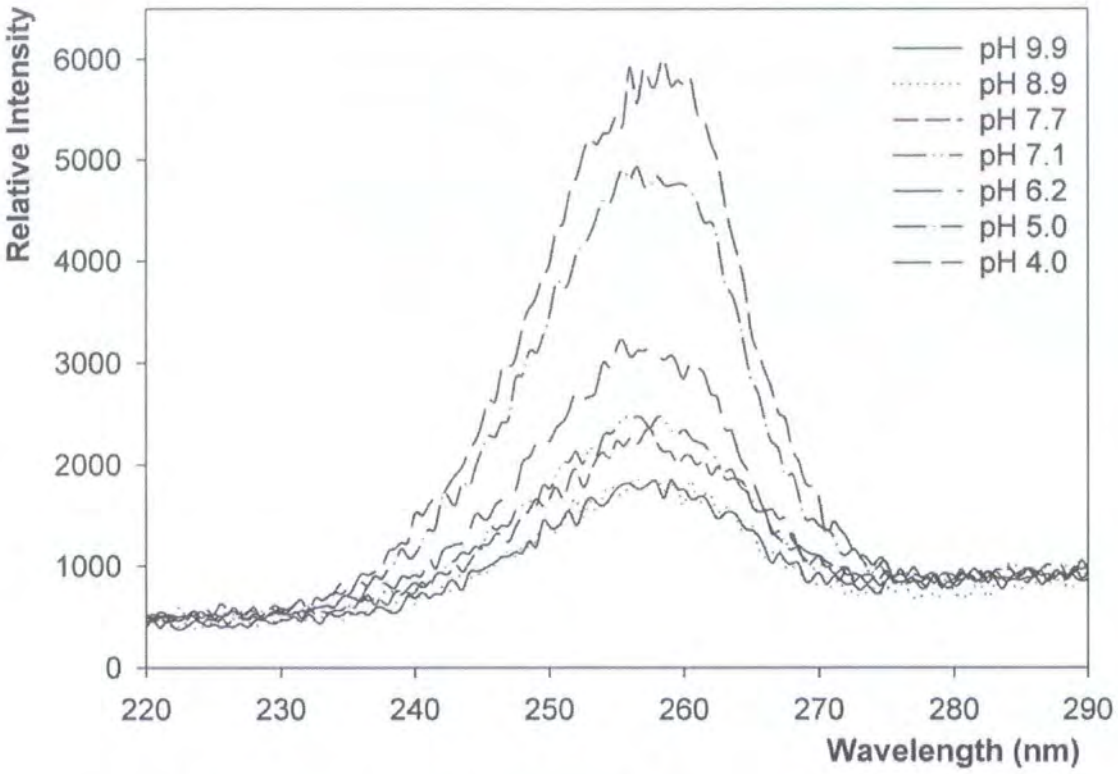

Figure 5.2 Excitation of [EuL^{12}] as a function of pH.

Although the intensity increases slightly, the form of the excitation spectrum of **[EuL^{12}]** remains unchanged with decreasing pH (Figure 5.2). This suggests that there is no change in the coordination environment of europium, thus no reversible ligation, with variation in pH.

5.3.3 Variation of [EuL^{12}] Absorption Spectra with pH

The absorption spectrum of **[EuL^{12}]** was also monitored as a function of pH. No significant variation in spectral form and intensity was observed with changing pH (λ_{max} 262 nm), suggesting that the coordination environment of the pyridyl chromophore was not changed.

5.3.4 Emission excited state lifetimes of Eu (III) complex: evaluation of q.

The number of water molecules (q) coordinated to the europium centre of **[EuL^{12}]** at pH 4 and 7 was assessed by measuring the rate constants for the depopulation of the Eu $^5D_0$ excited states in H_2O (k_{H_2O}) and D_2O (k_{D_2O}) as discussed in Section 3.3.[61]

Table 5.1 Rate constants for decay of Eu excited state and number of bound water molecules bound to [EuL^{12}] at pH 4 and 7.

[EuL^{12}]	pH 4	pH 7
k_{H_2O} (ms^{-1})	1.50	1.35
k_{D_2O} (ms^{-1})	0.54	0.53
q_{Eu}	0.8	0.7

Table 5.1 shows that there is one water molecule bound to **[EuL^{12}]** and the hydration state of the europium (III) centre does not change with increasing pH. This is also in agreement with the absence of pH dependent ligation of the europium (III) centre.

The value of q obtained is less than one, but the hydrophobic nature of the pyridyl and trifluoromethyl moieties may result in the outer sphere contribution being low, resulting in a decreased q value. The slight increase in the q value at pH 4 can probably be attributed to the protonation of the sulfonamide nitrogen resulting in slightly increased second sphere contribution.[128,129]

5.3.5 Effect of Zinc (II) on Luminescence of [EuL^{12}]

Information about the nature of the lanthanide (III) coordination environment as a function of zinc (II) concentration was provided by examination of the europium emission spectrum following sensitised excitation (262 nm). It was anticipated from the speciation plots of the model ligand (Section 2.9.1) that, as the concentration of zinc increased at neutral pH, the pyridyl and sulfonamide nitrogens would bind to the free zinc (II), Scheme 5.8. A consequence of this zinc (II) binding would be that the sulfonamide nitrogen could no longer bind to the lanthanide centre; this would result in the chromophore being further from the europium centre and allow more

water to bind to the lanthanide centre resulting in a change in form and decrease in the intensity of europium emission.[63]

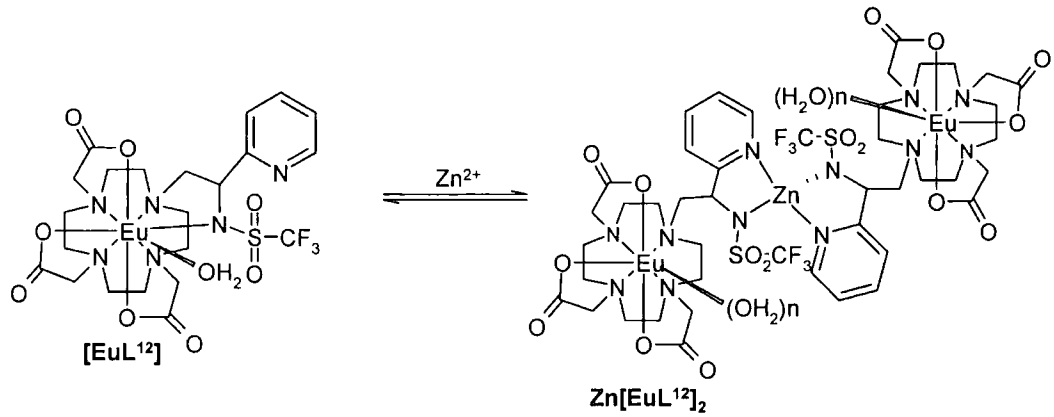

Scheme 5.8 Hypothesised Effect of Zinc (II) on [EuL^{12}].

The excitation and emission of **[EuL^{12}]** were monitored as a function of added zinc (II) while keeping the pH constant (pH 7.1). Zinc (II) acetate solution was added in small aliquots containing one equivalent of zinc until 10 equivalents had been added. EDTA was added to a sample of the **[EuL^{12}]** solution before the titration was undertaken to confirm that the complex had not already become bound to a metal ion. No change in the spectrum was observed so it was concluded that the sample was free from transition metal ions.

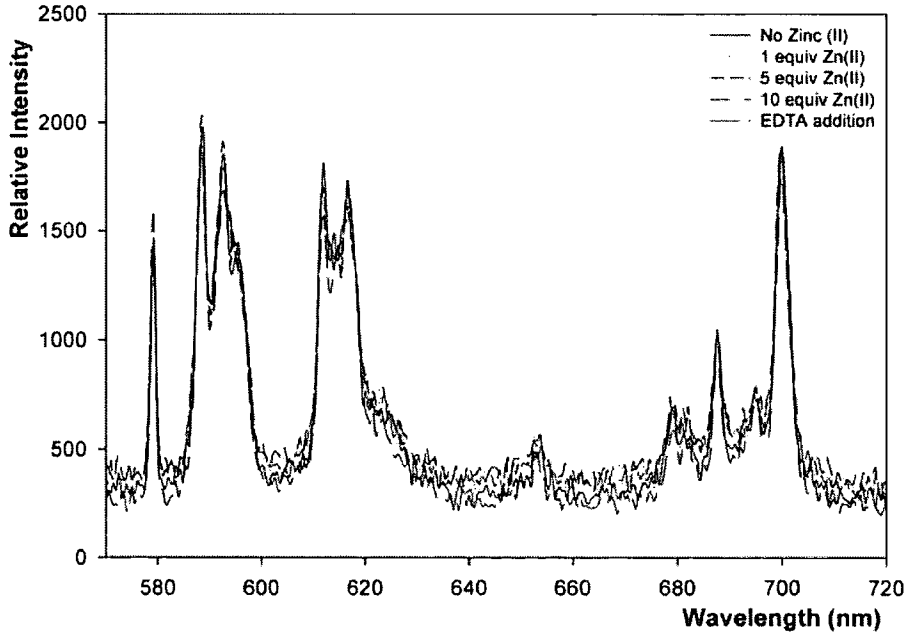

Figure 5.3 Sensitised emission (λ_{ex} 262 nm) of [EuL^{12}] as a function of zinc (II) concentration.

The emission spectrum (Figure 5.3) shows that there is no change in form or intensity as a function of zinc (II) concentration. There is similarly no change in the form or intensity of the excitation spectrum. It would be expected that if the pyridyl sulfonamide moiety bound zinc (II) as hypothesised, the binding of zinc would lead to an increase in the hydration state of the complex and thus a change in the europium (III) emission and excitation. This suggests that there is no change in the ligation or hydration state of the europium (III) centre as a function of added zinc (II).

5.4 Ligation of Pyridine?

Although it was predicted that the sulfonamide nitrogen would ligate the lanthanide (III) centre with a five-membered chelate ring, it would also be possible for a six-membered chelate ring to form between the lanthanide (III) centre and the pyridyl nitrogen atom (Figure 5.4).

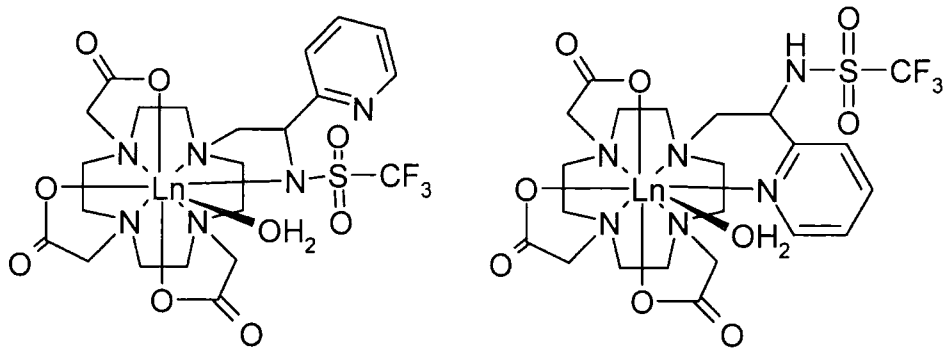

Figure 5.4 Possible ligation configurations of [LnL^{12}]. The sulfonamide nitrogen binds with a five-membered chelate ring or the pyridyl nitrogen could bind in a six-membered chelate ring.

A related EuDO3A complex appended with a pyridyl chromophore, synthesised by Lowe, **106** forms a five-membered chelate ring between the pyridyl nitrogen and the europium (III) centre.[149] The pyridyl nitrogen proved to be a very good donor for the europium centre and binds irreversibly in an equatorial position. The crystal structure obtained of the complex shows there to be one water of hydration in an axial position; this is in agreement with the relaxivity and k_{H_2O} data obtained.

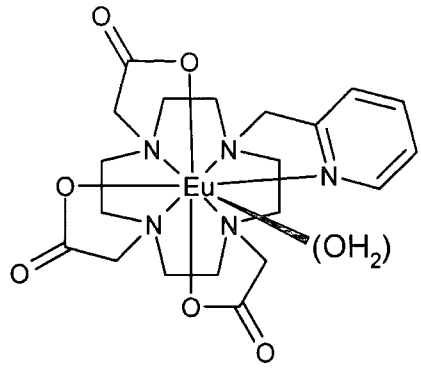

106

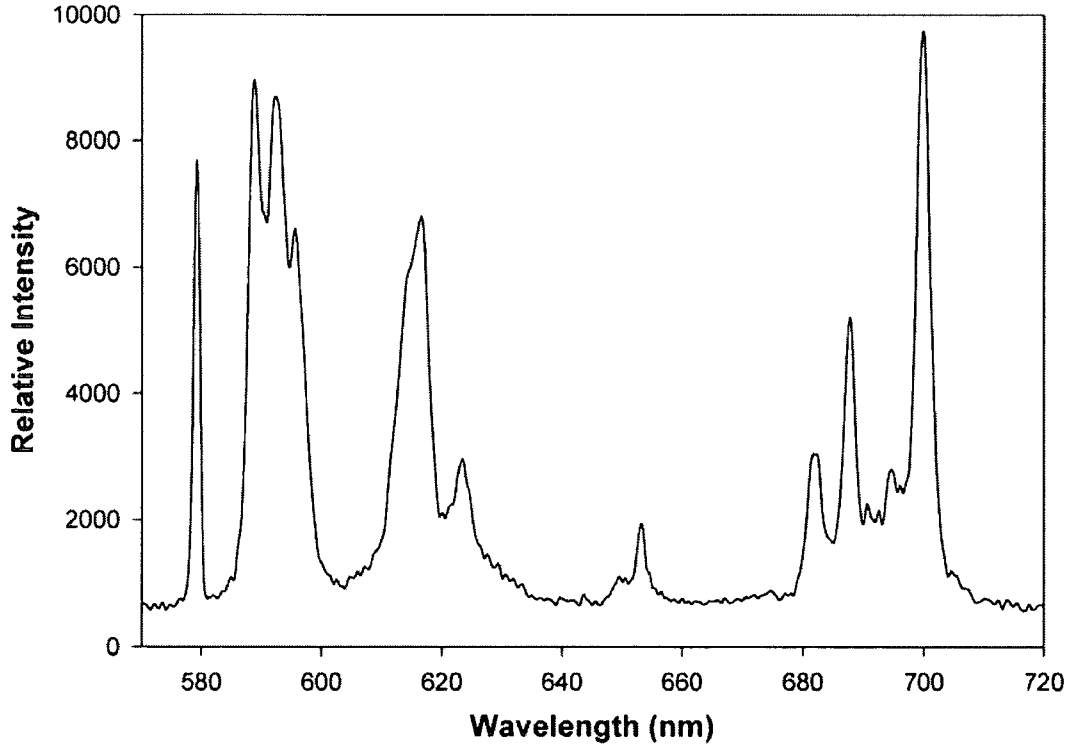

Figure 5.5 Emission spectrum (λ_{ex} 264 nm) of 106 (315 nm filter) The ΔJ = 2 and ΔJ = 1 bands have a similar relative intensity. The spectral form is similar to that of [EuL^{12}].

An emission spectrum (Figure 5.5) was recorded of europium complex **106** which had been synthesised by Dr Mark Lowe. The emission spectrum shows that a pyridyl nitrogen bound to a EuDO3A type complex in an equatorial position results in a ΔJ = 2 band of similar relative intensity to the ΔJ = 1 and ΔJ = 4 bands. The emission spectrum of **[EuL^{12}]** also has ΔJ = 2, ΔJ = 1 and ΔJ = 4 bands of similar relative intensity. This effect suggests that the pyridyl nitrogen of **[EuL^{12}]** binds to the europium centre in an equatorial fashion while the water is bound in an axial position.

Europium (III) complex **107** synthesised by Maffeo and Williams[150] has a quinoline moiety which forms a five-membered chelate ring between the quinoline nitrogen and the europium (III) centre. The complex has no bound water molecules as the space normally occupied by the water molecules is occupied by the benzyloxy group.

The europium emission spectrum obtained of complex **107** is of similar form, although the relative intensities of the ΔJ bands increases in the order $\Delta J = 4 > \Delta J = 2 > \Delta J = 1$. This change in the relative intensities of the ΔJ bands is probably a function of the change of hydration state.

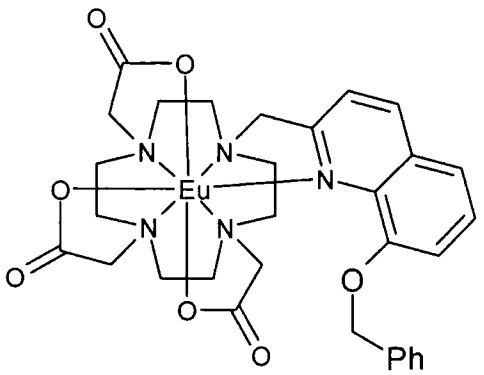

107

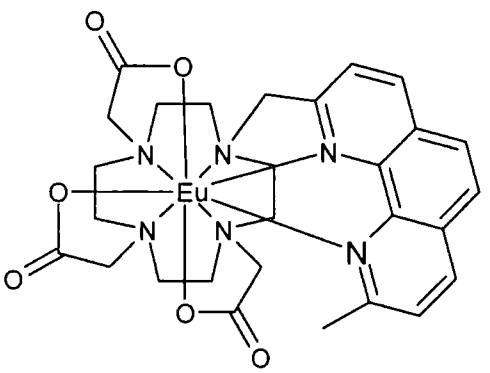

108

Another example of a EuDO3A complex with an aromatic nitrogen coordinated to the europium (III) centre in a five-membered chelate ring **108** was synthesised by Quici and coworkers.[151] The complex has a phenanthroline chromophore and no water is bound to the europium centre. The emission spectrum obtained is very similar in form to that obtained for **107**.

In summary, a comparison of the emission spectrum of **[EuL^{12}]** with that of other examples of EuDO3A complexes, with an aromatic nitrogen donor coordinated to the europium centre in a small chelate rings, shows the greatest similarity between **[EuL^{12}]** and **106.** This suggests that the pyridyl nitrogen is coordinated to the europium centre in an equatorial position and there is one water molecule coordinated in an axial position. The lack of change of the emission spectrum and excitation specta as a function of pH and increasing zinc (II) concentration suggests that the pyridyl nitrogen is an excellent donor for the europium (III) ion in such

tribasic N_5O_3 octadentate ligands, and is not susceptible to protonation, remaining irreversibly bound, as was the case for **106.**

5.5 Relaxivity Behaviour of [GdL^{12}] Complex

The behaviour of the gadolinium complex **[GdL^{12}]** was confirmed by relaxivity studies. The relaxivity values were determined from the measured T_1 values and calculated as described in Section 3.5.

The relaxivity of **[GdL^{12}]** was determined at both 60 MHz, 37°C and 65 MHz, 22°C (Table 5.2).

Table 5.2 Relaxivity of [GdL^{12}] at pH 7.

Complex	Relaxivity ($mM^{-1}s^{-1}$)	
	60 MHz, 37°C	65 MHz, 22°C
[GdL^{12}]	2.67	3.73

The relaxivity values obtained for **[GdL^{12}]** at the measured field and temperatures lie within the expected range for low molecular weight gadolinium systems with a q = 1 hydration state.[92]

5.5.1 Effect of pH on Relaxivity

The relaxivity of **[GdL^{12}]** was determined at pH 4, 7 and 9 using the Bruker Minispec mq60 (60 MHz, 37°C). The system was designed to increase in relaxivity with a decrease in pH. However, if the gadolinium and europium complexes behave in the same manner, with the pyridyl nitrogen being a very good donor for the lanthanide centre, no change in relaxivity would be expected with a decrease in pH.

Table 5.3 Relaxivity of [GdL^{12}] at pH 4, 7 and 9 (60 MHz, 37°C).

Relaxivity of [GdL^{12}] ($mM^{-1}s^{-1}$)		
pH 4	pH 7	pH 9
2.83	2.52	2.30

The relaxivity values (Table 5.3) show that there is no significant change in relaxivity with pH. This suggests that there is no change in the hydration state at

the Gd (III) centre. This is in agreement with the hypothesis that the pyridyl nitrogen is tightly bound to the lanthanide centre in an irreversible manner.

The slight increase in relaxivity value at low pH is probably caused by the protonation of the sulfonamide nitrogen, causing an increase in the hydration state of the complex, resulting in an increase in the second sphere contribution.

5.5.2 Effect of Zinc (II) on Relaxivity of [GdL^{12}]

The lumiscence studies suggested that the pyridyl nitrogen was bound tightly to the lanthanide ion centre and did not respond to the presence of zinc (II) ions. It was hypothesised that even if the pyridyl nitrogen remained bound to the lanthanide ion it still may be possible for a complex to form between the sulfonamide nitrogens and zinc (II) and possibly the bound pyridyl nitrogens. Although a change in the hydration state was not expected, a dimer would form with two gadolinium complexes per zinc (II) ion (Scheme 5.9). This increase in molecular size would lead to an increase in τ_R and thus an increase the relaxivity.

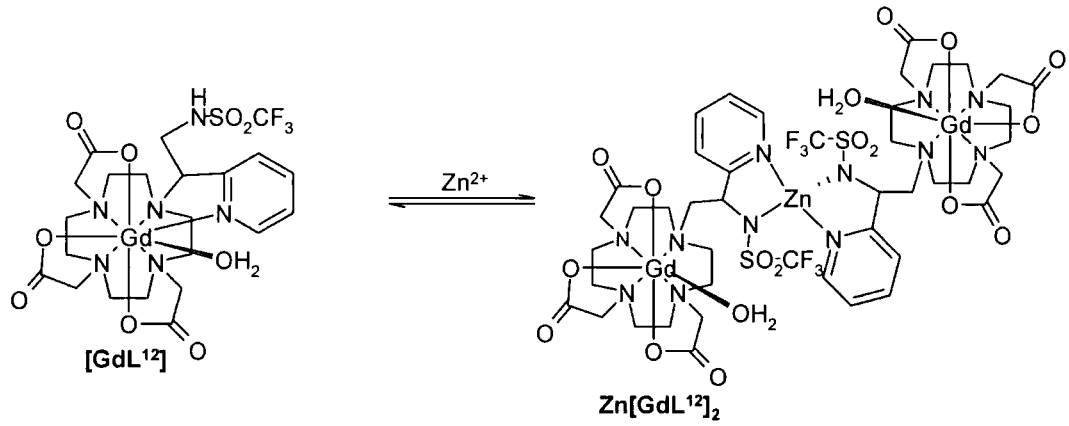

Scheme 5.9 Proposed dimerisation of [GdL^{12}] in the presence of zinc (II).

Small aliquots containing 0.25 equivalents of zinc (II) acetate were added to a 0.38 mM solution of **[GdL^{12}]**, the pH was kept constant at pH 7.4. The T_1 value was determined at both 65 MHz, 22°C and 60 MHz, 37°C.

Table 5.4 Relaxivity of [GdL^{12}] in the presence of various zinc (II) concentrations.

Number of zinc (II) equivalents added.	Relaxivity ($mM^{-1}s^{-1}$) of [GdL^{12}]	
	60 MHz, 37°C	65 MHz, 22°C
0	2.67	3.71
0.25		3.98
0.5		3.74
1	2.60	3.59

Table 5.4 shows that the presence of zinc (II) has no effect on the relaxivity of [GdL^{12}]. This would suggest that a dimer does not form between the gadolinium complex and zinc (II). This is in agreement with the hypothesis that the pyridyl nitrogen irreversibly binds to the gadolinium centre.

5.6 NMRD Profiles of Complex [GdL^{12}]

An NMRD profile of [GdL^{12}] was recorded and fitted in Durham according to the theoretical arguments presented in Section 3.6.

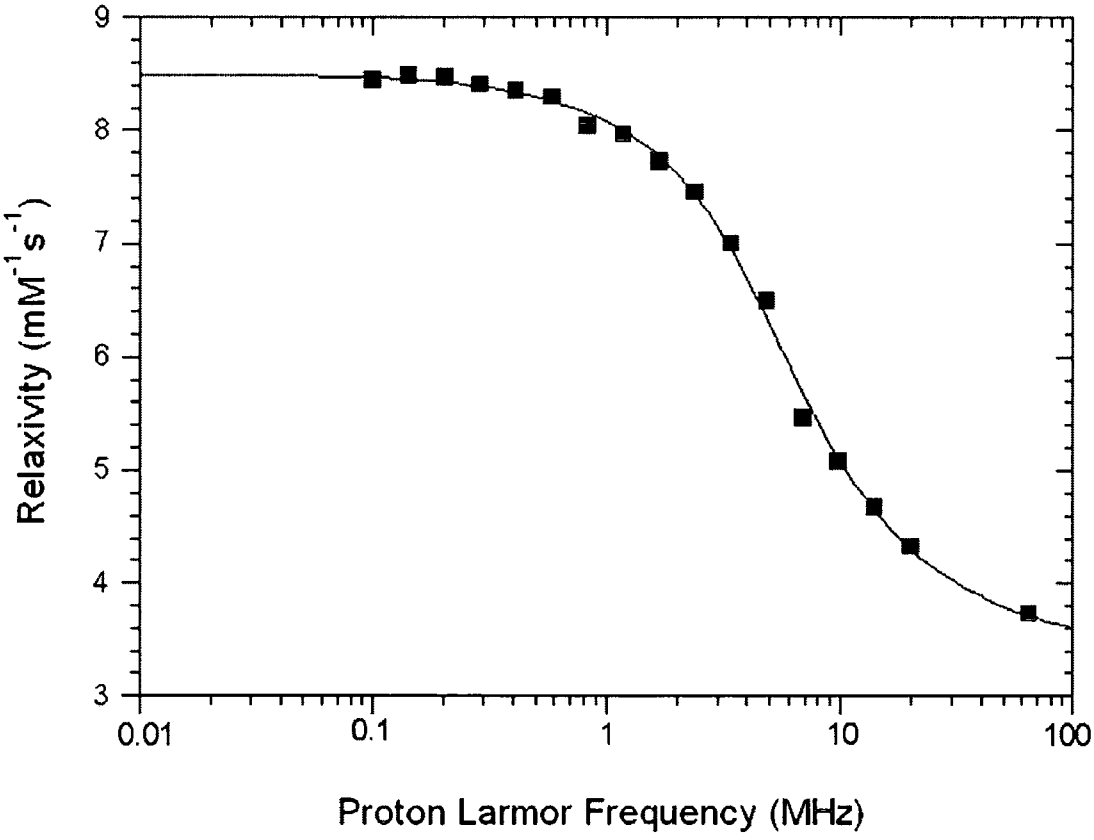

Figure 5.6 Experimental NMRD profile for [GdL^{12}] in aqueous solution (pH 6). The values were all obtained at 25°C with the exception of the 65 MHz value which was obtained at 22°C. The solid lines through the data are best fitting curves obtained using the parameters given in Table 5.5.

Table 5.5 Best fitting parameters obtained from the analysis of the NMRD profiles for the gadolinium (III) complex [GdL^{12}].

Complex	q	Δ^2 ($s^{-2}x10^{18}$)	τ_v (ps)	τ_R (ns)	τ_M (ns)	r (Å)	a (Å)	D ($cm^2s^{-1}x10^{-5}$)
[GdL^{12}]	1	9.9	28	56	2.4	3.13	4	1.72

[GdL^{12}] has an NMRD profile (Figure 5.6) typical of a small gadolinium (III) complex possessing a single coordinated water molecule.[128,129]

5.7 Conclusions

The octadentate N_5O_3 ligand L^{12} contains a coordinating pyridyl group that forms kinetically stable complexes with europium (III) and gadolinium (III) that resist protonation. The pyridyl group binds the lanthanide centre irreversiby, even in the presence of Zn (II) and Cu (II) ions, notwithstanding the putative high affinity of the pyridylsulfonamide moiety for the zinc (II) ions.

Lifetime and relaxivity studies show that the complex [LnL^{12}] has one water molecule coordinated to the lanthanide centre. The emission spectrum suggests that the water molecule is coordinated in an axial position while the pyridyl nitrogen coordinates to the lanthanide centre in an equatorial position.

As the pyridyl nitrogen is such an excellent donor for the lanthanide centre in this tribasic N_5O_3 octadentate ligand, the complex is rendered inappropriate for use as a pH and pZn responsive system. A more appropriate donor group with less strongly lanthanide ligating substituents is required.

Conclusions and Suggestions for Further Work

Although it was first shown that the trifluoromethanesulfonamide moieties in L^2 and L^3 have a high affinity for zinc (II), subsequent studies revealed that when this moiety was incorporated into a macrocyclic lanthanide complex, this affinity was lost. Zinc responsive lanthanide systems were not obtained. It may be possible to increase the affinity of the complex for zinc (II) by altering the sulfonamide to something with a greater number of zinc (II) donor atoms, Figure 7.1, giving a pentadentate binding site for Zn^{2+}.

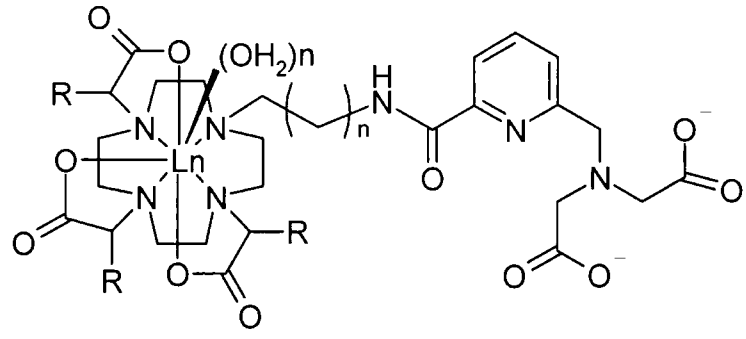

Figure 7.1

Investigations into DO3A systems with an appended pyridyl amide group revealed that the steric bulk introduced to the sytem by a seven-membered chelate ring between the amide carbonyl and lanthanide centre resulted in a very fast water exchange rate. Whereas the increased steric demands of an eight-membered chelate resulted in the lanthanide centre being unhydrated. This approach of increasing steric demand to promote rapid water exchange could be considered as a precursor for new higher molecular weight constrast agents in which a fast-water exchanging site at gadolinium is a prerequisite for maximal relaxivity enhancement.[69]

A remarkably high affinity and relaxivity enhancement in the presence of HSA was displayed by **[GdL^9]**. Unlike previous q = 2 systems, the binding of protein did not result in the displacement of water from the gadolinium centre and an unprecedented 700% enhancement in the relaxivity was observed. However, this system has the disadvantage that this relaxivity increase was not maintained in the

presence of anions or serum. The anions displaced the water bound to the lanthanide centre giving a small enhancement in relaxivity. Further work could try to understand which parts of the pyridyl sulfonamide moiety lead to this high HSA affinity, for example, by changing the sulfonamide group. As the formation of the sulfonamide occurs in the final stages of the ligand synthesis, it should be straightforward to form a variety of sulfonamide analogues, Figure 0.2. These analogues should exhibit different pK_a values at the sulfonamide nitrogen and so should have different hydrogen donor/acceptor properties leading to variation in the affinity for HSA. Also, the free amine and unsubsituted pyridylamide compounds may exhibit some interesting properties in the presence of albumin.

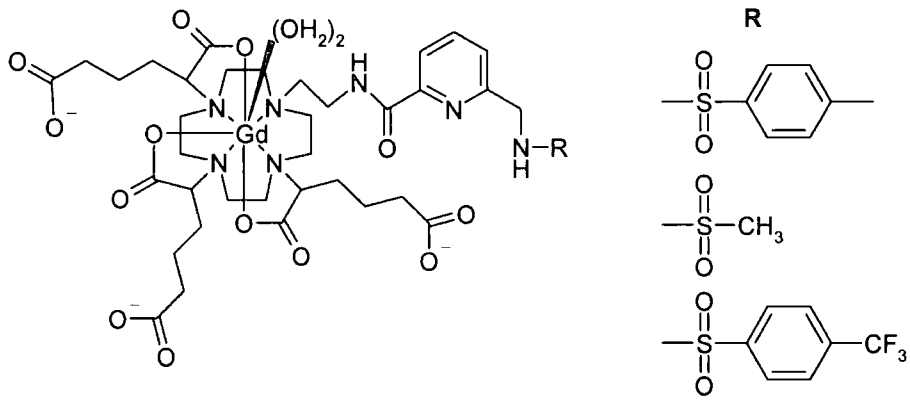

Figure 0.2 Possible target molecules.

Furthermore, the anion affinity of the lanthanide complex could perhaps be reduced by the addition of anion repelling phosphate groups, as in the structure below.

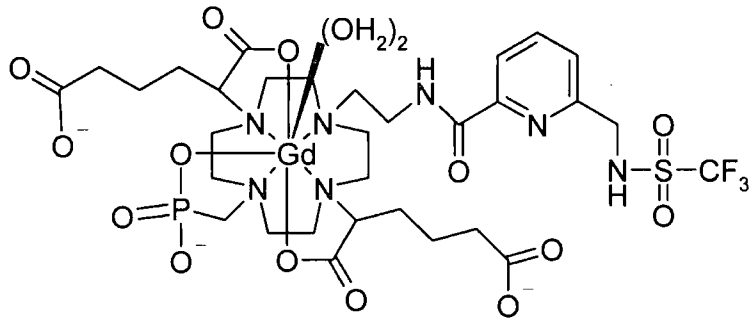

Chapter 6

Experimental

6 Experimental

6.1 Synthetic Procedures and Characterisation

Reactions requiring anhydrous conditions were carried out using Schlenk-line techniques under an atmosphere of dry argon. Solvents were dried from an appropriate drying agent where required.[152] Water was purified by the "Purite$_{STILL}$ plus" system and has a conductivity ≤ 0.04 μScm^{-1}. Reagents were used as supplied.

Thin layer chromatography was carried out using fluorescent (254 nm) silica plates (Merck Art 5554) and visualised by UV or iodine staining. Preparative column chromatography was carried out using silica (Merck silica gel 60, 230-400 mesh).

Mass spectra (ES MS) were recorded using a VG II Platform spectrometer (Fisons Instruments) with methanol as the carrier solvent. EI (EI MS) spectra were recorded on a Micromass AutoSpec. FAB spectra were recorded by the EPSRC Mass Spectrometry Service at the University of Wales at Swansea. Accurate mass spectra (Acc.Ms) were recorded at the University of Durham using a Micromass LCT at 5000 resolution using sodium iodide as the reference. Accurate mass spectra (Acc.Ms) of complexes **[EuL^5]**, **[GdL^5]**, **[EuL^6]**, **[GdL^6]**, **[EuL^{12}]** and **[GdL^{12}]** were recorded by the EPSRC Mass Spectrometry Service at the University of Wales at Swansea.

NMR Spectra were recorded on a Varian Unity 300 spectrometer at 299.91 MHz (^{1}H), 75.41 MHz (^{13}C) and 188 MHz (^{19}F) or a Varian Mercury 200 spectrometer at 199.99 MHz (^{1}H), 50.29 MHz (^{13}C) and 188.18 MHz (^{19}F) or a Varian Mercury 400 spectrometer at 399.97 MHz (^{1}H), 50.58 MHz (^{13}C) and 376.30 (^{19}F) or a Varian Inova 500 at 499.87 (^{1}H), 125.71 (^{13}C) and 376.35 (^{19}F). Variable-temperature ^{1}H NMR studies and two-dimensional spectra were recorded on a Varian Inova 500. Chemical shifts are quoted with reference to the residue residual protonated solvent and are given in ppm with coupling constants in Hz.

I.R. spectra were recorded on a Perkin-Elmer FT-IR 1720X spectrometer with GRAMS Analyst operating software. Melting points were determined on a

Reichert-Köfler block melting point apparatus and are uncorrected. Combustion analysis was performed using an Exeter Analytical Inc CE-440 elemental analyser.

Single crystal X-ray diffraction experiments were carried out using SMART CCD area detectors and graphite-monochromated MoK_α radiation. The structures were solved by direct methods and refined against F^2 of all data, using SHELXTL programs[106] and standard refinement techniques.

6.2 Photophysical Measurements

Ultraviolet absorbance spectra were recorded in a Unicam UV2-100 spectrometer operating with Unicam Vision software. Samples were contained in quartz cuvettes with a path length of 1cm. All spectra were run against a reference of pure solvent contained within a matched cell.

Luminescence spectra were recorded using a Perkin-Elmer LS 50B, operating with FL Winlab software, or an Instruments S.A. Fluorolog 3-11, operating with DataMax software. Quartz fluorescence cuvettes of path length 1 cm were employed. The absorbance of each solution at the excitation wavelength was below 0.3 to avoid any inner filter effect. Second order diffraction effects were obviated by using a cut-off filter to remove the scattered light before it enters the emission monochromator.

Excited state lifetime measurements were generally made on the Perkin-Elmer LS50 (using Phlemming data acquisition written by Dr A. Beeby, University of Durham), by monitoring the integrated intensity of light (at 616 nm for Eu) emitted during a fixed gate time, t_g, a delay time t_d, later. At least 20 different delay times were used covering two or more lifetimes. The gate time was 0.1 ms, the excitation and emission slits were set to 15 and 20 nm respectively. The lifetimes of **[EuL^9]** and **[EuL^{10}]** were measured using a time-resolved fluorescence spectrometer. The samples were excited by the fourth harmonic of a Nd : YAG laser (266 nm, 1 mJ per pulse). The luminescence was collected at 90° and the emission wavelength selected by a monochromator. The luminescence was recorded using a

photomultiplier tube (Hamamatsu R928); averaged and digitised using a digital storage oscilloscope (Tektronix TDS 320).

The pH measurements were made using a Jenway 3320 pH meter (fitted with a BDH glass + combination electrode-microsample) calibrated at pH 4, 7 and 10 buffer solutions. Luminescence pH titrations were carried out in a background of constant ionic strength (I = 0.1 M NaCl, 295 K) on solutions of absorbance of < 0.2 at wavelengths > λ_{ex} to avoid any errors due to the inner filter effect.

Cyclic voltammetry of the complexes (0.001 M) was carried out in a background electrolyte of tetrabutylammonium perchlorate, TBAP, (0.01 M) in acetonitrile controlled with potentiostat EG&G PARC Model 273. Computer control and data storage were achieved using EG&G PARC Model 270 Research Electrochemistry software. The auxiliary electrode was made of platinum foil, (area 1cm^2), connected to a copper wire mounted in a glass body. The working electrode was made of glassy carbon, purchased from BAS. The reference electrode was a non-aqueous silver/silver chloride electrode, self-assembly kit, purchased from BAS. The electrodes were mounted in a circular Teflon cap and placed in a cylindrical cell (diameter 20 mm, length 65 mm), which was filled with 1 ml of the desired solution and purged with argon. The cell assembly was placed inside a Faraday cage to eliminate strong field interference.

Potentiometric analyses were carried out using apparatus described previously.[153,154] Data were analysed using HYPERQUAD[118,119,120] and corrections to pK_W were applied to allow for solvent contribution.[117] All relevant hydrolysis constants used, were taken from the IUPAC Stability Constants database Version 5.12, published by IUPAC and Academic Software, 2000.

6.3 Relaxivity and ^{17}O Measurements

Longitudinal ^1H relaxation times at 60 MHz and 65 MHz were measured using a Bruker Minispec mQ 60, operating at 37.0°C and a home-made Varian 65.3 MHz instrument, at 22°C, by means of the inversion recovery technique.

Variable temperature ^{17}O NMR studies were determined on a Varian Inova 500 spectrometer at 67.08 MHz. The temperature of the probe head was determined using an ethylene glycol standard.

Variable-temperature proton-solvent longitudinal relaxation times were measured in the range 0.01 to 20 MHz in Durham on a Stelar Spinmaster-FFC 2000 Fast Field Cycling NMR relaxometer [Stelar, Mede (PV), Italy] by means of the inversion recovery technique (32 experiments, four scans). The reproducibility of T_1 measurements was within 1%. The temperature was controlled by a Stelar VTC 90 airflow heater equipped with a copper constantan thermocouple: the actual temperature in the probe head was measured with a Fluke 53 k/j digital thermometer with an uncertainty of 0.5 K.

Protein Titrations: Human Serum Albumin (crystallised and lyophilised) was purchased from Sigma (St. Louis, Mo., USA) and was used without any further purification. The molecular weight was assumed to be 67 kDa.

Human Serum was purchased from Sigma (St. Louis, Mo., USA) and was rehydrated and used without any further purification.

6.4 Chapter 2 Experimental

6.4.1 Ligand Synthesis

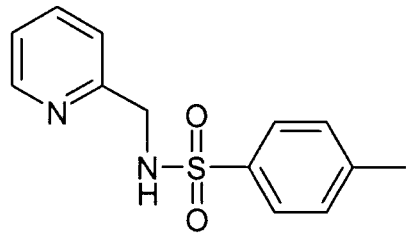

2-(p-Toluenesulfonylaminomethy)pyridine $\mathbf{L^1}$ To a stirred solution of p-toluenesulfonyl chloride (3.43 g, 0.018 mmol) in pyridine (10 ml) cooled to -10°C was slowly added 2-aminomethylpyridine (2.00 g, 0.018 mmol) in pyridine (5 ml). The resulting reaction mixture was stirred at -10°C for 3 hours and was held at 5°C overnight. The reaction mixture was poured onto crushed ice resulting in the precipitation of a

yellow solid, which was removed by filtration and washed with water. The precipitate was dissolved in dichloromethane, dried (Na_2SO_4) and the solvent evaporated yielding pale yellow crystals (2.12 g, 45%). m.p. 76-77°C; ^{1}H NMR (200 MHz, CD_3OD): δ_H 2.40 (s, 3H, CH_3), 4.15 (s, 2H, CH_2), 7.22 - 7.45 (4H, m, H3, H5, H3', H5'), 7.69 (3H, m, H4, H4', H6'), 8.37 (1H, d, *J* 4.4, H6); ^{13}C NMR (50.29 MHz, $CDCl_3$): δ_C 21.15 (Me), 47.47 (CH_2), 122.00 (C3 or C5), 122.32 (C3 or C5), 126.75 (C3'+C5'), 129.29 (C2'+C6'), 136.72 (C4), 142.92 (C4'), 148.59 (C2), 155.34 (C1'); *m/z* ES$^+$: 546.7 (100%, 2M+Na), 284.5 (85%, M+Na); υ_{max} (KBr)/cm^{-1} 3250 (νNH), 1599 (v py), 1574 (v py), 1441 (v py), 1385 (δ NH), 1329 (va SO_2), 1165 (vs SO_2), 1111 (δ CH), 1089 (δ CH), 1007, 901 (v N-S), 763 (δ py), 662 (γ NH), 543 (δ SO_2); Found: C, 57.12; H, 5.58; N, 10.25. $C_{13}H_{14}N_2O_2S.0.5H_20$ requires C, 57.54; H, 5.57; N, 10.32. Constitution confirmed by x-ray crystallography, CSD Refcode: HUGMEB01.

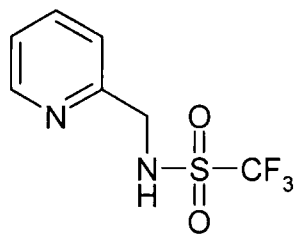

2-(*Trifluoromethylsulfonylaminomethyl)pyridine* **L^2** Under anhydrous conditions in an argon atmosphere, a solution of 2-aminomethylpyridine (0.64 g, 5.93 mmol) in anhydrous pyridine (5 ml) at -40°C was added dropwise, over 10 minutes, to a stirred solution of trifluoromethanesulfonyl chloride (1.0 g, 5.93 mmol) in pyridine (10 ml) at -40°C. The resulting bright yellow reaction mixture was stirred at -40°C for 2 hours and kept at 5°C overnight. The mixture was poured slowly onto crushed ice and stirred. The precipitate that formed was separated by filtration and washed with water. This precipitate was dissolved in dichloromethane (50 ml), washed with water (2 x 25 ml) and the organic phase was dried ($MgSO_4$), filtered and evaporated under reduced pressure to give a solid which was recrystallised from ethyl acetate and hexane (1 : 1) to yield pale brown crystals (0.36 g, 25%), m.p. 82-84°C; ^{1}H NMR (300 MHz, $CDCl_3$): δ_H 4.49 (2H, s, CH_2), 7.24 (2H, m, H3+H5), 7.69 (1H, t of d, *J 1.8, 7.8*, H4), 8.46 (1H, d, *J 5.1*, H6); ^{13}C NMR (50.3 MHz, $CDCl_3$): δ_C 48.05 (CH_2), 123.10 (C2), 123.87 (C4), 138.20 (C5), 149.30 (C6), 154.47 (q, CF_3); ^{19}F

NMR (188 MHz, CD_3CN): δ -79.44 (s, CF_3); m/z (ES^+): 263 (100%, $M+Na^+$), 241 (20%, $M+H^+$); υ_{max} (KBr)/cm^{-1} 1601 (ν py), 1434 (ν py), 1379 (δ NH), 1367 (ν_a SO_2), 1176 (ν_s SO_2), 1143 (δ CH), 1087 (δ CH), 599 (γ NH); Found: C, 35.30; H. 3.01; N. 11.52. $C_7H_7N_2O_2SF_3$ requires C. 35.00; H. 2.94; N. 11.66.

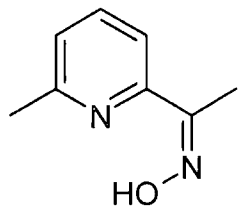

6-*Methylpyridine-2-aldoxime*[104,105] **44** Hydroxylamine hydrochloride (1.40 g, 20.14 mmol) dissolved in water (4 ml), was added to a solution of 6-methyl-2-pyrdinecarboxaldehyde (1.20 g, 9.90 mmol) in water (2 ml). Potassium carbonate (1.60 g, 11.50 mmol) was added and the resulting frothy white reaction mixture was heated at 35°C for two hours. The reaction mixture was cooled to room temperature, filtered under suction and washed with water to yield a white powder. Recrystallisation from ethanol and water yielded a white crystalline solid (1.13g, 84%). m.p. 120–122°C, (lit[104] 170-171°C, lit[105] 165°C); ^1H NMR (300 MHz, DMSO): δ_H 2.54 (3H, s, CH_3), 7.29 (1H, d, *J* 7.5, H5), 7.65 (1H, d, *J* 7.8, H3), 7.77 (1H, t, *J* 7.8, H4), 8.09 (1H, s, HC=C), 11.68 (1H, s, OH); ^{13}C NMR (300 MHz, DMSO): δ_C 24.77 (CH_3), 117.78 (C3), 124.12 (C5), 137.91 (C4), 149.95 (q, C6), 152.77 (q, C2), 158.71 (C=N); (ES^+): 158.8 (100%, MNa^+). Found: C, 61.75; H, 5.96; N, 20.71. $C_7H_8N_2O$ requires C, 61.75; H, 5.92; N, 20.57.

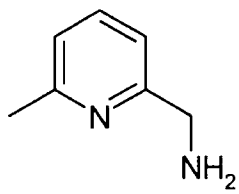

2-*Aminomethyl-6-methylpyridine* **45** 10%Pd/C (0.114 g) was added to 6-methylpyridine-2-aldoxime **44** (1.102g, 8.09 mmol) dissolved in absolute ethanol (60 ml). The mixture was hydrogenated in a Parr hydrogenation apparatus at room temperature under 40 psi H_2 for 4½ hours. The mixture was filtered through celite, which was washed thoroughly with ethanol and dichloromethane, the solvent was evaporated under reduced pressure to yield a clear colourless oil (0.915g, 93%); ^1H

NMR (200 MHz, $CDCl_3$): δ_H 2.47 (3H, s, CH_3), 3.87 (2H, s, CH_2), 6.93-7.08 (2H, m, H3, H5), 7.47 (1H, t, *J* 7.6, H4); ^{13}C NMR (200 MHz, $CDCl_3$): δ_C 24.56 (CH_3), 47.85 (CH_2), 118.35 (C5), 119.43 (q, C6), 121.61 (C3), 137.09 (C4), 158.12 (C2); m/z (ES^+): 122.9 (100%, MH^+).

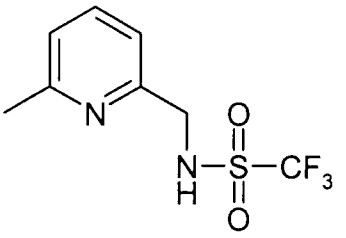

2-(*Trifluoromethanesulfonylaminomethyl)-6-methylpyridine* **L**^{3} Under anhydrous conditions in an argon atmosphere, a cooled solution of 2-aminomethyl-6-methylpyridine **45** (0.45g, 3.69 mmol) in anhydrous pyridine (2.4 ml) was added slowly to a stirred solution of trifluoromethanesulfonyl chloride (0.62g, 3.69 mmol) in anhydrous pyridine (6.6 ml), which had been cooled to -40°C. The resulting yellow solution was stirred at ~-40°C for two hours then kept at -18°C overnight before being added slowly to crushed ice. The ice was stirred and allowed to melt resulting in the formation of a green precipitate, which was filtered off under suction. This precipitate was dissolved in dichloromethane (10 ml), washed with water (2x10 ml), the combined organic phase was dried ($MgSO_4$), filtered and the solution evaporated under reduced pressure to yield a yellow oil. The aqueous phase was extracted with dichloromethane (3x50 ml), the combined organic extracts were dried ($MgSO_4$), filtered and evaporated under reduced pressure to yield a yellow oil which was purified by flash column chromatography (SiO_2, 1:1 ethyl acetate : hexane). Clear crystals formed on the evaporation of the reduced eluting solvent. (0.25g, 30%). m.p. 73-74°C. ^1H NMR (200 MHz, $CDCl_3$): δ_H 2.47 (3H, s, CH_3), 4.53 (2H, s, CH_2), 7.08 (2H, t, *J* 7, H3, H5), 7.61 (1H, t, *J* 7.8, H4); ^{13}C NMR (50.3 MHz, $CDCl_3$): δ_C 12.60 (CH_3), 47.80 (CH_2), 116.72 (q, C6), 119.49 (C5), 123.17 (C3), 137.64 (C4), 152.77 (C2), 158.34 (CF_3); ^{19}F NMR (188 MHz, $CDCl_3$): δ_F -77.70 (s, CF_3); m/z (ES^+): 255 (100%, MH^+); υ_{max} (KBr)/cm^{-1} 1606 (ν py), 1369 (ν_a SO_2), 1191 (ν_s SO_2), 1145 (δ CH), 1069 (δ CH), 611 (γ NH); Found: C, 37.73; H. 3.55; N. 10.91. $C_8H_9N_2O_2SF_3$ requires C. 37.80; H. 3.57; N. 11.02.

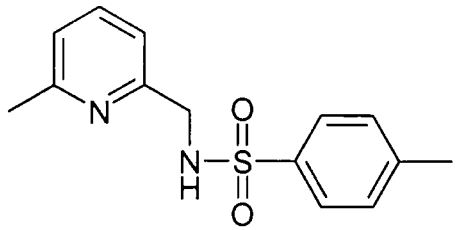

2-(*p-Toluenesulfonylamino)-6-methylpyridine* $\mathbf{L^4}$ To a stirred solution of p-toluene-sulfonyl chloride (192 mg, 1.0 mmol) in pyridine (0.6 ml) cooled to -10°C was slowly added a solution of 2-aminomethyl-6-methylpyridine (123 mg, 1.0 mmol) in pyridine (1 ml). The resulting yellow reaction mixture was stirred at -10°C for 3 hours and was held at 5°C overnight. The reaction mixture was poured onto crushed ice, which was allowed to melt resulting in the formation of an oil. A precipitate formed upon scratching. The solid was removed by filtration, dissolved in dichloromethane (5 ml) and washed with water (2 x 5 ml). The organic phase was dried ($MgSO_4$), filtered and evaporated under reduced pressure to yield a yellow oil which was crystallised from ethanol and water (1%) to form a white solid (0.53g, 53%); m.p. 83-84°C; ^{1}H NMR (200 MHz, $CDCl_3$): δ_H 2.38 (3H, s, CH_3), 2.46 (3H, s, CH_3), 4.18 (2H, d, *J 5.2,* CH_2), 5.92 (1H, s, NH), 6.97 (2H, t, *J 8.4,* H3, H5), 7.22 (2H, d, *J 7.8,* H3', H5'), 7.47 (1H, t, *J 7.8,* H4), 7.72 (2H, d, *J 6.6,* H2', H5'); ^{13}C NMR (50.3 MHz, $CDCl_3$): δ_c 21.37 (Me), 24.02 (Me), 47.35 (CH_2), 118.74 (C4'), 121.94 (C1'), 127.08 (C3'+ C5'), 129.45 (C2'+C6'), 136.63 (q, C6), 136.96 (C2), 143.17 (C3), 154.09 (C4), 157.68 (C2); *m/z* ES$^+$: 574.7 (25%, 2M+Na$^+$), 298.7 (100%, M+Na$^+$); υ_{max} (KBr)/cm^{-1} 1599 (v py), 1458 (v py), 1325 (ν_a SO_2), 1160 (ν_s SO_2), 1090 (δ CH), 816, 662 (γ NH), 551 (δ SO_2). Found: C, 60.57; H, 5.77; N, 10.39. $C_{13}H_{14}N_2O_2S$ requires C, 60.85; H, 5.84; N, 10.14.

6.4.2 Complex Synthesis

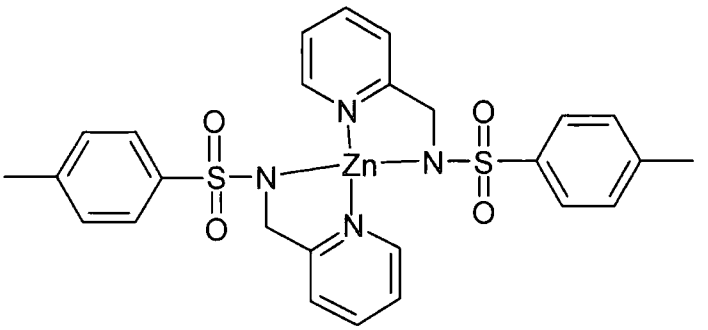

Zn($C_{13}H_{13}N_2O_2S)_2$ **[Zn(L^1)$_2$]** 2-*p*-Toluenesulfonylaminomethylpyridine **L^1** (72 mg, 0.27 mmol) and zinc acetate (30 mg, 0.14 mmol) were dissolved in methanol (6 ml), and the resulting solution was heated under reflux for 6 hours. The solution was allowed to cool to room temperature. On standing overnight white crystals formed. These were collected by filtration and washed with cold methanol. m.p. 220°C (dec.); ^{1}H NMR (200 MHz, CD_3OD): δ_H 8.4 (2H, d, *J* 5, H6), 8.0 (2H, t, *J* 5, H4), 7.8 (4H, d, *J* 8, tos), 7.5 (4H, m, H5,H3), 7.2 (4H, d, *J* 8, tos), 4.4 (4H, s, CH_2), 2.3 (6H, s, Me); *m/z* (FAB): 587 (100%, ZnL_2), 431 (39%, ZnL_2 - Tos), 325 (22%, ZnL), 263 (25%, LH); υ_{max} (KBr)/cm^{-1} 1611 (v py), 1568 (v py), 1442 (v py), 1277 (ν_a SO_2), 1151 (ν_s SO_2), 1104 (δ CH), 1087 (δ CH), 970, 762 (δ py), 670 (γ NH), 560 (δ SO_2); Found: C, 52.53; H, 4.44; N, 9.40. $Zn(C_{13}H_{13}N_2O_2S)_2$ .0.5MeOH requires C, 52.69; H, 4.67; N, 9.27. Constitution confirmed by x-ray crystallography, CSD Refcode: HUSCIH.

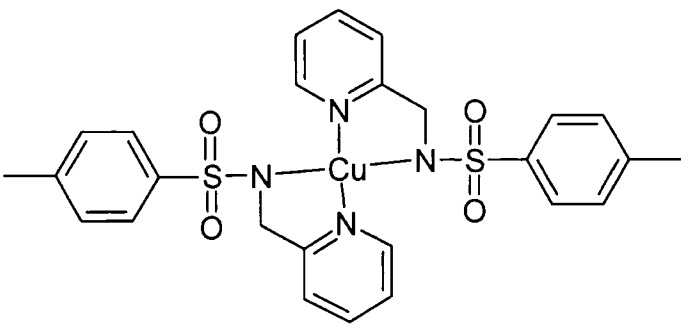

Cu($C_{13}H_{13}N_2O_2S)_2$ **[Cu(L^1)$_2$]** 2-(*p*-Toluenesulfonylaminomethyl)pyridine **L^1** (52 mg, 0.2 mmol) and copper acetate (40 mg, 0.2 mmol) were dissolved in methanol (10 ml) and the solution was heated under reflux for 18 hours. The solution was allowed to

cool to room temperature. On standing overnight, blue and brown cubic crystals formed. These were collected by filtration and washed with cold methanol. m.p. 180-182°C; *m/z* (FAB): 911 (11%, CuL_3), 650 (16%, Cu_2L_2), 608 (32%, CuL_2+Na), 586 (100%, CuL_2) 325 (71%, CuL), 263 (22%, L+H); υ_{max} (KBr)/cm^{-1} 1609 (v py), 1570 (v py), 1447 (v py), 1276 (v_a SO_2), 1139 (v_s SO_2), 1106 (δ CH), 1085 (δ CH), 844, 813, 673 (γ NH), 557 (δ SO_2); λ_{max}(MeCN) 638nm (ε 67$dm^3mol^{-1}cm^{-1}$); Found: C, 53.17; H, 4.46; N, 9.49. $Cu(C_{13}H_{13}N_2O_2S)_2$ requires C, 53.27; H, 4.47; N, 9.55. Constitution confirmed by x-ray crystallography, CSD Refcode: XEZQAU01.

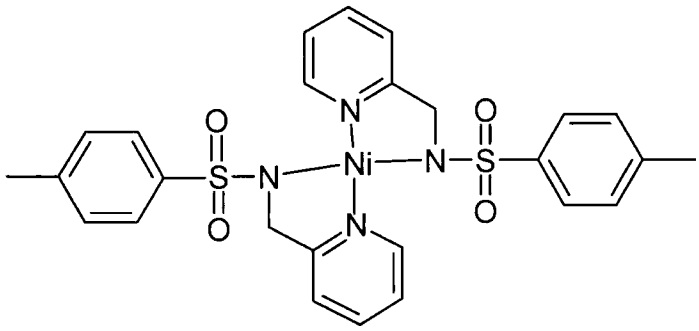

Ni($C_{13}H_{13}N_2O_2S$)$_2$ **[Ni(L^1)$_2$]** 2-(*p*-Toluenesulfonylaminomethyl)pyridine $\mathbf{L^1}$ (66 mg, 0.25 mmol) was dissolved in methanol (2.5 ml), and neutralised with 0.1M KOH solution (2.5ml, 0.25 mmol), the solvent was evaporated under reduced pressure. The resulting brown oil was dissolved in methanol (7 ml) and nickel acetate (31 mg, 0.12 mmol) was added. The resulting clear green solution was heated under reflux with stirring for one hour. The solution was allowed to cool to room temperature. An orange precipitate formed overnight, which was collected by filtration and washed with cold methanol and water, m.p. 220°C (dec); *m/z* (FAB): 603 (14%, NiL_2 + Na), 581 (63%, NiL_2), 425 (9%, NiL_2 - Tos), 263 (100%, LH); υ_{max} (KBr)/cm^{-1} 1611 (v py), 1478 (v py), 1281 (v_a SO_2), 1139 (v_s SO_2), 1084 (δ CH), 681 (γ NH), 557 (δ SO_2); Found: C, 53.57; H, 4.68; N, 9.58. $Ni(C_{13}H_{13}N_2O_2S)_2$ requires C, 53.72; H, 4.51; N, 9.64. Constitution confirmed by x-ray crystallography, CSD Refcode: HUSFAC.

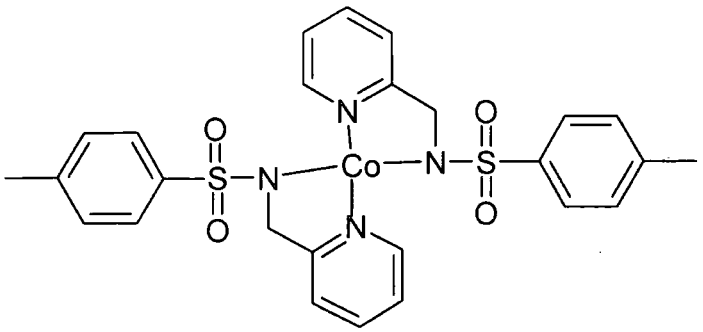

$Co(C_{13}H_{13}N_2O_2S)_2$ **[Co(L^1)$_2$]** 2-(*p*-Toluenesulfonylaminomethyl)pyridine L^1 (131 mg, 0.5 mmol) was dissolved in methanol (5 ml), and neutralised with 0.1M KOH solution (5ml, 0.5 mmol) and the solvent evaporated under reduced pressure. The resulting brown oil was dissolved in methanol (10 ml) and cobaltous acetate hexahydrate (62 mg, 0.25 mmol) was added. The resulting dark purple solution was heated under reflux with stirring for seven hours. The solution was allowed to cool to room temperature. On standing, purple crystals formed over a period of several days. These were collected by filtration and washed with cold methanol, m.p. 240°C (dec.); *m/z* FAB: 604 (37%, CoL_2+Na), 582 (100%, CoL_2), 426 (39%, CoL_2-tos), 320 (23%, CoL); υ_{max} (KBr)/cm^{-1} 1609 (ν py), 1439 (ν py), 1278 (ν_a SO_2), 1145 (ν_s SO_2), 1085 (δ CH), 947, 760 (δ py), 669 (γ NH), 559 (δ SO_2); λ_{max}(MeCN)/nm 513 and 579 (ε/$dm^3mol^{-1}cm^{-1}$ 302 and 291); Found: C, 53.20; H, 4.35; N, 9.51. $Co(C_{13}H_{13}N_2O_2S)_2.0.25MeOH$ requires C, 53.48; H, 4.61; N, 9.50. Constitution confirmed by x-ray crystallography, CSD Refcode: HUSFUW.

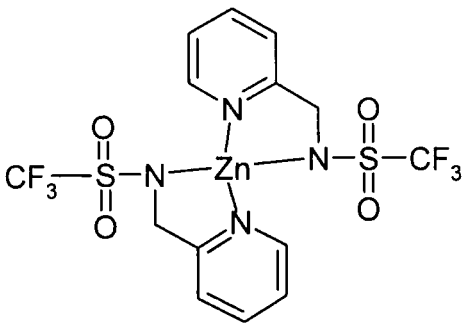

$Zn(C_7H_6F_3N_2O_2S)_2$ **[Zn(L^2)$_2$]** 2-Trifluoromethanesulfonylaminomethylpyridine L^2 (75 mg, 0.31 mmol) and zinc acetate (34.2 mg, 0.16 mmol) were dissolved in methanol (10 ml) and the solution heated under reflux for 3 hours. The solution was allowed to cool to room temperature and left standing to evaporate slowly. On standing, white crystals formed which were collected by filtration and washed with

cold methanol, m.p. 260°C (dec); ^{1}H NMR (300 MHz, CD_3CN): δ_H 4.78 (2H, s, CH_2), 7.54 (1H, t, *J 6.6*, H5), 7.61 (1H, d, *J 7.8*, H3), 8.08 (1H, t of d, *J 1.8, 8.1*, H4), 8.47 (1H, d, *J 5.4*, H6); ^{13}C NMR (65 MHz, CD_3CN): δ_C 49.81 (CH_2), 124.16 (C3 or C5), 124.71 (C3 or C5), 141.57 (C4), 148.14 (C6), 159.00 (q, C2); ^{19}F NMR (188 MHz, CD_3CN): δ_F -78.14 (s, CF_3); m/z (ES^+): 580 (22%, ZnL_2K), 564 (100%, ZnL_2Na), 262 (28%, L + Na); υ_{max} (KBr)/cm^{-1} 1614 (ν py), 1447 (ν py), 1334 (ν_a SO_2), 1196 (ν_s SO_2), 1098 (δ CH), 962, 603 (γ NH); Found: C, 30.87; H. 2.15; N. 10.08. $Zn(C_7H_6F_3N_2O_2S)_2$ requires C. 30.92; H. 2.22; N. 10.30; Constitution confirmed by x-ray crystallography, CSD Refcode: HUSCON.

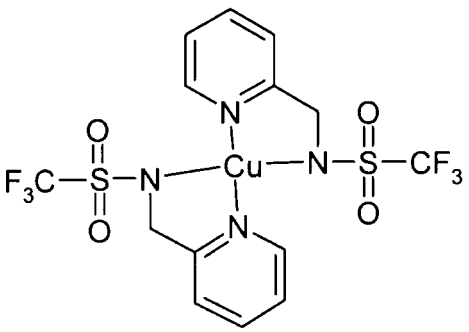

Cu($C_7H_6F_3N_2O_2S$)$_2$ **[Cu(L^2)$_2$].** The copper (II) complex was prepared as described for the zinc analogue to yield blue crystals, m.p. 220-223°C; m/z (ES^+): 579 (20%, CuL_2K), 563 (100%, CuL_2Na); υ_{max} (KBr)/cm^{-1} 1616 (ν py), 1448 (ν py), 1364 (δ NH), 1334 (ν_a SO_2), 1178 (ν_s SO_2), 1092 (δ CH), 605 (γ NH); λ_{max}(MeCN) 672nm (ε 227dm^{3}mol^{-1}cm^{-1}); Found: C, 30.64; H. 2.28; N. 10.27. $Cu(C_7H_6F_3N_2O_2S)_2$ requires C. 31.02; H. 2.23; N. 10.34; Constitution confirmed by x-ray crystallography, CSD Refcode: HUSDII.

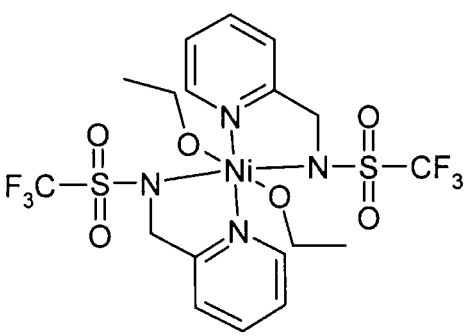

Ni($C_7H_6F_3N_2O_2S$)$_2$.2EtOH **[Ni(L^2)$_2$]** 2-Trifluoromethanesulfonylaminomethyl-pyridine L^2 (60 mg, 0.25 mmol) and nickel acetate (31 mg, 0.12 mmol) were

dissolved in methanol to form a pale green solution which was heated under reflux with stirring for four hours. The solution was allowed to cool to room temperature and the solvent slowly evaporated yielding a green oil which was dissolved in ethanol. Pale blue crystals formed on standing over a period of several days. The crystals were collected by filtration and washed with cold methanol. m.p. 120°C (dec); m/z (ES^+): 558 (100%, NiL_2Na); υ_{max} (KBr)/cm^{-1} 1609 (v py), 1444 (v py), 1305 (ν_a SO_2), 1182 (ν_s SO_2), 1084 (δ CH), , 601 (γ NH); λ_{max}(MeCN)/nm 367 and 597 (ε/$dm^3mol^{-1}cm^{-1}$ 52 and 32); Found: C, 34.15; H. 3.82; N. 8.97. $Ni(C_7H_6F_3N_2O_2S)_2.2EtOH$ requires C. 34.36; H. 3.84; N. 8.90; Constitution confirmed by x-ray crystallography, CSD Refcode: HUSFEG.

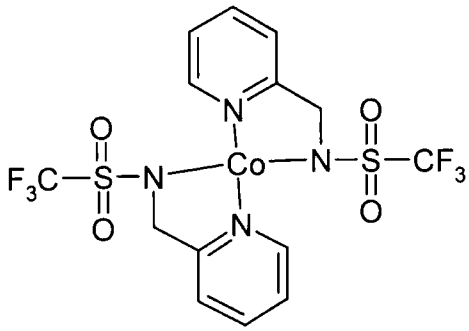

Co($C_7H_6F_3N_2O_2S)_2$ **[Co(L^2)$_2$]** The cobalt (II) complex was prepared as described for the nickel (II) analogue yielding deep pink crystals, m.p. 230°C; m/z (ES^+): 575 (26%, CoL_2K), 564 (100%, CoL_2Na); υ_{max} (KBr)/cm^{-1} 1613 (v py), 1446 (v py), 1335 (ν_a SO_2), 1186 (ν_s SO_2), 1164 (δ CH), 1095 (δ CH), 948, 602 (γ NH); λ_{max}(MeCN) 500nm (ε 46$dm^3mol^{-1}cm^{-1}$); Found: C, 31.58; H, 2.28; N, 10.44. $Co(C_7H_6F_3N_2O_2S)_2$ requires C. 31.29; H. 2.25; N. 10.43; Constitution confirmed by x-ray crystallography, CSD Refcode: HUSGAD.

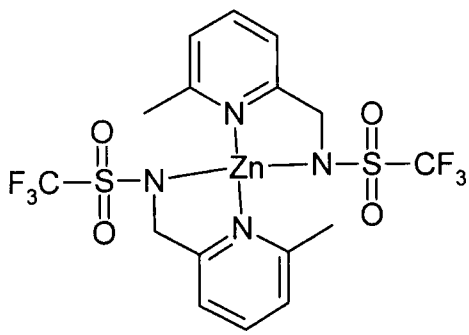

Zn($C_8H_8N_2O_2F_3S)_2$ **[Zn(L^3)$_2$].** 2-(Trifluoromethanesulfonylaminomethyl)-6-methyl-pyridine L^3 (25 mg, 0.11 mmol) and zinc acetate (12 mg, 0.05 mmol) were dissolved in methanol (4 ml). The resulting clear colourless solution was heated under reflux with stirring for four hours. After cooling to room temperature, colourless crystals formed on standing overnight. The crystals were collected by filtration and washed with cold methanol, m.p. 224-226°C; ^{1}H NMR (200 MHz, CD_3CN): δ_H 2.43 (3H, s, CH_3), 4.77 (2H, s, CH_2), 7.44 (2H, t, *J 6.8*, H3, H5), 8.00 (1H, t, *J 7.8*, H4); ^{13}C NMR (50.3 MHz, CD_3CN): δ_C 23.87 (CH_3), 49.77 (CH_2), 121.58 (C3 or C5), 124.81 (C3 or C5), 142.06 (C4), 157.73 (q, C2), 158.36 (CF_3). ^{19}F NMR (188 MHz, CD_3CN): δ_F -78.11 (s, CF_3); m/z (ES^+): 608 (12%, ZnL_2K^+), 592 (100%, ZnL_2Na^+), 276 (34%, LNa); υ_{max} (KBr)/cm^{-1} 1611 (v py), 1472 (v py), 1335 (ν_a SO_2), 1194 (ν_s SO_2), 1168 (δ CH), 1092 (δ CH), 604 (γ NH); Found: C, 33.48; H. 2.67; N. 9.69. $Zn(C_8H_8N_2O_2F_3S)_2$ requires C. 33.61; H. 2.82; N. 9.80. Constitution confirmed by x-ray crystallography, CSD Refcode: HUSCUT.

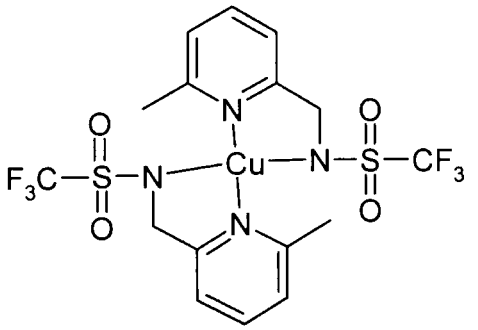

Cu($C_8H_8N_2O_2F_3S)_2$ **[Cu(L^3)$_2$].** The copper (II) complex was prepared as described for the zinc (II) analogue, yielding lime green crystals, m.p. 180°C (dec); m/z (ES^+): 592 (24%, CuL_2Na^+), 276 (100%, LNa^+); υ_{max} (KBr)/cm^{-1} 1611 (v py), 1472 (v py), 1340 (v py), 1324 (ν_a SO_2), 1186 (ν_s SO_2), 1167 (δ CH), 1088 (δ CH), 601 (γ NH); λ_{max}(MeCN) 410 and 764nm (ε 404 and 74 dm^{3}mol^{-1}cm^{-1}); Found: C, 33.53; H. 2.77; N. 9.60. $Cu(C_8H_8N_2O_2F_3S)_2$ requires C. 33.71; H. 2.83; N. 9.83. Constitution confirmed by x-ray crystallography, CSD Refcode: HUSDOO.

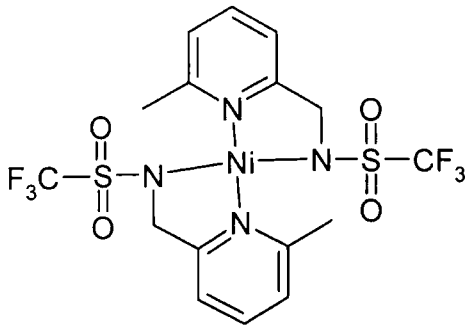

Ni($C_8H_8N_2O_2F_3S$)$_2$ **[Ni(L^3)$_2$]**, The nickel (II) complex was prepared as above, yielding purple crystals, m.p. 235-238°C; m/z (ES^+): 604 (18%, NiL_2K), 587 (40%, NiL_2Na), 276 (100%, LNa); υ_{max} (KBr)/cm^{-1} 1611 (v py), 1474 (v py), 1338 (ν_a SO_2), 1190 (ν_s SO_2), 1169 (δ CH), 1094 (δ CH), 605 (γ NH); λ_{max}(MeCN) 544 and 733 nm (ε 190 and 51 $dm^3mol^{-1}cm^{-1}$). A satisfactory microanalysis was not obtained for this compound; however the proposed constitution is in agreement with crystallographic data, CSD Refcode: HUSFIK.

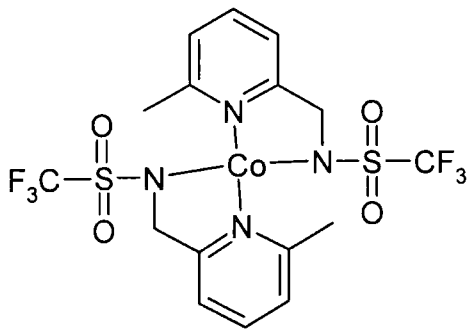

Co($C_8H_8N_2O_2F_3S$)$_2$ **[Co(L^3)$_2$]** The cobalt complex was prepared as described for the zinc (II) analogue, yielding purple crystals, m.p. 200°C (dec); m/z (ES^+): 588 (100%, CoL_2Na^+), 276 (41%, LNa^+); υ_{max} (KBr)/cm^{-1} 1611 (v py), 1473 (v py), 1335 (ν_a SO_2), 1188 (ν_s SO_2), 1167 (δ CH), 1090 (δ CH), 605 (γ NH); λ_{max}(MeCN) 533 and 564nm (ε407 and 380 $dm^3mol^{-1}cm^{-1}$); Found: C, 33.97; H. 2.84; N. 9.89. Co($C_8H_8N_2O_2F_3S$)$_2$ requires C. 33.99; H. 2.86; N. 9.91. Constitution confirmed by x-ray crystallography, CSD Refcode: HUSGEH.

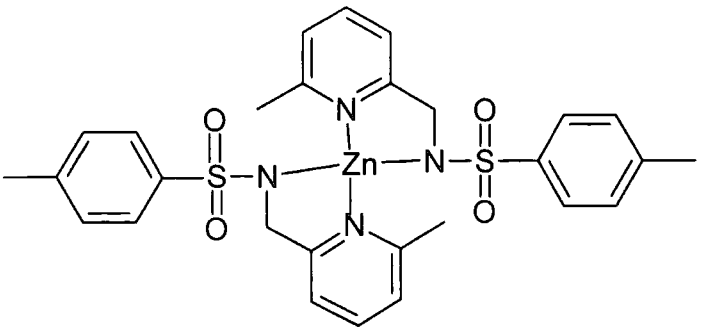

$Zn(C_{14}H_{15}N_2O_2S)_2$ **[Zn(L^4)$_2$]** 2-(*p*-Toluenesulfonylaminomethyl)-6-methylpyridine L^4 (500 mg, 18 mmol) and zinc acetate (190 mg, 9 mmol) were dissolved in methanol (35 ml), and the resulting clear solution was heated under reflux for 18 hours. The solution was allowed to cool to room temperature. On standing a white oil formed. This was crystallised from ethanol. The resulting white crystals were collected by filtration and washed with cold methanol. m.p. 220°C (dec); ^{1}H NMR (200 MHz, CD_3OD): δ_H 2.36 (6H, s, $2CH_3$), 2.41 (6H, s, $2CH_3$), 4.47 (4H, s, broad, $2CH_2$), 7.32 (4H, d, *J 8*, 2H3', 2H5'), 7.35 (4H, d, *J 7.6*, 2H2', 2H5'); 7.81 (4H, d, *J 8.2*, 2H3, 2H5), 7.88 (2H, t, *J 7.8*, 2H4); ^{13}C NMR (50.3 MHz, CD_3OD): δ_C 21.37 (Me), 23.79 (Me), 121.94 (C4'), 124.91 (C1'), 128.29 (C3'+ C5'), 130.39 (C2'+C6'), 140.40 (q, C6), 141.92 (C2), 143.24 (C3), 158.37 (C4), 159.86 (C2); *m/z* (ESMS): 615 (20%, ZnL_2), 637 (100%, ZnL_2Na); υ_{max} (KBr)/cm^{-1} 1607 (ν py), 1577 (ν py), 1448 (ν py), 1266(ν_a SO_2), 1149 (ν_s SO_2), 1095 (δ CH), 1085 (δ CH), 974, 788 (δ py), 669 (γ NH), 557 (δ SO_2); Found: C, 54.49; H, 4.86; N, 9.07. $Zn(C_{14}H_{15}N_2O_2S)_2$ requires C, 54.59; H, 4.91; N, 9.09. Constitution confirmed by x-ray crystallography, CSD Refcode: HUSDAA.

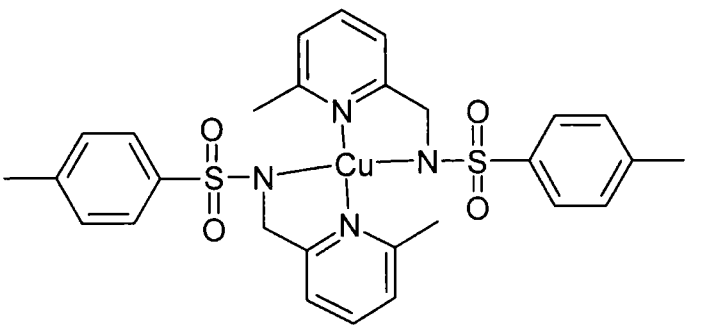

$Cu(C_{14}H_{15}N_2O_2S)_2$ **[Cu(L^4)$_2$]** 2-(*p*-Toluenesulfonylaminomethyl)-6-methylpyridine L^4 (50 mg, 0.18 mmol) and copper acetate (18 mg, 0.09 mmol) were dissolved in

methanol (10 ml) and the solution was heated under reflux for 15 hours. The resulting brown solution was allowed to cool to room temperature. On standing a brown oil formed, this was recrystallised from methanol to yield brown crystals which were collected by filtration and washed with cold methanol. m.p. 220°C(dec); *m/z* (FAB): 614 (46%, CuL_2),; υ_{max} (KBr)/cm^{-1} 1607 (v py), 1576 (v py), 1441 (v py), 1274 (ν_a SO_2), 1142 (ν_s SO_2), 1084 (δ CH), 958, 927 (δ py), 669 (γ NH), 555 (δ SO_2); λ_{max}(MeCN) 448, 784nm (ε 2017, 215 $dm^3mol^{-1}cm^{-1}$); Found: C, 54.79; H, 5.13; N, 8.84. $Cu(C_{13}H_{13}N_2O_2S)_2$ requires C, 54.75; H, 4.92; N, 9.12. Constitution confirmed by x-ray crystallography, CSD Refcode: HUSDUU.

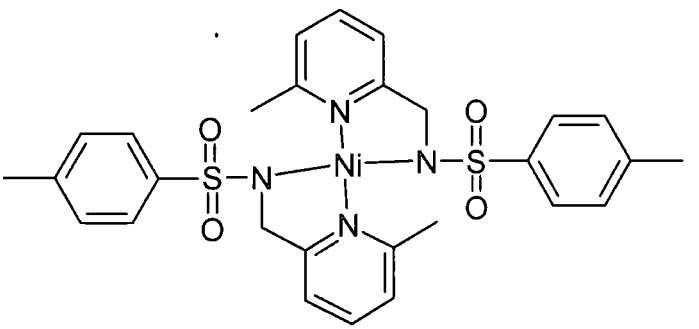

Ni($C_{14}H_{15}N_2O_2S$)$_2$ **[Ni(L^4)$_2$]** 2-*p*-Toluenesulfonylaminomethyl-6-methylpyridine L^4 (50 mg, 0.18 mmol) and nickel acetate (22 mg, 0.09 mmol) were dissolved in methanol (10 ml). The resulting clear pink solution was heated under reflux with stirring for eight hours. The solution was allowed to cool to room temperature and left standing, a purple-brown oil formed. This was crystallised from ethanol to form purple crystals which were collected by filtration and washed with cold methanol and water, m.p. 220°C (dec); υ_{max} (KBr)/cm^{-1} 1599 (v py), 1458 (v py), 1324 (ν_a SO_2), 1160 (ν_s SO_2), 1091 (δ CH), 662 (γ NH), 551 (δ SO_2); λ_{max}(MeCN) 544, 760nm (ε 71, 30 $dm^3mol^{-1}cm^{-1}$); Found: C, 55.01; H, 4.77; N, 8.79. $Ni(C_{13}H_{13}N_2O_2S)_2$ requires C, 55.19; H, 4.96; N, 9.19. Constitution confirmed by x-ray crystallography, CSD Refcode: HUSFOQ.

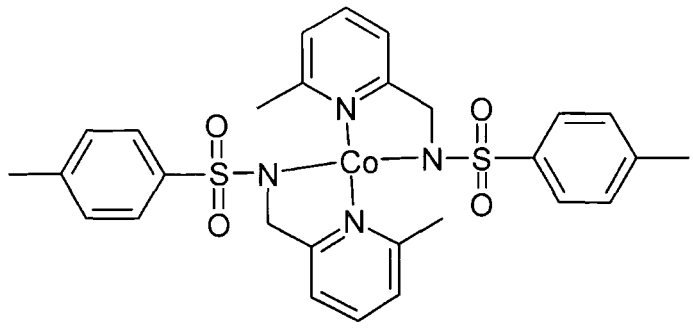

Co($C_{14}H_{15}N_2O_2S)_2$ **[Co(L^4)$_2$]** 2-(*p*-Toluenesulfonylaminomethyl)-6-methylpyridine L^4 (50 mg, 0.18 mmol) and cobaltous acetate hexahydrate (22 mg, 0.09 mmol) were dissolved in methanol (10 ml). The resulting purple solution was heated under reflux with stirring for eight hours. The solution was allowed to cool to room temperature. On standing a pink oil formed. This was recrystallised from ethanol to yield purple crystals. These were collected by filtration and washed with cold methanol, m.p. 240°C (dec); υ_{max} (KBr)/cm^{-1} 1610 (ν py), 1444 (ν py), 1335 (ν_a SO_2), 1166 (ν_s SO_2), 1090 (δ CH), 958, 789 (δ py), 643 (γ NH), 573 (δ SO_2); λ_{max}(MeCN)/nm 532 and 564 (ε/$dm^3mol^{-1}cm^{-1}$ 576 and 536); Found: C, 55.33; H, 5.12; N, 8.90. $Co(C_{13}H_{13}N_2O_2S)_2$ requires C, 55.17; H, 4.96; N, 9.19. Constitution confirmed by x-ray crystallography, CSD Refcode: HUSGIL.

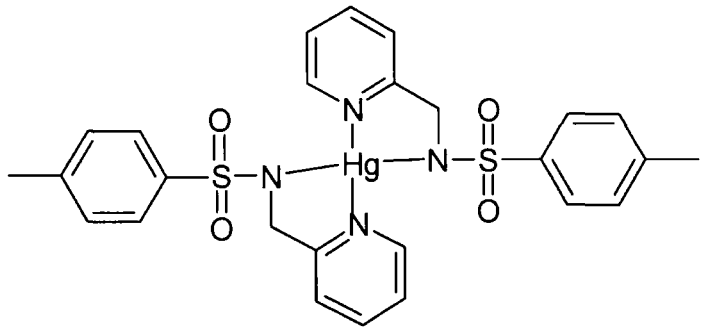

Hg($C_{13}H_{13}N_2O_2S)_2$ **[Hg(L^1)$_2$].** A clear colourless solution of mercury acetate (41 mg, 0.09 mmol) and 2-*p*-Toluenesulfonylaminomethylpyridine L^1 (66 mg, 0.19 mmol) in methanol (7 ml) was heated under reflux for 18 hours. It was then allowed to cool to room temperature. On standing clear colourless crystals formed. These were collected by filtration and washed with cold methanol. m.p. 220°C (dec.); ^{1}H NMR (200 MHz, CD_3OD): δ_H 8.1 (2H, d, *J* 5, H6), 7.8 (4H, d, *J* 8, tos), 7.7 (2H, t, *J* 6, H4), 7.3 - 7.2 (8H, m, tos, H3, H5), 4.5 (4H, s, CH_2), 2.3 (6H, s, Me); υ_{max} (KBr)/cm^{-1} 1598 (ν py), 1436 (ν py), 1282 (ν_a SO_2), 1144 (ν_s SO_2), 1102 (δ CH); A satisfactory

microanalysis was not obtained for this compound, however the proposed constitution is in agreement with crystallographic data.

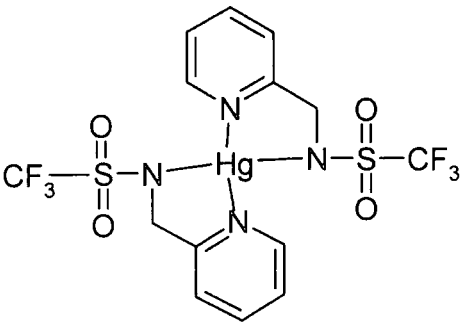

$Hg(C_7H_6F_3N_2O_2S)_2$ **[Hg(L^2)$_2$]** A clear colourless solution of mercury acetate (33 mg, 0.10 mmol) and L^2 (50 mg, 0.208 mmol) in methanol (7 ml) was heated under reflux for 18 hours. It was then allowed to cool to room temperature. On standing clear colourless crystals formed. ^{1}H NMR (200 MHz, CD_3CN): δ_H 4.85 (2H, s, CH_2), 7.48 (4H, m, H3 + H5), 7.95 (2H, t, *J 7.8*, H4), 8.41 (2H, d, *J* 5, H6); ^{13}C NMR (65 MHz, CD_3CN): δ_C 49.39 (CH_2), 124.68 (C3 or C5), 124.91 (C3 or C5), 140.40 (C4), 148.92 (C6); ^{19}F NMR (188 MHz, CD_3CN): δ_F -77.43 (s, CF_3); *m/z* (FAB): 703 (55%, ZnL_2Na), 681 (100%, ZnL_2H); υ_{max} (KBr)/cm^{-1} 1603 (v py), 1441 (v py), 1331 (v_a SO_2), 1176 (v_s SO_2), 1098 (δ CH); Found: C, 24.71; H, 1.73; N, 8.24. $Hg(C_7H_6F_3N_2O_2S)_2$ requires C, 24.76; H, 1.78; N, 8.25. Constitution confirmed by x-ray crystallography

6.5 Chapter 3 Experimental

6.5.1 Ligand synthesis

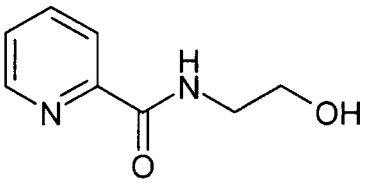

Pyridine-2-carboxylic acid (2-hydroxyethyl)-amide **46** 1-(3-Dimethylaminopropyl)-3-ethylcarbodiimide (5.00 g, 26.1 mmol), ethanolamine (1.45 g, 23.7 mmol) and HOBt (3 mg, catalytic) were added to a pale yellow solution of picolinic acid (2.92 g, 23.7 mmol) in water (25 ml). The resulting red solution was stirred at room temperature for 48 hours. The solvent was then removed under reduced pressure

to give an orange-brown oil. Flash column chromatography (SiO_2, 10% MeOH in EtOAc) isolated the desired product as a clear oil (0.462 g, 11.7%). R_f = 0.46 (SiO_2, 10% MeOH in EtOAc); ^{1}H NMR (200 MHz, $CDCl_3$): 3.66 (2H, quart, *J 5.6*, $\underline{CH_2}NH$), 3.85 (2H, t, *J 4.6*, $\underline{CH_2}OH$), 7.43 (1H, t, *J 6.1*, H5), 7.85 (1H, t, *J 7.6*, H4), 8.16 (1H, d, *J 7.8*, H3), 8.19 (1H, br s, NH), 8.55 (1H, d, *J 4.6*, H6); ^{13}C NMR ($CDCl_3$, 50 MHz) δ_C: 42.44 (CH_2), 62.06 (CH_2OH), 122.31 (C3), 126.31 (C5), 137.44 (C4), 148.17 (C6), 149.72 (q, C2), 165.37 (C=O); m/z (ES$^+$): 189 (100%, MH^+), 355 (100%, $2MNa^+$); IR (thin film): 1671 (C=O), 1524 (NH).

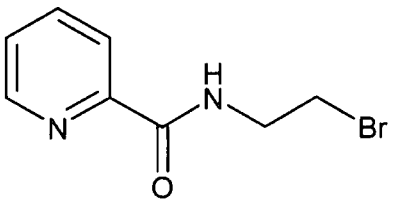

Pyridine-2-carboxylic acid (2-bromoethyl)-amide **47** Triphenyl phosphine (351 mg, 1.34 mmol) was added portionwise to a stirred, pale yellow solution of **46** (148 mg, 0.89 mmol) and carbon tetrabromide (370 mg, 1.11 mmol) which had been cooled with an ice bath. The resulting bright yellow solution was allowed to warm gradually to room temperature and stirred for 18 hours. The solvent was removed under reduced pressure. Flash column chromatography (SiO_2, 5% MeOH in EtOAc) gave the desired product as a clear oil (99 mg, 48%). R_f = 0.64 (10% SiO_2, MeOH in EtOAc); ^{1}H NMR (200 MHz, $CDCl_3$): 3.46 (2H, t, *J 5.4*, $\underline{CH_2}Br$), 3.61 (2H, quart, *J 6.6*, $\underline{CH_2}NH$), 7.41 (1H, t, *J 6.1*, H5), 7.82(1H, t, *J 7.6*, H4), 8.14 (1H, d, *J 7.8*, H3), 8.18 (1H, br s, NH), 8.52 (1H, d, *J 3.9*, H6); ^{13}C NMR ($CDCl_3$, 60 MHz) δ_C: 31.97 (CH_2), 41.27 (CH_2), 122.41 (C3), 126.52 (C5), 137.51 (C4), 148.35 (C6), 149.57 (q, C2), 164.60 (C=O); m/z (ES$^+$): 251 (100%, ^{79}Br MNa^+), 253 (100%, ^{81}Br MNa^+); IR (thin film): 1671 (C=O), 1524 (NH).

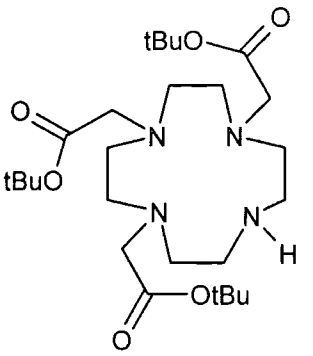

1,4,7-Tris(tert-butoxycarboxymethyl)-1,4,7,10-tetraazacyclododecane[155] **48** *Tert*-butyl bromoacetate (1.88 g, 9.6 mmol) was added to a solution of cyclen (0.55 g, 3.2 mmol), and sodium hydrogen carbonate (0.81 g, 9.6 mmol) in dry acetonitrile (15 ml). The suspension was stirred under argon for 18 hours. The solvent was then removed under reduced pressure and the resulting solid was dissolved in dichloromethane and filtered to remove the inorganic solids. The solvent was then evaporated under reduced pressure and the pale oil obtained was recrystallised from toluene to give needle shaped crystals (0.77 g, 47%). ^{1}H NMR (200 MHz, $CDCl_3$): 1.42 (27H, s, ^{t}Bu), 2.95 (16H, br m, ring CH_2), 3.26 (2H, s, acetate CH_2), 3.34 (4H, s, 2 acetate CH_2); ^{13}C NMR ($CDCl_3$, 60 MHz) δ_C: 30.2 ($C(\underline{C}H_3)_3$), 49.5 (CH_2), 50.4 (CH_2), 51.2 (CH_2), 53.1 (CH_2), 53.6 (CH_2), 60.4 (CH_2), 83.6 ($\underline{C}(CH_3)_3$), 171.4 (C=O), 172.2 (C=O); m/z (ES^+): 515 (100%, M^+).

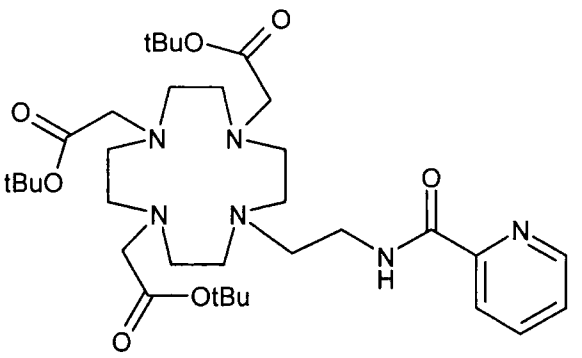

1,4,7-Tris-tert-butoxycarbonylmethyl-10-[2-(pyridine-2-carbamoylethyl)]-1,4,7,10tetraaza-cyclododecane **49** Under an argon atmosphere, a stirred suspension of **47** (99 mg, 0.43 mmol), **48** (222 mg, 0.43 mmol) and potassium carbonate (299 mg, 2.16 mmol) in acetonitrile (4 ml) was heated under reflux for 18hours. It was then cooled to room temperature and filtered; the filtercake was washed thoroughly with dichloromethane. The solvent was then evaporated under reduced pressure and the resulting brown oil was purified by flash column chromatography (SiO_2,

gradient elution 2% MeOH in DCM → 5% MeOH in DCM), a clear colourless oil (98 mg, 29%) was obtained. R_f = 0.65 (SiO_2, 10% MeOH in DCM). ^{1}H NMR (300 MHz, $CDCl_3$): 1.27 (18H, s, 2 *t*Bu), 1.35 (9H, s, *t*Bu), 2.27 - 3.54 (26H, br m, 13 CH_2), 7.36 (1H, t, *J 4.8,* H5), 7.69 (1H, t, *J 7.6,* H4), 8.02 (1H, d, *J 7.8,* H3), 8.23 (1H, br t, NH), 8.45 (1H, d, *J 5.7,* H6); ^{13}C NMR (75 MHz, $CDCl_3$) δ_C: 27.80 (C($\underline{CH_3}$)$_3$), 36.55, (CH_2), 50.37 (CH_2), 55.34 (br CH_2), 55.70 (CH_2), 56.54 (CH_2), 82.25 ($\underline{C}(CH_3)_3$), 122.17 (C3), 126.33 (C5), 137.17 (C4), 148.09 (C6), 149.60 (q, C2), 165.68 (C=O), 172.72 (C=O), 172.85 (C=O); m/z (ES^+): 685.5 (100%, MNa^+), 663.6 (90%, MH^+); Acc.MS (ES^+): Found 663.4497, $C_{34}H_{59}N_6O_7$ requires 663.4445.

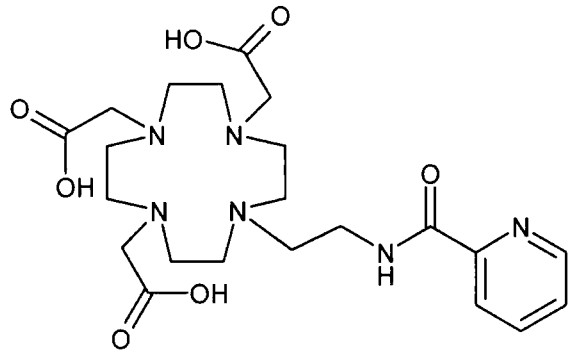

1,4,7-Tris-carboxymethyl-10-[3-(pyridine-2-carbamoylethyl)]-1,4,7,10tetraaza-cyclododecane **L**[5] Under an argon atmosphere, a solution of **49** (99 mg, 0.145 mmol) trifluoroacetic acid (2 ml) was left standing for 48 hours. The solvent was then removed under reduced pressure. The resulting solid was washed with dichloro-methane (3 x 2 ml) and the solvent removed under reduced pressure to give a pale yellow oil. ^{1}H NMR (300 MHz, D_2O): 3.10 - 3.99 (26H, br m, 13CH_2), 8.15 (1H, t, *J 6.6,* H5), 8.34 (1H, t, *J 7.8,* H4), 8.62 (1H, d, *J 7.8,* H3), 8.77 (1H, d, *J 5.7,* H6); ^{13}C NMR (75 MHz, D_2O) δ_C: 48.96 - 54.42 (br m, CH_2), 125.23 (C3), 129.93 (C5), 141.86 (C4), 143.16 (q, C2), 147.67 (C6), 161.05 ($\underline{C=O}$NH), 162.55 ($\underline{C=O}$NH), 163.03 (C=O).

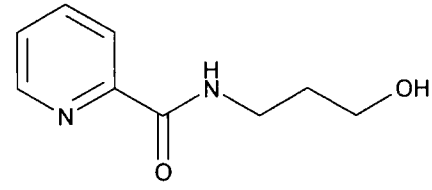

Pyridine-2-carboxylic acid (3-hydroxy-propyl)-amide **50** 3-Aminopropan-1-ol (1.78 g, 23.7 mmol) and a catalytic amount of HOBt (3 mg) were added to a stirred dark red

solution of picolinic acid (2.92 g, 23.7 mmol) and EDC (5.00 g, 26.0 mmol) in dichoromethane (25 ml). The reaction mixture was stirred at room temperature for 48 hours. Silica (~5 g) was then added to the black solution and the solvent evaporated under reduced pressure. Flash column chromatography (SiO_2, 10% methanol in ethyl acetate) was used to purify the product, which was obtained as a yellow oil (1.19 g, 28%). R_f = 0.29 (10% MeOH in EtOAc, SiO_2); ^1H NMR (300 MHz, $CDCl_3$): 1.80 (2H, quintet, *J 5.4*, $CH_2\underline{CH_2}CH_2$), 3.65 (4H, m, $\underline{CH_2}CH_2\underline{CH_2}$), 7.43 (1H, t, *J 7.6*, H5), 7.85 (1H, t, *J 7.6*, H4), 8.19 (1H, d, *J 7.8*, H3), 8.24 (1H, br s, NH), 8.53 (1H, d, *J 4.2*, H6); ^{13}C NMR ($CDCl_3$, 60 MHz) δ_C: 32.67 (CH_2 $\underline{CH_2}$ CH_2), 35.90 (CH_2NH), 59.07 (CH_2OH), 122.45 (C3), 126.45 (C5), 137.57 (C4), 148.25 (C6), 149.55 (q, C2), 165.68 (C=O); m/z (ES^+): 383 (90%, $2MNa^+$), 203 (100%, MNa^+), 181 (41%, MH^+); Acc.MS (EI^+): Found 180.0894, $C_9H_{12}N_2O_2$ requires 180.0898; IR (thin film) 3373 (OH), 1660 (C=O), 1534 (NH), 1434 (v py).

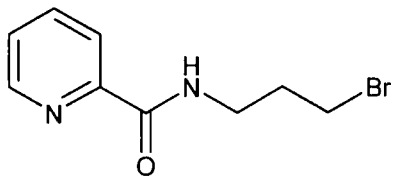

Pyridine-2-carboxylic acid (3-bromopropyl)-amide **51** Triphenylphosphine (725 mg, 2.77 mmol) was added portionwise to a stirred yellow solution of **50** (332 mg, 1.84 mmol) and carbon tetrabromide (765 mg, 2.31 mmol) in dichloromethane (10 ml) which had been cooled in an ice bath. The ice bath was then allowed to melt gradually and the resulting pale yellow solution was stirred for 18 hours at room temperature before the solvent was removed under reduced pressure yielding a pale brown oil. Flash column chromatography (SiO_2, 5% methanol in ethyl acetate) yielded the desired product as a clear colourless oil (119 mg, 27%). R_f = 0.48 (10% MeOH in EtOAc, SiO_2); ^1H NMR (300 MHz, $CDCl_3$): 2.18 (2H, quintet, *J 6.6*, $CH_2\underline{CH_2}CH_2$), 3.46 (2H, t, *J 5.4*, $\underline{CH_2}Br$), 3.61 (2H, quart, *J 6.6*, $\underline{CH_2}NH$), 7.41 (1H, t, *J 6.1*, H5), 7.82(1H, t, *J 7.6*, H4), 8.14 (1H, d, *J 7.8*, H3), 8.18 (1H, br s, NH), 8.52 (1H, d, *J 3.9*, H6); ^{13}C NMR ($CDCl_3$, 60 MHz) δ_C: 30.87 (CH_2), 32.48 (CH_2), 37.96 (CH_2), 122.27 (C3), 126.33 (C5), 137.52 (C4), 148.08 (C6), 149.65 (q, C2), 164.62 (C=O); m/z (ES^+): 242 (100%, M^+); IR (thin film): 1667 (C=O), 1529 (NH).

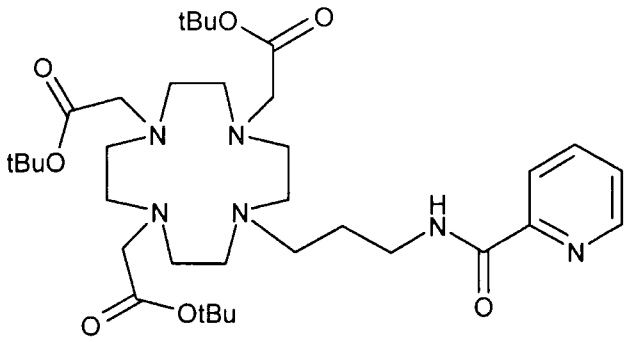

1,4,7-Tris-tert-butoxycarbonylmethyl-10-[3-(pyridine-2-carbamoylpropyl)]-1,4,7,10-tetraaza-cyclododecane **52** Under an argon atmosphere a suspension of **51** (119 mg, 0.49 mmol), **48** (252 mg, 0.49 mmol) and potassium carbonate (338 mg, 2.45 mmol) in acetonitrile (3 ml) was heated under reflux for 48 hours. It was then allowed to cool to room temperature before removing the inorganic salts by filtration and washing them thoroughly with dichloromethane. The solvent was then removed under reduced pressure to give a yellow oil (330 mg). Flash column chromatography (SiO_2, gradient elution DCM → 5% MeOH in DCM) yielded the desired product as a clear colourless oil (100 mg, 30%). R_f = 0.11 (SiO_2, 10% MeOH in EtOAc); ^{1}H NMR (300 MHz, $CDCl_3$): 1.36 (27H, s, 3*t*Bu), 1.73 (2H, quintet, *J 6.9*, $CH_2\underline{CH_2}CH_2$), 2.25 - 3.04 (20H, br m, ring CH_2 + $\underline{CH_2}CH_2\underline{CH_2}$), 3.14 (2H, s, $\underline{CH_2}CO$), 3.39 (4H, s, $2CH_2CO$), 7.40 (1H, t, *J 6.1*, H5), 7.80 (1H, t, *J 7.6*, H4), 8.10 (1H, d, *J 7.8*, H3), 8.94 (1H, d, *J 3.9*, H6); ^{13}C NMR ($CDCl_3$, 75 MHz) δ_C: 26.64 ($CH_2\underline{CH_2}CH_2$), 27.82 (*t*Bu), 27.95 (*t*Bu), 37.74 ($NH\underline{CH_2}CH_2$), 50.29, 50.46, 51.95 (br, ring CH_2s) , 55.76 ($N\underline{CH_2}CO$), 56.55 ($N\underline{CH_2}CO$), 82.45 ($\underline{C}(CH_3)_3$), 82.77 ($\underline{C}(CH_3)_3$), 122.06 (C3), 126.37 (C5), 137.44 (C4), 148.12 (C6), 149.59 (q, C2), 164.41 ($\underline{C}$=O NH), 172.64 (C=O), 173.57 (C=O); m/z (ES^+): 699.5 (100%, MNa^+), 677.6 (25%, MH^+).

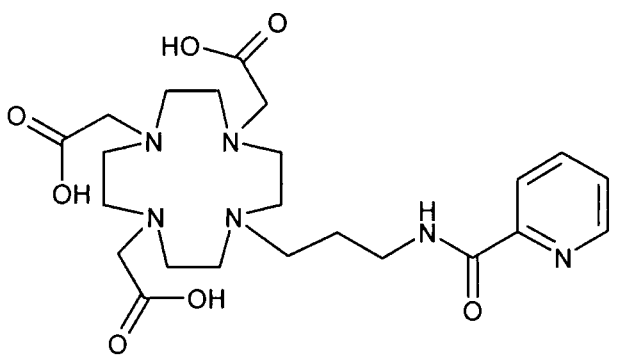

1,4,7-Bis-carboxymethyl-10-[3-(pyridine-2-carbamoylpropyl)]-1,4,7,10tetraaza-cyclododecane **L^6** Under an argon atmosphere, a solution of **52** (100 mg, 0.148 mmol)

in dichloromethane (1 ml) and trifluoroacetic acid (1 ml) was left standing for 18 hours. The solvent was then removed under reduced pressure. The resulting solid was washed with dichloromethane (3 x 2 ml) and the solvent removed under reduced pressure to give the trifluoroacetate salt as a pale yellow oil. ^{1}H NMR (300 MHz, D_2O): 2.03 (2H, br t, $CH_2\underline{CH_2}CH_2$), 2.90 - 3.46 (26H, br m, ring CH_2 + $\underline{CH_2}CH_2\underline{CH_2}$ + 3$\underline{CH_2}$CO), 8.12 (1H, t, *J 6.9*, H5), 8.34 (1H, t, *J 7.8*, H4), 8.62 (1H, d, *J 8.1*, H3), 8.77 (1H, d, *J 5.1*, H6); ^{13}C NMR (75 MHz, D_2O) δ_C: 23.14 ($CH_2\underline{CH_2}CH_2$), 37.74 (NH$\underline{CH_2}CH_2$), 48.13 (CH_2), 48.52 (CH_2), 50.10 (CH_2), 51.95 (CH_2), 52.20 (CH_2), 52.94 (CH_2), 53.97 (CH_2), 54.51 (CH_2), 125.01 (C3), 129.83 (C5), 142.15 (C4), 147.94 (C6), 160.18 (C=ONH), 162.33 (C=ONH), 162.81 (C=ONH), 174.32 (C=O); m/z (ES^+): 509.5 (100%, MH^+).

6.5.2 Complex synthesis

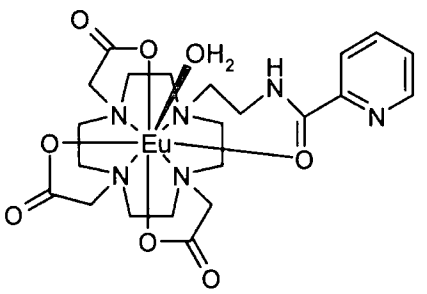

Eu($C_{22}H_{31}N_6O_7$) **[EuL^5]** Europium acetate (12 mg, 0.032 mmol) was added to a solution of **L^6** (pH 5.4, 16 mg, 0.032 mmol) in water (2 ml) and methanol (2 drops). The resulting pale yellow solution was heated under reflux for 48 hours before being cooled to room temperature. The pH was then increased to 10 using sodium hydroxide (1M solution) and the solution allowed to stand for 50 minutes. The europium hydroxide which formed was removed by filtration. The pH was adjusted back to pH 5.5 and the water removed by lyophilisation to yield a white solid. ^{1}H NMR (500 MHz, D_2O): the spectrum obtained was very complex; three major species were present, which were exchange broadened at 4°C; m/z (ES^-): 642.8 (100%, M-H); Acc.MS (ES^-): Found 643.1393, $C_{22}H_{31}N_6O_7Eu$ requires 643.1394; IR (KBr, cm^{-1}): 1699 (C=O), 1684 (C=O), 1560 (NH), 1407, 1206, 1131; k_{H_2O}: 1.65 ms^{-1}; k_{D_2O}: 0.53 ms^{-1}; q_{Eu} = 1.1.

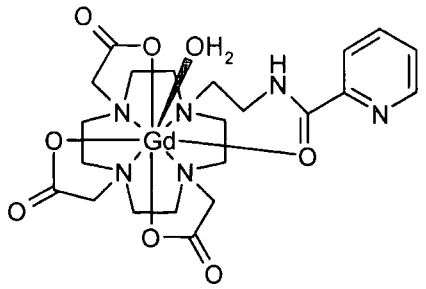

Gd($C_{22}H_{31}N_6O_7$) **[GdL^5]** Gadolinium acetate (12 mg, 0.032 mmol) was added to a solution of **L^5** (pH 5.5, 16 mg, 0.032 mmol) in water (2 ml) and methanol (2 drops). The resulting pale yellow solution was heated under reflux for 48 hours before being cooled to room temperature. The pH was then increased to 10 using sodium hydroxide (1M solution) and the solution allowed to stand for 50 minutes. The gadolinium hydroxide which formed was removed by filtration. The pH was adjusted back to pH 5.5 and the water removed by lyophilisation to yield the desired complex as a white solid. m/z (ES$^-$): 647.5 (85%, M-H$^-$); Acc.MS (ES$^-$): Found 648.1426, $C_{22}H_{31}N_6O_7Gd$ requires 648.1422; IR (KBr, cm^{-1}): 1699 (C=O), 1684 (C=O), 1560 (NH), 1407, 1206, 1131; r_{1p} (60 MHz, 37°C): 2.89 mM^{-1}s^{-1}; r_{1p} (65 MHz, 22°C): 3.50 mM^{-1}s^{-1}.

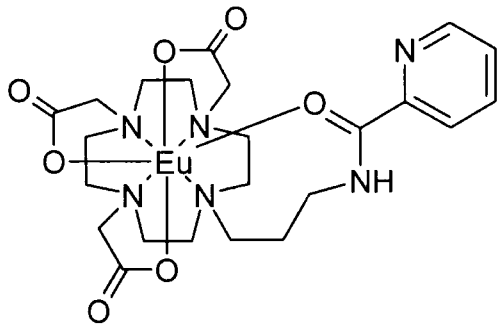

Eu($C_{23}H_{33}N_6O_7$) **[EuL^6]** The pH of a solution of **L^6** (0.073 mmol) in water (1.5 ml) and methanol (0.5 ml) was increased to pH 5.5 using KOH solution. Europium acetate (23 mg, 0.07 mmol) was added and the resulting solution was heated under reflux for 18 hours. After the solution was cooled, the pH was raised to 10 and the resulting suspension was filtered through a syringe filter to remove the excess europium as $Eu(OH)_3$. The pH was then lowered to 5.5 and the solution lyophilised to give the complex as a white powder. ^{1}H NMR (500 MHz, COSY, D_2O) was characteristic of a square antiprism constitution, one major and one minor isomer were present in ratio of 1 : 4. Partial assignment: 35.7 (0.2H, s, H_{ax},

minor isomer), 34.1 (0.2H, s, H_{ax}, minor isomer), 32.2 (1H, s, $H_{ax}(1)$), 29.3 (1H, s, H6), 27.5 (1H, s, $H_{ax}(2)$), 25.8 (1H, s, $H_{ax}(3)$), 23.41 (1H, s, $H_{ax}(4)$), 13.8 (1H, s), 11.3 (1H, s), 8.9 - 0 (br m), 4.6 ($H_{eq}(1)$), 1.8 ($H'_{ax}(1)$), -1.6 ($H'_{eq}(1)$), -3.6 ($H_{eq}(4)$), -3.9 ($H_{eq}(2)$), -4.6 ($H'_{eq}(2)$), -5.1 ($H'_{ax}(4)$), -7.4 ($H'_{ax}(2)$), -7.8 ($H_{eq}(3)$), -11.3 ($H'_{eq}(4)$), -11.5 ($H'_{eq}(3)$, -13.9 ($H'_{ax}(3)$), -14.9 ($\underline{CH_2}CO_2$), 16.7 ($\underline{CH_2}CO_2$), -18.0 ($\underline{CH_2}CO_2$), -20.0 ($\underline{CH_2}CO_2$), -20.2 ($\underline{CH_2}CO_2$); m/z (ES^+): 1351.2 (40%, $[KM_2 - H_2]^-$), 1312.9 (40%, $[M_2 - H_2]^-$), 656.8 (60%, $M\text{-}H^-$); Acc.MS (ES^+): Found 659.1696, $C_{23}H_{34}N_6O_7Eu$ requires 659.1696; IR (KBr, cm^{-1}): 1699 (C=O), 1684 (C=O), 1560 (NH), 1407, 1206, 1131; k_{H_2O}: 0.87ms^{-1}; k_{D_2O}: 0.58ms^{-1}; $q_{Eu} = 0$.

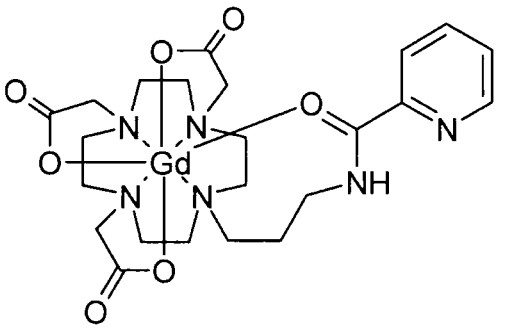

Gd($C_{23}H_{33}N_6O_7$) **[GdL^6]** Gadolinium acetate (26 mg, 0.07 mmol) was added to a solution of L^5 (0.07 mmol) in water (1.5 ml, pH 5.5) and methanol (0.5 ml). The resulting pale yellow solution was heated under reflux for 48 hours before being cooled to room temperature. The pH was then increased to 10 with sodium hydroxide (1M solution) for 50 minutes. The gadolinium hydroxide precipitate which formed was removed by filtration. The pH was then adjusted back to pH 5.5 and the water was removed by lyophilisation to yield the complex as a white solid. m/z (ES^-): 1323.7 (60%, $[M_2- H_2]^-$), 1361.7 (60%, $[KM_2 - H_2]^-$), 661.6 (40%, $M\text{-}H^-$); Acc.MS (ES^+): Found 702.1291, $C_{23}H_{33}N_6O_7GdK$ requires 702.1283; IR (KBr, cm^{-1}): 1699 (C=O), 1684 (C=O), 1560 (NH), 1407, 1206, 1131; r_{1p} (60 MHz, 37°C): 2.18 $mM^{-1}s^{-1}$; r_{1p} (65 MHz, 22°C): 2.45 $mM^{-1}s^{-1}$.

6.6 Chapter 4 Experimental

6.6.1 Ligand Synthesis

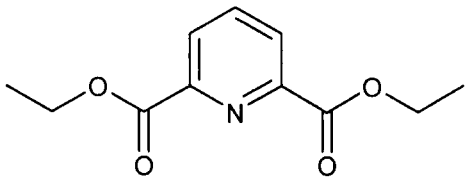

Pyridine-2,6-dicarboxylic acid diethyl ester[136] **55** Concentrated sulphuric acid (0.6 ml) was added to a suspension of 2,6-pyridinedicarboxylic acid (10.00 g, 59.8 mmol) in dry ethanol (100 ml) heating under argon at reflux. The reaction mixture, which gradually became clear and colourless, was boiled for 18 hours before being allowed to cool to room temperature and quenched with excess sodium hydrogen carbonate. The solvent was then evaporated under reduced pressure and the resulting residue was dissolved in dichloromethane (50 ml) and washed successively with water (50 ml) and aqueous sodium hydrogen carbonate solution (3 x 50 ml). The organic phase was then dried ($MgSO_4$), filtered, and concentrated under reduced pressure to yield a white crystalline solid (9.01 g, 67%). m.p. 38 - 39°C (no melting point given in literature[136]); ^{1}H NMR (200 MHz, $CDCl_3$): δ_H 1.46 (6H, t, *J* 7, 2Me), 4.47 (4H, quartet, *J* 7.2, $2CH_2$), 7.98 (1H, t, *J* 7.2, H4), 8.21 (2H, d, *J* 7.2, H3 + H5); ^{13}C NMR (50.3 MHz, $CDCl_3$): δ_C 14.24 (2Me), 62.33 ($2CH_2$), 127.87 (C4), 138.28 (C3 + C5), 148.67 (q, C2 + C6), 164.65 (C=O); m/z (ES^+): 469 (100%, $2M+Na^+$), 246 (42%, $M+Na^+$), 224 (17%, $M+H^+$).

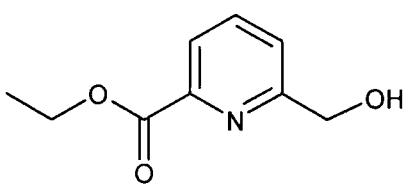

6-Hydroxymethyl-pyridine-2-carboxylic acid ethyl ester[136] **56** Sodium borohydride (0.91 g, 24.2 mmol) was added to a solution of **55** (9.01 g, 40.4 mmol) in dry ethanol (80 ml). The resulting suspension was heated under reflux for three hours before being allowed to cool to room temperature and quenched with water (60 ml). It was then concentrated under reduced pressure to ~70 ml and extracted with chloroform (3 x 80 ml). The combined organic phase was dried ($MgSO_4$), filtered

and concentrated under reduced pressure to yield a white solid (3.3 g), which was recrystallised from ethanol to give the desired product (3.22 g, 44%). m.p 91-92°C (no melting point given in literature[136]); ^{1}H NMR (200 MHz, $CDCl_3$): δ_H 1.42 (3H, t, *J* 7.2, Me), 3.76 (1H, br s, OH) 4.47 (2H, quartet, *J* 7.2, $\underline{CH_2}CH_3$), 4.85 (2H, s, $\underline{CH_2}OH$), 7.48 (1H, d, *J* 7.2, H5), 7.83 (1H, t, *J* 7.2, H4), 8.00 (1H, d, *J* 7.2, H3); ^{13}C NMR (50.3 MHz, $CDCl_3$): δ_C 14.45 (Me), 62.08 ($\underline{CH_2}CH_3$), 62.59 ($\underline{CH_2}OH$), 123.91 (C3), 123.98 (C5), 137.75 (C4), 160.04 (C=O); m/z (ES^+): 204.0 (100%, MNa^+).

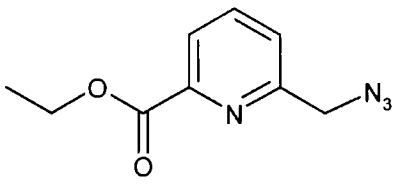

6-Azomethyl-pyridine-2-carboxylic acid ethyl ester[136] **57** Methanesulfonyl chloride (2.01 ml, 17.1 mmol) was added to a stirred suspension of **56** (3.10 g, 17.1 mmol) and triethylamine (2.38 ml, 17.1 mmol) in toluene (40 ml) which had been cooled in an ice bath. The reaction mixture was allowed to warm gradually to room temperature and stirred for 3 hours. Tetrabutylammonium bromide (0.606 g, 1.88 mmol), sodium azide (8.90 g, 136.86 mmol) and water (32 ml) were added and the resulting orange reaction mixture was heated at 90°C for 18 hours. The mixture was cooled to room temperature and the organic phase was separated. The aqueous phase was extracted with toluene (4 x 100 ml), and the combined organic extracts were dried ($NaSO_4$), filtered and concentrated under reduced pressure to yield a brown oil (4.01 g). Flash column chromatography (SiO_2, EtOAc) yielded the desired product as a pale yellow oil (2.21 g, 63%); R_f = 0.62 (SiO_2, EtOAc); ^{1}H NMR (200 MHz, $CDCl_3$): δ_H 1.42 (3H, t, *J* 7, Me), 4.48 (2H, *J* 7, $\underline{CH_2}CH_3$) 4.62 (2H, s, $\underline{CH_2}N_3$), 7.58 (1H, d, *J* 7.6, H3), 7.87 (1H, t, *J* 7.6, H4), 8.07 (1H, d, *J* 7.6, H5); ^{13}C NMR (50.3 MHz, $CDCl_3$): δ_C 14.39 (Me), 55.59 ($\underline{CH_2}N_3$), 62.17 ($\underline{CH_2}CH_3$), 124.32 (C3), 125.00 (C5), 138.13 (C4), 148.31 (q, C6) 156.58 (q, C2), 165.00 (C=O); m/z (ES^+): 435 (100%, $2M+Na^+$), 229 (56%, MNa^+), 207 (69%, MH^+).

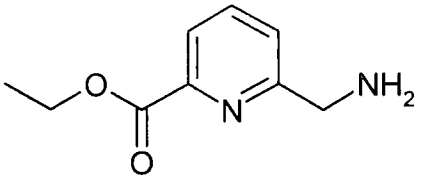

6-Aminomethyl-pyridine-2-carboxylic acid ethyl ester[136] **58** 10% Palladium on carbon (0.33 g) was added to a pale yellow solution of **57** (2.22 g, 10.8 mmol) in ethanol (50 ml). The resulting black suspension was hydrogenated on a Parr hydrogenator (30 psi) for 24 hours at room temperature. It was then filtered through celite and the filtercake washed with lots of ethanol. The filtrate was acidified with trifluoro-acetic acid (0.82 ml, 10.8 mmol) then the solvent was evaporated under reduced pressure to yield the trifluoroacetate salt as a yellow oil (3.43 g) which crystallised on standing. ^{1}H NMR (200 MHz, $CDCl_3$): δ_H 1.38 (3H, t, *J* 7.2, Me), 4.38 (2H, *J* 7.2, $\underline{CH_2}CH_3$) 4.44 (2H, s, $\underline{CH_2}NH_2$), 7.58 (1H, d, *J* 7.6, H3), 7.85 (1H, t, *J* 7.6, H4), 7.99 (1H, d, *J* 7.6, H5), 8.78 (2H, br s, NH_2); ^{13}C NMR (50.3 MHz, $CDCl_3$): δ_C 14.14 (Me), 43.61 ($\underline{CH_2}NH_2$), 62.38 ($\underline{CH_2}CH_3$), 124.91 (C3), 126.34 (C5), 138.64 (C4), 147.43 (q, C2) 153.15 (q, C6), 164.97 (C=O); m/z (ES^+): 167.1 (100%, $MH^+ - CH_2$), 180.1 (56%, MH^+).

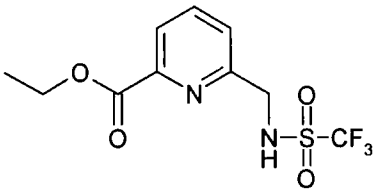

6-(Methanesulfonylamino-methyl)-pyridine-2-carboxylic acid ethyl ester **59** Under anhydrous conditions in an argon atmosphere, trifluoromethanesulfonyl chloride (1.65 ml, 10.87 mmol) was added to a solution of **58**.TFA (3.20 g, 10.87 mmol) in anhydrous pyridine (30 ml) which had been cooled to -40°C. The solution was stirred at -40°C for two hours before being allowed to warm gradually to room temperature. It was stirred at room temperature for 18 hours then poured onto ice (200 ml), which was allowed to melt. The resulting gloopy brown solution was extracted with diethyl ether (4 x 75 ml). The combined organic phase was then dried (Na_2SO_4), filtered and evaporated under reduced pressure. The resulting solid was then dissolved in dichoromethane and dried thoroughly under reduced pressure to remove all the residual pyridine. A pale brown solid was obtained

(2.35 g, 69%). m.p. 70 - 72°C; ^{1}H NMR (200 MHz, $CDCl_3$): δ_H 1.44 (3H, t, CH_3), 3.49 (1H, s, NH), 4.45 (2H, q, $\underline{CH_2}CH_3$), 4.70 (2H, d, *J 6.4*, $\underline{CH_2}NH$), 7.50 (1H, d, *J 7.6*, H3), 7.87 (1H, t, *J 7.8*, H4), 8.06 (1H, d, *J 7.8*, H5); After a D_2O shake, the NH peak disappeared and the $\underline{CH_2}NH$ peak became a singlet. ^{13}C NMR (50.3 MHz, $CDCl_3$): δ_C 14.29 (CH_3), 44.24 (CH_2), 62.15 (CH_2), 124.41 (C3), 125.53 (C5), 138.34 (C4), 147.89 (q, C2), 154.59 (q, C6), 164.78 (q, C=O); ^{19}F NMR (188 MHz, CD_3CN): δ -76.25 (s, CF_3); m/z (ES^+): 299 (100%, M- CH_2^+), 285 (80%, M- $C_2H_4^+$), transesterification occurs in methanol carrier solvent; υ_{max} (KBr)/cm^{-1} 3393 (NH), 1719 (C=O), 1590 (v py), 1421 (v py), 1372 (v_a SO_2), 1298, 1178 (v_s SO_2).

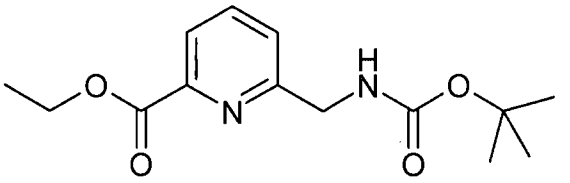

6-tert-Butoxycarbonylamino-methyl-pyridine-2-carboxylic acid ethyl ester **62** Following the method of Saito *et al.*,[137] BOC anhydride (3.89g, 17.88 mmol) and 10% palladium on carbon (0.307 g) was added to a clear solution of **100** (3.07 g)14.90 mmol) in ethyl acetate. The resulting black suspension was shaken under hydrogen (40psi) on a Parr hydrogentor for 18 hours at room temperature. The reaction mixture was then filtered through a pad of Celite which was then washed thoroughly with ethyl acetate. The resulting solution was concentrated under reduced pressure and then purified by flash column chromatography (SiO_2, EtOAc) to give the desired product as a clear oil (3.80 g, 91%). R_f = 0.52 (SiO_2, EtOAc); ^{1}H NMR (300 MHz, CD_3Cl): δ_H 1.48 (9H, s, *t*-Bu), 4.46 (2H, quintet, *J 6.9*, $\underline{CH_2}CH_3$), 4.51 (2H, d, *J 5.7*, $\underline{CH_2}NH$), 7.48 (1H, d, *J 7.8*, H5), 7.80 (1H, t, *J 7.5*, H4), 7.99 (1H, d, *J 7.2*, H3); ^{13}C NMR (50.8 MHz, $CDCl_3$): δ_C 28.38 ($C(\underline{CH_3})_3$), 45.93 (CH_2), 50.42 (CH_2), 52.88 (CH_2), 79.72 ($\underline{C}(CH_3)_3$), 123.76 (C4), 125.37 (C5), 137.79 (C3), 147.33 (C6), 156.15 (C2), 158.87 (C=O) 165.68 (C=O); m/z (ES^+): 303.2 (100%, MNa^+), 289.2 (70%, MNa^+ - CH_2 (tranesterification)); IR (thin film): 3373 (NH), 1693 (C=O), 1172; Acc.MS (ES^+): Found 303.1300, $C_{14}H_{20}N_2O_4Na$ requires 303.1321.

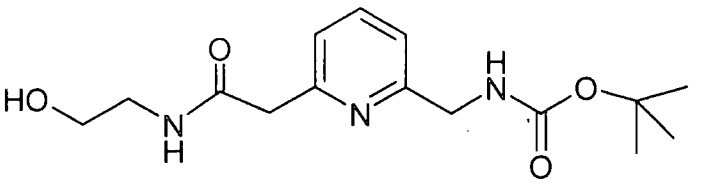

[6-(3-Hydroxy-ethylcarbamoyl)-pyridine-2-ylmethyl]-carbamic tert-butyl ester **63** A pale yellow solution of **62** (298 mg, 1.06 mmol) in ethanolamine (5 ml) and methanol (3 ml) was stirred at room temperature for 48 hours. The solvent was then removed using a Kügelrohr apparatus, purification of the resulting yellow oil by flash column chromatography (SiO_2, EtOAc) yielded the desired product as a clear colourless oil (68 mg, 22%). R_f = 0.66 (SiO_2, 10%MeOH in EtOAc); ^1H NMR (200 MHz, CD_3Cl): δ_H 1.46 (9H, s, *t*-Bu), 3.66 (2H, quartet, *J* 5.2, NH$\underline{CH_2}CH_2$), 3.84 (2H, t, *J* 5, HO$\underline{CH_2}CH_2$), 4.46 (2H, d, *J* 6.2, Ar$\underline{CH_2}$NH), 5.28 (1H, br s, NH), 7.40 (1H, d, *J* 7.6, H3), 7.82 (1H, t, *J* 7.8, H4), 8.05 (1H, d, *J* 7.6, H5), 8.38 (1H, br s, NH); ^{13}C NMR (75.4 MHz, $CDCl_3$): δ_C 28.52 (C($\underline{CH_3}$)$_3$), 42.67 (CH_2), 45.87 (CH_2), 62.53 (CH_2), 62.53 (CH_2), 120.99 (C4), 124.32 (q, C2), 138.26 (C3), 149.13 (C5), 156.17 (q, C6), 157.17 (C=O), 165.41 (C=O); m/z (ES^+): 318 (100%, MNa^+); Acc.MS (ES^+): Found 318.1414, $C_{14}H_{21}N_3O_4Na$ requires 318.1430; IR (thin film): 3200 (br OH), 1655 (C=O), 1526 (NH).

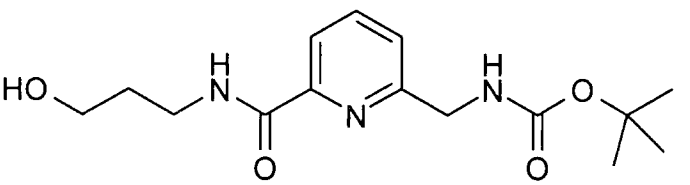

[6-(3-Hydroxy-propylcarbamoyl)-pyridine-2-ylmethyl]-carbamic tert-butyl ester **64** A solution of **62** (400 mg, 1.43 mmol) in 3-aminopropan-1-ol (4 ml) and methanol (2 ml) was stirred at room temperature for 48 hours. The solvent was then removed using a Kügelrohr apparatus, purification of the resulting yellow oil by flash column chromatography (SiO_2, EtOAc) yielded the desired product as a clear oil (262 mg, 59%). R_f = 0.67 (SiO_2, 10% MeOH in EtOAc), ^1H NMR (300 MHz, CD_3Cl): δ_H 1.48 (9H, s, *t*-Bu), 1.83 (2H, quintet, *J* 6, $CH_2\underline{CH_2}CH_2$), 3.62 - 3.73 (4H, m, $\underline{CH_2}CH_2\underline{CH_2}$), 4.46 (2H, d, *J* 5.1, $\underline{CH_2}$NH), 5.44 (1H, br s, NH), 7.40 (1H, d, *J* 7.5, H3), 7.83 (1H, t, *J* 7.8, H4), 8.06 (1H, d, *J* 7.8, H5), 8.49 (1H, br s, NH); ^{13}C NMR (75.4 MHz, $CDCl_3$): δ_C 28.64 (C($\underline{CH_3}$)$_3$), 32.31 (CH_2), 32.48 (CH_2), 36.68 (CH_2), 45.75

(CH_2), 121.07 (C4), 124.35 (C2), 138.45 (C3), 149.11 (C5), 157.05 (C6), 177.17 (C=O), 182.97 (C=O); m/z (ES^+): 332 (100%, MNa^+); Acc.MS (ES^+): Found 332.1570, $C_{15}H_{23}N_3O_4Na$ requires 332.1586.

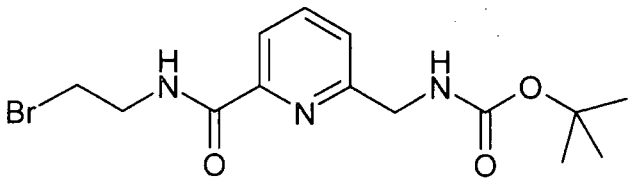

[6-(2-Bromo-ethylcarbamoyl)-pyridin-2-ylmethyl]-carbamic acid tert-butyl ester **68** Under an argon atmosphere, triphenylphosphine (1.107 g, 4.22 mmol) was added to a stirred clear solution of **63** (0.830 g, 2.81 mmol) and carbon tetrabromide (1.166 g, 3.52 mmol) in dichloromethane (35 ml) which had been cooled on an ice-bath. The resulting pale yellow solution was allowed to warm gradually to room temperature and stirred for 18 hours. The resulting red solution was concentrated under reduced pressure and purified by flash column chromatography (SiO_2, EtOAc) to give a clear colourless oil (0.833 g, 82%). ^1H NMR (300 MHz, CD_3Cl): δ_H 1.47 (9H, s, *t*-Bu), 3.59 (2H, t, *J 6*, HO$\underline{CH_2}CH_2$), 3.88 (2H, quartet, *J 6*, NH$\underline{CH_2}CH_2$), 4.48 (2H, d, *J 5.4*, Ar$\underline{CH_2}$NH), 5.28 (1H, br s, NH), 7.43 (1H, d, *J 7.5*, H3), 7.84 (1H, t, *J 7.8*, H4), 8.07 (1H, d, *J 7.6*, H5), 8.39 (1H, br s, NH); ^{13}C NMR (75.4 MHz, $CDCl_3$): δ_C 28.50 (C($\underline{CH_3}$)$_3$), 32.07 (CH_2), 41.17 (CH_2), 45.74 (CH_2), 120.97 (C4), 124.38 (q, C2), 138.25 (C3), 148.92 (C5), 156.12 (q, C6), 157.16 (C=O), 164.35 (C=O); m/z (ES^+): 382.0 (85%, MNa^+), 380.0 (100%, MNa^+); Acc.MS (ES^+): Found 380.0569, $C_{14}H_{21}N_3O_3BrNa$ requires 380.0586.

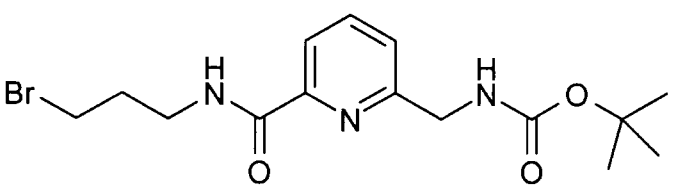

[6-(3-Bromo-propylcarbamoyl)-pyridine-2-ylmethyl]-carbamic tert-butyl ester **69** Triphenylphosphine (184 mg, 0.704 mmol) was added to a solution of **64** (145 mg, 0.469 mmol) and carbon tetrabromide (195 mg, 0.586 mmol) in dichloromethane (5 ml) which had been cooled in an ice bath. The resulting yellow solution was allowed to warm gradually to room temperature and then stirred at room

temperature for 18 hours. The solvent was then removed under reduced pressure and the resulting pink oil was purified by flash column chromatography (SiO_2, EtOAc) to yield a clear colourless oil (132 mg, 78%). R_f = 0.55 (SiO_2, EtOAc); ^1H NMR (200 MHz, $CDCl_3$): δ_H 1.45 (9H, s, *t*-Bu), 2.20 (2H, quintet, *J* 6.6, $CH_2\underline{CH_2}CH_2$), 3.48 (2H, q, *J* 6.6, $CH_2\underline{CH_2}NH$), 3.60 (2H, q, *J* 6.6, $Br\underline{CH_2}CH_2$), 4.46 (2H, d, *J* 2, $\underline{CH_2}NH$), 5.36 (1H, br s, NH), 7.38 (1H, d, *J* 6.6, H3), 7.80 (1H, t, *J* 6.6, H4), 8.03 (1H, d, *J* 6.6, H5), 8.84 (1H, br s, NH); ^{13}C NMR (75.4 MHz, $CDCl_3$): δ_C 28.50 ($C\underline{(CH_3)_3}$), 31.00 (CH_2), 32.48 (CH_2), 38.12 (CH_2), 45.79 (CH_2), 79.96 ($\underline{C}(CH_3)_3$), 120.90 (C4), 124.19 (C3), 138.24 (C5), 149.19 (C6), 156.06 (q, C2), 157.05 (C=O), 164.52 (C=O); m/z (ES^+): 394 (100%, $^{79}BrMNa^+$), 396 (94%, $^{81}BrMNa^+$); Acc.MS (ES^+): Found 394.0740, $C_{15}H_{22}N_3O_3NaBr$ requires 394.0742.

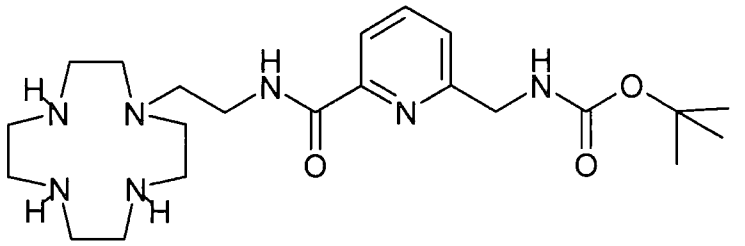

{6-[2-(1,4,7,10-Tetraaza-cyclododec-yl)-ethylcarbomoyl]-pyridin-2-ylmethyl}-carbamic acid tert-butyl ester **77** Under an argon atmosphere, a solution of **68** (291 mg, 0.815 mmol) in dry chloroform (50 ml) was added to a solution of cyclen (421 mg, 2.44 mmol) in dry chloroform (25 ml). The resulting clear colourless solution was stirred at room temperature for four days. The chloroform was then removed under reduced pressure and the resulting yellow oil was dissolved in dichloromethane (25 ml) and washed with water (2 x 10 ml). The organic phase was then evaporated under reduced pressure yielding a clear oil (347 mg, 94%). ^1H NMR (300 MHz, CD_3Cl): δ_H 1.40 (9H, s, *t*-Bu), 2.50 - 2.65 (18H, m, 8 ring CH_2, $N\underline{CH_2}CH_2$), 3.52 (2H, quartet, *J* 5.1, $NH\underline{CH_2}CH_2$), 4.32 (2H, d, *J* 5.7, $Ar\underline{CH_2}NH$), 7.33 (1H, d, *J* 7.5, H3), 7.74 (1H, t, *J* 7.5, H4), 8.03 (1H, d, *J* 7.5, H5); ^{13}C NMR (75.4 MHz, $CDCl_3$): δ_C 28.64 ($C\underline{(CH_3)_3}$), 37.88 (CH_2), 44.70 (CH_2), 45.77 (CH_2), 46.50 (CH_2), 51.92 (CH_2), 54.55 (CH_2), 78.92 ($\underline{C}(CH_3)_3$), 120.51 (C4), 124.56 (q, C2), 137.96 (C3), 149.72 (C5), 156.76 (q, C6), 157.12 (C=O), 164.21 (C=O); m/z (ES^+): 512.3 (15%, MCu^+), 450.3 (100%, MH^+); Acc.MS (ES^+): Found 450.3175, $C_{22}H_{40}N_7O_3$ requires 450.3193.

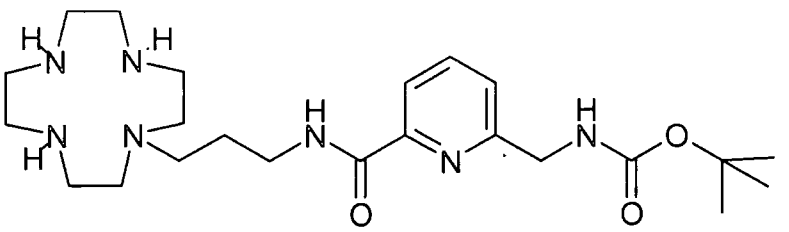

{6-[2-(1,4,7,10-Tetraaza-cyclododec-yl)-propylcarbomoyl]-pyridin-2-ylmethyl}-carbamic acid tert-butyl ester **78** Cyclen (323 mg, 1.871 mmol) was added in portions to a solution of **69** (232 mg, 0.623 mmol) in dry chloroform (75 ml) which was stirred under argon at room temperature. The resulting clear solution was stirred at room temperature under argon for 6 days until TLC (10% MeOH in DCM) showed no starting material to remain. The solvent was then evaporated under reduced pressure and the resulting clear oil was dissolved in dichloromethane (25 ml) and washed with water (20 ml). The organic phase was separated and evaporated under reduced pressure to give a clear oil (285 mg, 98% yield). ^{1}H NMR (300 MHz, CD_3Cl): δ_H 1.42 (9H, s, *t*-Bu), 1.85 (2H, t, *J 6.3*, $CH_2\underline{CH_2}CH_2$), 2.48 - 2.79 (18H, m, 8 ring CH_2, $N\underline{CH_2}CH_2$), 3.58 (2H, quartet, *J 6.3*, $NH\underline{CH_2}CH_2$), 4.35 (2H, br s, $Ar\underline{CH_2}NH$), 7.38 (1H, d, *J 7.8*, H3), 7.43 (1H, br s, NH), 7.78 (1H, t, *J 7.7*, H4), 8.03 (1H, d, *J 7.8*, H5), 8.31 (1H, br s, NH); ^{13}C NMR (75.4 MHz, $CDCl_3$): δ_C 26.53 (CH_2), 28.76 ($C(\underline{CH_3})_3$), 36.67 (CH_2), 44.97 (CH_2), 46.17 (CH_2), 46.37 (CH_2), 46.91 (CH_2), 50.67 (CH_2), 51.37 (CH_2), 54.55 (CH_2), 74.96 ($\underline{C}(CH_3)_3$), 120.65 (C4), 124.79 (q, C2), 138.26 (C3), 149.86 (C5), 157.34 (C=O), 164.45 (C=O); m/z (ES^+): 464.3 (100%, MH^+), 526.3 (12%, MCu); Acc.MS (ES^+): Found 464.3334, $C_{23}H_{42}N_7O_3Na$ requires 464.3349.

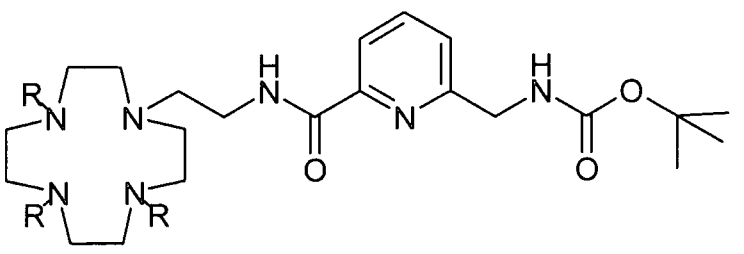

R = $CH_2CO_2{}^tBu$

{6-[2-(1,4,7,10-Tetraaza-cyclododec-yl)-ethylcarbomoyl]-pyridin-2-ylmethyl}-carbamic acid tert-butyl ester - N,N',N'',N'''-1,4,7,10-tert-butyl acetate **79** A suspension of **77** (401 mg, 0.89 mmol), t-butyl bromoacetate (573 mg, 2.94 mmol) and sodium carbonate (312 mg, 2.94 mmol) in dry acetonitrile (15 ml) were heated at 60°C for 18

hours under an argon atmosphere. The reaction mixture was then allowed to cool to room temperature and the solvent was evaporated under reduced pressure. The resulting oil was dissolved in dichloromethane (20 ml) and washed with water (3 x 10 ml). The organic phase was then dried (K_2CO_3) filtered and evaporated under reduced pressure to give the desired product as a pale brown oil (688 mg, 97%). ^{1}H NMR (300 MHz, CD_3Cl): δ_H 1.49 (36H, s, 4 x *t*-Bu), 1.92 - 3.37 (26H, m, 13 CH_2s), 4.20 (2H, d, *J 7.8*, Ar$\underline{CH_2}$NH), 5.77 (1H, br s, NH), 7.40 (1H, d, *J 7.8*, H3), 7.72 (1H, t, *J 7.8*, H4), 7.89 (1H, d, *J 7.8*, H5), 8.36 (1H, br s, NH); ^{13}C NMR (75.4 MHz, $CDCl_3$): δ_C 27.8 (C($\underline{CH_3}$)$_3$), 37.7 (CH_2), 45.8 (CH_2), 50.2 (CH_2), 51.9 (CH_2), 55.6 (CH_2), 56.5 (CH_2), 82.4 ($\underline{C}$(CH_3)$_3$), 120.4 (C4), 124.0 (C2), 138.0 (C3), 149.0 (C5), 157.7 (q, C6), 164.4 (C=O), 172.5 (C=O), 173.6 (C=O); m/z (ES$^+$): 814.9 (100%, MNa$^+$), 792.5 (48%, MH$^+$).

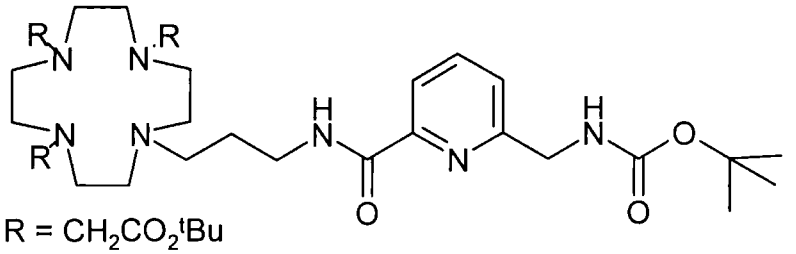

{6-[2-(1,4,7,10-Tetraaza-cyclododec-yl)-propylcarbomoyl]-pyridin-2-ylmethyl}-carbamic acid tert-butyl ester - N,N',N''-1,4,7,-tert-butyl acetate **80** A suspension of **78** (207 mg, 0.45 mmol), *t*-butyl bromoacetate (287 mg, 1.47 mmol) and sodium carbonate (156 mg, 1.47 mmol) were heated at 60°C for 18 hours under an argon atmosphere. The reaction mixture was then allowed to cool to room temperature and the solvent was evaporated under reduced pressure. The resulting oil was dissolved in dichloromethane (20 ml) and washed with water (3 x 10 ml). The organic phase was then dried (K_2CO_3) filtered and evaporated under reduced pressure to give the desired product as a yellow oil. ^{1}H NMR (300 MHz, CD_3Cl): δ_H 1.39 (36H, s, 4 x *t*-Bu), 1.89 (2H, br t, $CH_2\underline{CH_2}CH_2$), 2.25 - 3.38 (26H, m, 13 CH_2s), 4.40 (2H, br s, Ar$\underline{CH_2}$NH), 5.78 (1H, br s, NH), 7.39 (1H, d, *J 7.2*, H3), 7.73 (1H, t, *J 7.8*, H4), 7.92 (1H, d, *J 7.2*, H5), 8.22 (1H, br s, NH); m/z (ES$^+$): 806.6 (100%, MH$^+$), 828.4 (30%, MNa$^+$).

As the synthetic pathway is analogous for the C_2 and C_3 appended DO3A ligand systems L^7 and L^8; the synthetic details will only be described for the C_3 variant.

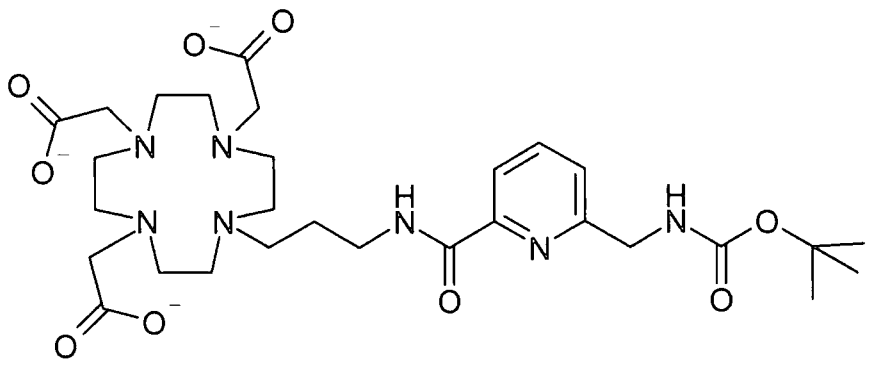

1,4,7-Tris(carboxymethyl)-{6-[2-(1,4,7,10-Tetraaza-cyclododec-yl)-propylcarbomoyl]-pyridin-2-ylmethyl}-carbamic acid tert-butyl ester $\mathbf{L^{11}}$ A solution of **80** (397 mg, 0.92 mmol) in TFA (4 ml) was left standing under an argon atmosphere for 18 hours. The solvent was then removed under reduced pressure. The resulting pale brown oil was resuspended in dichloromethane (3 x 4 ml) which was then evaporated in order to remove all residual TFA. ^{1}H NMR (300 MHz, D_2O): δ_H 2.07 (2H, br quintet, $CH_2\underline{CH_2}CH_2$), 2.92 - 3.51 (26H, m, 13 CH_2s), 4.36 (2H, s, $Ar\underline{CH_2}NH$), 7.56 (1H, t, *J* 7.2, H4), 7.80 (2H, m, H3 + H5); m/z (ES^+): 566.4 (100%, MH^+).

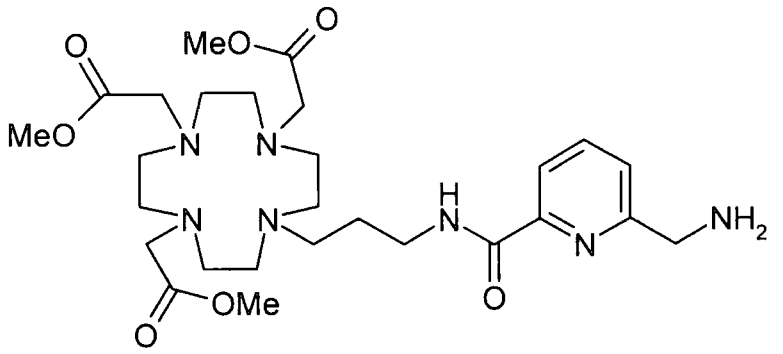

1,4,7-Tris(methoxycarboxymethyl)-{6-[2-(1,4,7,10-Tetraaza-cyclododec-yl)-propylcarbomoyl]-pyridin-2-ylmethyl}-amine **83** The TFA salt of $\mathbf{L^{11}}$ (0.92 mmol) was dissolved in dry methanol (3 x 5 ml) which was then evaporated under high vacuum. The resulting oil was then redissolved in dry methanol (10 ml) and acetyl chloride (0.5 ml) was added to generate dry HCl *in situ*. The resulting solution was heated under reflux for 48 hours. It was then allowed to cool to room temperature and the solvent was evaporated to yield the desired product. ^{1}H NMR (300 MHz,

CD_3Cl): δ_H 2.02 (2H, br s, $CH_2\underline{CH_2}CH_2$), 2.79 - 4.36 (28H, m, 13 x CH_2), 3.47 (9H, s, 3 $O\underline{CH_3}$), 7.33 (1H, d, *J 7.5*, H5), 7.72 (1H, t, *J 7.5*, H4), 7.83 (1H, d, *J7.8*, H3); m/z (ES^+): 290.9 (100%, MH^{2+}), 314.7 (52%, MNa^{2+}), 580.4 (90%, MH^+); Acc.MS (ES^+): Found 580.3412, $C_{27}H_{46}N_7O_7$ requires 580.3459.

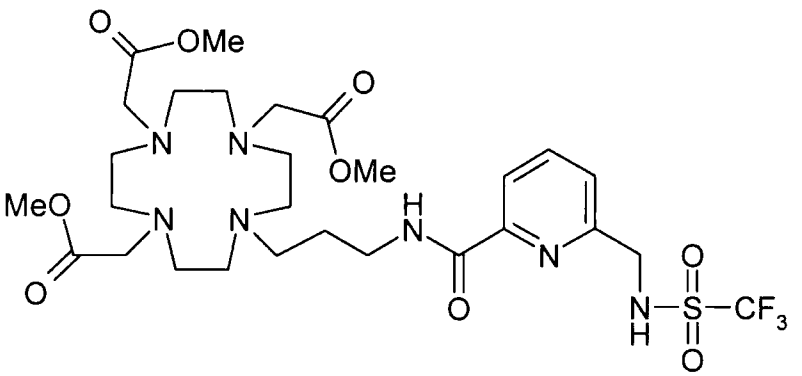

1,4,7-Tris(methoxycarboxymethyl)-{6-[2-(1,4,7,10-Tetraaza-cyclododec-yl)-propylcarbomoyl]-pyridin-2-ylmethyl}-trifluoromethanesulfonamide **85** Under an argon atmosphere trifluoromethane sulfonyl chloride (225 mg, 1.34 mmol) was added to a solution of **83** (258 mg, 0.446 mmol) and Hünig's base (172 mg, 1.34 mmol) in dichloromethane (5 ml) which had been cooled to -40°C. The solution was held at -40°C for one hour, then allowed to warm to -20°C and kept at this temperature for 18 hours. The solvent was then removed under reduced pressure and the resulting brown oil was purified by flash column chromatography (SiO_2, 5% MeOH in DCM) to give the desired product contaminated with Hünig's base as a pale yellow oil. R_f = 0.61 (SiO_2, 10% MeOH in DCM); ^1H NMR (300 MHz, CD_3Cl): δ_H 2.75 - 3.64 (26H, m, 13 x CH_2), 3.88 (9H, s, 3 $O\underline{CH_3}$), 4.13 (2H, s, $\underline{CH_2}NH_2$), 7.76 (1H, d, *J 7.2*, H5), 8.00 (1H, d, *J 6.9*, H5), 8.12 (1H, t, *J 8.1*, H4); ^{19}F NMR (282 MHz, $CDCl_3$): δ_F -78.8 (s, CF_3); m/z (ES^+): 712.4 (65%, MH^+).

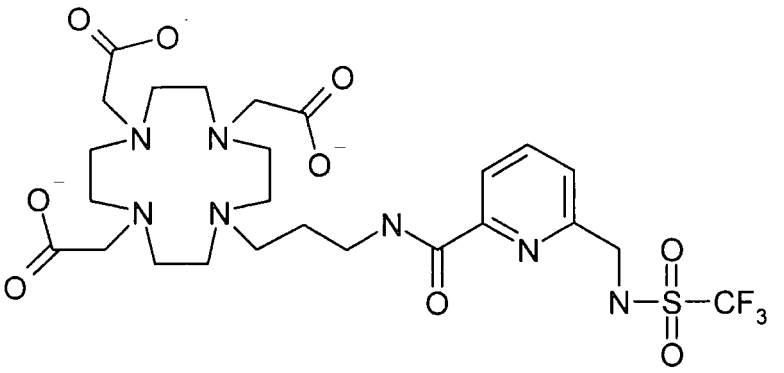

1,4,7-Tris(carboxymethyl)-{6-[2-(1,4,7,10-Tetraaza-cyclododec-yl)-propylcarbomoyl]-pyridin-2-ylmethyl}-trifluoromethanesulfonamide $\mathbf{L^8}$ A suspension of **85** (23 mg, 0.033 mmol) and lithium hydroxide (15 mg) in deuterium oxide (0.7 ml) was left standing at room temperature for 24 hours. The hydrolysis of the methyl esters was monitored by ^{1}H NMR. The ligand was complexed *in situ*. δ_H 2.75 - 3.64 (26H, m, 14 CH_2s), 7.76 (1H, d, *J 7.2*, H5), 8.00 (1H, d, *J 6.9*, H5), 8.12 (1H, t, *J 8.1*, H4); ^{19}F NMR (282 MHz, D_2O): δ_F -78.8 (s, CF_3).

As the synthetic pathway is analogous for the C_2 and C_3 appended aDO3A ligand system $\mathbf{L^9}$ and $\mathbf{L^{10}}$; the synthetic details will only be described for the C_2 variant.

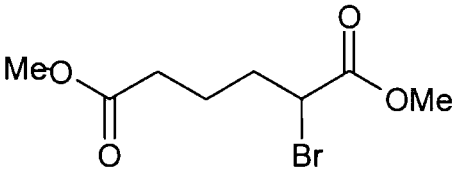

Dimethyl α-bromo adipate[142] **76** A solution of monomethyladipic acid (21g, 131 mmol) in thionyl chloride (38 ml) and carbon tetrachloride (60 ml) were heated to 65°C for 40 minutes. N-bromosuccinimide (27.8g, 157 mmol), carbon tetrachloride (50 ml) and hydrogen bromide (5 drops) were then added and the resulting orange solution was heated at 85°C for 2 hours. The resulting brown solution was then cooled with an ice bath and quenched with methanol (80 ml), the suspension which formed was stirred overnight. The succinimide precipitate was removed by filtration and washed with methanol. The methanol was then removed under reduced pressure; the resulting brown oil was dissolved in dichloromethane (150 ml) and washed with water (100 ml), then saturated sodium hydrogen carbonate (100 ml), then more water (100 ml). The organic phase was then dried (Na_2SO_4), filtered and concentrated under reduced pressure to yield a purpley oil

(42.3 g). Fractional distillation (125-126°C, 0.1 mm Hg) yielded the desired product in 71% yield. ^{1}H NMR (250 MHz, $CDCl_3$) δ_H: 1.64 (2H, m, C<u>H</u>CH$_2$CHBr), 2.05 (2H, m, C<u>H</u>$_2$CHBr), 2.34 (2H, bt, *J* 7.2, C<u>H</u>$_2$CO$_2$CH$_3$), 3.66 (3H, s, CHBrCO$_2$<u>CH</u>$_3$), 3.77 (3H, s, CH$_2$CO$_2$<u>CH</u>$_3$), 4.22 (1H, dd *J* 6.6, 7.9, C<u>H</u>Br); ^{13}C NMR (62.9 MHz, $CDCl_3$) δ_C: 22.41 (<u>C</u>H$_2$CH$_2$CHBr), 32.79 (<u>C</u>H$_2$CO$_2$CH$_3$), 33.88 (<u>C</u>H$_2$CHBr), 44.91 (<u>C</u>HBr), 51.42 (CH$_2$CO<u>C</u>H$_3$), 52.76 (CHBrCO$_2$<u>C</u>H$_3$), 169.79 (CH$_2$<u>C</u>O$_2$CH$_3$), 172.99 (CHBr<u>C</u>O$_2$CH$_3$); m/z (ES$^+$): 528.7 (64%, 2MNa$^+$), 276.8 (100%, MNa$^+$).

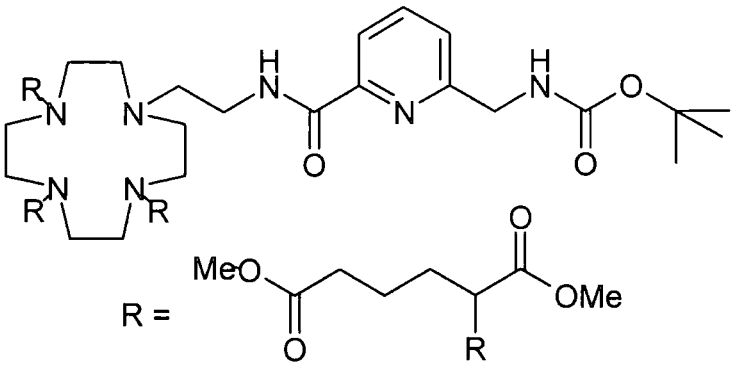

1,4,7-Tris-[(4'-methoxycarbonyl)-1'methoxycarbonylbutyl]-{6-[2-(1,4,7,10-Tetraaza-cyclododec-yl)-ethylcarbomoyl]-pyridin-2-ylmethyl}-carbamic acid tert-butyl ester **86**

Under anhydrous conditions and an argon atmosphere, a stirred suspension of **77** (68 mg, 0.151 mmol), α-bromoadipate **76** (170 mg, 0.499 mmol) and sodium carbonate (53 mg, 0.499 mmol) in dry acetonitrile (3 ml) was heated at reflux for 10 days. The reaction mixture was then allowed to cool to room temperature and filtered to remove the inorganic solids, evaporation of the solvent yielded a yellow oil which was purified by gradient elution column chromatography (SiO_2, 1% MeOH in DCM → 5% MeOH in DCM). The desired product was obtained as a yellow oil (67 mg, 46% yield). R_f = 0.22 (SiO_2, 10% MeOH in DCM). ^{1}H NMR (300 MHz, CD_3Cl): δ_H 1.42 (9H, s, *t*-Bu), 1.59 -3.55 (41H, br m, CH_2s), 3.60 (18H, s, 6 CH_3), 4.42 (2H, s, Ar<u>CH$_2$</u>NH), 7.40 (1H, d, *J* 6.6, H3), 7.76 (1H, t, *J* 7.5, H4), 7.98 (1H, d, *J* 7.2, H5); ^{13}C NMR (75.4 MHz, $CDCl_3$): δ_C 22.18 (CH_3), 28.51 (C(<u>CH$_3$</u>)$_3$), 33.63, 39.99, 45.73, 50.49, 51.63, 74.81 (<u>C</u>(CH$_3$)$_3$), 120.68 (C4), 137.94 (C3), 149.72 (C5), 156.29 (q, C6), 157.67 (C=O), 173.61 (C=O); m/z (ES$^+$): 966.4 (100%, MH$^+$); Acc.MS (ES$^+$): Found 966.5485, $C_{46}H_{76}N_7O_{15}$ requires 966.5399.

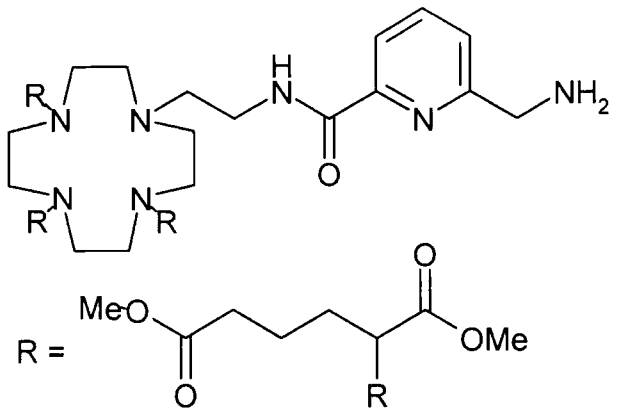

1,4,7-Tris-[(4'-methoxycarbonyl)-1'methoxycarbonylbutyl]-{6-[2-(1,4,7,10-Tetraaza-cyclododec-yl)-ethylcarbomoyl]-pyridin-2-ylmethyl}-amine **88** Under an argon atmosphere, a solution of **86** (55 mg, 0.067 mmol) in trifluoroacetic acid (1.5 ml) was left standing for 18 hours. The solvent was then removed under reduced pressure and the resulting brown oil was redissolved in dichloromethane (1 ml) and the solvent evaporated under reduced pressure. This was repeated three times to remove the residual TFA. ^{1}H NMR (300 MHz, CD_3Cl): δ_H 1.59 -3.55 (41H, br m, CH_2s), 3.60 (18H, s, 6 CH_3), 4.42 (2H, s, Ar$\underline{CH_2}$NH), 7.40 (1H, d, *J 6.6*, H3), 7.76 (1H, t, *J 7.5*, H4), 7.98 (1H, d, *J 7.2*, H5); m/z (ES^+): 434.1 (100%, MH^{2+}), 866.3 (12%, MH^+). Acc.MS (ES^+): Found 866.4825, $C_{41}H_{68}N_7O_{13}$ requires 866.4875.

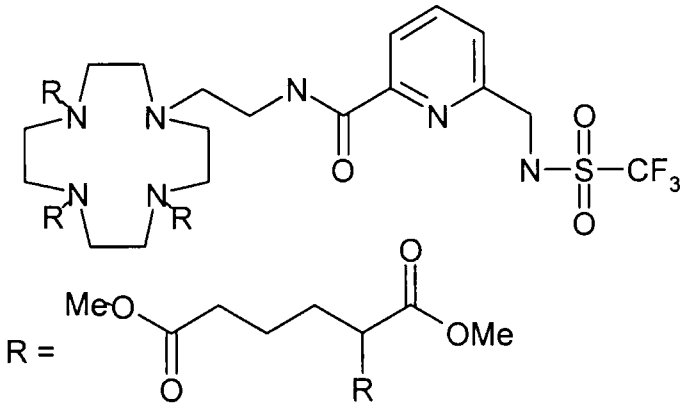

1,4,7-Tris-[(4'-methoxycarbonyl)-1'methoxycarbonylbutyl]-{6-[2-(1,4,7,10-Tetraaza-cyclododec-yl)-ethylcarbomoyl]-pyridin-2-ylmethyl}-trifluoromethanesulfoanmide **90**

Under anhydrous conditions and an argon atmosphere, trifluoromethanesulfonyl chloride (0.0072ml, 0.067 mmol) was added to a stirred solution of **88** (0.0673 mmol) in dichloromethane (0.5 ml) and Hunig's base (0.012ml, 0.0673 mmol) which had been cooled to -40°C. The reaction mixture was stirred at -40°C for two hours, then

held at -18°C for 18 hours. The solvent was removed under reduced pressure and the resulting brown oil was purified by flash column chromatography (SiO_2, 2% MeOH in DCM). The desired product was obtained as a clear oil (15 mg, 22% yield). ^{1}H NMR (300 MHz, CD_3Cl): δ_H 1.63 -3.46 (44H, br m, CH_2s), 3.66 (18H, m, 6 CH_3), 3.96 (2H, s, Ar$\underline{CH_2}$NH), 7.36 (1H, d, *J 7.8*, H3), 7.83 (1H, t, *J 7.8*, H4), 8.01 (1H, d, *J 8.1*, H5); ^{19}F NMR (282 MHz, CD_3Cl): δ_F -79.10 (s, CF_3); *m/z* (ES^+): 998.6 (100%, MH^+); Acc.MS (ES^+): Found 998.4404, $C_{44}H_{67}N_7O_{15}F_3S$ requires 998.4368.

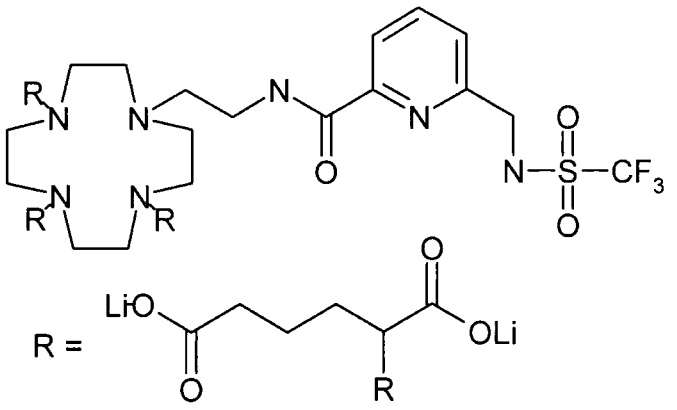

1,4,7-Tris-[(4'-carbonxy)-1'carbonylbutyl]-{6-[2-(1,4,7,10-Tetraaza-cyclododec-yl)-ethylcarbomoyl]-pyridin-2-ylmethyl}-trifluoromethanesulfoanmide **L**[9] A suspension of **90** (15 mg, 1.5 μmol) and lithium hydroxide (29 mg, 0.69 mmol) in D_2O (0.7 ml) and dMeOH (0.4 ml) was agitated at room temperature for 24 hours. The reaction was monitored by ^{1}H NMR. The hydrolysed product was complexed without further purification. ^{1}H NMR (300 MHz, CD_3Cl): δ_H 1.30 -3.52 (44H, br m), 7.44 (1H, d, *J 7.8*, H3), 7.70 (2H, m, H4, H5); ^{19}F NMR (282 MHz, D_2O): δ_F -78.79 (s, CF_3).

6.6.2 Complex Synthesis

The lanthanide complexes were all formed in a similar fashion: an aqueous solution containing the ligand and the lanthanide chloride hexahydrate in a 1 : 1 ratio, was adjusted to pH 5.5 using 1M NaOH solution and heated at 90°C for 18 hours. The solution was then cooled, the pH was raised to 10 and the solution was filtered to remove excess lanthanide as insoluble $Ln(OH)_3$. The pH was then lowered to 5.5 and the solution lyophilised to give the desired complex as a white powder. H^+ loaded Amberlite IRC-50 weakly acidic cation exchange resin was used to remove the salt from the complexes.

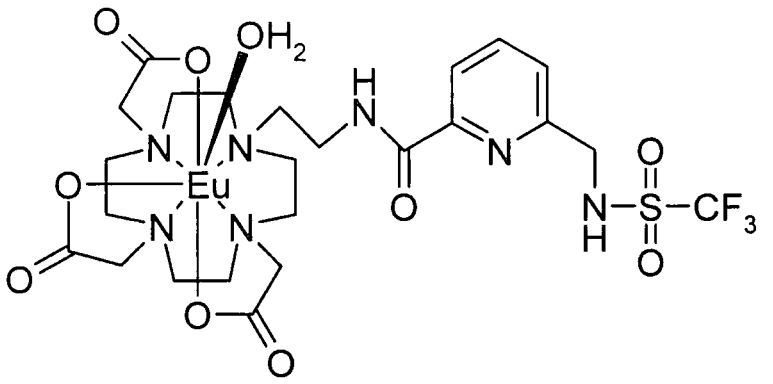

Eu($C_{24}H_{33}N_7O_9SF_3$) **[EuL^7]** ^{1}H NMR (500 MHz, D_2O): The spectrum was exchange broadened. ^{19}F NMR (500 MHz, D_2O): 79.35; k_{H_2O} 1.57 ms-1; k_{D_2O} 0.50 ms-1; q = 0.98; $\lambda_{max}(H_2O)$ 271 nm (ε 4693 $dm^3mol^{-1}cm^{-1}$).

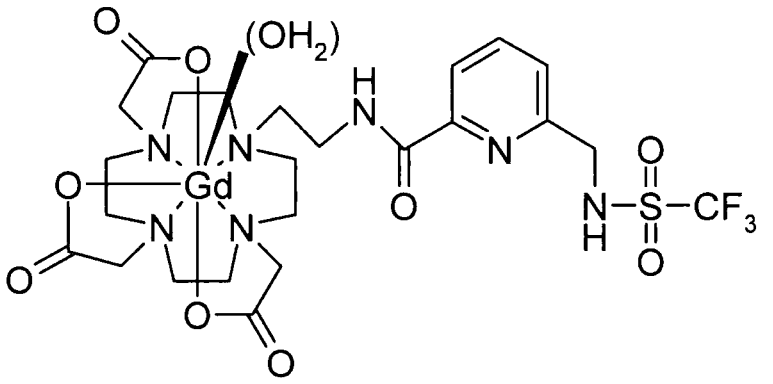

Gd($C_{24}H_{33}N_7O_9SF_3$) **[GdL^7]** r_{1p}: 6.74 $mM^{-1}s^{-1}$ (65 MHz, 22°C); 4.34 $mM^{-1}s^{-1}$ (60 MHz, 37°C).

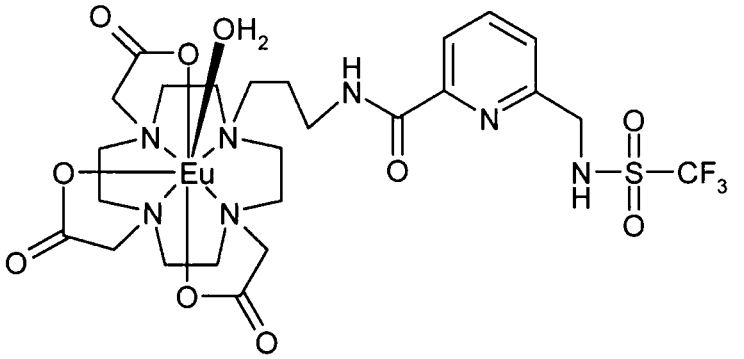

Eu($C_{25}H_{35}N_7O_9SF_3$) **[EuL^8]** ^{1}H NMR (500 MHz, D_2O): The spectrum was exchange broadened. ^{19}F NMR (500 MHz, D_2O): 79.20; k_{H_2O} 1.69 ms-1; k_{D_2O} 0.49 ms-1; q = 1.14; $\lambda_{max}(H_2O)$ 271 nm (ε 4693 $dm^3mol^{-1}cm^{-1}$).

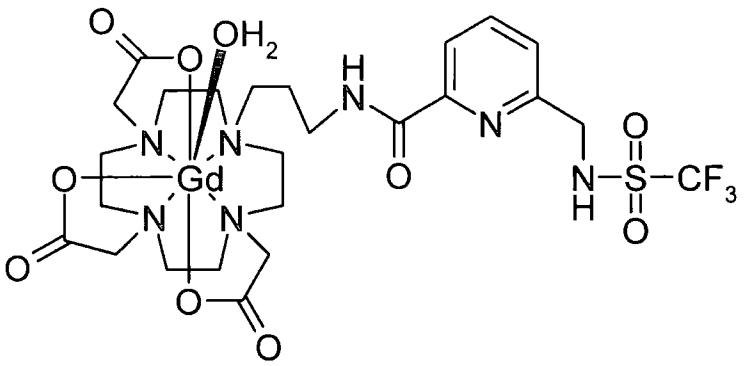

Gd($C_{25}H_{35}N_7O_9SF_3$) **[GdL^8]** r_{1p}: 6.56 $mM^{-1}s^{-1}$ (65 MHz, 22°C); 4.34 $mM^{-1}s^{-1}$ (60 MHz, 37°C).

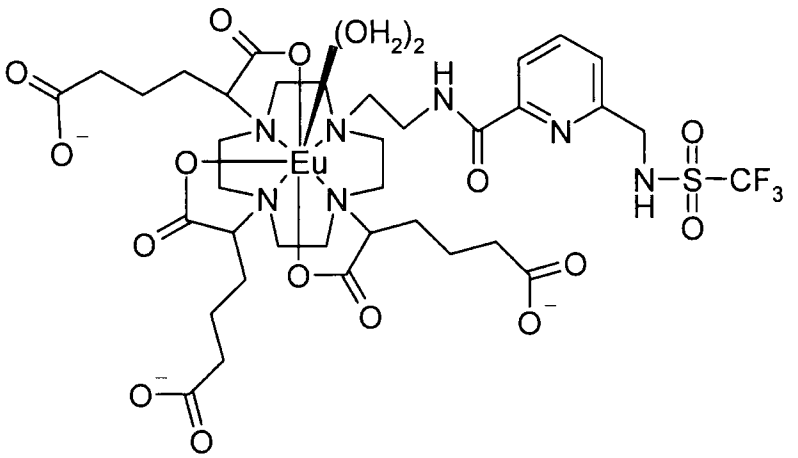

Eu($C_{42}H_{54}N_7O_{21}SF_3$) **[EuL^9]** ^{1}H NMR (500 MHz, D_2O): The spectrum was exchange broadened. ^{19}F NMR (500 MHz, D_2O): 79.20; k_{H_2O} 2.05 ms-1; k_{D_2O} 0.26 ms-1; q = 1.85; $\lambda_{max}(H_2O)$ 271 nm (ε 4693 $dm^3mol^{-1}cm^{-1}$).

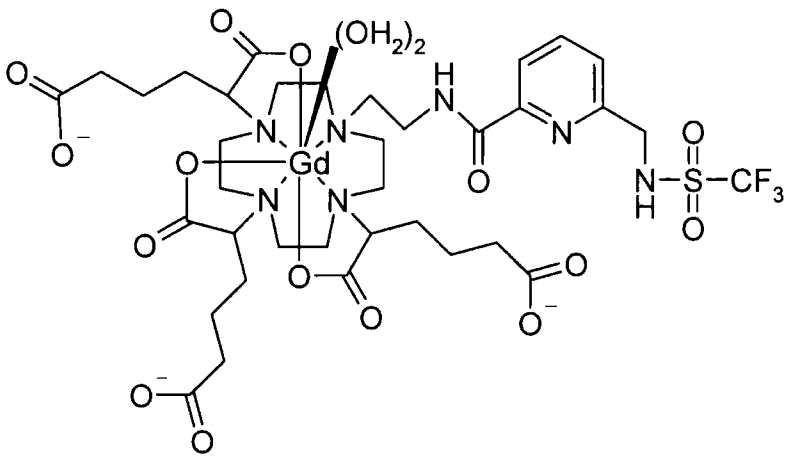

Gd($C_{42}H_{54}N_7O_{21}SF_3$) **[GdL^9]** r_{1p}: 13.40 $mM^{-1}s^{-1}$ (65 MHz, 22°C); 8.70 $mM^{-1}s^{-1}$ (60 MHz, 37°C).

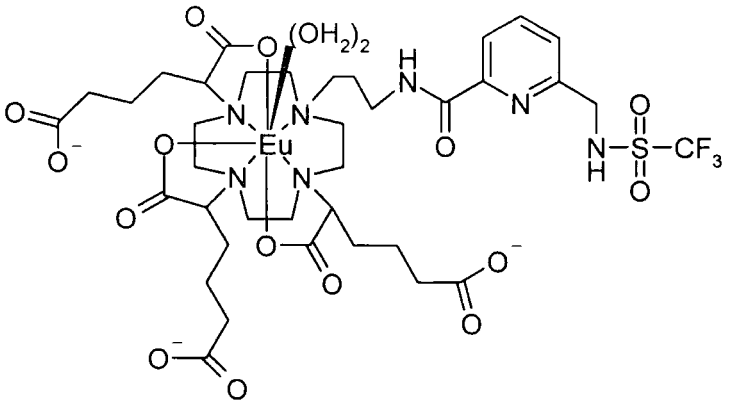

Eu($C_{43}H_{56}N_7O_{21}SF_3$) **[EuL^{10}]** ^{1}H NMR (500 MHz, D_2O): The spectrum was exchange broadened; ^{19}F NMR (500 MHz, D_2O): 77.35; k_{H_2O} 1.84 ms-1; k_{D_2O} 0.22 ms^{-1}; q = 1.65; $\lambda_{max}(H_2O)$ 271 nm (ε 4693 dm^{3}mol^{-1}cm^{-1}).

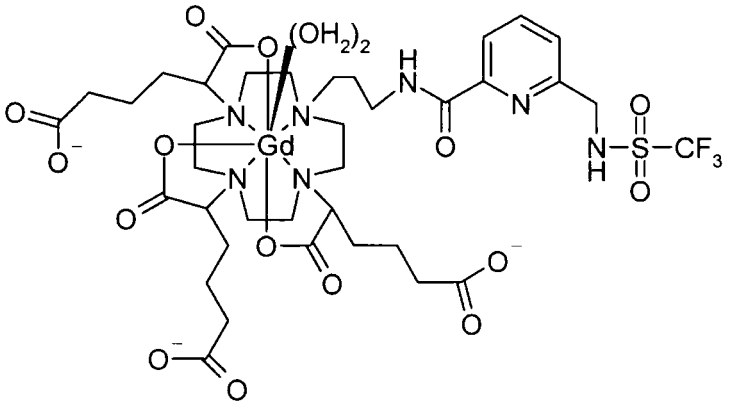

Gd($C_{43}H_{56}N_7O_{21}SF_3$) **[GdL^8]** r_{1p}: 19.9 mM^{-1}s^{-1} (65 MHz, 22°C); 13.63 mM^{-1}s^{-1} (60 MHz, 37°C).

6.7 Chapter 5 Experimental

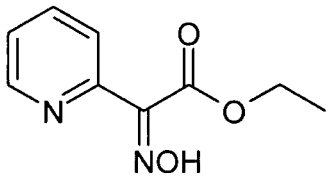

Ethyl 2-Hydroxyimino-2-(pyridyl-2')acetate **97**[147,148] A solution of sodium nitrite (0.96 g, 13.9 mmol) in water (2.42 ml) was added in portions over 30 minutes to a stirred solution of ethyl (2-pyridyl) acetate (2.00 g, 12.1 mmol) in glacial acetic acid (3 ml), cooled in an ice-bath. The reaction mixture was allowed to warm to room temperature and stirred for 40 minutes before water (7 ml) was added. The resulting two phase system was stirred at room temperature for two hours. The

organic and aqueous phases were separated, the organic phase was washed with water (20 ml) and the aqueous phase was washed with dichloromethane (20 ml). The combined organic phases were dried ($MgSO_4$), filtered and evaporated under reduced pressure to yield a yellow oil which crystallised on standing. The solid was recrystallised from methanol to yield a white crystalline solid (2.00 g, 85%), m.p. 130-132 °C (lit[147] m.p. 149-150°C); ^{1}H NMR (300 MHz, $CDCl_3$): δ_H 1.38 (3H, 2t, CH_3), 4.45 (2H, 2d, CH_2), 7.30 (m, Ar), 7.48 (t, Ar), 7.72 (m, Ar), 7.94 (td, Ar), 8.04 (d, *J 7.2,* Ar), 8.56 (d, *J 5.1,* Ar), 8.60 (d, *J 4.8,* Ar), 8.88 (broad s, OH); the compound appears to exist in two forms (E and Z isomers); ^{13}C NMR (65 MHz, $CDCl_3$): δ_C 14.10 (CH_3), 62.03 (CH_2), 123.79 (C5), 125.45 (C3), 138.46 (C4), 143.01 (q, C2), 145.23 (C6), 149.61 (C=N), 163.65 (C=O); (ES^+): 411 (48%, $2M+Na^+$), 216 (100%, MNa^+).

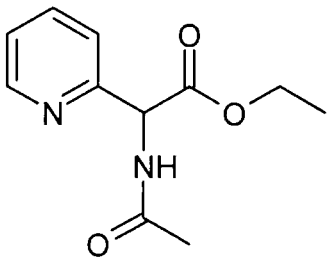

Ethyl N-acetyl-2-(pyridyl-2')glycinate **98** Following the method of Kolar *et al.*[156,157] for a related quinoline compound, zinc dust (1.472 g, 65.39 mmol) was added portion-wise to a clear colourless solution of **97** (965 mg, 192.89 mmol) in glacial acetic acid (15 ml) and acetic anhydride (5 ml). The resulting suspension was stirred at room temperature for two hours, diluted with ice-water (100 ml) and stirred for a further 40 minutes before being extracted with chloroform (3 x 100 ml). The combined organic extracts were washed with 5% aqueous sodium hydrogen carbonate solution (100 ml) and water (100 ml), dried ($MgSO_4$), filtered and solvent removed under reduced pressure to yield a yellow oil which was purified by column chromatography (SiO_2, EtOAc, R_f = 0.26), to yield a clear oil (0.441 g, 40%); ^{1}H NMR (200 MHz, $CDCl_3$): δ_H 1.20 (3H, t, MeCH$_2$), 2.09 (3H, s, MeC=O), 4.17 (2H, m, CH_2), 5.63 (1H, d, *J 7.2,* CH), 7.28 (2H, m, H5 + NH), 7.50 (1H, d, *J 7.8,* H3), 7.70 (1H, td, *J 7.6, 1.6,* H4), 8.53 (1H, d, *J 4.8,* H6); ^{13}C NMR (50.3 MHz, $CDCl_3$): δ_C 13.92 (Me CH_2), 22.86 (MeC=O), 57.36 (CH_2), 61.77 (CH), 123.26 (C5), 123.29 (C3),

137.07(C4), 149.10 (C6), 154.15 (q, C2), 169.71 (C=O), 169.88 (C=O); m/z (ES^+): 467 (100%, M_2Na^+), 245 (62%, MNa^+); $C_{11}H_{14}N_2O_3.{}^1/_5H_20$ requires C: 58.50%, H: 6.43%, N: 12.24%, found C: 58.42%, H 6.22%, N: 12.24%. Constitution confirmed by x-ray crystallography (03srv088): $C_{11}H_{14}$ N_2 O_3; formula weight 222.24 (gM^{-1}); T = 120(2) K; λ 0.71073 Å (Mo Kα); cystal system orthorhombic; space group Fdd2; Unit cell dimensions : a = 38.06(3) Å, α= 90°, b = 8.236(6) Å, β = 90°, c = 14.590(11) Å, γ = 90° ; Volume = 4573(6) $Å^3$; Z = 16 ; density (calculated) 1.291 Mg/m^3; crystal size 0.20 x 0.18 x 0.10 mm^3; theta range for data collection 2.14 to 23.29°; total number of reflections collected = 4772; independent reflections = 1472; [R(int) = 0.0878]; completeness to theta = 23.29°; 99.7 %; refinement method: full-matrix least-squares on F^2; data / restraints / parameters: 1472 / 1 / 145; final R indices [I>2sigma(I)]: R_1 = 0.0460, wR_2 = 0.0909; R indices (all data): R_1 = 0.0728, wR_2 = 0.0989.

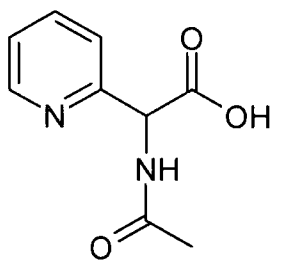

N-Acetyl-2-pyridylglycine **96** Sodium hydroxide solution (0.02M, 30 ml) was added to ethyl N-acetyl-2-(2'-pyridyl)glycinate **98** (100 mg, 0.45 mmol), the resulting solution was stirred at room temperature for 18 hours. The reaction mixture was neutralised to pH 7 using 0.1M HCl(aq). The water was removed by lyophilisation to yield as white solid. ^{1}H NMR (200 MHz, D_2O): δ_H 2.07 (3H, s, Me), 5.31 (1H, s, CH), 7.36 (1H, t, *J 5.6*, H5), 7.46 (1H, d, *J 7.8*, H3), 7.84 (1H, t, *J 7.6*, H4), 8.44 (1H, d, *J 4.8*, H6); ^{13}C NMR (50.3 MHz, $CDCl_3$): δ_C 22.86 (Me), 61.03 (CH), 123.28 (C5), 123.66 (C3), 138.57 (C4), 148.90 (C6), 156.98 (q, C2), 173.49 (C=O), 175.17 (C=O).

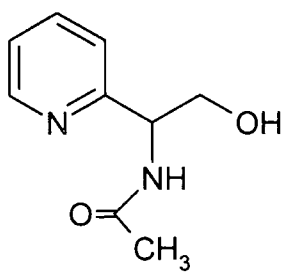

N-(2-Hydroxy-1-pyridin-2-yl-ethyl)-acetamide **99** following the proceedure of Gilbertson and Chang,[158] lithium borohydride (0.19 g, 18.0 mmol) was added in portions to a stirred solution of **98** (2.0 g, 9.0 mmol) in dry THF (80 ml) which was cooled in an ice bath. The resulting pink reaction mixture was allowed to warm gradually to room temperature; stirring was continued for a further 18 hours. The reaction was then quenched with 1M HCl (10 ml), neutralised with aqueous sodium hydrogen carbonate, and extracted with dichloromethane (3 x 70 ml). Then combined organic extracts were dried ($MgSO_4$) and concentrated under reduced pressure to give a white solid which was recrystallised from ethanol to give the desired product as a white crystalline solid (0.66 g, 41%). m.p. 112-114°C; R_f = 0.39 (SiO_2, 10% MeOH in DCM); ^{1}H NMR (200 MHz, $CDCl_3$): δ_H 2.06 (2H, s, CH_3), 3.91 (1H, dd, J_{BA} *4.5*, J_{BX} *11.3*, $CH_A\underline{H_B}OH$), 3.95 (1H, dd, J_{AB} *4.5*, J_{AX} *11.5*, $C\underline{H_A}H_BOH$), 4.91 (1H, m, $\underline{CH}CH_2$), 7.16 (1H, br s, NH), 7.25 (1H, t, *J 6.6*, H5), 7.37 (1H, d, *J 7.8*, H3), 7.71 (1H, t, *J 7.8*, H4), 8.51 (1H, d, *J 4.8*, H6); ^{13}C NMR (50.3 MHz, $CDCl_3$): δ_c 23.47 (CH_3), 54.76 (CH_2), 66.69 (CH), 123.12 (C3 or C5), 123.37 (C3 or C5), 137.42 (C4), 148.80 (C6), 158.57 (q, C2); *m/z* ES$^+$: 181.0 (100%, MH$^+$); $C_9H_{12}N_2O_2$ requires C: 59.99%, H: 6.71%, N: 15.33%, found C: 59.69%, H: 6.70%, N: 15.54%.

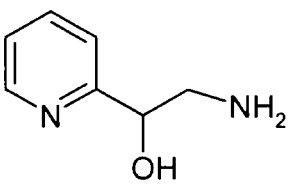

2-Amino-1-pyridin-2-yl-ethanol **100** A solution of **99** (0.300 g, 1.66 mmol) in 6M hydrochloric acid (15 ml) and heated under reflux for four hours. The solution was then allowed to cool to room temperature and the solvent was evaporated to yield the salt of the desired product as a yellow oil. ^{1}H NMR (300 MHz, D_2O): δ_H 3.98 (1H, dd, J_{BA} *4.8*, J_{BX} *12.4*, $CH_A\underline{H_B}OH$), 4.10 (1H, dd, J_{AB} *4.8*, J_{AX} *12.5*, $C\underline{H_A}H_BOH$), 4.91 (2H, t, *J 4.8*, $\underline{CH}CH_2$), 8.04 (1H, t, *J 6.6*, H5), 8.12 (1H, d, *J 8.1*, H3), 8.61 (1H, t, *J 8.1*, H4), 8.79 (1H, d, *J 6.3*, H6); ^{13}C NMR (75.4 MHz, D_2O): δ_c 52.95 (CH_2), 60.55 (CH), 126.00 (C3 or C5), 127.81 (C3 or C5), 142.60 (C4), 147.15 (q, C2), 148.10 (C6); *m/z* ES$^+$: 139.2 (100%, MH$^+$).

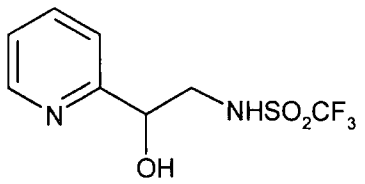

(±)-N-(2-Hydroxy-1-pyrindin-2-yl-ethyl)-triflurомethanesulfonamide **101** An aqueous solution of **100** (0.536 g, 3.88 mmol), was eluted through an OH^- loaded Amberlite anion exchange column, the solvent was then removed under reduced pressure. Under an atmosphere of argon, the resulting solid was dissolved in dry dichloromethane (9 ml) and Hünig's base (0.67 ml, 3.9 mmol) and the solution cooled to -40°C. Trifluoromethanesulfonyl chloride (0.41 ml, 3.9 mmol) was added and the reaction mixture was stirred at -40°C for one hour then warmed gradually to -20°C and held at this temperature for 18 hours, before being allowed to warm to room temperature. The solvent was removed under reduced pressure and the resulting oil was purified by flash column chromatography (SiO_2, EtOAc). The product was obtained as a pale yellow solid (0.826 g, 79%). R_f = 0.42 (SiO_2, EtOAc), m.p. 86 - 87°C; ^{1}H NMR (200 MHz, $CDCl_3$): δ_H 3.86 (1H, dd, J_{AB} *4.1*, J_{AX} *11.6*, $C\underline{H}_A H_B OH$), 3.91 (1H, dd, J_{BA} *4.2*, J_{BX} *11.7*, $CH_A\underline{H}_B OH$), 4.68 (2H, t, *J 4.0*, $\underline{CH}CH_2$), 7.54 (1H, t, *J 6.6*, H5), 7.61 (1H, d, *J 7.8*, H3), 8.08 (1H, t, *J 8.1*, H4), 8.47 (1H, d, *J 5.4*, H6); ^{13}C NMR (50.29 MHz, $CDCl_3$): δ_c 59.20 (CH_2), 65.71 (CH), 122.99 (C3 or C5), 123.88 (C3 or C5), 137.95 (C4), 149.12 (C6), 156.81 (q, C2); ^{19}F NMR (188 MHz, $CDCl_3$): δ_F -77.94 (s, CF_3); *m/z* ES^+: 624.6 (100%, $(M\text{-}H)_2Cu^+$), 292.9 (20%, MNa^+), 270.9 (5%, MH^+); (KBr)/cm^{-1} 3285 (ν OH), 1597 (ν py), 1375 (δ NH), 1229 (ν_a SO_2), 1192 (ν_s SO_2), 1147 (δ CH), 1074 (δ CH), 604 (γ NH); Found: C, 35.81; H, 3.40; N, 10.22. $C_8H_9N_2O_3F_3S$ requires C, 35.56; H, 3.35; N, 10.36.

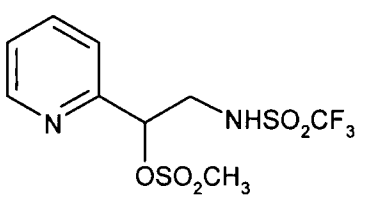

(±)-N-(2-Methanesulfoxy-1-pyrindin-2-yl-ethyl)-triflurомethanesulfonamide **104**
Methanesulfonyl chloride (21 mg, 0.18 mmol) was added to a solution of **101** (50 mg, 0.18 mmol) and triethylamine (0.026ml, 0.18 mmol) in dichloromethane (2 ml) which had been cooled with an ice bath. The reaction mixture was then

allowed to warm gradually to room temperature and was stirred for 4 hours. The formation of the mesylate was monitored by TLC; R_f = 0.57 (SiO_2, 10% MeOH in DCM). The product was not isolated but reacted on *in situ*.

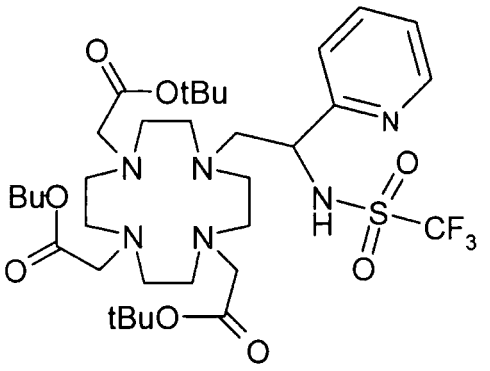

1,4,7-Tris-tert-butoxycarbonylmethyl-10-[(±)-N-(2-Hydroxy-1-pyrindin-2-yl-ethyl)-trifluromethanesulfonamide]-1,4,7,10tetraaza-cyclododecane **105** Under an argon atmosphere, a yellow solution of **104** in dichloromethane (2 ml) was added to a suspension of **48** (95 mg, 0.18 mmol) and caesium carbonate (301 mg, 0.92 mmol) in dry acetonitrile (3 ml). The resulting suspension was heated under reflux for 18 hours before being allowed to cool to room temperature. The reaction mixture was filtered to remove inorganic solids and washed thoroughly with dichloromethane. Flash column chromatography (SiO_2, gradient elution 2% MeOH in DCM → 15% MeOH in DCM) isolated the desired product as a pale brown oil (31 mg, 22%). R_f = 0.43 (SiO_2, 10% MeOH in DCM). ^{1}H NMR (300 MHz, $CDCl_3$): The aromatic region of the ^{1}H NMR suggests that this molecule exists in two different conformations in chloroform solution. 1.37 (18H, s, 2 *t*Bu), 1.44 (9H, s, *t*Bu), 1.98 - 3.61 (22H, br m, 11 CH_2), 6.99 (0.5H, d, *J* 7.5, H3), 7.07 (0.5H, t, *J* 6.0, H5), 7.18 (0.5H, t, *J* 6.0, H5), 7.35 (0.5H, d, *J* 7.8, H3), 7.60 (1H, m, H4), 8.40 (0.5H, d, *J* 3.6, H6), 8.45 (0.5H, d, *J* 3.6, H6); ^{13}C NMR (125 MHz, $CDCl_3$) δ_C: 27.71 ($C(\underline{CH_3})_3$), 29.61, (CH_2), 39.02 (CH_2), 43.33 (CH_2), 44.87 (CH_2), 45.35 (CH_2), 52.62 (CH_2), 53.22 (CH_2), 53.43 (CH_2), 56.71 (CH_2), 57.34 (CH_2), 57.79 (CH_2), 64.69 (CH), 86.69 ($\underline{C}(CH_3)_3$), 123.44 (C3), 124.48 (C5), 136.61 (C4), 149.33 (C6), 154.49 (q, C2), 175.54 (C=O), 176.25 (C=O), 176.66 (C=O); ^{19}F NMR (188 MHz, $CDCl_3$): δ_F -77.70 (s, CF_3); m/z (ES^+): 805.3 (100%, MCa^+); Acc.MS (ES^+): Found 805.3524, $C_{34}H_{56}N_6O_8SF_3Ca$ requires 805.3458.

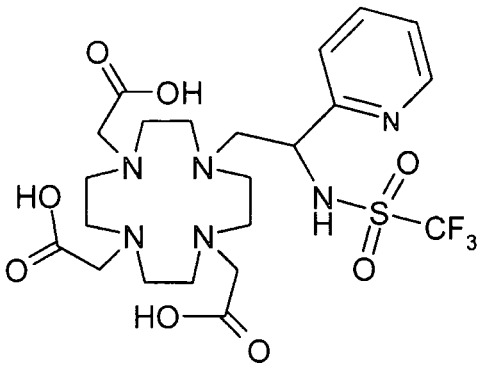

1,4,7-Tris-carboxymethyl-10-[(±)-N-(2-Hydroxy-1-pyrindin-2-yl-ethyl) trifluromethane sulfonamide]-1,4,7,10tetraaza-cyclododecane $\mathbf{L^{12}}$ Under an argon atmosphere, a solution of **105** (31 mg, 0.04 mmol) in trifluoroacetic acid (1 ml) was left standing for 48 hours. The solvent was then removed under reduced pressure. The resulting solid was washed with dichloromethane (3 x 2 ml) and the solvent removed under reduced pressure to give a pale yellow oil. ^{1}H NMR (300 MHz, D_2O): 1.98 - 3.61 (22H, br m, 11 CH_2), 7.65 (0.5H, br , H3), 7.95 (0.5H, m, H5), 8.06 (0.5H, m, H5), 8.26 (0.5H, d, *J 7.8,* H3), 8.59 (1H, m, H4), 8.74 (0.5H, d, *J 6.0,* H6), 8.83 (0.5H, d, *J 5.1,* H6); ^{19}F NMR (282 MHz, D_2O): δ_F -76.10 (s, CF_3); m/z (ES^+): 657.1 (36%, $MNaCa^+$), 317.3 (100%, MCa^{2+}).

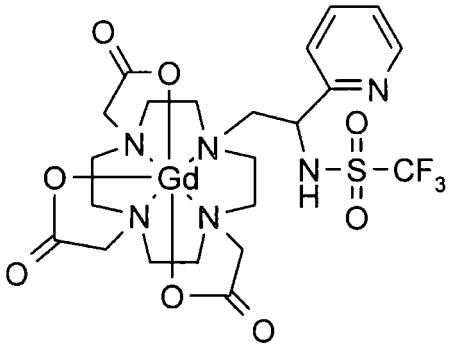

Gd($C_{22}H_{30}N_6O_8SF_3$) **[GdL^{12}]** An aqueous solution (2 ml) containing $\mathbf{L^{11}}$ (26 µmol) and gadolinium chloride hexahydrate (10 mg, 26 µmol) was adjusted to pH 5.5 using 1M NaOH solution and heated at 90°C for 18 hours. After the solution was cooled, the pH was raised to 10 and the solution was filtered to remove excess gadolinium as $Gd(OH)_3$. The pH was then lowered to 5.5 and the solution lyophilised to give the complex as a white powder. m/z (ES^-): 751.5 (100%, $[M-H]^-$); Acc.MS (ES^-): Found 752.0969, $C_{22}H_{29}N_6O_8\ SF_3Gd$ requires 752.0966; r_{1p} (60 MHz, 37°C): 2.67 $mM^{-1}s^{-1}$; r_{1p} (65 MHz, 22°C): 3.73 $mM^{-1}s^{-1}$.

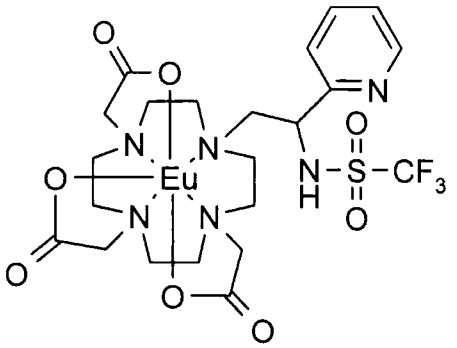

Eu($C_{22}H_{30}N_6O_8SF_3$) **[EuL^{12}]** An aqueous solution (2 ml) containing **L**^{11} (13 μmol) and europium chloride hexahydrate (5 mg, 13 μmol) was adjusted to pH 5.5 using 1M NaOH solution and heated at 90°C for 18 hours. After the solution was cooled, the pH was raised to 10 and the solution was filtered to remove excess europium as $Eu(OH)_3$. The pH was then lowered to 5.5 and the solution lyophilised to give the desired complex as a white powder. ^{1}H NMR (200 MHz, D_2O): shows that at least three isomers were present; the peaks were characteristic of a major (A) and a minor (B) square antiprism (SAP) conformation and a minor (C) twisted square antiprism (TSAP) in a ratio of 21 : 4 : 9. Partial assignment 35.1 (1H, s, H_{ax}, B), 34.2 (1H, s, H_{ax}, B), 32.9 (1H, s, H_{ax}, A), 30.8 (1H, s, H_{ax}, A), 29.5 (1H, s, H_{ax}, B), 27.1 (1H, s, H_{ax}, B), 26.4 (1H, s, H_{ax}, A), 23.2 (1H, s, H_{ax}, C), 22.6 (1H, s, H_{ax}, C), 22.3 (1H, s, H_{ax}, C), 19.8 (1H, s, H_{ax}, C), 14.0 (1H, s, H_{ax}, A), 12.9 (1H, s, H_{ax}, B), the remaining resonances span 11.8 to - 20.2ppm; ^{19}F NMR (188 MHz, D_2O): δ_F -76.03 (s, CF_3); m/z (ES^-): 746.6 (48%, $[M-H]^-$); Acc.MS (ES^-): Found 747.0942, $C_{22}H_{29}N_6O_8SF_3Eu$ requires 747.0937; k_{H_2O} (λ_{ex} 262 nm, λ_{em} 616 nm): 1.35 ms^{-1}; k_{D_2O}: 0.53 ms^{-1}; q_{Eu} = 0.7.

References

1 L. Stryer, Biochemistry, W.H. Freeman and Company, New York, 1995.

2 L. Prodi, F. Bolletta, M. Montalti, N. Zaccheroni, *Coordination Chemistry Reviews*, 2000, **205**, 59 - 83.

3 W. Kaim, B. Schwederski, *Bioinorganic Chemistry: Inorganic Elements in the Chemistry of Life. An Introduction and Guide*, John Wiley and Sons, Chichester, 1994.

4 J. M. Berg, Y. Shi, *Science*, 1996, **271**, 1081 - 1085.

5 R. W. Hay, *Bioinorganic Chemistry*, Ellis Horwood, Chichester, 1984.

6 C. J. Fahrni, T. V. O'Halloran, *J. Am. Chem. Soc.*, 1999, **121**, 11448 - 11458.

7 M.C. Kimber, I.B. Mahadevan, S.F. Lincoln, A.D. Ward, E.R.T. Tiekink, *J. Org. Chem.*, 2000, **65**, 8204 - 8209.

8 C.E. Outten and T. V. O'Halloran, *Science*, 2001, **292**, 2488 - 2491.

9 C. J. Fahrni, K. D. Simon, D. A. Suhy, M. S. Nasir, R. Dwivedi, T. V. O'Halloran, *J. Inorg. Biochem.*, 1999, **74**, 125 - 125.

10 G. K. Walkup, S. C. Burdette, S. J. Lippard, R. Y. Tsien, *J. Am. Chem. Soc.*, 2000, **122**, 5644 - 645.

11 J. J. R. Frausto da Silva, R. J. P. Williams, *The Biological Chemistry of the Elements*, Clarendon Press, Oxford, 1994, 299 - 318.

12 H. Haase, D. Beyersmann, *Biometals*, 1999, **12**, 247 - 254.

13 T. Koike, T. Watanabe, S. Aoki, E. Kimura, M. Shiro, *J. Am. Chem. Soc.*, 1996, **118**, 12696 - 2703.

14 S.C. Burdette, S.J. Lippard, *Coordination Chemistry Reviews*, 2001, **216-217**, 333 - 361.

15 T. Budde, A. Minta, J. A. White, A. R. Kay, *Neuroscience*, 1997, **79** (2), 347 - 358.

16 D. Bryce-Smith, *Chemistry in Britiain*, 1989, 783 - 786.

17 D.W. Choi, J.Y. Koh, *Ann. Rev. Neurosci.*, 1998, **21,** 347 - 375.

18 F. A. Cotton, G. Wilkinson, *Advanced Inorganic Chemistry, 5th Edition,* John Wiley and Sons, New York, 1988.

19 R. D. Shannon, *Acta Cryst* **AC32**, 1976, 751 - 767

20 D. F. Shriver, P. W. Atkins, C. H. Langford, *Inorganic Chemistry 2nd Edition,* Oxford University Press, Oxford, 1994.

21 H. M. N. H. Irving, R. J. P. Williams, *J. Chem. Soc.*, 1953, 3192 - 3210.

22 G. B. Bates, *Synthesis of Tetrahedrally Coordinating Ligands,* Ph. D. Thesis, University of Durham, 1995.

23 T. Koike, T. Watanabe, S. Aoki, E. Kimura, M. Shiro, *J. Am. Chem. Soc.*, 1996, **118**, 12696 - 12703.

24 C. J. Fahrni, T. V. O'Halloran, *J. Am. Chem. Soc.*, 1999, **121**, 11448 - 11458.

25 A.P. de Silva, H.Q.N. Gunaratne, T. Gunnlaugsson, A.J.M. Huxley, C.P. McCoy, J.T. Rademacher, T.E. Rice, *Chem. Rev.*, 1997, **97**, 1515 - 1566.

26 D. Parker, J.A.G.Williams, *Metal Ions in Biological Systems, Volume 40, The Lanthanides and their Interactions,* Eds. A. Sigel, H. Sigel, Marcel Dekker Inc., New York, Basel, 2003.

27 J.R. Lakowicz, *Principles of Fluorescence Spectroscopy,* 2nd Edition, Kluwer Academic/ Plenum Publishers, New York, 1999.

28 T. Koike, E. Kimura, I. Nakamura, Y. Hashimoto, M. Shiro, *J. Am. Chem. Soc.*, 1992, **114,** 7338 - 7345.

29 T. Koike, T. Abe, M. Takahashi, K. Ohtani, E. Kimura, M. Shiro, *J. Chem. Soc., Dalton Trans.*, 2002, 1764- 1768.

30 S. Aoki, H. Kawatani, T. Goto, E. Kimura, M. Shiro, *J. Am. Chem. Soc.*, 2001, **123**, 1123 - 1132.

31 T. Hirano, K. Kikuchi, Y. Urano, T. Higuchi, T. Nagano, *Angew. Chem. Int. Ed.* 2000, **39** (6), 1052 - 1054.

32 C. Sauden, V. Balzeni, M. Gorka, S. Lee, M. Maetri, V. Vicinelli, F. Vögtle, *J. Am. Chem. Soc.*, 2003, **125,** 4424 - 4425.

33 S.C. Burdette, S.J. Lippard, *PNAS,* 2003, **100,** (7), 3605 - 3610.

34 S. C. Burdette, C.J. Frederickson, W. Bu, S. J. Lippard, *J. Am. Chem. Soc.,* 2003, **125,** 1778 - 1787.

35 S.C. Burdette, S.J. Lippard, *PNAS,* 2003, **100,** (7), 3605 - 3610.

36 T. Hirano, K. Kikuchi, Y. Urano, T. Nango, *J. Am. Chem. Soc.,* 2002, **124,** 6555 - 6562.

37 T. Hirano, K. Kikuchi, Y. Urano, T. Higuchi, T. Nango, *J. Am. Chem. Soc.,* 2000, **122,** 12399 - 12400.

38 K.R. Gee, Z.L. Zhou, W.J. Qian, R. Kennedy, *J. Am. Chem. Soc.,* 2002, **124,** 776 - 778.

39 T. Gunnlaugsson, T.C. Lee, R. Parkesh, *Org. Biomol. Chem.,* 2003, **1,** 3265 - 3267.

40 S. Maruyama, K. Kikuchi, T. Hirano, Y. Urano, T. Nango, *J. Am. Chem. Soc.,* 2002, **124,** 10650 - 10651.

41 W. Goodall, J.A.G. Williams, *Chem. Commun.,* 2001, 2514 - 2515.

42 C.J.Frederickson, E.J. Kasarkis, D. Ringo, R.E. Frederickson, *J. Neurosci. Methods,* 1987, **20,** 91 - 103.

43 D.A. Pierce, N. Jotterand, I.S. Carrico, B. Imperiali, *J. Am. Chem. Soc.,* 2001, **123,** 5160 - 5161.

44 M.C. Kimber, I.B. Mahadevan, S.F. Lincoln, A.D. Ward, W.H. Betts, *Aust. J. Chem.* 2001, **54,** 43 - 49.

45 S.P. Creaser, S.M. Pyke, S.F. Lincoln, *Aus. J. Chem.,* 2003, **56,** 61- 64.

46 M. Ghedini, M. La Deda, I. Aiello, A. Grisolia, *J. Chem. Soc., Dalton Trans.,* 2002, 3406 - 3409.

47 L.S. Sapochak, F.E. Benincasa, R.S. Schofield, J.L. Baker, K.K.C. Ricco, D. Fogarty, H. Kohlmann, K.F. Ferris, P.E. Burrows, *J. Am. Chem. Soc.,* 2002, **124,** 6119 - 6125.

48 P. D. Zalewski, S. H. Millard, I. J. Forbes, O. Kapaniris, A. Slavotinek, W. H. Betts, A. D. Ward, S. F. Lincoln, *J. Histochem Cytochem.,* 1994, **42,** 877 – 888.

49 M. S. Nasir, C. J. Fahrni, D. A. Suhy, K. J. Kolodsick, C. P. Singer, T. V. O'Halloran, *JBIC*, 1999, **4**, 775 - 783.

50 S.C. Burdette, S.J. Lippard, *Coordination Chemistry Reviews*, 2001, **216-217**, 333 - 361.

51 G. K. Walkup, B. Imperiali, *J. Org. Chem.* 1998, **63**, 6727 - 6731.

52 G. K. Walkup, B. Imperiali, *J. Am. Chem. Soc.*, 1997, **119**, 3443 - 3450.

53 G.K. Walkup, B. Imperiali, *J. Am. Chem. Soc.*, 1996, **118**, 3052 - 3054.

54 D.M. Shults, D.A. Pearce, B. Imperiali, *J. Am. Chem. Soc.*,2003, **125** (35), 10591 - 10597.

55 H. A. Godwin, J. M. Berg, *J. Am. Chem. Soc.*, 1996, **118**, 6514 - 6515.

56 D.P. Barondeau, C.J. Kassmann, J.A. Tainer, E.D. Getzoff, *J. Am. Chem. Soc.*, 2002, **124**, 3522 - 3524.

57 R.B. Thompson, D. Peterson, W. Mahoney, M. Cramer, B.P. Maliwal, S.W. Suh, C. Frederickson, C. Fierke, P. Herman. *Journal of Neuroscience Methods*, 2002, **118**, 63 - 75.

58 D. Parker, *Coordination Chemistry Reviews*, 2000, **205**, 109 - 130.

59 G. Bobba, Interaction of Chiral Lanthanide Complexes with Nucleic Acids, Ph. D. Thesis, University of Durham, 2002.

60 D. Parker, J.A.G. Williams, *J. Chem. Soc., Dalton Trans.*, 1996, 3613 - 3628.

61 A. Beeby, I.M. Clarkson, R.S. Dickins, S. Faulkner, D. Parker, L. Royle, A.S. de Sousa, J.A.G. Williams, M. Woods, *J. Chem. Soc, Perkin Trans. 2.*, **1999**, 493 - 503.

62 D. Parker, R.S. Dickins, H. Puschmann, C. Crossland, J.A. K. Howard, *Chem. Rev.*, 2002, **102**, 1977 - 2010

63 M.P. Lowe, D. Parker, O. Reany, S. Aime, M. Botta, G. Castellano, E. Gianolio, R. Pagliarin, *J. Am. Chem. Soc.*, 2001, **123**, 7601-7609.

64 J.I. Bruce, R.S. Dickins, L.J. Glovenlock, T. Gunnlaugsson, S. Lopinski, M.P. Lowe, D. Parker, R.D. Peacock, J.J.B. Perry, S. Aime, M. Botta, *J. Am. Chem. Soc.*, 2000, **122**, 9674 - 9684.

65 Y. Bretonniére, M.J. Cann, D. Parker, R. Slater, *Chem. Commun.*, 2002, 1930 - 1931.

66 M. J. Abrams, B. A. Murrer, *Science*, 1993, **261**, 725 - 730

67 D. Parker, *Comprehensive Supramolecular Chemistry*, Eds. J.L. Atwood, J.E.D. Davies, F. Vogtle, D.D. MacNicol, Pergamon Press, 1996, **10**, 509 - 535.

68 M.P. Lowe, *Aust. J. Chem.*, 2002, **55**, 551 - 556.

69 A.E. Merbach, E. Tóth, *The Chemistry of Contrast Agents in Medical Magnetic Resonance Imaging;* Wiley: New York, 2001.

70 D. Parker, J.A.G. Williams, *J. Chem. Soc., Dalton Trans.*, **1996**, 3613 - 3628.

71 M. Botta, *Eur. J. Inorg. Chem.* 2000, 399 - 401.

72 I. Solomon, *Phys. Rev.*, 1955, **99**, (2), 559 - 565.

73 N. Bloembergen, *J. Chem. Phys.*, 1957, **27**, 572 - 573.

74 N. Bloembergen, L.O. Morgan, *J. Chem. Phys.*, 1961, **34**, 842 - 850.

75 J.H. Freed, *J. Chem. Phys.*, 1978, **68**, 4034 - 4037.

76 S. Aime, A. Barge, M. Botta, J.A.K. Howard, R. Kataky, M.P. Lowe, J.M. Moloney, D. Parker, A.S. de Sousa, *Chem. Commun.*, 1999, 1047 - 1048.

77 M.P. Lowe, D. Parker, *Chem. Commun.*, 2000, 707 - 708.

78 M.P. Lowe, D. Parker, *Inorganica Chimica Acta.*, 2001, **317**, 163 - 173.

79 S. Zhang, K. Wu, A.D. Sherry, *Angew. Chem., Int Ed.*, 1999, **38**, 3192 - 3194.

80 S. Aime, M. Botta, S. G. Crich, G. Giovenzana, G. Palmisano, M. Sisti, *Chem. Comm.*, 1999, 1577 - 1578.

81 R. Hovland, C. Glogård, A.J. Aasen, J. Klaveness, *J. Chem. Soc., Perkin Trans. 2.*, 2001, 929 - 933.

82 W.Li, G. Parigi, M. Fragai, C. Luchinat, and T.J. Meade; *Inorg. Chem.*, 2002, **41**, 4018 - 4024.

83 W. Li, S.E. Fraser, and T.J. Meade, *J. Am. Chem. Soc.*, 1999, **121**, 1413 - 1414.

84 K. Hanaoka, K. Kikuchi, Y. Urano, T. Nagano, *J. Chem. Soc., Perkin Trans. 2*, 2001, 1840 - 1843.

85 S. Aime, M. Botta, E. Gianolio, E. Terreno, *Angew. Chem. Int. Ed.*, 2000, **39**, 747 - 750.

86 S. Seibig, E. Tóth, A.E. Merbach, *J. Am. Chem. Soc.*, 2000, **122**, 5822 - 5830.

87 L. Burai, E. Tóth, S. Seibig, R. Scopelliti, A.E. Merbach, *Chem. Eur. J.*, 2000, **6**, 3761 - 3770.

88 R.A. Moats, S.E. Fraser, T.J. Meade, *Angew. Chem., Int. Ed.*, 1997, **36**, 726 - 728.

89 A.L. Nivorozhkin, A.F. Kolodziej, P. Caravan, M.T. Greenfield, R.B. Lauffer, T.J. McMurry, *Angew. Chem. Int. Ed.*, 2001, **40**, 2903 - 2906.

90 L.M. De Leon-Rodriguez, A. Ortiz, A.L. Weiner, S. Zhang, Z. Kovacs, T. Kodadek, A.D. Sherry, *J. Am. Chem. Soc.*, 2002, **124**, 3514 - 3515.

91 R.S. Dickins, T. Gunnlaugsson, D. Parker, R.D. Peacock, *Chem. Comm.*, 1998, 1643 - 1644.

92 P. Caravan, J.J. Ellison, T.J. McMurry, R.B. Lauffer, *Chem. Rev.*, 1999, **99**, 2293 - 2352.

93 D. Messeri, M.P. Lowe, D. Parker , M. Botta, *Chem. Commun.*, 2001, 2742 - 2743.

94 D.M. Corsi, L. Vander Elst, R.N. Muller, H. van Bekkum, J.A. Peters, *Chem. Eur. J.*, 2001, **7**, 64 - 71.

95 S. Aime, M. Botta, S.G. Crich, G. Giovenzana, G. Palmisano, M. Sisti, *Bioconjugate Chem.* 1999, **10**, 192 - 199.

96 E. Tóth, D. Pubanz, S. Vauthey, L. Helm, A.E. Merbach, *Chem. Eur. J.*, 1996, **2**, 1607 - 1610.

97 P. Caravan, N.J. Cloutier, M.T. Greenfield, S.A. McDermid, S.U. Dunham, J.W.M. Bulte, J.C. Amedio, R.J. Looby, R.M. Supkowski, W.D. Horrocks, T.J. McMurry, *J. Am. Chem. Soc.*, 2002, **124** (12): 3152 - 3162.

98 O. Reany, T. Gunnlaugsson, D. Parker, *J. Chem. Soc. Perkin Trans. 2*, 2000, 1119 – 1131.

99 O. Reany, T. Gunnlaugsson, D. Parker, *Chem.Commun.*, 2000, 473 - 474.

100 K. Hanaoka, K. Kikuchi, H. Kojima, Y. Urano, T. Nagano, *Angew. Chem. Int. Ed.*, 2003, **42**, 2996 - 2999.

101 B. Nyasse, L. Grehn, U. Ragnarsson, H.L.S. Maia, L.S. Moneiro, I. Leito, I. Koppel, J. Koppel, *J. Chem. Soc., Perkin Trans. 1,* 1995, 2025 - 2031.

102 K. Hakansson, A Liljas, *FEBS Lett.,* 1994, 350, 319 - 322.

103 *Anal. Chem.,* 1974, **46**, 692.

104 O. Fuentes, W. W. Paudler, *J. Org. Chem.,* 1975, **40** (9), 1210 - 1213.

105 Goodwin, F. Lions, *J. Am. Chem. Soc.,* 1959, **81,** 6415 - 6422.

106 SHELXTL version 6.12, Bruker AXS, Madison, Wisconsin, USA, 2001.

107 L. Gutierrez, G. Alzuet, J. A. Real, J. Cano, J. Borras, A. Castineiras, C. T. Supuran, *Inorg. Chem.,* 2000, **39**, 3608 - 3614.

108 L. Gutierrez, G. Alzuet, J. Borras, M. Liu-Gonzalez, F. Sanz, A. Castineiras, *Polyhedron,* 2001, **20**, 703 - 709.

109 F.H. Allen, O. Kennard, *Chem. Des. Autom. News,* 1993, **8**, 30.

110 S. E. Denmark, S. P. O'Connor, S. R. Wilson, *Angew. Chem., Int. Ed.,* 1998, **37**, 1149 - 1151.

111 S. Z. Haider, K. M. A. Malik, M. B. Hursthouse, S. Das, *Acta Crystallogr., Sect. C,* 1984, **40**, 1147 - 1150.

112 U. Hartmann, H. Vahrenkamp, *Z. Naturforsch. B.,* 1994, **49**, 1725 - 1729.

113 S. L. Sumalan, J. Casanova, G. Alzuet, J. Borras, A. Castineiras, C. T. Supuran, *J. Inorg. Biochem.,* 1996, **62**, 31 - 39.

114 N.N. Greenwood, A. Earnshaw. Chemistry of the Elements, second edition, 1997, Butterworth-Heinemann, Oxford.

115 C. H. Hamann, A. Hamnet, W. Vielstich, *Electrochemistry 2nd Edition,* Wiley - VCH, 1998

116 A. H. Alberts, J. M. Lehn, D. Parker, *J. Chem. Soc. Dalton Trans.,* 1985, 2311 - 2317.

117 S. Rondini, P. R. Mussini, T. Mussini, *Pure Appl. Chem.,* 1987, **59,** 1549 - 1560.

118 P. Gans, A. Sabbatini, A. Vacca, *Talanta,* 1996, **43,** 1739 - 1753.

119 L. Alderighi, P. Gans, A. Ienco, D. Peters, A. Sabbatini, A. Vacca, *Coord. Chem. Rev.*, 1999, **184**, 311 - 318.

120 P. Gans, A. Sabbatini, A. Vacca, *J. Chem. Soc., Dalton Trans.*, 1985, 1195 - 1200.

121 K. Hakansson, A. Liljas, *FEBS Lett.*, 1994, **350**, 319 - 322.

122 B. Nyasse, L. Grehn, U. Ragnarsson, H. L. S. Maia, L. S. Monteiro, I. Leito, I. Koppel, J. Koppel, *J. Chem. Soc., Perkin Trans. 1*, 1995, 2025 - 2031.

123 A. Beeby, I.M. Clarkson, R.S. Dickins, S. Faulkner, D. Parker, L. Royle, A.S. de Sousa, J.A.G. Williams, M. Woods, *J. Chem. Soc, Perkin Trans. 2.*, 1999, 493 - 503.

124 J.G. Kang, M.K. Na, S.K. Yoon, *Inorg. Chim. Acta.*, 2000, **310**, (1), 56 - 64.

125 J.I. Bruce, R.S. Dickins, D. Parker, D.J. Tozer, *Dalton Trans.*, 2003, 1264 - 1271.

126 J.C.G. Bunzli, *Lanthanide Probes in Life, Chemical and Earth Sciences*, Eds. J.C.G. Bunzli, G.R. Choppin, Elsevier, Amsterdam, 1989.

127 S. Aime, A.S. Batsanov, M. Botta, J.A.K. Howard, D. Parker, K. Senanayake, J.A.G. Williams, *Inorg. Chem.* 1994, **33**, 4696 - 4706.

128 S. Aime, M. Botta, D. Parker, J.A.G. Williams, *J. Chem. Soc, Dalton Trans.*, 1995, 2259 - 2266.

129 S. Aime, M. Botta, D. Parker, J.A.G. Williams, *J. Chem. Soc, Dalton Trans.*, 1996, 17 - 23.

130 S. Aime, M. Botta, M. Fasano, E. Terreno, *Chem.Soc. Rev.*, 1998, **27**, 19 - 29.

131 S. Loms, R. Ruloff, E. Tòth, A.E. Merbach, *Chem. Eur. J.*, 2003, **9**, 3555 - 3556.

132 L. Burai, R. Scopelliti, E. Tòth, *Chem. Comm.*, 2002, 2366 - 2367.

133 R. Ruloff, E. Tòth, R. Scopelliti, R. Tripier, H. Handel, A.E. Merbach, *Chem. Comm.*, 2002, 2630 - 2631.

134 D.Parker, J.M. Lehn, J. Rimmer, *J. Chem. Soc.*, 1985, 1517 - 1521.

135 S. Aime, E. Gianolio, E. Terrano, G.B. Giovenzana, R. Pagliarin, M. Sisti, G. Palmisano, M. Botta, M.P. Lowe, D. Parker, *J. Biol. Inorg. Chem.*, 2000, **5**, 488 - 497.

136 Y. Bretonniére, 'Chimie de coordination des ions lanthanides (III) avec des ligands tripodes azotés et oxygénés' 2001, Université Joseph Fourier, Grenoble (France).

137 S. Saito, H. Nakajima, M. Inaba and T. Moriwake *Tet. Lett.* 1989, **30** (7), 837 - 838.

138 S. Aime, E. Gianolio, E. Terreno, G.B. Giovenzana, R. Pagliarin, M. Sisti, G. Palmisano, M. Botta, M.P. Lowe, D. Parker, *JBIC,* 2000, 488 - 497.

139 A.J. Stewart, C.A. Blindauer, S. Berezenko, D. Sleep, P.J. Sadler, *PNAS,* 2003, **100**, (7), 3701 - 3706.

140 J. Masuoka, J. Hegenauer, B.R. Van Dyke, P. Saltman, *J. Biol. Chem.,* 1993, **268**, (29), 21533 - 21537.

141 P. Caravan, C. Comuzzi, W. Crooks, T.J. McMurry, G.R. Choppin, S.R. Woulfe, *Inorg. Chem.,* 2001, **40**, 2170 - 2176.

142 D. Messeri, Ph. D. Thesis, Targeted and High Relaxivity Contrast Agents, University of Durham, 2002.

143 C.A. Hunter and D.H. Purvis, *Angew. Chem. Int. Ed.* 1992, **31**, (6), 792 - 795.

144 A. R. Battersby, M. Nicoletti, J. Staunton, R. Vieggaar, *J. Chem. Soc. Perkin Trans 1.* 1980, **1**, 43 - 51.

145 M. Viscontini, H. Raschig, *Helvetica Chimica Acta,* 1959, **62**, 570 - 577.

146 C. Herdeis, R. Gebhard, *Heterocycles,* 1986, **24** (4), 1019 - 1024.

147 G. Van Zyl, D. L. DeVries, R. H. Decker, E. T. Niles, 1961, **26**, 3373 - 3375.

148 P. Kolar, M. Tišler, *J. Heterocyclic Chem.,* 1993, **30**, 1253 - 1260.

149 S. Aime, A.S. Batsanov, M. Botta, J.A.K. Howard, M.P. Lowe, D. Parker, *New J. Chem.,* 1999, **23**, 669 - 670.

150 D. Maffeo, J.A.G. Williams, *Inorganica Chimica Acta,* article in press.

151 S. Quici, G. Marzanni, M. Cavazzini, P.L. Anelli, M. Botta, E. Gianolio, G. Accorsi, N. Armaroli, F. Barigelletti, *Inorg. Chem.,* 2002, 41, 2777 - 2784.

152 J. Leonard, B. Lygo, G. Proctor, *Advanced Practical Organic Synthesis, 2nd Edition,* Blackie Academic and Professional, 1995, Glasgow.

153 G.B. Bates, E. Cole, R. Kataky, D. Parker, *J. Chem. Soc., Dalton Trans.,* 1996, 2693 - 2698.

154 G.B. Bates, D. Parker, *J. Chem. Soc., Perkin Trans. 2,* 1996, 1109 - 1115.

155 A. Dadabhoy, S. Faulkner, P.G. Sammes, *Perkin Trans. 2.,* 2002, 348 - 357.

156 P. Kolar, M. Tišler, *J. Heterocyclic Chem.,* 1995, **32**, 141 – 143.

157 P. Kolar, A. Petrič, M. Tišler, *J. Heterocyclic Chem.,* 1991, **28**, 1715 – 1720.

158 S.R. Gilbertson and C.T. Chang, *J. Org. Chem.,* 1998, **63**, 8424 - 8431.

Appendix

Lecture Courses Attended 2000/2001

Separation Methods
Practical Spectroscopy

Conferences Attended

RSC Perkin Group Meeting. University of Durham. 5th May 2002.

RSC UK Macrocycles and Supramolecular Chemistry Group Meeting. University of Birmingham. 19 - 20th December 2001.*

ICCC35. XXXVth International Conference on Coordination Chemistry. Heidelberg. July 21 - 26th 2002.*

RSC Dalton Division. Coordination Chemistry in Action. University of Edinburgh. 6th November 2002.

UK Macrocyclic and Supramolecular Group. University of York. 18 - 19th December 2002.

RSC Perkin Group Meeting. University of York. 8th April 2002.

Biomolecular Probes Mini-Symposium. University of Durham. 16th January 2003.

* Poster presented

Seminars Attended

2000

October 11	Dr Victor Christou, ICL, Oxford University Recent Developments in Organic LED Technology: Organolanthanide Phosphors
October 25	Dr S.F. Campbell, Former Senior Vice President of Pfizer Science, art and drug discovery. A personal perspective
October 31	Dr V. McKee, Loughborough University

Polymetallic arrays - Controlling assembly and communicating restraints

November 7 Dr C. Ludman, Durham University
Explosions - A demonstration lecture

November 8 J.P.L. Cox, Bath University
Cosmic: a universal, DNA-based language for communicating with aliens and other intelligent lifeforms

November 22 Dr Wayne Hayes, University of Reading
Synthesis of Novel Dendrimers and Hyperbranched Polymers

November 29 Professor T. George Truscott, University of Keele
Life, Death and the Carotenoids

December 5 Dr D. Kelly, Cardiff University
The chemistry of sexual attraction

December 6 Professor Richard Compton, University of Oxford
Dual activation approaches to electroanalysis: ultrasound, microwaves and laser activation

2001

January 10 Professor S. P. Armes, School of Chemistry, Physics and Environmental Science, University of Sussex
Micelles, reversed micelles and shell-crosslinked micelles based on tertiary amine methacrylates

January 23 Professor C. Sterling, Sheffield University
Why should the public bother with science anyway?

January 24 Dr Andrew deMello, Department of Chemistry, Imperial College, London
Chemical Integrated Circuits: organic synthesis and analysis on a small scale

January 31 Dr Paul Wright, University of St Andrews
Making Space for Molecules: Designed Synthesis of Novel Molecular Sieves

February 13	Professor D. Leigh, Warwick University Tooling up for the nanoworld - The race for molecular machinery
February 15	Prof. Christopher Brett, University of Coimbra, Portugal New materials and strategies for electroanalytical sensing of biotoxic metals
February 21	Professor Rob Richardson Department of Physics, University of Bristol Liquid Crystals of All Shapes and Sizes
February 27	G. Ferry Dorothy Hodgkin - A woman's life in science
March 14	Dr Dave Keen, ISIS Facility Rutherford Appleton Laboratory Probing structural disorder with diffuse neutron scattering
March 28	Dr. John P. Richard, University of Buffalo, N.Y. Proton Transfer in Water and at Enzymes
May 2	Professor Robin Perutz, Department of Chemistry, University of York Escapades with Arenes and Transition Metals: from Laser Spectroscopy to Synthetic Applications
May 2	Dr. AWG Platt, University of Staffordshire Transition Metal Complexes of Alkylsufonated phosphines and their Antitumor Properties
May 9	Professor Rabindranath Mukherjee, Department of Chemistry, Indian Institute of Technology, Kanpur, INDIA Spin-State Regulation in Iron(II) and Iron(III) Complexes with Pyrazolylpyridine and Deprotonated Pyridine Amide Ligands
May 16	Dr Steve Marsden, Department of Chemistry, Imperial College, London Silicon-based methods for stereoselective and solid-phase syntheses
May 23	Dr Paul Smith, GlaxoWellcome Sialidase inhibitors for the treatment of influenza
October 9	Dr Roy S Lehrle, Birmingham

Forensics, Fakes and Failures

October 24 Prof Bob Denning, University of Oxford
Photonic Crystals

October 31 Dr Colin Raston, School of Chemistry, Univ of Leeds
Towards benign supramolecular chemistry: synthesis - self organisation

November 6 Dr Cliff Ludman, Durham University
Explosions - a demonstration lecture

November 14 Professor John Goodby, Department of Chemistry, University of Hull
Supermolecular liquid crystals - multipodes and dendrimers

November 20 Professor Peter Atkins
A Century of Physical Chemistry

November 21 Dr Roy Copely, GlaxoSmithKline
Crystallography in the Pharmaceutical Industry

November 27 Professor Ian G M Cowie, Herriot-Watt University
Cellulose - An old polymer with new applications
In association with The North East Polymer Association

November 28th Dr Jeremy Kilburn, Department of Chemistry, University of Southampton
Synthetic Receptors for Peptides - Rational and Combinatorial Approaches

December 5 Dr Mike Eaton, Celltech
Drugs of the Future

2002

January 22 Dr Ian Fallis, University of Cardiff
Size is Everything

January 23 Dr W. Huck, Melville Laboratory, Cambridge University
Control over polymeric materials at the (sub)-micron level

January 29 Dr Paul Monks, University of Leicester

	Ozone - the good, the bad and the ugly
January 30	Dr Peter Hore, PCL, University of Oxford Chemistry in a spin: effects of magnetic fields on chemical reactions
February 13	Dr Helen Aspinall, Department of Chemistry, University of Liverpool Defining effective chiral binding sites at lanthanides - enantioselective reagents and catalysts
February 20	Dr Elizabeth Hall, Institute of Biotechnology, Cambridge University The Heart of the Matter
February 26	Dr Mike Griffin, Forensic Science Service, Metropolitan Police Smack, Crack, Speed and Weed: A forensic chemist's tale
March 12	Professor David Williams, Cardiff Beer and Health: 7000 years of history
March 15	Dr Graham Saunders, Queens University, Belfast Dehydrofluorinative Carbon-Carbon Coupling as a Route to Complexes of Hybrid Cyclopentadienide- and Arene-Phosphine Ligands
October 2	Professor Gideon Davies, Department of Chemistry, University of York Structural Enzymology of Glycosyl Transfer: How Enzymes Make and Degrade Polysaccharides
October 15	Professor Mike Zaworotko from the University of South Florida Suparamolecular Synthesis of Functional Molecules & Materials
October 16	Dr. Hubert LeBozec, Université de Rennes 1, France Design of Molecular and Supramolecular Metal Polypyridine Complexes for Nonlinear Optics
October 23	Professor Marcetta Darensbourg, Department of Chemistry, Texas A&M University Functioning Catalysts Inspired by Active Sites in Bio-Organometallic Chemistry: The Hydrogenases
October 30	Professor Tim Bugg, Department of Chemistry, Warwick University

Enzymes in Aromatic Degradation

November 5 Dr Cliff Ludman, University of Durham
Explosions: a demonstration lecture

November 6 Professor Steve Perkins, Department of Biochemistry and Molecular Biology, UCL
Modelling large uncrystallisable protein structures using X-ray and neutron scattering

November 12 Dr Dave Alker, Pfizer
The Discovery of a New Medicine

November 13 Professor Geoffrey Lawrance, Newcastle University, Australia
Designer Ligands: Macrocyclic and alicyclic molecules for metal complexation and biocatalysis

November 27 Professor Marc Lemaire, University Claude Bernard, Lyon
Organic Synthesis and Heterogenous Asymmetric Catalysis

2003

January 15 Professor Pat Bailey, Department of Chemistry, UMIST
Planned and unplanned routes to bio-active target molecules

January 22 Dr David Procter, Department of Chemistry, University of Glasgow
New Strategies and Methods for Organic Synthesis

February 11 Dr John Emsley, University of Cambridge
False Alarms: Chemistry & the Media

February 19 Professor Tony Ryan, Department of Chemistry, University. of Sheffield
Introducing Soft Nanotechnology

March 4 Professor Richard Taylor, University of York
Adventures in Natural Product Synthesis

March 12 Professor David Lilley, School of Life Sciences, University of Dundee
Structure, folding and catalytic activity in RNA molecules

Publications

Examination of cobalt, nickel, copper and zinc (II) complex geometry and binding affinity in aqueous media using simple pyridylsulfonamide ligands.
A. Congreve, R. Kataky, M.Knell, D. Parker , H. Puschmann, K. Senanayake, L. Wylie, *New J. Chem.*, 27 (1): 98-106 2003.

Steric control of lanthanide hydration state: fast water exchange at gadolinium in a mono-amide 'DOTA' complex.
A. Congreve, D. Parker, E. Gianolio, M. Botta, *Dalton Trans.*, in press.